The University Of Sheffield.

The role of FRMPD2 in cell polarisation and zebrafish development

by

Agnieszka Skowronek

A thesis submitted in partial fulfilment of the requirements for the degree of

Doctor of Philosophy

The University of Sheffield

Faculty of Science

Department of Biomedical Science

October 2017

DECLARATION

I hereby declare that my thesis entitled: ***"The role of FRMPD2 in cell polarisation and zebrafish development"*** has been composed entirely by myself and has been solely the result of my work, unless where stated otherwise by reference or acknowledgement. I confirm that this work has not been submitted, in whole or in part, in any previous application for a degree.

27.10.2017

Date

Agnieszka Skowronek

Signature

ABSTRACT

The establishment of cell polarity is one of the most interesting symmetry-breaking events occurring in almost all physiological and developmental processes. One of the multi-PDZ domain proteins, the protein FRMPD2, has been implicated in the regulation of epithelial cell polarisation as well as playing a role in the immune host defence of epithelial cells of the human intestine. The aim of the current study was to explore the FRMPD2-mediated protein complex and to characterise its components with respect to signalling relevant to inflammatory bowel disease and epithelial cell polarisation as well as the in vivo analysis of FRMPD2 function in zebrafish.

The current study revealed several potential protein-protein interactions allowing a better understanding of the FRMPD2 role in epithelial cell polarisation. Here we described a novel interaction of FRMPD2 with the serine/threonine protein kinase N2 (PRK2) identified using the proximity-dependent biotin identification (BioID) method followed by western-blotting. In-depth analysis revealed that PRK2 interacts selectively with a PDZ3 domain of FRMPD2 and the extreme C-terminal cysteine of PRK2 is indispensable for this binding. We demonstrated that FRMPD2 can colocalize with PRK2 at cell-cell contacts and tight junctions of polarised epithelial cells. Our results suggest that FRMPD2 can recruit PRK2 to the basolateral membrane and potentially regulate PRK2-mediated signalling, however, more experiments are needed to identify the precise role of the FRMPD2-PRK2 complex in epithelial polarisation. Additionally, in line with previously published data using bronchial epithelial cells, we show here that PRK2 appears to play a similar role in colon and kidney epithelial cells.

In this study, we have also defined a possible role of FRMPD2 and PRK2 in cell mechanics. We discovered that altered expression of these two genes resulted in changes in cell stiffness and increased cell deformability. As a likely functional consequence, we observed accelerated migration of FRMPD2 and PRK2 depleted cells in a transwell filter assay. We also demonstrated that subcellular localisation of FRMPD2 in migrating cells is in line with a potential role in contributing to front-rear polarity.

Our in vivo study shows that *frmpd2* is expressed in zebrafish during early development. We also generated a homozygous zebrafish line only expressing a truncated version of FRMPD2, however, no obvious phenotype was detected and more careful analysis is necessary. Spatial expression pattern, as well as the precise role of FRMPD2 in zebrafish development and physiology, require further investigation beyond this thesis.

In conclusion, we identified a novel role of FRMPD2 in the regulation of PRK2-mediated signalling as well as cell mechanical properties and both phenomena place FRMPD2 as an important regulator of processes relevant to epithelial polarity.

ACKNOWLEDGEMENT

Undertaking PhD has been a truly life-changing experience, however, making me stronger and teaching me not give up too early. There are many people out there I really want to thank for their support and guidance during last four years of my life. The most important one is my supervisor Dr Kai Erdmann whose enthusiasm and constructive criticism helped me in carrying out my research. He always had an open door when I needed to talk and pushed me to trust myself and my work.

I also want to thank my advisors Dr Louise Robson and Dr Andrew Peden for their support and invaluable advice throughout my PhD. Huge thanks go to Prof Jochen Guck and his lab members who helped me to carry out my experimental work in their lab in Dresden and answered thousands of questions concerning biology and biophysics. I would like to express my gratitude to other Principal Investigators and colleagues from Department of Biomedical Science who not only shared reagents and protocols, but many times helped to solve problems with experiments.

Without my best friends, Shruti and Zainab, the time during my PhD would not be as great as it was. You two deserve a big thank you for all your support, company in the lab until late hours and being with me in the happiest, but also difficult moments in my life. Thanks for your trust, tolerance, making me laugh and loving me. Zainab, thank you for all your support during my writing-up time, reading all chapters and your comments. I also want to thank my friends, Iza and Paweł, who always found time for me to chat, listen to my complaints and kept fingers crossed for my success since I have left Poland.

I want to thank my parents and sister for their constant support during my whole life, and their deep belief in my capabilities, as well as helping me to be the person I am today. They taught me that nothing in life is free and that hard work always eventually pays off.

Finally, I want to thank my beloved husband Rafał, for the faith he has in my person and my abilities and to make me believe in them, too.

ABBREVIATIONS

16HBE14o-	human bronchial epithelial cell line
AF-6	afadin
AFM	atomic force microscopy
AJ	adherens Junction
ANOVA	analysis of variance
APC	adenomatous polyposis coli
aPKC	atypical protein kinase C
AP-MS	affinity-purification mass spectrometry
APS	ammonium persulfate
ARVCF	armadillo repeat gene deleted in Velo-Cardio-Facial syndrome
BANK1	B cell-specific adaptor protein with ankyrin repeats 1
BCIP	5-bromo-4-chloro-3-indolyl phosphate
BioID	proximity-dependent biotin identification
BirA*	mutant (R118A) of Biotin ligase
BSA	bovine serum albumin
Caco-2	human colon colorectal adenocarcinoma epithelial cell line
CD	Crohn's disease
Cdc42	cell division cycle 42
CFTR	cystic fibrosis transmembrane conductance regulator
CIP	calf intestinal alkaline phosphatase
Co-IP	co-immunoprecipitation
Crb3	Crumbs 3 protein
CRISPR	clustered regularly interspaced short palindromic repeats
DAPI	4',6-diamidino-2-phenylindole
DIG	digoxigenin
Dlg1	*Drosophila* disc large tumor suppressor
DMEM	Dulbecco's Modified Eagle Medium
DMSO	dimethyl sulfoxide
DNA	deoxyribonucleic acid
dNTP	deoxynucleotide

dNTP	deoxynucleotide triphosphates
ECM	extracellular matrix
EDTA	ethylenediaminetetraacetic acid
EGFR	epidermal growth factor receptor
EMT	epithelial-mesenchymal transition
ENU	*N*-ethyl-*N*-nitrosourea
FA	focal adhesion
FAK	focal adhesion kinase
FCS	fetal calf serum
FERM	four-point-one, ezrin, radixin, moesin
FRMPD2	FERM and PDZ containing 2 protein
GAPDH	glyceraldehyde 3-phosphate dehydrogenase
GDP	guanosine diphosphate
GEF	guanine exchange factor
GFP	green fluorescent protein
GGF	global geometric factor
GST	glutathione S-transferase
GTP	guanosine triphosphate
HBS	HEPES buffer saline
HEK293	human embryonic kidney cell line
HeLa	human cervical cancer cell line
HEPES	(4-(2hydroxyethyl)-1piperazineethanesulfonic acid
HF	high fidelity
HM	hybridization mix
HRP	horseradish peroxidase
IBD	Inflammatory bowel disease
IF	Immunofluorescence
IGF-1	insulin-like growth factor 1
INAD	Inactivation no afterpotential D protein
IPTG	Isopropyl β-D-1-thiogalactopyranoside
JAM	Junctional adhesion molecule
kDa	kilodalton
KIND	Kinase non-catalytic C-lobe

LARG	leukaemia-associated Rho-GEF
LB	Luria-Bertani
Lgl1	Lethal giant larvae 1
MAGUK	membrane-associated guanylate kinases
MCS	multiple cloning site
MDA-MB-231	human breast adenocarcinoma
MDCK II	Madin-Darby canine kidney cell line
MDP	muramyl dipeptide
MEM	Minimum Essential Medium
MRLC	myosin regulatory light chain
MUPP1	Multiple PDZ Domain Protein-1
MW	molecular weight
NBT	nitro blue tetrazolium
NEAA	non-essential amino acids
NF-κB	nuclear factor kappa-light-chain-enhancer of activated B cells
NHERF	Na+/H+ exchanger regulatory factor
NOD	nucleotide-binding oligomerization domain-containing protein 2
NTC	no template control
OCRL	Lowe oculocerebrorenal syndrome protein
Opti-MEM	reduced serum media
ORF	open reading frame
OS	optical stretcher
PALS1	Protein Associated with Lin-Seven 1
Par3	partitioning defective-3
Par6	partitioning defective-6
PATJ	PALS1 associated Tight Junction Protein
PBM	PDZ binding motif
PBS	phosphate-buffered saline
PBST	phosphate buffered saline with Tween20
PCP	planar cell polarity
PCR	polymerase chain reaction

PDMS	polydimethylsiloxane
PDZ	PSD95/Dlg1/ZO-1
PFA	paraformaldehyde
PRK2/PKN2	serine/threonine-protein kinase N2
PSD-95	postsynaptic density protein 95
PTEN	phosphatase and tensin homolog
PTP-BL	Protein tyrosine phosphatase Basophil-like
Rac1	Ras-related C3 botulinum toxin substrate 1
RFP	red fluorescent protein
RhoA	Ras homolog gene family member A
RI	refractive index
RNA	ribonucleic acid
ROCK	Rho-associated protein kinase
RT	room temperature
RT-DC	real-time deformability cytometry
RT-qPCR	quantitative reverse transcription PCR
Scrib	Scribble protein
SDS-PAGE	sodium dodecyl sulphate polyacrylamide gel electrophoresis
SEM	standard error of the mean
SH3	Src homology 3 domain
shRNA	short hairpin RNA
siRNA	small interfering RNA
SSC	saline-sodium citrate buffer
TAE	tris-acetate buffer
TALEN	transcription activator-like effector nuclease
TAP	tandem affinity purification
TBST	tris buffered saline with Tween20
Tiam1	T-cell lymphoma invasion and metastasis 1 protein
TJ	tight junction
UC	ulcerative colitis
UTP	uridine triphosphate
VASP	Vasodilator-stimulated phosphoprotein

WASP	Wiskott-Aldrich syndrome protein
WAVE	WASP-family verprolin-homologous protein
WB	Western Blot
WISH	whole-mount in situ hybridization
WT	wild type
ZO-1/-2/-3	zonula occludens 1/2/3

Table of contents

List of figures

List of tables

List of publications

The following publications resulted from the work carried out during my PhD, but not directly relevant to this thesis:

SHARMA, S., **SKOWRONEK, A.** & ERDMANN, K. S. 2015. The role of the Lowe syndrome protein OCRL in the endocytic pathway. *Biol Chem,* 396**,** 1293-300.

YU, F., SHARMA, S., **SKOWRONEK, A.** & ERDMANN, K. S. 2016. The serologically defined colon cancer antigen-3 (SDCCAG3) is involved in the regulation of ciliogenesis. *Sci Rep,* 6**,** 35399.

CHAPTER 1 - Introduction

1.1 Cell polarity

Asymmetric distribution of proteins and lipids within cell membranes and intracellular spaces is a hallmark of cell polarity. The ability of the cells to establish and maintain spatial asymmetry is an evolutionarily conserved feature observed in single cell systems, like yeast, as well as in multicellular organisms, like mammals. Cell polarity is essential for many biological processes such as cell division, cell migration or differentiation and must be coordinated to enable cells to maintain tissue organisation and function.

There are different types of polarity regulating morphogenesis of epithelial structures (Figure 1.1): ***planar cell polarity*** (PCP), which coordinates polarity between the cells and maintains tissue order, ***apical-basal polarity*** reflected in asymmetrically distributed proteins and cellular components along the apical-basal axis, ***front-rear polarity*** used by migrating cells to control directionality and ***mitotic-spindle polarity***, regulating the plane of cell division and position of daughter cells (Muthuswamy and Xue, 2012).

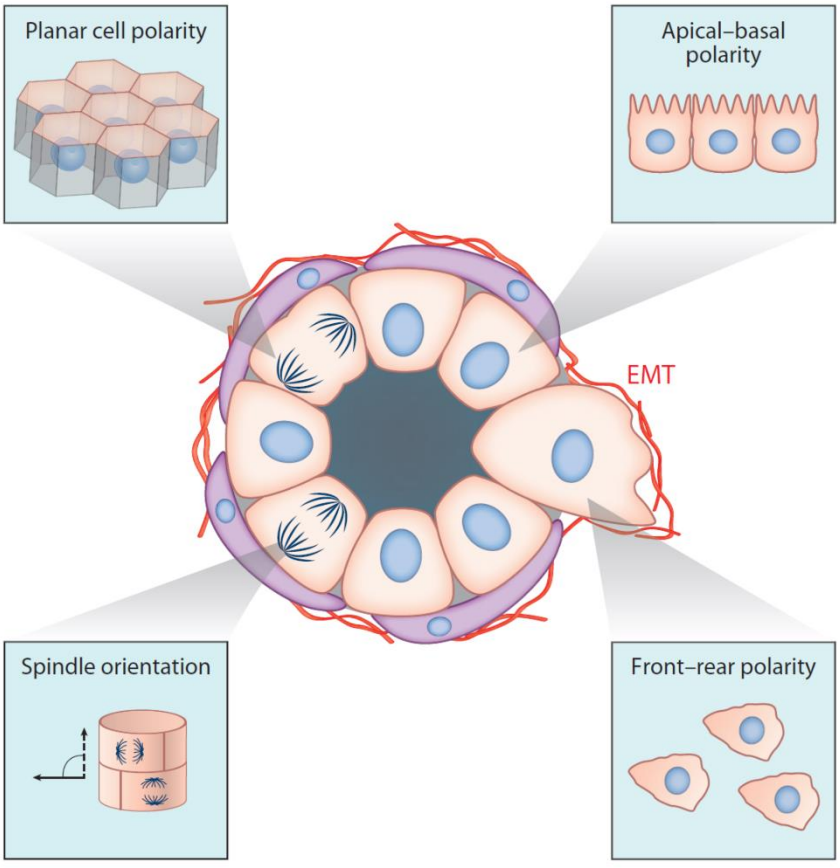

Figure 1.1 Different types of cell polarity

Figure represents different types of cell polarity that regulate morphogenesis of epithelial structures: planar cell polarity, apical-basal polarity, front-rear polarity and mitotic spindle polarity. Figure adapted from others (Muthuswamy and Xue, 2012)

1.1.1 Apical-basal cell polarisation

The structure of epithelial cells allows them to form a continuous monolayer lining the tubular network of epithelial organs, like intestine or kidney, which form a barrier between the lumen and the underlying tissue. Polarised epithelial cells are split into two different regions characterised by an unequal distribution of proteins and lipids, resulting in an asymmetry in structure and function of these subdomains. The apical surface, facing the luminal space, contains a network of microvilli and regulates the exchange of biological components, while the basolateral surface provides the contact between the cell and the extracellular matrix or basement membrane. Formation and maintenance of three-dimensional tissues are mediated and facilitated by junctional multiprotein complexes, which are positioned asymmetrically in polarised epithelial cells (Figure 1.2) (Bryant and Mostov, 2008, Shin et al., 2006). Below a short summary of these protein complexes follows.

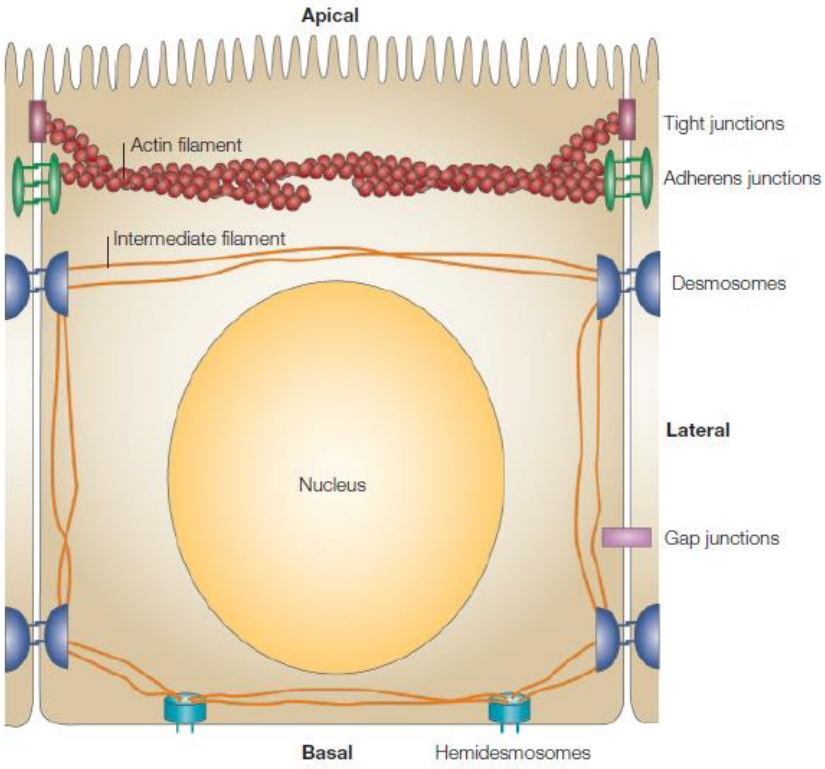

Figure 1.2 Arrangement of junctions in polarised epithelial cells

Figure represents an example of polarised epithelial cell with intracellular junctions: tight junctions, adherens junctions, desmosomes and gap junctions as well as cell-extracellular matrix junctions called hemidesmosomes. Figure adapted from others (Matter and Balda, 2003)

Tight junctions (TJ) are the most apical junctions which mark the boundary between the apical and lateral membranes. They create a barrier and regulate the paracellular permeability of the molecules and ions (gate function), but also prevent mixing of the components between the apical and basolateral membranes (fence function). Tight junctions are constituted of transmembrane proteins such as Claudins, Occludin, and junctional adhesion molecules (JAM) as well as cytoplasmic actin-binding zonula occludens (ZO) proteins. Claudins are the most important components of the tight junctions forming their backbone and regulating their gate function by selecting the molecules by their size (Tsukita et al., 2008). The permeability of the tight junctions varies between different types of epithelial cells and depends on the specific content of claudin family members incorporated into TJs (Balkovetz, 2009). At the C-terminus claudins contain PDZ binding motif and have the ability to interact with scaffold proteins containing PDZ-domains (Itoh et al., 1999, Roh et al., 2002a). Occludin maintains stability and barrier function of tight junctions but its role in tight junction assembly is dispensable (Schulzke et al., 2005). Occludin mediates connections between adjacent cells and these interactions help to maintain the size selective barrier and separation between apical and basolateral membranes (McCarthy et al., 1996). Similarly to claudins, the C-terminus of occludin mediates protein-protein interactions and binds for example ZO proteins (Balda et al., 1996). All zonula occludens (ZO) proteins, ZO-1, ZO-2 and ZO-3, have a similar modular structure and contain two types of domains mediating protein-protein interactions. PDZ and SH3 domains of ZO proteins bind components of tight and adherens junctions like claudins and JAMs as well as catenins, therefore they are thought to link these two junctional complexes (Rajasekaran et al., 1996, Itoh et al., 1999, Ebnet et al., 2000). Moreover, as scaffold molecules, ZO-family proteins link other transmembrane proteins to the cytoskeleton (Fanning et al., 1998). The last component of the tight junctions are the junctional adhesion molecules (JAM). The extracellular domains of JAMs stabilise cell-cell junctions between

neighbouring cells, while their cytoplasmic tail mediates protein-protein interactions, similarly to claudins and occludin. JAMs localise to the tight junctions and together with other protein complexes support their formation (Ebnet et al., 2003).

Adherens junctions (AJ) are found in the lateral membrane of polarised epithelial cells, below the tight junctions and are formed by two complexes of adhesive receptors: the nectins and the cadherins. Extracellularly these two molecules mediate adhesion of the adjacent cells but intracellularly interact with the range of proteins connected to cytoskeleton and signalling pathways. Interestingly, the formation of tight and adherens junctions is mutually dependent. It has been shown, that generation of tight junctions depends on established cadherin- and nectin-mediated adhesions, while depletion of tight junction proteins affects maturation of adherens junctions (Ikenouchi et al., 2007). The main component of the cadherin-based adhesions is E-cadherin interacting with catenin family proteins and other actin-binding proteins (Aberle et al., 1994, Yap et al., 1998). E-cadherin directly binds β-catenin at cell-cell contacts and thereby prevents β-catenin from transfer to the nucleus (Nelson and Nusse, 2004). Additionally, β-catenin interacts with α-catenin linking the adherens junction complex to the actin cytoskeleton (Aberle et al., 1994), however simultaneous binding of β-catenin to α-catenin and actin filaments is only possible in cells under force (Buckley et al., 2014). Interaction of E-cadherin with the third p120-catenin stabilises E-cadherin at the membrane and also activates Rho GTPases (Noren et al., 2000), which further, through their effector proteins, modulate cytoskeleton dynamics. The connection between E-cadherin and actin filaments makes epithelia susceptible to changes of the cell shape and tissue remodelling during morphogenesis. Similarly to cadherins, nectins mediate cell-cell adhesion, however, they are not as strong as cadherin-mediated adhesions. Like other components of tight or adherens junctions, nectins interact with other proteins by their C-terminal PDZ binding motif (Takahashi et al., 1999, Takai and Nakanishi, 2003). Nectins anchor the junctional complex to the actin cytoskeleton through the adaptor protein afadin (AF-6) (Takai et al., 2008). It has

been shown that loss of interaction between nectin and afadin delays junctional localisation of E-cadherin resulting in weak adhesion (Sato et al., 2006).

In addition to tight and adherens junctions there are also other important cell connections including ***gap junctions*** directly connecting the cytoplasm of epithelial cells and thereby regulating the exchange of molecules and ions between the cells. ***Desmosomes*** link adhesion proteins to intermediate filaments, while ***hemidesmosomes*** attach epithelial cells to the extracellular matrix.

1.1.2 Front-rear cell polarisation

During embryonic development, tissue regeneration as well as cancer progression and metastasis, polarised epithelial cells undergo multiple biochemical processes known as epithelial-mesenchymal transition (EMT). During EMT, polarised epithelial cells, which normally interact with the basement membrane via their basal surface, lose their apical-basal polarity and acquire a mesenchymal phenotype with enhanced migratory capacity and invasiveness (Kalluri and Neilson, 2003). Cells can migrate individually as well as collectively and front-rear polarity can be acquired by isolated or cohesive cells. Remodelling from apical-basal to front-rear polarity can be initiated by many external stimuli including growth factors and the extracellular matrix but conversion from tightly packed and non-migrating epithelial cells into directionally migrating cells requires global changes in cell organisation (Lauffenburger and Horwitz, 1996). The new polarised phenotype is characterised by extended membrane protrusions in the direction of migration, assembly and disassembly of focal adhesions, extensive reorganisation of the actin cytoskeleton and re-orientation of the Golgi apparatus and microtubule organising centre (Figure 1.3) (Lauffenburger and Horwitz, 1996, Casanova, 2002, Grande-Garcia et al., 2007).

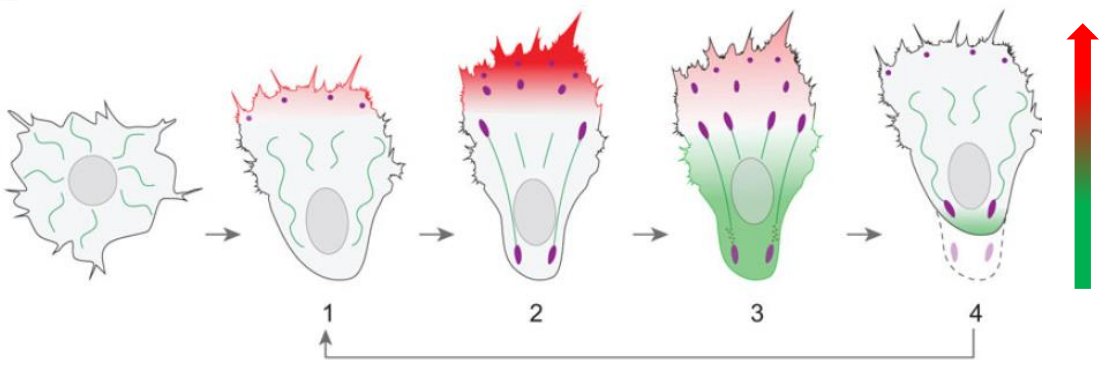

Figure 1.3 Stages of cell migration

Figure represents stages of cell migration. Cells migrate in the repeated cycle: (1) formation of the leading edge and immature adhesions, (2) maturation of cell adhesions, (3) translocation of the cell body, (4) disassembly of focal adhesions and rear retraction. Processes dependent on actin polymerization are highlighted in red, myosin II-dependent in green and cell adhesions in purple. An arrow indicates the direction of cell migration from the rear to the front of the cell. Figure adapted and modified from others (Reig et al., 2014).

At the initial stage of migration, a cell must first polarise and form its leading edge (front) with dynamic lamellipodia (Chou et al., 2003), which form contacts with the extracellular matrix (ECM) and enable stabilisation of the cell cytoskeleton (Gupton and Waterman-Storer, 2006). The process of protrusion formation requires extensive actin polymerisation and is regulated by signaling molecules including Rho GTPases (Cdc42 and Rac), the Arp2/3 complex activated by WASP/WAVE, and also Ena/VASP proteins, which localise at the leading edge of migrating cells (Krause et al., 2003, Ridley et al., 2003, Grande-Garcia et al., 2007). The initial formation of protrusions is followed by generation of additional extensions known as focal adhesions (FAs), also connecting the cell to the ECM, but utilising traction forces to drive migration (Burridge and Chrzanowska-Wodnicka, 1996). FAs are linked to the actin cytoskeleton via stress fibers, regulating and maintaining tension on the cell axis (Ridley et al., 2003). Mature cell-ECM contacts anchored to actomyosin form longitudinal stress fibers, which create strong tension and as a consequence adhesion sites are disassembled and the rear of the cell retracts (Ridley et al., 2003). Retraction of the trailing edge is regulated by Rho GTPase, Rho kinase, interaction with myosin II and phosphorylation of myosin light chain (Katoh et al., 2001). In summary, establishment of front-rear polarity and cell migration require a high level of regulation associated with the appropriate orientation of the actin cytoskeleton and adhesive structures.

1.2 PDZ domain proteins

1.2.1 Structure

PDZ domains were initially recognised as conserved sequence motifs within three proteins: postsynaptic density protein 95 (PSD-95), *Drosophila* disc large

tumor suppressor (Dlg1) and zonula occludens protein (ZO-1). Although the discovered domains were originally named from the characteristic amino acid sequence motif as GLGF domains, currently they are known by an acronym derived from the names of these three proteins (PDZ: PSD95/Dlg1/ZO-1) (Kennedy, 1995). Each PDZ domain is 80 – 100 amino acids residues long and structurally contains six β-strands (βA–βF) and two α-helices (αA and αB) which together form a globular structure. The carboxyl terminus of the interacting protein binds to a specific conserved motif containing an R or KXXXGLGF (GLGF motif) within the carboxylate-binding loop of a PDZ domain (Figure 1.4) (Doyle et al., 1996). The basic amino acid within the carboxylate-binding loop (arginine – R or lysine – K) is a key determinant of the target protein binding and its substitution can alter the affinity of PDZ domains for their ligand (Gee et al., 2000).

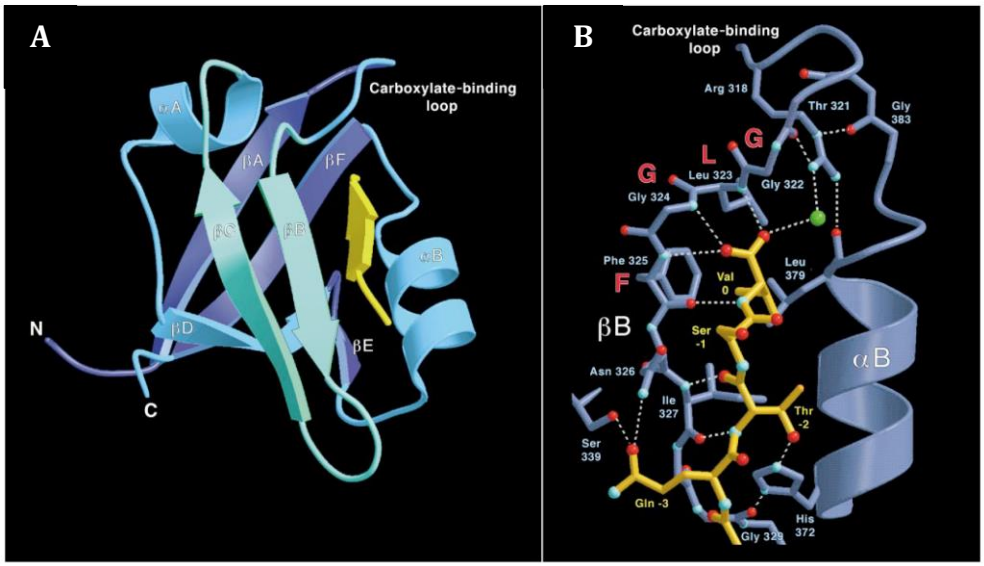

Figure 1.4 Structure of the PDZ3 domain of PSD-95

(A) *Ribbon diagram of the PDZ3 domain with the carboxyl terminus of the interaction partner (yellow).* ***(B)*** *Detailed diagram representing bound peptide (yellow) of the ligand in the carboxylate-binding loop of PDZ domain. Dashed white lines represent hydrogen bonds created during the interaction between peptide and protein. Figures adapted and modified from others (Doyle et al., 1996).*

In view of the binding specificity, PDZ domains were classified into three groups distinguished upon the sequences of the C-terminal peptide ligands (Hung and Sheng, 2002). Although specific sequence motifs at the carboxyl terminus of the target proteins are typical ligands bound by PDZ domains, these domains differ

in their stringency and specificity. PDZ domains can also bind internal sequences (Brenman et al., 1996), and also interact with other PDZ domains and form homo- and heterooligomers like ZO-1 or NHERF protein (Fanning et al., 1998, Maudsley et al., 2000). Proteins bearing PDZ domains are localised at specific subcellular sites near the plasma membrane and such membrane association may also be related to their affinity for phosphatidylinositols (Kachel et al., 2003). The majority of PDZ domain-containing proteins represent molecules with the higher-order organisation and very often they comprise multiple PDZ domains or multidomain arrangements like MAGUK (membrane-associated guanylate kinase) proteins (Figure 1.5).

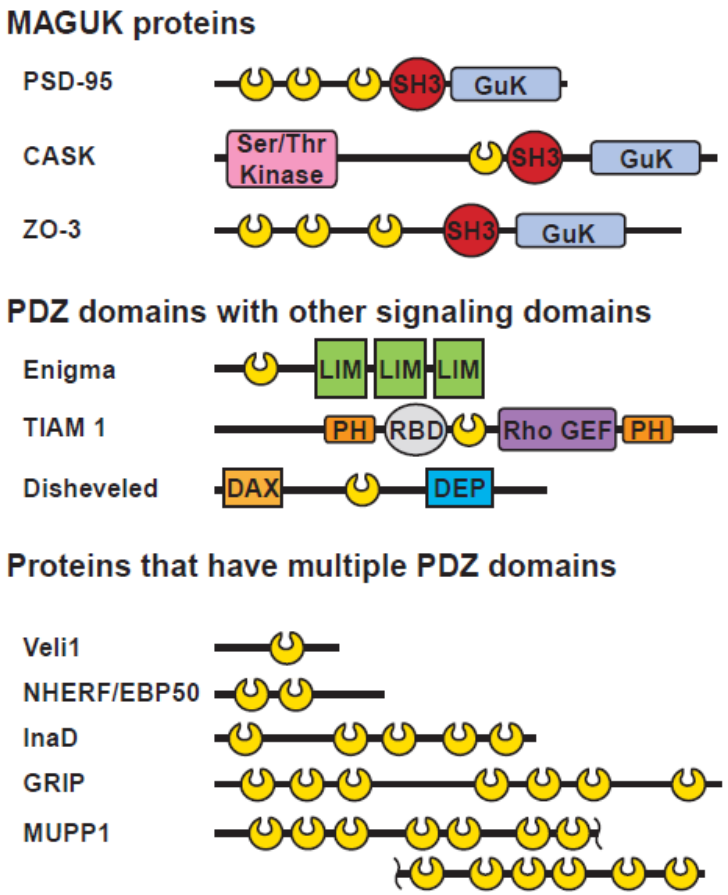

Figure 1.5 Examples of PDZ domain-containing proteins

Figure represents examples of PDZ domain-containing proteins considering their modular structure. PDZ domains are shown in yellow. Figure adapted from others (Harris and Lim, 2001).

1.2.2 Function

PDZ domains function as protein-protein interaction modules and proteins that bear them contribute to many cellular processes. They mainly organise large multiprotein complexes involved in signalling cascades and organisation of cytoarchitecture, both important in establishment and maintenance of epithelial polarity. A large number of PDZ-domain containing proteins form polarity complexes, whose role in epithelial polarisation and polarised cell migration is described in more detail later in this chapter in section 1.2.3.

1.2.2.1 Formation of protein complexes at the plasma membrane

In polarised epithelial cells, PDZ domain proteins indicate distinct subcellular localisation at the apical and basolateral membrane as well as junctional regions, thus they are responsible for targeting their ligands to the appropriate membrane compartments. In most cases, PDZ domain-containing proteins interact and colocalize with transmembrane and cytosolic binding partners (Fanning and Anderson, 1996).

Proteins containing PDZ domains that are associated with ion channels and receptors influence their stability and function in the membrane. They also often regulate their trafficking and downstream signalling pathways (Kaech et al., 1998, Romero et al., 2011, Short et al., 1998). For example, the CFTR (cystic fibrosis transmembrane conductance regulator) associates with the PDZ domain protein Erb50, which functions as an adaptor linking this apical membrane molecule to the cortical actin cytoskeleton (Short et al., 1998). Such anchoring may potentially enable transmission of the cytoskeletal changes, which are known to regulate CFTR activity (Cantiello, 1996, Ismailov et al., 1997, Prat et al., 1995). Furthermore, interactions with other multi-PDZ domain proteins, CAP70 and NHERF, modulate channel activity and potentially promote CFTR multimerization (Raghuram et al., 2001, Wang et al., 2000).

Proper localisation at the membrane, facilitated by PDZ domain-containing proteins, also regulates the function of tyrosine kinase receptors (Kaech et al., 1998, Maudsley et al., 2000). A complex of three PDZ proteins, LIN-2/Lin-7/LIN-

10, interacts with and targets Let-23 (the epidermal growth factor receptor in *Caenorhabditis elegans*) to the basolateral membrane, while loss of function of any of the components of the LIN complex leads to receptor mislocalisation and disturbance of further related signalling cascades (Kaech et al., 1998). Activation of the tyrosine kinase receptor signalling pathways by PDZ domain-containing proteins has also been demonstrated by Maudsley et al. (Maudsley et al., 2000). It has been shown that clustering and autophosphorylation of the platelet-derived growth factor (PDGF) receptor is more efficient when it interacts with NHERF and strengthens PDGF-mediated activation of the MAPK pathway. Localisation of the NHERF at the apical membrane of polarised epithelial cells has also been shown to play an important role in beta2-adrenergic receptor-mediated regulation of Na^+/H^+ exchange (Hall et al., 1998). NHERF binds directly to the β_2-adrenergic receptor and NHE-3 (sodium hydrogen exchanger-3) via two PDZ domains. Disruption of the interaction between receptor and NHERF alters the activity of NHE-3 and results in ionic homeostasis disorders.

Formation of multi-protein complexes mediated by PDZ domain-containing proteins may also be affected by the ability of these proteins to interact with the cortical actin cytoskeleton. Some PDZ proteins, like ZO-1 and AF-6, which are components of tight junctions, bind directly to actin filaments (Fanning et al., 1998, Mandai et al., 1997), but also function as regulators of the actin cytoskeleton (Willott et al., 1993, Yamamoto et al., 1997). Other PDZ proteins like NHERF or PSD-95 also associate with the actin cytoskeleton or microtubules respectively, however they do so through interacting with actin-binding proteins (Reczek et al., 1997, Niethammer et al., 1998). These interactions act to anchor the PDZ domain-containing proteins to the cortical cytoskeleton, which brings them into close contact with membrane-associated proteins and additionally stabilise their supramolecular complexes.

1.2.2.2 Organisation of postsynaptic density

Postsynaptic density (PSD) is a specific membrane-associated region of excitatory neuronal synapses that is responsible for transduction and processing of postsynaptic signals (Kennedy, 2000, Scannevin and Huganir, 2000, Sheng and Hoogenraad, 2007) and is characterised by a very complex and organised core

structure (Chen et al., 2008) (Figure 1.6). These specialised membrane domains are organised by abundant PDZ domain-containing scaffold proteins, which regulate clustering of glutamate receptors as well as trafficking of receptors and ion channels, organise large signalling complexes and coordinate the dynamic of cytoskeletal architecture (Elias and Nicoll, 2007, Kim and Sheng, 2004, Scannevin and Huganir, 2000, Sheng and Hoogenraad, 2007). PSD contains three specific layers of which the first one is enriched with membrane receptors like NMDA (N-methyl-D-aspartic acid glutamate) receptors and AMPA (α-amino-3-hydroxy-5-methyl-isoxazole-4-propionic acid) receptors, ion channels and transmembrane cell-adhesion molecules. The second layer contains MAGuK scaffold proteins and PSD-95 (postsynaptic density protein of 95 kilodaltons) is one of the most abundant of these, providing direct contact with ion channels and membrane receptors (Feng and Zhang, 2009). Possession of three PDZ domains as well as an SH3 and GuK domain allows PDS-95 to form multiprotein complexes at the postsynaptic density region. It clusters NMDA receptors at the synapse (Kornau et al., 1995, Niethammer et al., 1996), while its GuK domain associates with GKAP (guanylate kinase-associated protein) (Naisbitt et al., 1999). GKAP, together with another protein Shank, forms the third layer of the PSD and connects protein complexes to the actin cytoskeleton. Such functional supramodules created by many scaffolding proteins regulate the dynamic architecture of the postsynaptic density during developmental processes and in response to synaptic activity.

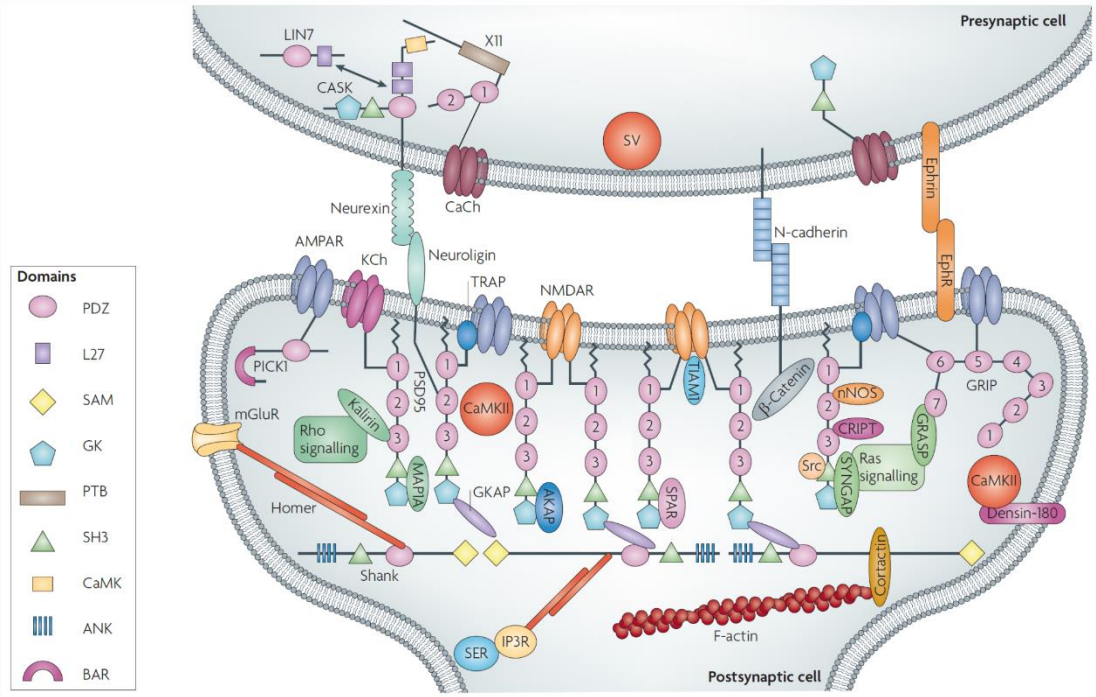

Figure 1.6 Organisation of architecture in the postsynaptic density (PSD)

The postsynaptic density is comprised of membrane receptors, ion channels, scaffold and adaptor proteins, signaling mlecules, cell adhesion moleculs and cytoskeleton components. All molecules form specific layers in the PSD and regulate the dynamic architecture of the PSD during development and in response to synaptic activity. Figure adapted from others (Feng and Zhang, 2009)

1.2.3 Polarity complex proteins in epithelial cell polarisation and polarised cell migration

The majority of polarity proteins are highly conserved among the multicellular species (Stern, 2006), however crucial for their function is localisation. Assembly and asymmetric distribution of junctional complexes in polarised epithelial cells are regulated by conserved complexes containing PDZ domain proteins (Nelson, 2003). The polarity proteins are grouped into three functional complexes: apically localised **Crumbs complex** (Crb/PALS1/PATJ), subapically localised **Par complex** (Par3/Par6/aPKC) and basolaterally localised **Scribble complex** (Scrib/Dlg/Lgl) (Bryant and Mostov, 2008) (Figure 1.7 a). Establishment and maintenance of epithelial polarity are coordinated by all three protein complexes, which positively or negatively cross-regulate each other (Bilder, 2003). Polarity proteins that control apical-basal polarity adapt to processes that generate front-rear polarity in migrating cells and that is reflected in the transition of their

localisation to the leading edge in polarised migrating cells as well as in the modification of their functions for different cellular activities (Figure 1.7 b).

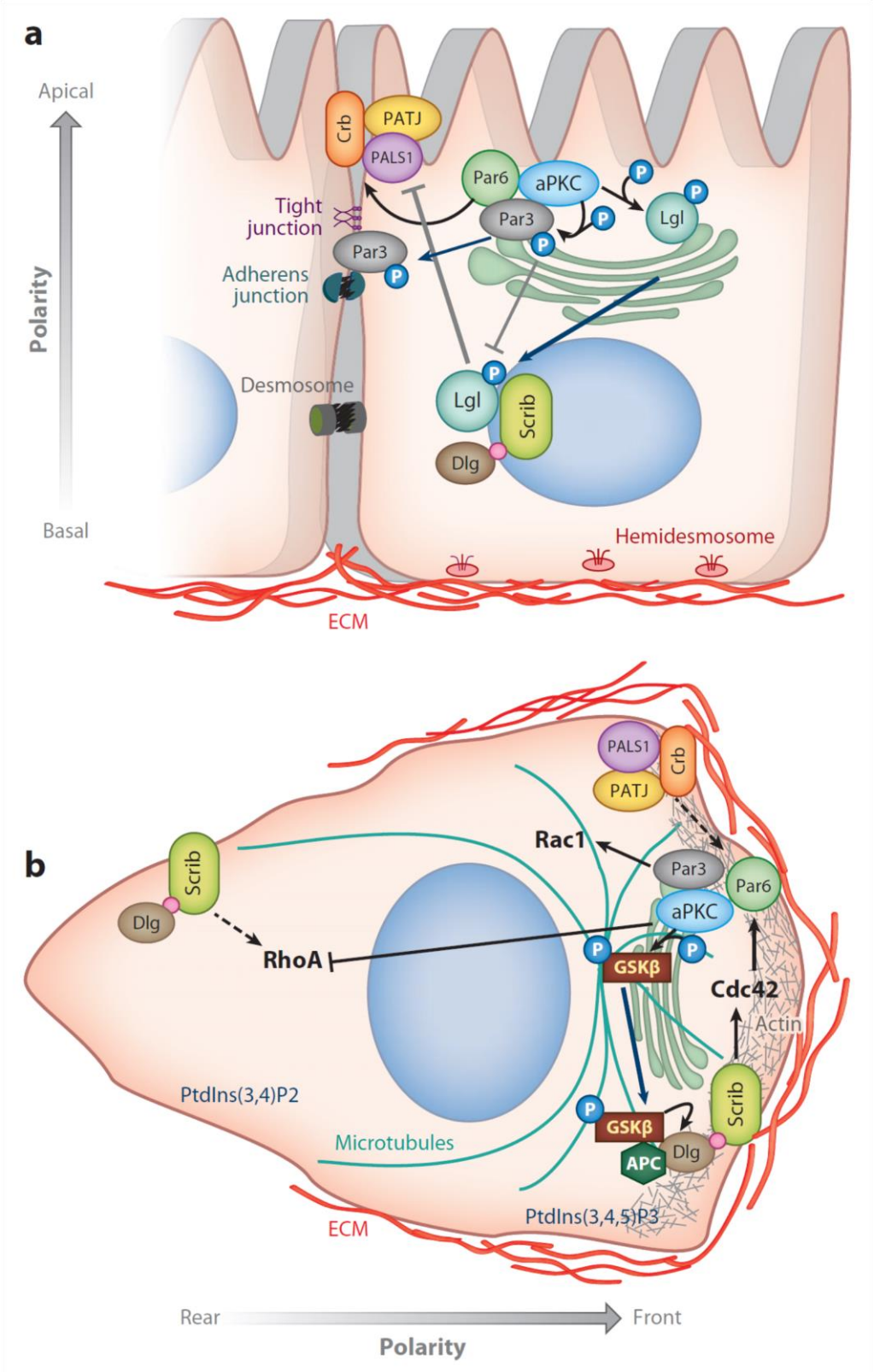

Figure 1.7 Localisation of polarity complexes in polarised epithelial cells

Figure represents changes in the localisation of polarity complexes during the transition between (a) apical-basal to (b) front-rear polarity. Abbreviations: Crb (Crumbs), PATJ (Pals1 associated tight junction), PALS1 (Protein associated with Lin-Seven 1), Par3 (Partioning defective-3), Par6 (Partioning defective-6), aPKC (atypical protein kinase C), Lgl (Lethal giant larvae), Dlg (Discs Large), Scrib (Scribble). Figure adapted from others (Muthuswamy and Xue, 2012).

1.2.3.1 Crumbs complex

The Crumbs complex consists of four major components: Crumbs3 (Crb3), Protein Associated with Lin-Seven 1 (PALS1), PALS1 associated Tight Junction Protein (PATJ) and Multiple PDZ Domain Protein-1 (MUPP1), which are highly conserved among the species (den Hollander et al., 1999, Lemmers et al., 2002, Medina et al., 2002a, Roh et al., 2002b, Makarova et al., 2003).

Crumbs3 (Crb3) is a transmembrane protein with an extracellular N-terminus and cytoplasmic C-terminus containing FERM and PDZ binding domains (Makarova et al., 2003). *Crb3* exists in two isoforms, Crb3a and Crb3b (Fan et al., 2007, Makarova et al., 2003), which differ from each other in the sequence encoding the PDZ domain at the C-terminus of the protein. The Crb3b isoform has been found to localise to the spindle poles during mitosis as well as primary cilia in polarised epithelial cells where it controls cytokinesis and ciliogenesis, respectively (Fan et al., 2007). The second isoform, Crb3a, localizes to the apical subdomain of polarised epithelial cells where it is involved in apical membrane growth (Schluter et al., 2009) as well as tight junction formation (Fogg et al., 2005, Hurd et al., 2003b, Makarova et al., 2003). Both Crb3 isoforms are essential for epithelium function, however only the Crb3a isoform is included in the Crumbs polarity complex. Crb3a protein forms a complex with PALS1 and PATJ at tight junctions and links this group of proteins with the Par complex via interaction with Par6 (Hong et al., 2001, Roh et al., 2002b, Hurd et al., 2003b, Lemmers et al., 2004). Simultaneous binding of Crb3 to both PALS1 and Par6 proteins is required for undisturbed tight junction formation (Hurd et al., 2003b, Roh et al., 2003, Lemmers et al., 2004). Additionally, during cell polarisation, actin cytoskeleton regulators, moesin and βH-spectrin are recruited by the FERM domain of the

Crb3 protein and stabilise the cortical cytoskeleton and establish cell polarity (Medina et al., 2002b).

Another component of the Crumbs polarity complex, **PALS1**, is an essential PDZ domain-containing scaffolding molecule providing an important link between Crumbs and Par complexes via its interaction with the PDZ domain of Par6 protein (Hurd et al., 2003a, Penkert et al., 2004, Wang et al., 2004). PALS1 interacts with Crb3 via its PDZ domain, while binding to other component of the Crumbs complex, PATJ, is mediated by its L27N domain (Li et al., 2004). It has been shown that PALS1 presence in the Crumbs polarity complex is indispensable for tight junction formation (Li et al., 2004, Straight et al., 2004), but also it is necessary for PATJ stability as well as aPKC localisation to the tight junctions (Straight et al., 2004, Wang et al., 2004). It has been shown that in mammalian epithelium PALS1 protein is stabilised by small PDZ domain-containing protein Lin-7 (Lineage defective protein-7) (Olsen et al., 2002, Straight et al., 2006, Bohl et al., 2007). In Lin-7 depleted MDCK cells, tight junction formation is delayed, but not completely abrogated, therefore it suggests that PALS1 plays an essential role in the establishment of the tight junctions (Straight et al., 2006). On the other hand, it has been shown that knockdown of PALS1 in MDCK cells leads not only to a tight junction defect but also changes the architecture of the lateral membrane (Wang et al., 2007). PALS1 depletion was found to cause mislocalization of the exocyst complex which most likely disrupt E-cadherin trafficking and finally leads to severe adherens junction defect.

Two remaining main components of Crumbs polarity complex, **PATJ and MUPP1**, have been shown to directly interact with PALS1 (Roh et al., 2002b, van de Pavert et al., 2004) and to localise to the tight junctions. Both proteins are highly modular multi-PDZ domain proteins that act as scaffolds at apical junctions (Ullmer et al., 1998, Lemmers et al., 2002). PATJ protein has been shown to interact with tight junction structural proteins ZO-3 and Claudin1 (Roh et al., 2002a), while MUPP1 was linked to proteins from Claudin family and JAMs (Lee et al., 2003, Hildebrandt et al., 2009). Whereas PATJ is necessary for tight junction formation, MUPP1 does not seem to play a significant role in this process (Adachi et al., 2009). Depletion of PATJ does not affect the stability of the Crumbs polarity

complex (Shin et al., 2005), however, its absence in epithelial cells affects the localisation of other components of adherens and tight junctions (Michel et al., 2005).

There is not much known about the function of Crumbs polarity complex in cell migration, however, it has been shown that PATJ is recruited to the leading edge of migrating cells, where it controls localisation of Par3 and aPKC (Hurd et al., 2003b, Wang et al., 2004). PATJ is involved in directional migration during wound healing in epithelial cells and its depletion alters cell orientation and slows down wound closure (Shin et al., 2007).

1.2.3.2 Par complex

The Par complex comprises three components: Par3 (Partitioning defective-3), Par6 (Partitioning defective-6) and atypical protein kinase C, aPKC. Initially the complex has been described as an important regulator of asymmetric division in *C. elegans* (Watts et al., 1996, Kemphues, 2000), however, later several groups have shown the importance of the Par complex in tight junction formation and epithelial polarisation. The Par complex exists transiently during the formation of apical surface and tight junctions (Morais-de-Sa et al., 2010, Nagai-Tamai et al., 2002). Interactions between Par3 and Par6 as well as Par3 and aPKC are indispensable for the establishment of cell polarity (Joberty et al., 2000, Lin et al., 2000, Horikoshi et al., 2009).

Par3 is a PDZ domain protein that, similarly to other proteins from the same family, acts as a scaffold at tight junctions and is essential for tight junction formation (Kohjima et al., 2002). It has been shown that the N-terminus of Par3 protein is necessary for its recruitment to the most apical side of cell-cell contacts and proper localisation of other components of the Par complex (Mizuno et al., 2003). Par3 binds to the extreme C-terminus of JAM, a component of tight junctions, suggesting that JAM anchors the Par complex at tight junctions (Ebnet et al., 2001, Itoh et al., 2001). It also has been demonstrated that two PDZ domains of Par3 protein link the Par complex to the plasma membrane and phosphoinositide signaling (Wu et al., 2007, Feng et al., 2008). Membrane

localisation of Par3 provides spatial regulation of Rac1 signaling pathways leading to the stabilisation of epithelial junctions (Chen and Macara, 2005). Such subcellular restriction also supports Par3 role in membrane biogenesis, in which via an interaction with kinesin-2, Par3 participates in a process of cilia growth and elongation (Sfakianos et al., 2007).

The other component of the Par complex, **Par6**, is a multifunctional protein that mediates the interaction of Par polarity complex with Crumbs and Scribble complexes (Hurd et al., 2003b, Lemmers et al., 2004, Wang et al., 2004). The PDZ domain of Par6 is implicated in the interaction with a member of the Crumbs complex, the Crb3 protein (Hurd et al., 2003b, Lemmers et al., 2004) as well as with the Lgl protein, a component of the lateral Scribble complex (Plant et al., 2003, Yamanaka et al., 2003). Interestingly, during cell polarisation, Lgl colocalises with Par6/aPKC in the cell-cell contact region, however this complex remains inactive for tight junction formation. Upon aPKC activation, Lgl separates from the complex and that enables it to form the active form of the Par complex with Par3, which finally triggers formation of tight junctions (Yamanaka et al., 2003). As mentioned before, Par6 binds to aPKC and in the presence of GTP-bound Cdc42 it is thought to activate aPKC (Joberty et al., 2000), which subsequently phosphorylates Par3 (Izumi et al., 1998, Nagai-Tamai et al., 2002). Activated Par3 then localises to apical junctions where it can function independently from Par6 and aPKC (Morais-de-Sa et al., 2010). Similar mechanisms of Par complex activation are observed in migrating cells in which Par6, together with aPKC, acts as a downstream target of Cdc42 (Joberty et al., 2000, Lin et al., 2000) and regulate cell polarity during scratch-induced migration of astrocytes and fibroblasts (Etienne-Manneville and Hall, 2001, Gomes et al., 2005). Localisation of the Par6 protein and its interaction with aPKC at the leading edge of migrating cells is crucial for aPKC activation (Etienne-Manneville and Hall, 2001, Wang et al., 2003). It has been shown that such localised activation of aPKC enables appropriate cell orientation as well as polarised organisation of microtubules. Moreover, through the recruitment of Smurf1 (Smad ubiquitination regulatory factor-1), which controls RhoA degradation, Par6/aPKC complex establishes front-rear polarity inhibiting cell contraction at

the sites of actin polymerization and at the same time enabling dynamic membrane movements at the leading edge of migrating cells.
aPKC localisation and activation at the leading edge of migrating cells can be also supported by components of other two polarity complexes: Crumbs and Scribble (Shin et al., 2007, Etienne-Manneville et al., 2005). It has been shown that PATJ, a member of Crumbs complex, regulates directional migration by controlling the organisation of the microtubule network through the appropriate localisation of aPKC and Par3 to the leading edge (Shin et al., 2007). On the other hand, aPKC activation at the membrane is also required for polarisation of the microtubule network, which is stabilised by spatially localised association of Dlg, a component of Scribble complex, with the APC protein (adenomatous polyposis coli protein) (Etienne-Manneville et al., 2005). Stabilised microtubules enable appropriate orientation of the centrosome which is critical for maintaining epithelial cell polarisation and directional migration (Etienne-Manneville and Hall, 2003).

Whereas Par6 and aPKC control cell orientation through Cdc42, the third component of Par complex, Par3, through its interaction with Tiam1, is connected to Rac1 protein. It has been shown that interaction with Tiam1 enables Par3 to control tight junction assembly in polarised epithelial cells (Chen and Macara, 2005, Mertens et al., 2006), however in polarised migrating cells, Par3-Tiam1 complex regulates directionality of cell migration by microtubule stability (Pegtel et al., 2007).

1.2.3.3 Scribble complex

The Scribble complex consists of three main components: Scribble (Scrib), Discs Large (Dlg) and Lethal giant larvae (Lgl) proteins, however, the exact nature of the physical interaction between these proteins is not yet recognised. The Scribble complex in mammalian cells localises at the lateral membrane of polarised epithelia and is required for restricting the apical domain by antagonising the Par polarity complex (St Johnston and Sanson, 2011).

Scribble is a large PDZ domain-containing protein associated with the lateral membrane of epithelial cells (Dow et al., 2003, Legouis et al., 2003, Navarro et al.,

2005), however, Scribble also colocalises with ZO-1 and ZO-2 proteins at tight junctions (Ivanov et al., 2010b, Metais et al., 2005, Nguyen et al., 2005). The association of Scrib with the lateral membrane was shown to be E-cadherin-dependent (Navarro et al., 2005), however, Scrib has also been demonstrated as a regulator of adherens junction stability (Qin et al., 2005).

Another component of Scribble polarity complex, **Dlg1**, is a multi-PDZ domain-containing protein which forms a complex with MPP7 (membrane palmitoylated protein 7) and Lin-7 proteins that regulate tight junction formation and at the same time stabilises Dlg1 (Bohl et al., 2007, Stucke et al., 2007). Interaction with Lin-7 functionally links Crumbs and Scribble complexes and potentially can establish tight junctions (Straight et al., 2006). Additionally, the role of Dlg1 in cell polarity is controlled by its post-translational modifications. It has been shown that phosphorylation of Dlg1 in epithelial cells is required for adherens junction assembly (Laprise et al., 2004), while Dlg1 stability is regulated by ubiquitination (Mantovani and Banks, 2003, Mantovani et al., 2001). Interestingly, Dlg1 can be ubiquitinated upon infection with oncogenic viruses and such modification may modulate Dlg1 interactions and therefore affect downstream pathways regulating cell polarity (Mantovani et al., 2001, Tomaic et al., 2009).

Basolateral restriction of the other component of Scribble polarity complex, **Lgl1** protein, depends on its phosphorylation which is mediated by aPKC during the establishment of epithelial cell polarisation (Musch et al., 2002, Yamanaka et al., 2003). Lgl1 function in epithelial cells seems to be regulated by the Par complex (Plant et al., 2003, Yamanaka et al., 2003). Lgl1 binds to Par6 and aPKC, components of the Par complex, however this interaction exists only in the absence of Par3. Moreover, it has been demonstrated that Lgl1 is required for apical membrane disassembly, which is controlled by the inhibition of Par complex activity (Yamanaka et al., 2006). Additionally, Lgl1 has been shown to interact with molecules involved in intracellular trafficking. It has been found in the complex with syntaxin 1 in neuronal cells suggesting that it may contribute to cell polarity by regulation of polarised exocytosis (Fujita et al., 1998). In fact, Lgl1 interacts with syntaxin 4 which is specific for the lateral membrane of

polarised epithelial cells suggesting that it may regulate basolateral exocytosis (Musch et al., 2002).

Similarly to other polarity complexes, Scribble complex was found to be implicated in migration of astrocytes and mammalian epithelial cells by controlling their velocity (Dow et al., 2007, Osmani et al., 2006). Without Scrib the microtubule network does not polarise, therefore interfering with the orientation of the centrosome and Golgi. It has been shown that depletion of Scrib induces random cell movement, suggesting that it also controls cell orientation (Dow et al., 2007). Through the interaction with βPix, Scrib regulates Cdc42-mediated APC and Dlg1 recruitment to the leading edge, where they are involved in the process of polarisation of the microtubule network and thereby promoting cell orientation (Osmani et al., 2006). As mentioned above, Dlg1 is also targeted to the leading edge of migrating cells and this recruitment depends on a number of proteins including Scrib, Cdc42, Par6 and aPKC (Etienne-Manneville et al., 2005). Depletion of Dlg1 affects cell orientation, however, protrusion formation appears to be normal. Moreover, Dlg1 regulates microtubules network at the front edge of migrating cells and most likely via its interaction with APC protein is involved in the capture of microtubule plus ends at the membrane (Etienne-Manneville et al., 2005). The function of Lgl1 in polarised cell migration has not been studied in detail, however, its phosphorylation mediated by aPKC suggests that Lgl1 may control cell orientation like other two components of Scribble polarity complex.

In summary, PDZ domain-containing proteins mainly act as scaffolds assisting in the localisation of other proteins, but also as direct regulators of different cellular pathways. They represent a protein family with the multitude of protein interactions important for the establishment and maintenance of epithelial polarisation as well as polarised cell migration.

1.3 FRMPD2

1.3.1 FRMPD protein family

FRMPD2 belongs to the FERM protein superfamily characterised by the presence of a FERM (Four-point-one, ezrin, radixin, moesin) domain, which is conserved across a variety of proteins and usually located at the N-terminus of the FERM-containing molecules (Chishti et al., 1998). Most of them are directly associated with other cytoplasmic or membrane proteins as well as phosphoinositides and function as a linkage between the cytoskeleton and the plasma membrane at specific cellular locations (Chishti et al., 1998). The FERM domain-containing proteins have been initially classified into five groups based on protein sequence similarity (Takeuchi et al., 1994) and later into three groups mainly based on their biological functions (Frame et al., 2010). Among many potential smaller subgroups of the FERM protein superfamily we can also distinguish FRMPD protein family consisting of four members: FRMPD1, FRMPD2, FRMPD3 and FRMPD4. A common feature of all FRMPD proteins is possession of both FERM and PDZ domains (Figure 1.7) as well as their function as scaffolding molecules (Moleirinho et al., 2013). Interestingly, FRMPD2 is more structurally similar to its paralog, the protein tyrosine phosphatase PTPN13, than to other members of FRMPD protein family (Figure 1.8).

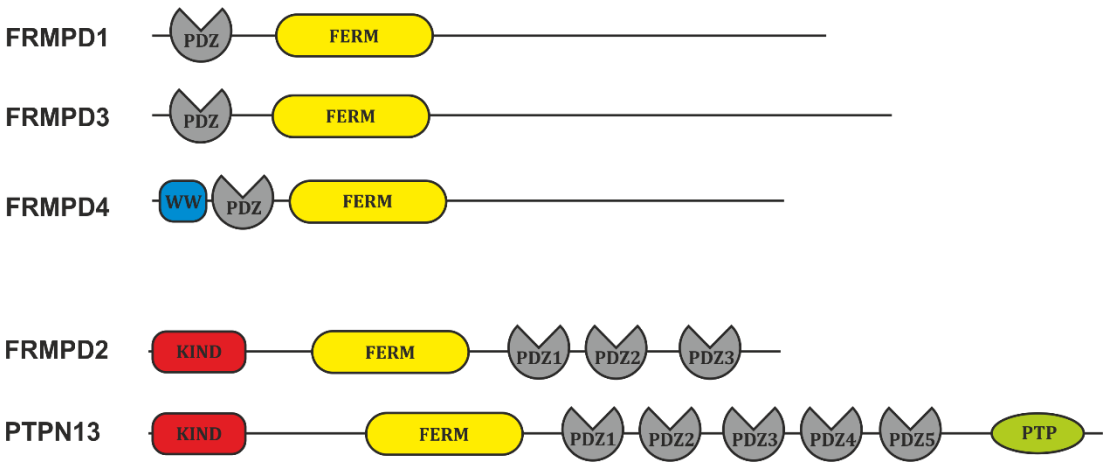

Figure 1.8 Domain organisation of FRMPD2 and related proteins in human

FRMPD2 and related proteins can be classified into two different groups according to the similarity of domain organisation. FRMPD1 and FRMPD3 consist of a PDZ (PSD95/Dlg/ZO1-homologous peptide-binding) domain and a FERM (Four-point-one, ezrin, radixin, moesin) domain. FRMPD4 contains a WW domain upstream of the PDZ and

FERM domains. FRMPD2 consists of a KIND (kinase non-catalytic C-lobe) domain, a FERM domain and three PDZ domains. PTPN13 consists of a KIND domain, a FERM domain, five PDZ domains and a PTP (protein tyrosine phosphatase) domain.

FRMPD proteins are not very well-known and apart from just a few publications reporting their basic biological functions, their importance in cellular processes is still undiscovered. It has been shown that theFRMPD1 protein interacts with AGS3 (activator of G-protein signalling 3) via its C-terminus and is responsible for AGS3 positioning at the plasma membrane (An et al., 2008). Moreover the same study shows that the membrane distribution of FRMPD1 protein depends on both the FERM and PDZ domains. Another protein, FRMPD4, is mainly expressed in the brain and interacts with the PDZ domain of the PSD-95 (postsynaptic density protein 95) protein responsible for dendritic spine morphogenesis (Lee et al., 2008). It has been shown that spine density is positively regulated by FRMPD4 and requires a contribution of its WW, PDZ and FERM domains mediating interactions with the synaptic plasma membrane, actin filaments and the Rac1 signalling pathway (Lee et al., 2008). In addition, loss of FRMPD4 activity in vivo affects synaptic plasticity and pain perception, therefore it suggest that FRMPD4 may play a very important role in neuronal functions (Hu et al., 2012). Apart from identification at the genomic level, at the moment there is no other information about FRMPD3 function. FRMPD2, as a protein of interest of the current study, was described separately in more detail in the sections below.

1.3.2 Evolutionary conservation of *frmpd2*

To date, the human *frmpd2* is the best characterised gene from a variety of species, however finding its corresponding counterpart in other organisms is important for the determination of the FRMPD2 protein conserved function as well as future perspective of an in vivo study and the right choice of a research model. To find out the evolutionary history and orthologs of *frmpd2* gene we have used the TreeFam database (Li et al., 2006, Ruan et al., 2008, Schreiber et al., 2014), which covers fully sequenced genomes of 109 species and compares results with Ensembl genome database. The results depicted in Figure 1.9 show that during genetic duplication event the *frmpd2* gene was separated from its

paralogs, *ptpn13* and *ptpn20* genes. A full version of the phylogenetic tree (available on the website: http://www.treefam.org/family/TF315388#tabview =tab1) shows that the *frmpd2* gene has orthologs in many different species, which evolved from the common ancestral gene in the speciation event. Interestingly, *frmpd2* orthologs can be found for example in chimpanzee, dog, rabbit, rat, zebrafish or *C. elegans*, however none of the genes in *Drosophila melanogaster* were indicated in this analysis.

(SI:DKEY-191M6.5 gene corresponds to zebrafish *frmpd2* gene, however for some reason TreeFam refers to its older annotation in Ensembl database, therefore the protein domain information is also not updated; the protein domain structure of zebrafish *frmpd2* should be similar to human *frmpd2*).

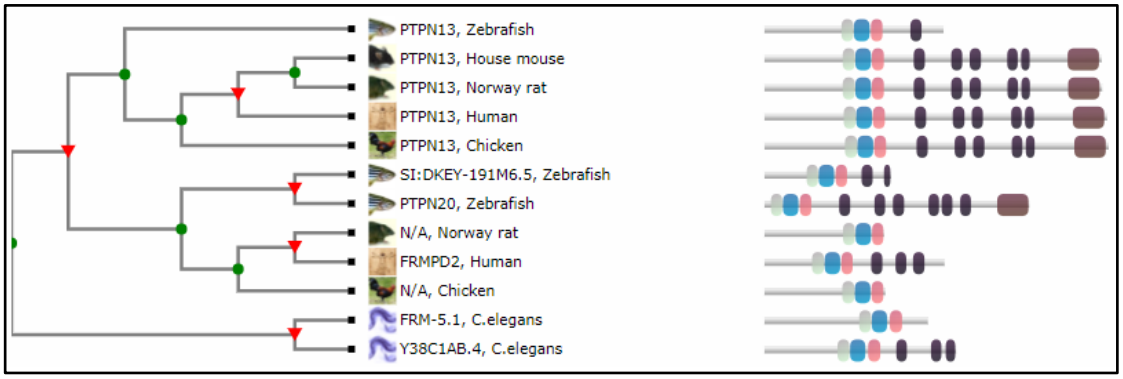

Figure 1.9 frmpd2 phylogenetic tree

The pruned gene tree for TreeFam family TF315388 (FRMPD2) presenting model species only. Gene tree demonstrates Pfam protein domain information as well; legend: grey: FERM N domain, blue: FERM M domain, pink: FERM C domain, black: PDZ domain, brown: phosphatase domain. Data presented in this thesis were obtained from the TreeFam database (http://www.treefam.org/family/TF315388#tabview=tab1) on 05.09.2017.

1.3.3 FRMPD2 expression

According to published data, FRMPD2 is expressed in many cell lines of epithelial origin and is therefore considered as a key component of a complex regulating establishment and maintenance of polarised epithelial cells (Stenzel et al., 2009, Lipinski et al., 2012). Apart from these two publications, our knowledge about FRMPD2 protein expression is limited. However, analysis of global RNA expression in the Genotype-Tissue Expression (GTEx) Project demonstrates that the highest tissue-specific *frmpd2* gene expression occurs in testis, brain, heart, prostate, thyroid, lungs, bladder and kidney (Figure 1.10). Another independent

study, performed in much smaller scale using quantitative transcriptomics analysis (RNA-Seq) (Fagerberg et al., 2014), also confirmed that *frmpd2* was found in the above-mentioned tissues. Taken together these data support the hypothesis that the function of the FRMPD2 protein may be related to cell polarisation.

Figure 1.10 frmpd2 gene expression in human tissues

Diagram on page 51. frmpd2 gene expression from 53 human tissues by analysing global RNA expression. Expression values are shown in RPKM (Reads Per Kilobase of transcript per Million mapped reads) calculated from a gene model with isoforms collapsed to a single gene. Box plots are shown as median and 25th and 75th percentiles; points are displayed as outliers if they are above or below 1.5 times the interquartile range. Data presented in this thesis were obtained from the Genotype-Tissue Expression (GTEx) Portal (https://www.gtexportal.org/) on 05.09.2017.

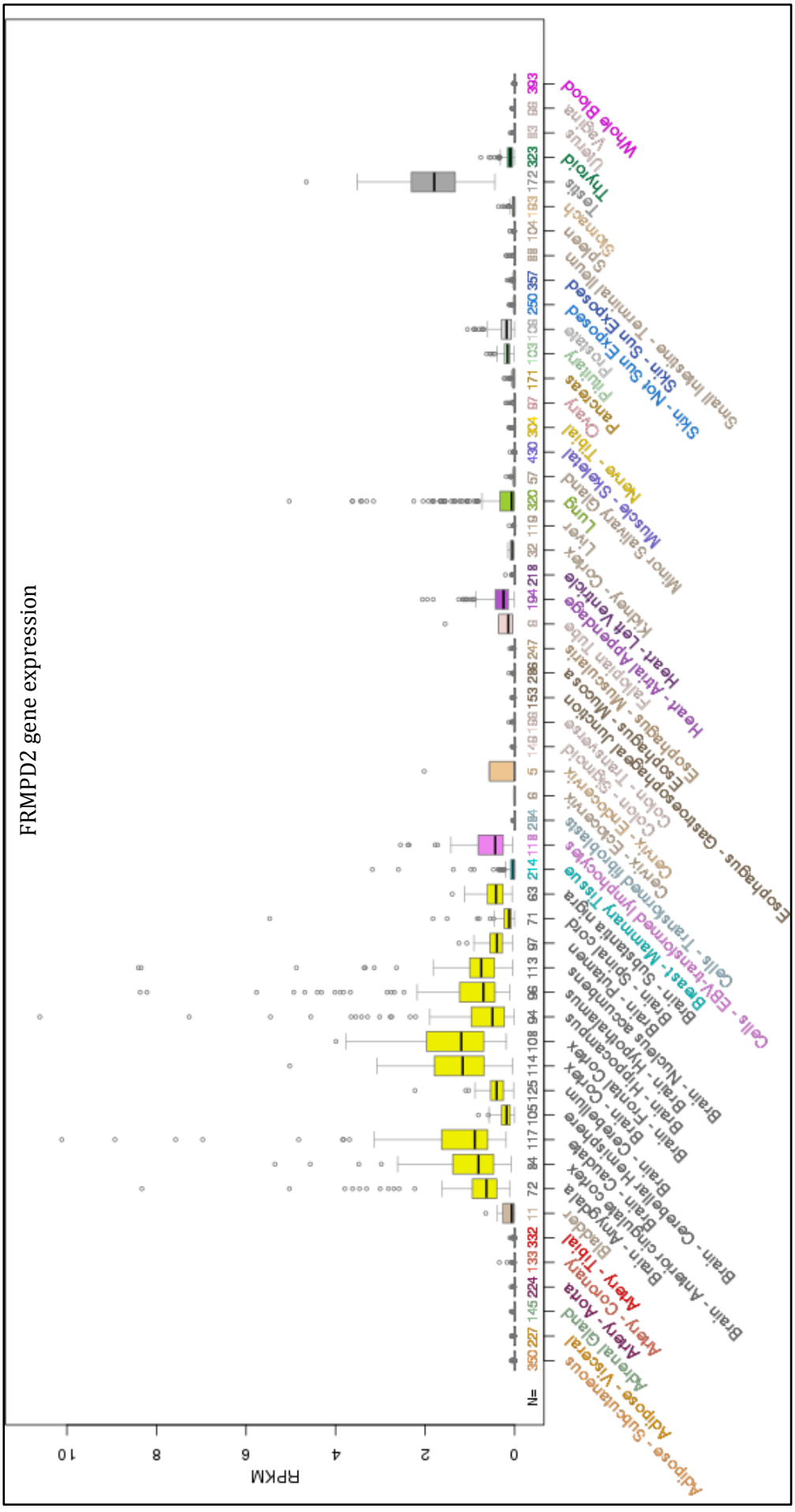
FRMPD2 gene expression
RPKM
0
2
4
6
8
10
N=
Adipose - Subcutaneous
Adipose - Visceral
Adrenal Gland
Artery - Aorta
Artery - Coronary
Artery - Tibial
Bladder
Brain - Amygdala
Brain - Anterior cingulate cortex
Brain - Caudate
Brain - Cerebellar Hemisphere
Brain - Cerebellum
Brain - Cortex
Brain - Frontal Cortex
Brain - Hippocampus
Brain - Hypothalamus
Brain - Nucleus accumbens
Brain - Putamen
Brain - Spinal cord
Brain - Substantia nigra
Breast - Mammary Tissue
Cells - EBV-transformed lymphocytes
Cells - Transformed fibroblasts
Cervix - Ectocervix
Cervix - Endocervix
Colon - Sigmoid
Colon - Transverse
Esophagus - Gastroesophageal Junction
Esophagus - Mucosa
Esophagus - Muscularis
Fallopian Tube
Heart - Atrial Appendage
Heart - Left Ventricle
Kidney - Cortex
Liver
Lung
Minor Salivary Gland
Muscle - Skeletal
Nerve - Tibial
Ovary
Pancreas
Pituitary
Prostate
Skin - Not Sun Exposed
Skin - Sun Exposed
Small Intestine - Terminal Ileum
Spleen
Stomach
Testis
Thyroid
Uterus
Vagina
Whole Blood

1.3.4 FRMPD2 function

FRMPD2 (FERM and PDZ domain containing 2) is a highly modular multi-PDZ domain protein composed of an N-terminal KIND (kinase non-catalytic C-lobe) domain, followed by a FERM (Four-point-one, ezrin, radixin, moesin) domain and three PDZ domains (Figure 1.7). The first study about FRMPD2 defined this molecule as a peripheral membrane protein and demonstrated its specific basolateral localisation in polarised epithelial cells (Stenzel et al., 2009). A large fraction of FRMPD2 was found to colocalize with adherens junctions, but partial colocalization was also observed with ZO-1, indicating localisation of FRMPD2 at tight junctions (Stenzel et al., 2009). It has been shown that depletion of FRMPD2 leads to impairment of tight junction formation and to loss of epithelial cell polarisation (Stenzel et al., 2009). Furthermore, basolateral restriction of FRMPD2 requires the FERM domain together with the PDZ2 domain, but this membrane targeting is also mediated by PtdIns(3,4)P_2, which binds to the FERM domain of the protein (Stenzel et al., 2009). FRMPD2 localizes to cell-cell contacts in an E-cadherin-dependent manner, what was further supported by the fact that FRMPD2 interacts with p0071, ARVCF and δ-catenin – members of the catenin family (Stenzel et al., 2009). FRMPD2 was demonstrated as a protein which potentially acts as a scaffold, assembling components of signalling mechanisms relevant to epithelial cell polarisation, however, its role in establishment and maintenance of epithelial integrity still requires further investigation.

In a recent study, FRMPD2 was presented as a positive modulator of NOD2-dependent activation of NF-κB signalling in intestinal epithelial cells (Lipinski et al., 2012). It has been shown that upon muramyl dipeptide (MDP) stimulation FRMPD2 interacts with and recruits NOD2 from the cytosol to the basolateral membrane of epithelial cells and that interaction is further enhanced by the presence of ERBB2IP protein. Subsequent recruitment of RIPK2 adaptor protein to the already formed complex leads to activation of innate immune responses (Lipinski et al., 2012). The most striking result, presented in this study, demonstrated that genetic variant of NOD2 (L1007fsinsC), associated with Crohn's disease (Ogura et al., 2001a), does not bind to FRMPD2, therefore its spatial restriction to the membrane is abolished. As a consequence, other components of NOD2 signalling complex are not recruited as well and fail to

activate NF-κB-mediated immune responses (Figure 1.11). Lipinski et. al. (Lipinski et al., 2012) demonstrated that FRMPD2 acts as a scaffold protein which spatially assembles and recruits signalling complexes to the membrane, but more interestingly it can modulate immune responses, which are disturbed in inflammatory bowel disease.

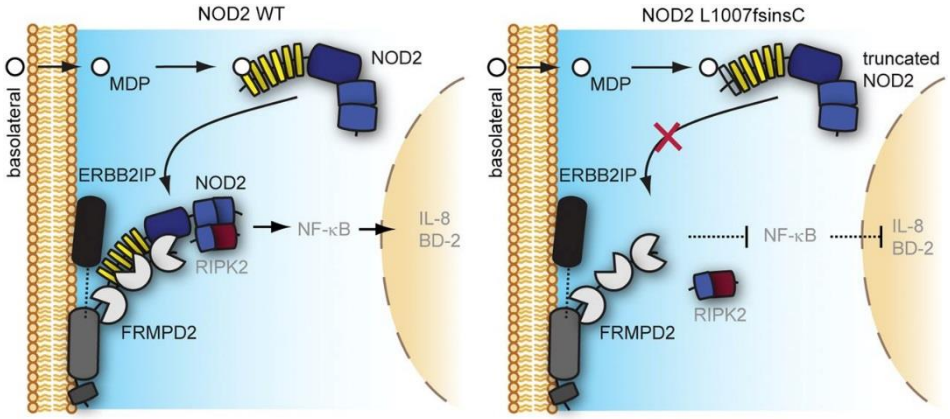

Figure 1.11 Model of basolateral translocation of NOD2 via interaction with FRMPD2.

The frameshift mutation L1007fsinsC, strongly associated with Crohn's disease, leads to a truncated NOD2 variant, which is unable to be recruited by FRMPD2 (Lipinski et al., 2012).

1.4 Advantages and perspectives of zebrafish use as a model organism in the current study

1.4.1 Zebrafish as a research model

Danio rerio, also called zebrafish, is a vertebrate tropical water fish that has become an appreciated animal model to study embryogenesis and pathology of human diseases. Fully sequenced genome and significant homology with the human genome suggest that many genes associated with human disorders could have a conserved function in zebrafish (Howe et al., 2013). Usage of zebrafish in the current studies became an appealing model for researchers due to many advantages. Zebrafish is a highly fecund organism, producing more than 100 embryos per clutch, that develop very rapidly and are ready to use for larval experiments already within 72 hours post fertilisation (hpf). Zebrafish embryos develop externally, outside the mother's body, and their high transparency allows to follow early developmental changes and organogenesis (Kimmel et al., 1995). This, in turn, facilitates genetic manipulations, which in conjunction with high-

resolution fluorescent technology enables tracking of signalling molecules or even whole cellular entities of living zebrafish embryos or larvae and follow changes in the biological processes utilising time-lapse imaging. In comparison to other vertebrates, zebrafish is easy to maintain and due to the low cost, it is conceivable to keep a large amount of fish at a sensible cost. Moreover, last decades resulted in the massive development of genetic manipulation techniques, including forward (e.g. ENU mutagenesis, transgenic) and reverse (e.g. morpholino-knockdown, TALEN, CRISPR) approaches, which enable to manipulate and recognise zebrafish gene functions.

1.4.2 NOD2 signalling in Crohn's disease

Inflammatory bowel disease (IBD), including Crohn's disease (CD) and ulcerative colitis (UC), is characterised by chronic relapsing intestinal inflammation, which has been explained as an effect of environmental factors (Loftus, 2004). A genetic study has revealed that genes associated with inflammatory bowel disease regulate innate immune responses, mucosal barrier function and bacterial killing, however, the precise mechanisms of the disease still remain elusive. The first identified and the most well-defined gene was the CARD15 gene encoding NOD2 (nucleotide-binding oligomerization domain 2) protein, which is involved in the innate immune responses triggered by bacterial infections. NOD2 is localised in the cytosol and is broadly expressed in the intestinal epithelial cells including Paneth cells, dendritic cells and myelomonocytic cells (monocytes/macrophages, granulocytes), where it induces pro- and anti-inflammatory cytokines, epithelial cell defences and participates in T cell activation (Ogura et al., 2001b, Gutierrez et al., 2002, Hisamatsu et al., 2003, Berrebi et al., 2003, Ogura et al., 2003, Barnich et al., 2005). Thus, in mammals NOD2 is an important part of the innate immune system of intestinal epithelia, recruited to the plasma membrane and activating NF-κB pathway (Barnich et al., 2005). A genetic study has identified NOD2 as a protein closely associated with Crohn's disease. Three major genetic variants of NOD2 have been found in patients suffering from CD: two missense mutations R702W, G908R, and a frameshift insertion mutation L1007fsinsC, which results in truncated NOD2 protein (Hugot et al., 2001, Ogura et al., 2001a). All mutations have been associated with an impaired ability to activate NF-κB signalling (Bonen

et al., 2003), however only truncated NOD2 (L1007fs variant) could not be translocated to the membrane of intestinal epithelial cells (Barnich et al., 2005). Interestingly, this NOD2 variant does not interact with FRMPD2, which is responsible for the recruitment of NOD2 to the basolateral membrane of epithelial cells and therefore provides spatial specificity to NOD2 signalling (Figure 1.8) (Lipinski et al., 2012). Hence, interaction of NOD2 with FRMPD2 places NOD2 in a larger protein complex with potential relevance for inflammatory bowel disease.

1.4.3 NOD2 signalling in zebrafish

NOD1 and NOD2 have been identified from the zebrafish genome and there is an evidence that these two genes are conserved among the species and the proteins have an identical domain structure to mammalian proteins (Laing et al., 2008) Other regulators of NOD2 signalling in mammals also have their analogues in zebrafish. It has been demonstrated that NOD1, NOD2 and genes encoding components of the NOD signalling pathway are expressed throughout the gastrointestinal system of zebrafish larvae, which suggests their potential role in gastrointestinal inflammation. Knockdown of NOD1 and NOD2 proteins resulted in less embryonic resistance to infection caused by *Salmonella enterica* (Oehlers et al., 2011) and this finding suggests that NOD proteins have conserved antibacterial roles in zebrafish, which is relevant to inflammatory bowel disease.

Among many vertebrates, zebrafish was chosen as an animal model with the future perspective to establish a model for inflammatory bowel disease based on FRMPD2 protein complex. It is expected that FRMPD2/NOD2 interaction and complex function is conserved in zebrafish, therefore it would be essential to demonstrate a conserved role of FRMPD2 in zebrafish as well.

AIMS

Epithelial cell polarisation is established and maintained by many biological processes including membrane trafficking, signalling cascades and cytoskeletal dynamics. Dysregulation of cell polarity leads to loss of tissue homoeostasis which results in human diseases such as kidney disease, inflammatory bowel disease and cancer. The contribution of PDZ domain proteins in cell polarisation is versatile and should be considered with respect to protein-protein interactions leading to the formation of large supramolecular complexes involved in signalling and construction of cytoskeleton architecture. Multi-PDZ domain protein FRMPD2 has been implicated in tight junction assembly and has been shown to act as a scaffold protein that localises NOD2 to the basolateral membrane of epithelial cells, providing spatial specificity to the NOD2-mediated immune responses. These findings became interesting due to the fact that functional defects of NOD2 were observed in Crohn's disease. FRMPD2 brought our attention as a potential scaffolding protein integrating signalling and membrane trafficking mechanism relevant to epithelial cell polarisation and inflammatory bowel disease. Potential FRMPD2 functions are highly relevant for epithelial integrity, however the precise role of FRMPD2 in establishment and maintenance of epithelial polarity remains elusive and will be investigated in the current study by:

1) identification and characterisation of the components of FRMPD2-mediated protein complex;
2) analysis of the role of FRMPD2 in cell mechanical properties;
3) analysis of FRMPD2 in vivo function in zebrafish development.

CHAPTER 2 - Materials and Methods

2.1 Materials

2.1.1 Devices

3D gyratory rocker SSM3	Stuart Equipments
Analogue tube rollers SRT6	Stuart Equipments
Avanti J-26 XP	Beckmann Coulter
Blue LED Illuminator	Nippon Genetics Europe
CFX96 Touch™ Real-Time PCR Detection System	Bio-Rad Laboratories
Class II Biological Safety Cabinet	ESCO
Confocal microscope A1	Nikon
Dry block heating system QBD2	Grant Instruments
Entris® Analytical Balance	Sartorius
Galaxy 170S CO_2 Incubator	New Brunswick Scientific
Gel Doc™ EZ System	Bio-Rad Laboratories
iMark™ Microplate Absorbance Reader	Bio-Rad Laboratories
Incubator (Heratherm)	Thermo Fisher Scientific
Innova® 44 incubator shaker series	New Brunswick Scientific
Jenway 3510 Bench pH/mV meter	JENWAY
Mini-PROTEAN Tetra Cell	Bio-Rad Laboratories
Mini Trans-Blot electrophoretic transfer cell	Bio-Rad Laboratories
neoLab-Rotator with Vortex RM-2M	neoLab
Neubauer-improved counting chamber	Labor Optik
Odyssey Sa® Infrared Imaging System	LI-COR
PerfectBlue™ Gel System Mini M	Peqlab

PerfectSpin mini	Peqlab
PerfectSpin 24 Plus	Peqlab
PeqMIXplus	Peqlab
peqSTAR Dual 48-Well PCR Thermal Cycler	Peqlab
peqTWIST vortex mixer	Peqlab
PGW 753M Precision Balance	Adam Equipment Ltd
Sigma 1-14K Refrigerated Microfuge	SIGMA
Soniprep 150	MSE
Spinning disc confocal Perkin Elmer Ultraview VoX spinning inverted Olympus IX81	Perkin Elmer
Nikon SMZ1500 stereomicroscope	Nikon

2.1.2 Consumables and kits

Amersham Hyperfilm™ ECL	GE Healthcare Life Sciences
Amersham™ Protran™ 0.2 µm NC	GE Healthcare Life Sciences
cOmplete™, EDTA-free Protease Inhibitor Cocktail	Roche
DIG-RNA labeling mix	Roche
DNase I Amplification Grade	Thermo Fisher Scientific
DC Protein Assay	Bio-Rad Laboratories
Gel Loading Dye Purple (6X)	New England BioLabs
GeneJET Gel Extraction Kit	Thermo Fisher Scientific
GeneJET Plasmid Miniprep Kit	Thermo Fisher Scientific
GFP-Trap®_A	ChromoTek
Hard-Shell® PCR plates 96-well, thin-wall	Bio-Rad Laboratories
Lipofectamine® 2000 Transfection Reagent	Thermo Fisher Scientific

Myc-Trap®_A	ChromoTek
NucleoBond® Xtra Midi	Macherey-Nagel
PageRuler™ Prestained Protein Ladder	Thermo Fisher Scientific
Pierce® ECL Western Blotting Substrate	Thermo Fisher Scientific
Pierce™ NeutrAvidin™ Agarose	Thermo Fisher Scientific
Pronase	Sigma-Aldrich
Protein A-agarose saline suspension	Sigma-Aldrich
Proteinase K	Roche
Protino® Glutathione Agarose 4B	Macherey-Nagel
Quick-Load Purple 2-Log DNA Ladder	New England BioLabs
RNA Loading Dye (2X)	New England BioLabs
RNase-free DNase I	Promega
RNeasy® Mini Kit	Qiagen
Sheep serum	Sigma-Aldrich
SigmaSpin™ Sequencing Reaction Clean-Up	Sigma-Aldrich
Slyde-A-Lyzer™ dialysis cassette, 20 000 MWCO	Thermo Fisher Scientific
StarSeal SealingTape Polyolefin Film	STARLAB International GmbH
SuperScript™ II Reverse Transcriptase	Invitrogen
Supersignal® West Femto Maximum Sensitivity Substrate	Thermo Fisher Scientific
SYBR® Safe DNA Gel Stain	Thermo Fisher Scientific
T7/T3 RNA polymerase	Promega
Takyon™ No Rox SYBR® MasterMix dTTP Blue	Eurogentec
ThinCerts™ Inserts, 24-well, 8.0 µm, TC treated, sterile	Greiner Bio-one Int

VECTASHIELD® HardSet Antifade Mounting Medium with DAPI	Vector Laboratories
Whatman™ chromatography paper, 3 mm	GE Healthcare Life Sciences

2.1.3 Chemicals

All chemicals used in this thesis were purchased from reputable suppliers like Sigma-Aldrich, Thermo Fisher Scientific, Roche and Roth.

2.1.4 Antibodies

All antibodies were used according to the manufacturer's instructions or dilution and incubation conditions were optimised if required.

2.1.4.1 Primary antibodies

Antibody	Host	Application	Supplier
anti-BANK1	*rabbit*	WB (1:100)	Santa Cruz Biotechnology (sc-133359)
anti-c-myc 9E10	*mouse*	WB (1:2000) IF (1:150)	Gentaur (04-CMYC-9E10)
anti-c-myc (A14)	*rabbit*	WB (1:1000) IF (1:40)	Santa Cruz Biotechnology (sc-789)
anti-β-catenin	*mouse*	WB (1:1000) IF (1:250)	BD biosciences (610153)
anti-Digoxigenin-AP Fab fragments	*sheep*	in situ hybridization	Roche (11093274910)
anti-E-cadherin	*mouse*	WB (1:500) IF (1:100)	BD Biosciences (610181)
anti-FRMPD2(1)	*rabbit*	WB (1:500)	Sigma-Aldrich (HPA018872)
anti-FRMPD2(2)	*goat*	WB (1:100)	Santa Cruz Biotechnology (sc-138284)
anti-FRMPD2(3)	*rabbit*	WB (1:2000)	Eurogentec, custom made

anti-FRMPD2(4)/(5) (150aa, C-terminus)	*rabbit*	WB (1:500)	Eurogentec, custom made
anti-FRMPD2(6)/(7) (like HPA018872)	*rabbit*	WB (1:500)	Eurogentec, custom made
anti-FRMPD2(8)/(9) (150aa, C-terminus)	*rabbit*	WB (1:500)	Biogenes, custom made
anti-GFP	*rabbit*	WB (1:2000)	Gift from Andrew Peden
anti-Myosin IIa	*rabbit*	WB (1:1000)	Sigma-Aldrich (M8064)
anti-PRK2	*mouse*	WB (1:500)	Thermo Scientific (MA5-15887)
anti-phospho-PRK2	*rabbit*	WB (1:1000)	Cell Signaling (#2611)
anti-Plectin-1	*rabbit*	WB (1:1000)	Cell Signaling(#2863)
anti- β-tubulin	*mouse*	IF (1:500)	Sigma-Aldrich (T4026)
anti-ZO-1	*rabbit*	WB (1:500) IF (1:100)	Invitrogen (61-7300)

* WB – Western Blot, IF – Immunofluorescence

Table 2.1 Primary antibodies

2.1.4.2 Secondary antibodies

Antibody	Application	Supplier
goat anti-mouse IgG (H + L) HRP	WB (1:5000)	Life Technologies™ (G-21040)
goat anti-rabbit IgG (H + L) HRP	WB (1:5000)	Life Technologies™ (G-21234)
donkey anti-goat IgG (H + L) HRP	WB (1:5000)	Santa Cruz Biotechnology (sc-2020)
Pierce® High Sensitivity Streptavidin-HRP	WB (1:5000)	Thermo Scientific (21134)
DyLight™ 800 4X PEG conjugate anti-mouse IgG (H + L)	WB (1:10 000)	Thermo Scientific (SA5-35521)

donkey anti-rabbit IgG (H+L) Alexa Fluor® 350 (a gift from Dr Jason King)	IF (1:500)	Thermo Scientific (A-11046)
donkey anti-rabbit IgG (H+L) Alexa Fluor® 488	IF (1:500)	Thermo Scientific (A-11034)
donkey anti-mouse IgG (H+L) Alexa Fluor® 488	IF (1:500)	Thermo Scientific (A-11001)
donkey anti-rabbit IgG (H+L) Alexa Fluor® 568	IF (1:500)	Thermo Scientific (A-11011)
donkey anti-mouse IgG (H+L) Alexa Fluor® 568	IF (1:500)	Thermo Scientific (A-11004)
donkey anti-rabbit IgG (H+L) Alexa Fluor® 594	IF (1:500)	Thermo Scientific (A-11012)
donkey anti-mouse IgG (H+L) Alexa Fluor® 594	IF (1:500)	Thermo Scientific (A-11005)
donkey anti-rabbit IgG (H+L) Alexa Fluor® 647	IF (1:500)	Thermo Scientific (A-21245)
donkey anti-mouse IgG (H+L) Alexa Fluor® 647	IF (1:500)	Thermo Scientific (A-21235)
donkey anti-rabbit IgG (H+L) Alexa Fluor® 680	WB (1:5000)	Thermo Scientific (A-21109)
Streptavidin Alexa Fluor® 594 conjugate (gift from Dr Jason King)	IF (1:1000)	Thermo Scientific (S11227)
Streptavidin Alexa Fluor® 680 conjugate (gift from Dr Jason King)	WB (1:10 000)	Thermo Scientific (S21378)

* WB – Western Blot, IF – Immunofluorescence

Table 2.2 Secondary antibodies

2.1.5 Primers

All primers used for sequencing, cloning, mutagenesis were designed by myself. Primers for qPCR were designed using Primer-Blast available on the website: https://www.ncbi.nlm.nih.gov/ tools/primer-blast/. All primers were purchased from Sigma-Aldrich.

CLONING

No	Primer name	Sequence	Length [bp]	T_m [°C]
1	FLNB_fwd_BamHI	AAAAA**GGATCC**CGCGGCCTGTCA GAAGGCCGG	32	86.0

2	FLNB_rev_XhoI	AAAAA**CTCGAG**TTAGTTACCAGG CTCTTGGGC	32	73.8
3	RAPGEF2_fwd_NotI	TATAA**GCGGCCGC**TAAACCACTA GCAATCCCAGCTAACC	39	80.5
4	RAPGEF2_rev_XbaI	CAGCG**TCTAGA**TTAAACAGCAGA AACTTGTTCATCTTC	38	74.0
5	hFRMPD2_fwd_NotI	ATA**GCGGCCGC**CACAGCCTTTAA CGAAGGACG	32	82.9
6	hFRMPD2_rev_BamHI	AGGAC**GGATCC**TCAGAAAATATC TGTCGAAAG	32	73.4
7	PRK2_fwd_BamHI	TATTAT**GGATCC**GCGTCCAACCC CGAACGG	30	81.7
8	PRK2_rev_DEL_EcoRI	CGGC**GAATTC**TTAAGCAATGTAG TCAAAATC	31	71.8
9	PRK2_rev_C/S_EcoRI	CGGC**GAATTC**TTAAGACCAATCA GCAATGTAG	32	74.6
10	hFRMPD2_fwd_BamHI_trun	GATCA**GGATCC**CAGCCTTTAACG AAGGACGCAG	33	80.1
11	hFRMPD2_rev_EcoRI_trun	CGCGC**GAATTC**TTAGACTATGAC ACCCTTGGC	32	78.8
12	zFRMPD2_fwd_EcoRI	AGCTC**GAATTC**CATTGAATGCAG CACCAGCAA	32	80.7
13	zFRMPD2_rev_XhoI	ATATT**CTCGAG**CTCGTAGCTGCG CTCGTTCAG	32	77.8
14	zFRMPD2_fwd_BamHI	GACT**GGATCC**GTTTGGACACAGA AAGGGAAC	31	77.1
15	zFRMPD2_rev_EcoRI	CAGC**GAATTC**GTGCGGCAGTTAT TAATAAC	30	73.2
16	zPTPN13_fwd_EcoRI	CACGC**GAATTC**TTCCTGACGGTC ACTACACG	31	79.3
17	zPTPN13_rev_XhoI	TAGAT**CTCGAG**ATCTGCGTCTTT GCTGATTAG	32	79.1

* sequences of restriction sites in bold and underlined

Table 2.3 Primers used for molecular cloning

MUTAGENESIS

No	Primer name	Sequence	Length [bp]	T_m [°C]
1	FR_PDZ3_fwd_K/E_1084	GTTTGAAGTCAAACTAAAAGAGAA TGCCAATGGTTTGGG	39	77.1
2	FR_PDZ3_rev_K/E_1084	CCCAAACCATTGGCATTCTCTTTTA GTTTGACTTCAAAC	39	77.1

Table 2.4 Primers used for site-directed mutagenesis

SEQUENCING

No	Primer name	Sequence	Length [bp]	T_m [°C]
1	GFP	GTCCGCCCTGAGCAAAGACCC	21	73.1
2	GST	GTACTTGAAATCCAGCAAG	19	54.8
2	BGH reverse	TAGAAGGCACAGTCGAGG	provided*	
3	T7 forward	TAATACGACTCACTATAGGG	provided*	
4	RAPGEF2_fwd_seq1	CTTTCTGTTGACCTATAGGAC	21	54.5
5	RAPGEF2_fwd_seq2	TGTCAGTGGAACCTTATCATCC	22	62.7
6	RAPGEF2_fwd_seq3	CAATAGTCAAAATCTACAACC	21	52.9
7	RAPGEF_fwd_seq4	ACGTCACAAGAAACAGGCTGAAG	23	66.5
8	BioID_fwd_1801	CTCCAGAGGAATCGACAAGC	20	63.9
9	FRMPD2__seq1	CGGGCAGCACCTGGAGGTAAAATG	24	74.5
10	FRMPD2__seq2	CTTAGAGAGAAGAGTCCCCAGG	22	62.2
11	PRK2_seq880	GAAGAACTTTCACTTGTTG	19	52.0
12	PRK2_seq1876	CCTGATACTCCTCAGTCAGG	20	58.9

*provided – primers were provided by Core Genomic Facility of University of Sheffield

Table 2.5 Primers used for sequencing

qPCR

No	Primer name	Sequence	Length [bp]	T_m [°C]
1	RT_hFRMPD2_fwd1	CAGTGACAGATGGTCCTAAGTTTG	24	63.6
2	RT_hFRMPD2_rev1	CCTCTCAGTAAATGCAGCACCT	22	64.4
3	RT_hFRMPD2_fwd2	CAGTCAAAAGGTGTTGGTGGAAAT	24	66.8
4	RT_hFRMPD2_rev2	GAGGACAAGAAGAACCAGCACC	22	66.1

5	RT_hFRMPD2_fwd3	CCGTTAAAGGGTGCTGGTTC	20	65.4
6	RT_hFRMPD2_rev3	ACACTGAATCCAAGTGTCCCA	21	64.4
7	RT_hFRMPD2_fwd4	CAGGAAGTCACGCTCCTCCTTT	22	67.8
8	RT_hFRMPD2_rev4	TACATGTTGCCCTGGTGAATTCTT	24	67.2
9	RT_hFRMPD2_fwd5	GTTGTCCCATGATGAAGGCC	20	66.6
10	RT_hFRMPD2_rev5	GAATCGTTGCGGAGGTCTTC	20	65.9
11	RT_hFRMPD2_fwd6	AGTGGAGAGAAACCGGGAAG	20	64.4
12	RT_hFRMPD2_rev6	TGTGCAGGACTCAAATTGGC	20	66.2
13	RT_hFRMPD2_fwd7	ACTTCAACGTGGACGGCAGCAA	22	72.9
14	RT_FRMPD2_rev7	GGTCATTGGCTTCTGGATCACAC	23	68.8
15	PrimePCR™ Assay	Bio-Rad, Cat. #10025636	-	-
16	RT_hFR_fwd8	TCAGTTTCGTGCAGATGGAG	20	64.1
17	RT_hFR_rev8	CAGTACATGTTGCCCTGGTG	20	64.1
18	RT_hFR_fwd9	ATCTTGTGAGGATTAAGAGGCTC	23	61.5
19	RT_hFR_rev9	GCCCCTCTCAGTAAATGCAG	20	63.7
20	GAPDH_fwd	GGTGAAGGTCGGAGTCAACG	20	67.0
21	GAPDH_rev	ATCTCGCTCCTGGAAGATGG	20	65.6
22	GAPDH_fwd_116bp	TCGCTCTCTGCTCCTCCTGTTC	22	69.3
23	GAPDH_rev_116bp	CGACCAAATCCGTTGACTCCGACC	24	74.9
24	RT_MDCK_FRMPD2_fwd	GCTCCACTTACTTCGAGGGG	20	64.9
25	RT_MDCK_FRMPD2_rev	AGCACAGGTGTATCGCATCT	20	62.4
26	RT_MDCK_GAPDH_fwd	AGATTGTCAGCAATGCCTCCTG	22	67.5
27	RT_MDCK_GAPDH_rev	GGTCTTCTGGGTGGCAGTGA	20	67.7
28	RT_zFRMPD2_fwd1	ATCATTTCACAGCCCAAAGCTCA	23	68.7
29	RT_zFRMPD2_rev1	AGAGACGCTGATCTGGAATAATCA	24	64.9
30	RT_zFRMPD2_fwd2	GATGATTATTCCAGATCAGCGTCT	24	64.2
31	RT_zFRMPD2_rev2	CTTCCAACAGTCTGTCTCCTGTC	23	64.1
32	RT_bACTIN_fwd	TTCACCACCACAGCCGAAAGA	21	70.0
33	RT_bACTIN_rev	TACCGCAAGATTCCATACCCA	21	66.1

Table 2.6 Primers used for qPCR

GENOTYPING

No	Primer name	Sequence	Length [bp]	T_m [°C]
1	Tubby_fwd	CGAGCTCTACTGGAACAGAAGCAGAAGA	28	61.1

2	Tubby_rev	GTTGTATTTGAACTGTAGTTTGTACCGTGG	30	57.8
3	zFR_4_fwd	CCCGAGAGAAGAAGCCTGTG	20	66.3
4	zFR_5_fwd	TATGGTGTGCTGTTTCACCG	20	64.6
5	zFR_9_rev	AGTTGAGGTGATGCTGCTCG	20	65.6

Table 2.7 Primers used for zebrafish genotyping

2.1.6 siRNAs

No	siRNA name [name in the thesis]	Sequence or Catalogue number	Company
1	siRNA control **[siCTRL]**	AllStar Negative Control siRNA #1027280	Qiagen
2	siGenome Human PKN2 **[PRK2 duplex 1]**	PRK2 duplex 1, #D-004612-03 GACAGAAGAUCUCAGCAAA	Dharmacon
3	siGenome Human FRMPD2 **[siFRMPD2]**	siGENOME SMARTpool siRNA FRMPD2, #D-008854-01	Dharmacon
4	PKN2 duplex 1 **[siPRK2_1]**	custom made, canine PKN2 GCAAAGAAGGAAUGGGAUA	Dharmacon
5	PKN2 duplex 2 **[siPRK2_2]**	custom made, canine PKN2 CCUUGGAGCUGGUGAGAAA	Dharmacon
6	FRMPD2 duplex 1 **[siFRMPD2_1]**	custom made, canine FRMPD2 GAUCAAGAAUAUAGCCAAA	Dharmacon
7	FRMPD2 duplex 2 **[siFRMPD2_2]**	custom made, canine FRMPD2 GGACCAAGACCUAGAGAGA	Dharmacon

Table 2.8 siRNAs used in this study

2.1.7 Plasmids DNA

All DNA constructs used in this study were verified by sequence analysis performed with appropriate primers listed in Table 2.5 at University of Sheffield Core Genomic Facility.

Plasmid name	Description and source
pcDNA3-myc	pcDNA3 with myc tag from the library of Dr Erdmann lab

pcDNA3-GFP	pcDNA3 with GFP tag from the library of Dr Erdmann lab
pEGFP-C1	vector with GFP tag from the library of Dr Erdmann lab
pcDNA3-myc-BANK1	myc-tagged human BANK1 from the library of Dr Erdmann lab
pcDNA3-GFP-BANK1	GFP-tagged human BANK1 from the library of Dr Erdmann lab
pcDNA3-myc-SEPTIN-10	myc-tagged human SEPTIN-10 from the library of Dr Erdmann lab
pcDNA3-GFP-SEPTIN-10	GFP-tagged human SEPTIN-10 from the library of Dr Erdmann lab
pcDNA3-myc-FRMPD2	myc-tagged human FRMPD2 from the library of Dr Erdmann lab
pcDNA3-GFP-FRMPD2	GFP-tagged human FRMPD2 from the library of Dr Erdmann lab
pEGFP-C1-KIND	GFP-tagged KIND domain of human FRMPD2 from the library of Dr Erdmann lab
pEGFP-C1-FERM	GFP-tagged FERM domain of human FRMPD2 from the library of Dr Erdmann lab
pEGFP-C1-PDZ1-3	GFP-tagged PDZ1-3 domains of human FRMPD2 from the library of Dr Erdmann lab
pEGFP-C1-FERM+PDZ1	GFP-tagged FERM and PDZ1 domains of human FRMPD2 from the library of Dr Erdmann lab
pEGFP-C1-FERM+PDZ2	GFP-tagged FERM and PDZ2 domains of human FRMPD2 from the library of Dr Erdmann lab
pEGFP-C1-FERM+PDZ3	GFP-tagged FERM and PDZ3 domains of human FRMPD2 from the library of Dr Erdmann lab
pACT2-FILAMIN B	pACT2 vector with the fragment of human FILAMIN B corresponding to 2041-2290aa from the library of Dr Erdmann lab
pcDNA3-myc-FILAMIN $B_{2041-2290}$	myc-tagged fragment of human Filamin B (2041-2290aa) made by PCR using pACT2-FILAMIN B as a template and primers 1 and 2 (Table 2.3) BamHI/XhoI fragment was cloned into BamHI/XhoI pcDNA3-myc
pcDNA3-GFP-FILAMIN $B_{2041-2290}$	GFP-tagged fragment of human FILAMIN B (2041-2290aa) made by PCR using pACT2-FILAMIN B as a template and primers 1 and 2 (Table 2.3) BamHI/XhoI fragment was cloned into BamHI/XhoI pcDNA3-GFP

R777-E225 Hs.RAPGEF2	pDonor-255 vector with human RAPGEF2 was a gift from Dominic Esposito (Addgene plasmid #70509)
pcDNA3-myc-RAPGEF2	myc-tagged RAPGEF2 made by PCR using R777-225 Hs.RAPGEF2 as a template and primers 3 and 4 (Table 2.3) NotI/XbaI fragment was cloned into NotI/XbaI pcDNA3-myc
pcDNA3-GFP-RAPGEF2	GFP-tagged RAPGEF2 made by PCR using R777-225 Hs.RAPGEF2 as a template and primers 3 and 4 (Table 2.3) NotI/XbaI fragment was cloned into NotI/XbaI pcDNA3-GFP
pcDNA3.1-mycBioID	pcDNA3.1 vector with BirA* tag was a gift from Kyle Roux (Addgene plasmid #35700)
myc-BirA*-FRMPD2	myc-BirA*-tagged FRMPD2 made by PCR using pcDNA3-GFP-FRMPD2 as a template and primers 5 and 6 (Table 2.3) NotI/BamHI fragment was cloned into NotI/BamHI pcDNA3.1-mycBioID
pcDNA3-myc-PRK2	myc-tagged human PRK2 from the library of Dr Erdmann lab
pcDNA3-myc-PRK2 K686R	myc-tagged human PRK2 with the mutation K686R from the library of Dr Erdmann lab
pcDNA3-myc-PRK2 DEL	myc-tagged human PRK2 with the deletion of last three amino acids made by PCR using pcDNA3-myc-PRK2 as a template and primers 7 and 8 (Table 2.3) BamHI/EcoRI fragment was cloned into BamHI/EcoRI pcDNA3-myc
pcDNA3-myc-PRK2 C/S	myc-tagged human PRK2 with the mutation of last amino acid made by PCR using pcDNA3-myc-PRK2 as a template and primers 7 and 9 (Table 2.3) BamHI/EcoRI fragment was cloned into BamHI/EcoRI pcDNA3-myc
pcDNA3-GFP-FRMPD2 K/E	GFP-tagged human FRMPD2 with the mutation K1084E made by site-directed mutagenesis using pcDNA3-GFP-FRMPD2 as a template and primers 1 and 2 (Table 2.4)
pEGFP-C1-PDZ1-3 K/E	GFP-tagged PDZ1-3 domains of human FRMPD2 with the mutation K1084E made by site-directed mutagenesis using pEGFP-C1-PDZ1-3 as a template and primers 1 and 2 (Table 2.4)

pEGFP-C1-FERM+PDZ3 K/E	GFP-tagged FERM and PDZ3 domains of human FRMPD2 with the mutation K1084E made by site-directed mutagenesis using pEGFP-C1-FERM+PDZ3 as a template and primers 1 and 2 (Table 2.4)
pcDNA3-GFP-FRMPD2trun	GFP-tagged truncated human FRMPD2 made by PCR using pcDNA3-GFP-FRMPD2 as a template and primers 10 and 11 (Table 2.3) BamHI/EcoRI fragment was cloned into BamHI/EcoRI pcDNA3-GFP
pBSK(+)-zFRMPD2 – probe1	pBSK(+) vector with zebrafish FRMPD2 made by PCR using cDNA (RNA isolated from zebrafish embryos 120 hpf) as a template and primers 12 and 13 (Table 2.3) EcoRI/XhoI fragment was cloned into EcoRI/XhoI pBSK(+)
pBSK(+)-zFRMPD2 – probe2	pBSK(+) vector with zebrafish FRMPD2 made by PCR using cDNA (RNA isolated from zebrafish embryos 120 hpf) as a template and primers 14 and 15 (Table 2.3) BamHI/EcoRI fragment was cloned into BamHI/EcoRI pBSK(+)
pBSK(+)-zPTPN13	pBSK(+) vector with zebrafish PTPN13 made by PCR using cDNA (RNA isolated from zebrafish embryos 120 hpf) as a template and primers 16 and 17 (Table 2.3) EcoRI/XhoI fragment was cloned into EcoRI/XhoI pBSK(+)

Table 2.9 Plasmids DNA used in this study

2.1.8 shRNAs

shRNA name [name in the thesis]	**Sequence or Catalogue number**	**Company**
shRNA control **[shCTRL]**	Non-effective scrambled shRNA #TR30012	OriGene
shRNA human FRMPD2 **[shFRMPD2_1]**	#TR312922A/TI351681 AGGAATGGCAGACACCTGAACTCTCAGCT	OriGene
shRNA human FRMPD2 **[shFRMPD2_2]**	#TR312922C/TI351683 CTGTGTCTCAGTGACAGATGGTCCTAAGT	OriGene

Table 2.10 shRNA constructs used in this study

2.1.9 Mammalian cell lines

16HBE14o-	human bronchial epithelial cell line, SV40-transformed; supplier: gift from Dr. Dieter Grünert (California Pacific Medical Center, San Francisco, CA)
Caco-2	human colon colorectal adenocarcinoma epithelial cell line; supplier: ATCC
Cos-7	African green monkey kidney fibroblast-like cell line, SV40-transformed; supplier: ECACC
HEK293	Human Embryonic Kidney cell line; supplier: ECACC
HeLa	human cervical cancer cell line; supplier: ECACC
MDCKII	Madin-Darby Canine Kidney epithelial cell line; supplier: ECACC

2.1.10 Bacterial strains

E.coli Nova Blue (XL1)	bacterial strain used for plasmid DNA isolation, general cloning and subcloning applications; genotype: *recA1 endA1 gyrA96 thi-1 hsdR17 supE44 relA1 lac* [*F' proAB lacI^{q}ZΔM15 Tn10 (*Tet^I*)*] supplier: Stratagene GmbH, Heidelberg, Germany
E.coli BL21 Rosetta™ 2(DE3)	bacterial strain strain used for protein expression; genotype: F$^-$ *ompT hsdS*$_B$(r_{B^-} m_{B^-}) *gal dcm* (DE3) pRARE2 (Cam^R) supplier: Novagene, New Jersey (USA)

2.1.11 Culture media and plates

2.1.11.1 Mammalian cell lines

DMEM	DMEM (1X) + GlutaMAX™-I - Dulbecco's Modified Eagle Medium [+] 4.5 g/L D-glucose [+] Pyruvate supplier: gibco®, Life Technologies™ (31966-021)
MEM	MEM (1X) - Minimum Essential Medium [+] Earle's Salts [+] L-Glutamine

	supplier: gibco®, Life Technologies™ (11095-080)
Opti-MEM	Opti-MEM® I (1X) - Reduced Serum Medium [+] L-Glutamine [+] HEPES [-] Phenol Red supplier: gibco®, Life Technologies™ (11058-021)

2.1.11.2 Bacteria

LB	10 g/l peptone 5 g/l yeast extract 10 g/l NaCl up to 1l ddH2O
LB plates	15 g/l agar in LB medium

2.2 Methods

2.2.1 NUCLEIC ACID METHODS

2.2.1.1 PURIFICATION

2.2.1.1.1 RNA extraction and purification

Total RNA was extracted from zebrafish embryos/larvae or adult fish according to the published protocol (Peterson and Freeman, 2009). The same protocol, with some modifications, was adapted for mammalian cells. As RNA is relatively unstable, analysis of gene expression level was performed using cDNA, which was directly synthesised using RNA as a template.

INITIAL PREPARATION OF MAMMALIAN CELLS

Cells grown in the T-75 flask or 10 cm cell culture dish were washed with 1x PBS and using cell scraper cells were subsequently scraped off the bottom of the flask or dish into 1x PBS. The cell suspension was transferred to a 1.5 ml tube and cells were pelleted in microcentrifuge for 10 min at the maximum speed 15 000 rpm and RT.

TOTAL RNA EXTRACTION

Homogenisation in *TRIzol® Reagent* was prepared as follows:

a) the cell pellet was resuspended in 250 µl of *TRIzol® Reagent* and homogenised using *VWR® Disposable Pellet Mixer and Cordless Motor* until the suspension was homogenous. 750 µl of *TRIzol® Reagent* was added additionally to the tubes to equal the total volume of 1 ml;
b) 50 – 100 zebrafish embryos or early larvae were anaesthetised with Tricaine and pooled in a 1.5 ml tube. All the supernatant was removed, 250 µl of *TRIzol® Reagent* was added and embryos or early larvae were homogenised using *VWR® Disposable Pellet Mixer and Cordless* until the suspension was homogenous. 750 µl of *TRIzol® Reagent* was added additionally to the tubes to equal the total volume of 1 ml;
c) adult fish anaesthetised with Tricaine and subsequently immersed in 3 ml of *TRIzol® Reagent* was precisely crushed using mortar and pestle until all organs and tissues were sufficiently disrupted. Each 1ml of obtained suspension and non-disrupted tissues were transferred into three 5 ml tubes and further homogenised using *VWR® Disposable Pellet Mixer and Cordless Motor*.

Homogenised samples were incubated for 5 min at RT in order to ensure complete dissociation of nucleoprotein complexes. At that stage samples were frozen at -80°C or RNA extraction was conducted. 0.2 ml of chloroform was added to each sample, the tube was vortexed for 15 sec to mix the content and samples were incubated for 2 min at RT. Subsequently all samples were centrifuged for 15 min at 12 000 rpm and 4°C resulting in separation into three phases: lower red organic phase containing DNA, white interphase containing DNA and proteins, the upper colourless aqueous phase containing RNA. Without interphase disruption, the top phase containing RNA (around 0.5 – 0.6 ml) was transferred to the fresh 1.5 ml tube, where it was mixed with 0.5 ml of isopropanol to precipitate the RNA. After 10 min incubation at RT, samples were centrifuged for 10 min at 12 000 rpm and 4°C, and the supernatant was removed. White RNA pellet formed on the bottom of the tube was washed with 70% ethanol and centrifuged for 5 min at 7500 rpm and 4°C. Finally, the ethanol was removed and RNA pellet was air-dried for at least 15 min. RNA was resuspended in 100 µl of nuclease-free water, incubated for 10 min at 55°C with frequent vortexing and further purified using *Qiagen RNeasy® Mini Kit* according to the manufacturer's

instruction. Concentration and purity of RNA samples were assessed using *Thermo Scientific NanoDrop Lite Spectrophotometer* as described in section 2.2.1.2.1. Additionally, RNA integrity was checked by agarose gel electrophoresis. RNA samples were stored at -80°C until cDNA synthesis was performed.

2.2.1.1.2 DNase treatment

RNA purification was completed with DNase treatment which helped to eliminate possible gDNA contamination. Reaction was prepared in duplicates as indicated in Table 2.11 and incubated for 15 min at RT. To inactivate *DNase I*, 1 µl of 25 mM EDTA solution was added directly to the reaction mixture and incubated for 10 min at 65°C.

Reaction component	Amount
RNA sample	1 µg
10x DNase I Reaction Buffer	1 µl
DNase I, Amp Grade (1 U/ µl)	1 µl
nuclease-free water	up to 10 µl

Table 2.11 DNase treatment reaction components

2.2.1.1.3 Plasmid preparation

2.2.1.1.3.a Preparation of chemically competent E.coli

Chemically competent cells were treated with calcium chloride. Bacteria stock was thawed at RT and using inoculation loop bacteria were spread on LB agar plate without antibiotic and incubated overnight at 37°C. Subsequently, one single colony was inoculated into 2 ml of LB medium without antibiotic and incubated in the shaking incubator overnight at 220 rpm and 37°C. The next day 1 ml of the overnight culture was inoculated into 100 ml of LB medium without antibiotic and incubated again in the shaking incubator for around 2 h at 220 rpm and 37°C. Bacterial growth was controlled by measurement of OD_{600} every 1 h until the desired optical density was obtained: OD_{600} = 0.4 – 0.5, which indicated the exponential phase of bacterial growth. The culture was then chilled on ice for 30 min and centrifuged for 10 min at 3000 rpm and 4°C. The supernatant was

discarded, the bacteria pellet resuspended in ice cold sterile 40 ml of 0.1 M $CaCl_2$ and incubated on ice for 30 min. Bacteria were centrifuged again as described above, the supernatant was removed and bacteria pellet was resuspended in ice-cold sterile 6 ml of 0.1 M $CaCl_2$ containing 15% glycerol. Aliquots of 100 µl competent cells were prepared in the sterile 1.5 ml eppendorf tubes and stored at -80°C. In order to check the efficiency of freshly prepared competent cells, they were transformed with plasmid DNA.

2.2.1.1.3.b Bacterial transformation

Chemically competent XL1-Blue *E.coli* were thawed on ice for 10 min. One of the following plasmids or mixture:

a) 0.5 µl (from 1 µg/µl stock) of the desired plasmid DNA or
b) 5 ul of mutagenized plasmid or
c) 7 µl of ligation mixture

was mixed with chilled cells and incubated on ice for 15 min to allow the plasmid to come into close contact with the cells. The plasmid-cell mixture was then heated at 42°C for 45 sec to induce DNA uptake by the cell through its disrupted membrane and then immediately chilled on ice for 2 min to retain plasmid inside the bacteria. Subsequently, 900 µl of LB was added into the tube with transformed bacteria and incubated in the shaking incubator for 1 h at 220 rpm and 37°C. After incubation, the procedure was as follows (depending on the type of transformation mentioned above):

a) 100 µl from 1 ml culture of the bacteria transformed with the desired plasmid DNA were spread on LB agar plate containing appropriate antibiotic: ampicillin (100 µg/ml) or kanamycin (50 µg/ml)
b) and c) 1 ml of bacteria culture was centrifuged for 2 min at 7000 rpm and RT and 900 µl of supernatant was removed. The cell pellet was then resuspended in the remaining 100 µl of LB medium and plated on the LB agar plate containing appropriate antibiotic: ampicillin (100 µg/ml) or kanamycin (50 µg/ml).

Plates were incubated overnight at 37°C and the next day checked for the presence of bacterial colonies.

2.2.1.1.3.c Plasmid DNA isolation and purification

One single colony was picked from the LB agar plate and inoculated into 5 ml of LB medium in a sterile culture tube (for miniprep) or 100 ml of LB medium in a sterile flask (for midiprep) containing appropriate antibiotic: ampicillin (100 μg/ml) or kanamycin (50 μg/ml). The culture was incubated in a shaking incubator overnight at 220 rpm and 37°C. The next day bacteria were pelleted and plasmid DNA was isolated and purified using GeneJET Plasmid Miniprep Kit (typical yield 10-15 μg) or Nucleo Bond® Xtra Midi kit (typical yield 0,75-1,0 mg) following the manufacturer's instructions.

2.2.1.1.4 DNA precipitation

Purification and/or concentration of DNA after for example site-directed-mutagenesis reaction was performed by ethanol precipitation. Initially, DNA-containing solution was mixed with 1/10 volume of 3 M sodium acetate, pH 5.2 by pipetting. Subsequently, 2.5 volumes of 100% ethanol, kept beforehand for at least 30 min in -20°C, was added and DNA was incubated for 30 min at -80°C or on dry ice. After incubation, DNA was pelleted by centrifugation for 20 min at the maximum speed of 15 000 rpm at 4°C. The supernatant was removed, the white pellet of DNA was washed with 300 μl of 70% ethanol and centrifuged again as above for 5 min. The supernatant was removed again and DNA was air-dried for at least 20 min until the ethanol evaporated and subsequently resuspended in 10 μl of nuclease-free water.

2.2.1.2 QUANTIFICATION

2.2.1.2.1 Assessment of nucleic acid concentration and purity

Very often experiments that use DNA or RNA necessitate their particular amount and purity for optimum efficiency. In order to determine nucleic acid concentration and purity, the spectrophotometric analysis was applied using *Thermo Scientific NanoDrop Lite Spectrophotometer*. DNA was accepted as pure when $A_{260/280} = \sim 1.8$ and for RNA when $A_{260/280} = \sim 2.0$.

2.2.1.2.2 Assessment of nucleic acids size - agarose gel electrophoresis

BUFFERS

1x TAE buffer	40 mM Tris, 20 mM acetic acid, 1 mM EDTA
Agarose gel	1% agarose, 1x TAE

DNA or RNA fragments were separated on and visualised in an agarose gel. Agarose gels were prepared by dissolving the correct amount of agarose in 1x TAE buffer by heating in a microwave and to visualise DNA, *SYBR® Safe DNA Gel Stain* was added into the gel solution in dilution 1:10 000. Subsequently, the mixture was loaded into the gel tray with the comb in it and left to solidify for approximately 30 min at RT. Solidified gel was placed in the electrophoresis chamber and 1x TAE buffer was added until the gel was completely submerged by the buffer. Gel comb was carefully removed and DNA/RNA samples were mixed with *6x DNA Loading Dye*/*2x RNA Loading Dye*, before being loaded into the wells along with DNA/RNA ladder. The gel was run for approximately 1 h at 100 V and DNA or RNA was visualised using *Gel Doc™ EZ System*.

Some of the procedures like PCR and restriction digest required isolation and purification of DNA fragments from the agarose gel. After gel running, DNA was visualised under *Blue LED Illuminator*, the desired DNA fragments were excised from the gel and purified using *GeneJET Gel Extraction Kit* according to the manufacturer's instructions. The amount of obtained DNA was assessed by DNA concentration measured on the *NanoDrop*.

2.2.1.3 SYNTHESIS

2.2.1.3.1 Transcription – RNA synthesis

Non-radioactive labelled RNA sense and anti-sense probes were synthesised using linearized plasmid DNA as a template and T7 or T3 RNA polymerases for the incorporation of digoxigenin-UTP (DIG-UTP) into the RNA transcript. Specific DNA fragments were cloned into the vector within a dual promoter cassette with the T7 promoter at one end and T3 promoter at the other end (Figure 2.1).

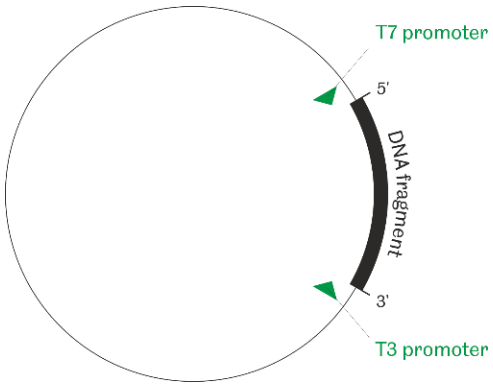

Figure 2.1 Dual promoter plasmid DNA

Plasmid DNA was linearized with a specific restriction enzyme (section 2.2.1.4.1) used beforehand for DNA fragment cloning and subsequently purified (section 2.2.1.2.2). 5' restriction site and T3 RNA polymerase were used to create the anti-sense probe while 3' restriction site and T7 RNA polymerase was used to synthesise the sense probe. The reaction mixture was prepared as indicated in Table 2.12 and incubated for 2 h at 37°C.

Reaction component	Amount
Transcription Optimized 5x buffer	4 µl
DTT (100mM)	2 µl
DIG-UTP	2 µl
RNasin	1 µl
linearized plasmid DNA	1 µg
T7/T3 RNA polymerase	1 µl
nuclease-free water	up to 20 µl

Table 2.12 RNA transcription reaction components

To remove DNA template, 2 µl of *RQ1 RNase-Free DNase* and 18µl of nuclease-free water were added directly to the transcription reaction and incubated further for 30 min at 37°C. Synthesized RNA probes were subsequently purified using *SigmaSpin™ Post-Reaction Clean-up Columns* according to the manufacturer's instructions. RNA concentration and purity were assessed using *NanoDrop* and its quality by agarose gel electrophoresis.

2.2.1.3.2 Reverse Transcription - cDNA synthesis

First-strand cDNA library was synthesised using oligo(dT)15 primers what allowed the study of gene expression of many different targets from the same cDNA pool. cDNA synthesis (*+RT* sample) was performed using RNA treated with DNase as a template and *Super-Script™ II Reverse Transcriptase* according to the manufacturer's instructions. Second RNA sample after DNase treatment (section 2.2.1.1.2) was prepared in the same way but instead of enzyme 1 µl of nuclease-free water was added. This sample served as a negative control for reverse transcription (*-RT* sample). Synthesised cDNA was used as a template in standard PCR to amplify DNA fragments used for molecular cloning or in qPCR to determine gene expression level.

2.2.1.3.3 Polymerase chain reaction

2.2.1.3.3.a Standard PCR

DNA fragments used for molecular cloning were amplified by PCR from existing plasmid DNA or cDNA.

Primers were designed to be around 30 bases in length and contained sequences recognised by specific restriction enzymes used further in the cloning procedure (section 2.2.1.4.1). The PCR was performed with *Phusion Green High-Fidelity DNA Polymerase* and the reaction was prepared as indicated in the Table 2.13.

Reaction component	Amount
5x Phusion Green HF buffer	10 µl
template DNA (plasmid DNA)	20 ng
the primer I (forward) (10µM)	2.5 µl
primer II (reverse) (10µM)	2.5 µl
10 mM dNTP mix	1 µl
Phusion DNA Polymerase	0.5 µl
H_2O	up to 50 µl

Table 2.13 PCR reaction components

Amplification of the DNA fragments was carried out in the thermal cycler with a heated lid using the parameters outlined in the Table 2.14.

Cycle step	Temperature	Time	Cycles
Initial denaturation	98°C	30 sec	1
Denaturation	98°C	10 sec	35
Annealing	T_m - 3°C * < 70°C	30 sec	
Extension	72°C	30 sec/kb of plasmid length	
Final extension	72°C	10 min	1

* T_m – primers melting temperature

Table 2.14 Cycling parameters for standard PCR reaction

After PCR, amplified DNA fragments were separated on an agarose gel (section 2.2.1.2.2) and purified. DNA concentration was measured using *NanoDrop* and DNA was prepared for further cloning procedures.

2.2.1.3.3.b Site-directed-mutagenesis

Single point mutants and siRNA-resistant contructs were created by site-directed mutagenesis. The mutagenic primers were designed to be between 30-40 bases in length with a melting temperature $T_m \geq 78$°C. Depending on the type of created construct, primers contained one missense mutation or 3 silent mutations with at least 15-20 bp of correct DNA sequence flanking on both sides. Primers were designed according to the primer design guidelines provided by *Agilent Technologies* and subsequently, PCR reaction was prepared as indicated in the Table 2.15.

Reaction component	Amount
10x reaction buffer	5 µl
template DNA (plasmid DNA)	20 ng
primer I (forward)	125 ng
primer II (reverse)	125 ng

10 mM dNTP mix	1 µl
H_2O	up to 50 µl
+/- *PfuUltra* HF DNA polymerase (2.5 U/µl)*	1 µl

*control reaction - *PfuUltra* HF DNA polymerase

Table 2.15 Site-directed mutagenesis reaction components

Amplification of the plasmid DNA was carried out in the in the thermal cycler with a heated lid using the parameters outlined in the Table 2.16.

Cycle step	Temperature	Time	Cycles
Initial denaturation	95°C	1 min	1
Denaturation	95°C	50 sec	18
Annealing	60°C	50 sec	
Extension	68°C	1 min/kb of plasmid length	
Final extension	68°C	7 min	1

Table 2.16 Cycling parameters for site-directed-mutagenesis

Parental DNA template was removed after PCR. 10x reaction buffer and 1 µl of *DpnI* restriction enzyme were added directly to each amplification reaction and incubated for 1.5 h at 37°C. Restriction digest in the reaction tube without *PfuUltra HF DNA polymerase* served as a control for digestion efficiency. Digested DNA was subsequently purified by ethanol precipitation as described in section 2.2.1.1.3 and transformed into bacteria using a protocol from section 2.2.1.1.2.b. Absence of bacterial colonies on the control plate confirmed successful digestion of parental DNA template.

2.2.1.3.3.c qPCR

Real-time quantitative PCR was used to determine and compare gene expression level during zebrafish development into adulthood and to confirm gene knockdown efficiency in mammalian cells. Quantitative real-time PCR was performed using *SYBR Green*-based system (*Takyon™ No Rox SYBR® MasterMix dTTP Blue)*, which measured a fluorescent signal proportional to the amount of

amplified gene. Primers specific to all target genes were designed using Primer-Blast available on the website: https://www.ncbi.nlm.nih.gov/tools/primer-blast/. The reaction mix was prepared under sterile conditions as indicated in the Table 2.17.

Reaction component	Amount
Takyon™ MasterMix	5 µl
template (*+RT* sample, *-RT* sample or H_2O)	1 µl
primer mix (forward + reverse) (1 µM)	1 µl
nuclease-free water	3 µl

Table 2.17 qPCR reaction components

Hard-Shell® 96-well PCR plate was kept on ice for at least 15 min and 1 µl template (non-diluted *+RT* sample, non-diluted *-RT* sample or H_2O) was aliquoted into the wells. All samples were prepared in triplicate or at least in duplicate. The reaction mix (with an excess) containing water, appropriate primer pair and *Takyon™ MasterMix* was prepared in 1.5 ml sterile tube by pipetting up and down several times and with limited light exposure. 9 µl reaction mix was subsequently added into the wells ensuring that no bubbles were present and the plate was centrifuged for 2min at 2000 rpm.

The real-time PCR was run in the thermocycler *CFX96 Touch™ Real-Time PCR Detection System* using the following parameters presented in the Table 2.18.

Cycle step	Temperature	Time	Cycles
Takyon™ activation	95°C	3 min	1
Denaturation	95°C	10 sec	40
Annealing/extension	60°C /63.3°C * or gradient 55-65°C	45 sec	
Denaturation	95°C	10 sec	1
Melt curve	65-95°C the increment of 0.5°C/5 sec	3 min	1

* annealing/extension temperature 63.3°C was specific for zebrafish experiments

Table 2.18 Regular cycling parameters for qPCR

qPCR data were analysed using *CFX Manager™ Software*. The main outcome obtained after qPCR run and used further for analysis was **C_t value** (threshold cycle) which indicated the number of the cycles where the first fluorescent signal from amplified product in the exponential phase was detected. Results obtained for all target genes were normalised to one of the housekeeping genes like *β-actin* (for zebrafish) or *GAPDH* (for mammalian cells) and normalised gene expression level was determined using relative quantification method called comparative $\Delta\Delta C_t$ (delta delta C_t). First, C_t value of the target gene was normalised to C_t value of the housekeeping gene for both the sample and the calibrator*:

$$\Delta C_{t\,(sample)} = C_{t\,(target\ gene,\ sample)} - C_{t\,(housekeeping\ gene,\ sample)}$$

$$\Delta C_{t\,(calibrator)} = C_{t\,(target\ gene,\ calibrator)} - C_{t\,(housekeeping\ gene,\ calibrator)}$$

Second, the ΔC_t of the sample was normalised to ΔC_t of the calibrator:

$$\Delta\Delta C_t = \Delta C_{t\,(sample)} - \Delta C_{t\,(calibrator)}$$

Finally expression fold change (increase or decrease) of the target gene in the sample relative to the calibrator as normalised to the housekeeping gene was calculated:

$$fold\ change\ (normalised\ gene\ expression) = 2^{-\Delta\Delta Ct}$$

* - calibrator: for zebrafish experiments - it was sample representing the earliest developmental stage; for gene knockdown efficiency - it was sample treated with control siRNA

Results from three independent experiments were analysed using *GraphPad Prism* software and represented as bar charts with error bars corresponding to the SEM (Standard Error of the Mean). Statistical significance was calculated using one-way ANOVA.

2.2.1.4 MOLECULAR CLONING

2.2.1.4.1 Restriction digest

Most of the DNA constructs used in this thesis were created by general cloning and subcloning procedures which required restriction digests. Using NEBcutter® – an online tool provided by NEB (*New England BioLabs*®Inc.), DNA fragments (inserts) were checked for enzymes which do not cut them and at the same time match multiple cloning site (MCS) within the cloning vector. Double-stranded DNA (plasmid DNA or PCR product) was cut with the restriction endonucleases, which recognised specific sequences of nucleotides and created sticky-ends, in the appropriate reaction buffer and incubation temperature providing optimum enzyme activity. Where possible, double digestion was performed and appropriate reaction conditions were chosen using another online tool provided by NEB - Double Digest Finder. The amount of enzyme required to digest DNA was calculated based on the amount of DNA according to the standard rule that 1 unit of enzyme digests 1 µg of DNA. The restriction digest was performed for 1 h at 37°C as follows:

Reaction component	Sequential digestion	Double digestion
DNA (vector or PCR product)	1 – 3 µg	1 – 3 µg
10x reaction buffer	5 µl	5 µl
enzyme I	1 – 3 units	1 – 3 units
enzyme II	-	1 – 3 units
H_2O	up to 50 µl	up to 50 µl

Table 2.19 Restriction digest reaction components

Digestion of the cloning vector was followed by dephosphorylation using Calf Intestinal Alkaline Phosphatase (CIP) to prevent re-circularization during ligation. Digested vector was incubated with 2 units of CIP for 30 min at 37°C. Subsequently digested DNA insert and cloning vector were run on an agarose gel, isolated and purified as described in section 2.2.1.2.2. DNA concentration was measured using the NanoDrop.

2.2.1.4.2 Ligation

Purified DNA insert and dephosphorylated cloning vector were ligated using T4 ligase in the provided buffer for 1.5 – 6 h at RT. Ligation time strongly depended on the DNA insert length – shorter insert required shorter ligation time. The amount of DNA insert and linear cloning vector was calculated as a molar ratio 5:1 (insert over vector) according to the formula:

$$ng\ of\ linearized\ vector = \frac{length\ of\ the\ insert\ (kb)}{length\ of\ the\ vector\ (kb)} = (ng\ of\ insert) \times 5$$

Ligation was performed at RT as indicated in the Table 2.20 and ligation mixture was subsequently transformed into bacteria as described in section 2.2.1.1.2.b.

Reaction component	DNA insert ligation into linearized vector	Self-circularization of linear vector (control)
linear cloning vector	50 µg	50 µg
DNA insert	5:1 molar ratio over vector	-
10x T4 DNA ligase buffer	2 µl	2 µl
T4 ligase	1 unit	1 unit
H_2O	up to 20 µl	up to 20 µl

Table 2.20 Ligation reaction components

2.2.2 PROTEIN METHODS

2.2.2.1 AFFINITY PURIFICATION

2.2.2.1.1 Fusion tag protein expression and purification from bacteria

BUFFERS

Lysis buffer 0,5% Triton X-100, 1x PBS protease cocktail inhibitor

Elution buffer 50 mM Tris-HCl pH 7.9, 50 mM glutathione in water, adjusted to pH 8.0

BL21 (DE3) bacteria were transformed with an appropriate pGEX vector as described in section 2.2.1.1.3.b. The next day one single colony was inoculated in 50 ml LB medium containing ampicillin (100 µg/ml) and incubated in the shaking incubator overnight at 220 rpm and 37°C. The next day culture was diluted 1:10 in the LB media containing ampicillin and incubated again in the shaking incubator for around 2-3 h at 220 rpm and 37°C until it reached an OD_{600} = 0.6 – 0.7. The culture was cooled to RT and expression of the recombinant protein was induced by addition of 0.5 mM IPTG under continuous shaking for 6 h at 220 rpm and 18°C. Bacteria were centrifuged for 20 min at 6000 rpm and RT, subsequently resuspended in 20 ml of ice-cold lysis buffer and incubated on ice for 30 min. Next, samples were sonicated with 15 seconds on/off cycles for 5 min in the glass beaker kept on the ice. Bacteria lysate was cleared by centrifuging for 30 min at 10 000 rpm and 4°C, the supernatant was collected and kept on ice. In the meantime 400 µl of *Protino® Glutathione Agarose 4B* suspension was centrifuged in 50 ml tube for 4 min at 1800 rpm and 4°C and subsequently, the supernatant was removed. Beads were equilibrated with 10 ml of ice-cold lysis buffer, mixed by inversion and centrifuged three times as described above. The supernatant was subsequently added to the equilibrated beads and mixed under continuous rotation for 4-6 h at 4°C. After incubation, beads were washed 3 times with 10 ml of ice-cold lysis buffer and centrifuged three times for 4 min at 1800 rpm and 4°C. After the final wash supernatant was removed, beads were resuspended in 1 volume of ice-cold lysis buffer to prepare 50% suspension and transferred into 1.5 ml tube. Beads were centrifuged for 2 min at 7000 rpm and 4°C and the supernatant was removed. GST-tagged recombinant protein was eluted from the beads by incubating them with 0.5 ml of glutathione containing elution buffer under constant rotation for 30 min at RT. Beads were centrifuged, the eluate was collected in the fresh tube and elution was repeated 2 more times. All three eluates were combined, the recombinant protein solution was dialysed into 1x PBS using *Slide-A-Lyzer™* according to the manufacturer's instruction and protein concentration was measured. To assess the recombinant protein production efficiency, purity and quality, the SDS-PAGE and Coomassie staining were performed as described in sections 2.2.2.2.2 and 2.2.2.2.3b respectively.

2.2.2.1.2 Co-immunoprecipitation

To characterise and verify protein-protein interactions between two overexpressed proteins or between overexpressed and endogenous proteins co-IP was conducted using specific antibody coupled to *Protein A-agarose* resin, *GFP-Trap®_A* or *Myc-Trap®_A*. Cell lysate, from 2 – 4 dishes 35 mm in total 1 ml HEPES lysis buffer, was prepared 48 hours post transfection from cells overexpressing GFP- or myc-tagged proteins as described in section 2.2.2.2.3.a. For Western Blot analysis, 5 – 10% of the cell lysate was taken, mixed with 4x Laemmli sample buffer (as described in section 2.2.2.2.3.a) and boiled for 5 min at 95°C (refer to as INPUT). 15 µl of *Protein A-agarose*, *GFP-Trap®_A* or *Myc-Trap®_A* beads were equilibrated in 200 µl of ice-cold HEPES lysis buffer and centrifuged for 2 min at 7000 rpm and 4°C. The supernatant was discarded and beads were washed two more times with lysis buffer. After the final wash supernatant was removed and: cell lysate containing overexpressed tagged proteins was added to the equilibrated *GFP-Trap®_A* or *Myc-Trap®_A* beads and incubated under continuous rotation for 3 h at 4°C or cell lysate pre-incubated with antibody under continuous rotation for 1 h at 4°C was added to the equilibrated *Protein A-agarose* and incubated under continuous rotation for 3 h at 4°C. After incubation, beads were washed 3 times with 500 µl of ice-cold lysis buffer and centrifuged for 2 min at 7000 rpm and 4°C. After the final wash supernatant was removed, 60 µl of 2x Laemmli sample buffer was added to the beads and samples were boiled for 5 min at 95°C (refer to as BOUND). Samples INPUT and BOUND were run on SDS-PAGE gel and Western Blot was performed as described in sections 2.2.2.2.3.b and c respectively.

2.2.2.1.3 Pull-down assays

Pull-down assays were performed using streptavidin-biotin system. Stable MDCKII cell lines expressing myc-tagged BirA* or myc-tagged BirA*-FRMPD2 were grown in duplicates in 60 mm dishes until they reached 80% confluency, biotin was added to the final concentration 50 µM and cells were incubated for 18 h. Control plates were incubated without biotin. Cell lysate collection and further procedures were conducted as described in section 2.2.2.1.2. Pull-down assay was performed using *Pierce™ NeutrAvidin™ Agarose* to capture all

biotinylated proteins which were later detected by Streptavidin-HRP antibody or Alexa Fluor® 680 Streptavidin secondary antibody.

2.2.2.2 PROTEIN DETECTION

2.2.2.2.1 Assessment of protein concentration

Protein concentration was estimated using colorimetric *Bio-Rad DC Protein Assay* which principle is based on improved Lowry method. The procedure was carried out according to the manufacturer's instruction for microplate assay protocol and absorbance was read by *iMark™ Microplate Absorbance Reader* at wavelength 750 nm.

For knockdown experiments the set of all samples was equalised according to the formula:

$$\mu l\ of\ the\ sample = \left(\frac{the\ lowest\ A_{750}\ in\ the\ set\ of\ samples}{A_{750}\ of\ the\ sample} \right) \times total\ volume\ (\mu l)$$

If experiments or further analysis required estimation of the specific amount of protein, a standard curve was prepared with serial dilutions of Albumin Standard (2.0 mg/ml) in the same buffer as the samples in the range from 0.0 – 1.5 mg/ml. Concentrations of albumin dilutions and corresponding absorbances were plotted on X and Y axis of the graph respectively, linear regression was applied and if the R-squared value was ≥ 0.95 , the unknown protein concentration of the sample was determined by interpolation on the graph (using the equation of the linear regression line). All samples were finally adjusted to the same volume with the appropriate buffer and contained the same amount of protein.

2.2.2.2.2 Coomassie staining

BUFFERS

Fixing solution	50% methanol, 10% glacial acetic acid
Staining solution	50% methanol, 10% glacial acetic acid, 0.1% Coomassie Brilliant Blue R-250

Destaining solution	40% methanol, 10% glacial acetic acid

Purified recombinant proteins separated on a SDS-PAGE gel were visualised by Coomassie staining. All steps of gel staining were carried out at RT and with gentle agitation. After gel running, the gel was initially fixed in a fixing solution for 1 h. Fixing solution was discarded and the gel was stained with a staining solution for 20 min. Subsequently, the gel was destained with a destaining solution which was changed several times until the background of the gel was completely transparent and proteins were clearly visible on the gel. The gel was washed with ddH_2O and a picture was taken using *Gel Doc™ EZ System*.

2.2.2.2.3 Western Blot

BUFFERS

1x PBS	137mM NaCl, 2.7mM KCl, 10mM Na_2HPO_4, 1.8mM KH_2PO_4
Lysis buffer	50 mM HEPES pH 7.5, 150 mM NaCl, 1.5 mM $MgCl_2$, 1 mM EDTA, 10% glycerol, 1% Triton X-100, protease cocktail inhibitor
4x Laemmli sample buffer	250 mM Tris-HCl pH 6.8, 40% glycerol, 20% β-mercaptoethanol, 8% SDS, 1% bromophenol blue
10x Running buffer (diluted 10-fold in water)	0.192 M glycine, 0.025 M Tris, 0.1 % SDS
10x Transfer buffer (diluted 10-fold in water)	0.192 M glycine, 0.025 M Tris +20% methanol
Ponceau S	30% trichloroacetic acid, 2% Ponceau S
PBST	0.05% Tween20, 1x PBS
TBST	50 mM Tris, 150 mM NaCl, 0.1% Tween20, pH 7.6

2.2.2.2.3.a Cell lysate preparation

The cell lysate was prepared from cells grown in cell culture dishes either as wild type or after transfection. When cells reached the desired confluency or 48/72/96 h post transfection, cell culture dishes were taken out from the incubator and put on the ice. The medium was aspirated and cells were washed twice with 1x PBS. Subsequently, ice-cold HEPES lysis buffer supplemented with protease cocktail inhibitor was added to each well/dish in the volume indicated in the Table 2.21.

Cell type	35mm dish/ 6-well plate	60mm dish
WT	150 µl	250 µl
knockdown	150 µl	-
overexpression	250 µl	300 µl

Table 2.21 Volume of lysis buffer depending on cell culture dishes size and type of experiment

Cells were harvested from the wells/dishes using a cell scraper and cell lysate was transferred into an ice-cold 1.5 ml tube and incubated on ice for 60 min with vortexing at 5-10 min intervals. The cell lysate was cleared by centrifuging for 20 min at the maximum speed 15 000 rpm and 4°C. The supernatant was transferred into the new ice-cold 1.5 ml tube and the cell pellet was discarded. If necessary protein concentration was assessed and protein samples were prepared by adding 4x Laemmli sample buffer (to give a final concentration of 1x Laemmli sample buffer) into the protein lysate. To denature proteins, samples were boiled for 5 min at 95°C. Before loading on the gel, samples were briefly centrifuged and cooled down to RT.

2.2.2.2.3.b SDS-PAGE gel electrophoresis and protein transfer

Proteins from the cell lysate samples were separated using SDS-PAGE gel electrophoresis according to their molecular weight. SDS-PAGE gels were prepared and electrophoresis was run according to *Bio-Rad Mini-PROTEAN*® *Tetra Cell* manufacturer's instruction. Samples were loaded on the gel along with

PageRuler™ Prestained Protein Ladder and run on the gel in the 1x running buffer. During first 30 min electrophoresis was carried out at 50 V until the samples were concentrated and formed the leading front. Subsequently, the voltage was increased up to 120 V and the gel was run until the die front was run off the bottom of the gel. At that stage, depending on the experimental approach, proteins on the gel were either stained with Coomassie or transferred onto the membrane for Western Blot. Protein transfer was performed using *Mini Trans-Blot® Electrophoretic Transfer Cell* in 1x transfer buffer containing 20% methanol for 90 min at constant current 250 mA. For high molecular weight proteins larger than 200 kDa protein transfer was performed overnight (~ 16 h) at a constant voltage 25 V or using *Trans-Blot® Turbo™ Transfer System* and *Bio-Rad* preprogrammed protocol HIGH MW for 10 min at constant current 1.3 A and voltage up to 25 V. Protein transfer efficiency was assessed by membrane Ponceau S staining (section 2.2.2.2.3.d).

2.2.2.2.3.c Blocking and incubation with antibody

Membrane stained with Ponceau S was washed with washing buffer (1x PBST or 1x TBST) until staining was removed. Depending on the antibody and manufacturer's recommendations membrane was blocked with 5% non-fat dry skimmed milk in 1x PBST or 5% BSA in 1x TBST for 1 h at RT with gentle agitation. Subsequently, the membrane was incubated with the primary antibody diluted in the appropriate blocking buffer overnight at 4°C or for 2 h at RT (Table 2.1). After incubation with the primary antibody, the membrane was washed 3 times for 10 min with the washing buffer and later incubated with the secondary antibody (HRP-conjugated or fluorescently-conjugated, Table 2.2) diluted in the appropriate blocking buffer for 1 h at RT. The membrane was washed again 3 times for 10 min with the washing buffer and subjected for protein detection.
If custom made antibody was used, primary and secondary antibody were diluted in 0.5% milk and the membrane was incubated for 2 h and 1 h at RT respectively.

2.2.2.2.3.d Detection and quantification

Protein detection was performed using 2 methods:

a) *Pierce ™ ECL Western Blotting Substrate* and *X-ray films*

After washing, membranes probed with secondary HRP-conjugated antibody were put in the *Amersham hypercassette autoradiography cassette* overlaid with the clear plastic sheet. Detection solution was freshly prepared by mixing Detection Reagent 1 and 2 at a 1:1 ratio, added on the blot and incubated for 1 min at RT in the dark. The blot was covered with a clear plastic sheet and exposed to X-ray *Amersham Hyperfilm™ ECL* film in the dark room. Exposure time varied depending on the used antibody. X-ray film with detected protein signal was scanned and densitometry analysis was performed using Image J.

b) *Odyssey Sa® Infrared Imaging System* from *LI-COR*

After washing, membranes probed with fluorescently-conjugated antibody was dried at RT and subsequently put into the machine. The blot was scanned for 3 min with one or two channels at the same time. If the proteins were detected using LI-COR system, membranes were not stained with Ponceau S, as it produced a non-specific background during scanning. Brightness and contrast adjustment, as well as signal intensity analysis, were performed using *Image Studio™ Lite* software.

2.2.3 CELL CULTURE METHODS

2.2.3.1 Cell lines and culture conditions

A few adherent mammalian cell lines were used in this thesis and culture conditions for each cell line are indicated below in the Table 2.22.

Cell line	Organism	Tissue	Morphology	Complete growth medium
16HBE14o-	human	bronchus	epithelial	MEM + 10% FCS + 1% P/S
Caco-2	human	colon	epithelial	DMEM + 10% FCS + 1% P/S
Cos-7	monkey	kidney	fibroblast	
HEK293	human	embryonic kidney	epithelial	

HeLa	human	cervix	epithelial	
MDCKII	dog	kidney	epithelial	

Table 2.22 Cell line characteristics and culture conditions

2.2.3.2 Cell sub-culturing

SOLUTIONS

1x PBS	137mM NaCl, 2.7 mM KCl, 10 mM Na_2HPO_4, 1.8 mM KH_2PO_4; pH 7.2-7.4
HBS (filter sterilised)	19.04g HEPES, 28.52g NaCl, 0.8g glucose, 6.8g Na_2HPO_4 x $7H_2O$, 0.5% phenol red; pH 7.4-7.6
Trypsin	Trypsin-EDTA (0.25%), gibco®, Life Technologies™
PET (sterile)	36 ml HBS 2 ml of 10% Polyvinylpyrrolidone in HBS 5 ml of 0.2% EGTA in HBS 4 ml Trypsin 0.25% with 0.02% EDTA

Cells were grown in a T-75 flask (T-75 flask coated with fibronectin for 16HBE14o- cells) placed in an incubator at 37°C with 5% CO_2. When cells reached 80-100% confluency, the medium was aspirated and cells were rinsed once with 5 ml of sterile 1x PBS (5ml of HBS solution for 16HBE14o- cells) to remove FCS residues which could inhibit the trypsinization step. Subsequently, 2 ml of trypsin (2ml of PET solution for 16HBE14o- cells) was added to the flask and spread across the cell surface. The flask was placed in the incubator at 37°C to allow the trypsin to work. After 3-5 min cells were examined under the microscope. If cells were still attached, the flask was placed back in the incubator for a few more minutes and later examined again. After 80-90% cells detached from the surface, 8ml of the medium was added to the flask to stop trypsinization and cells were

pipetted repeatedly to break up any clumps. The cell suspension was transferred into a 15 ml centrifuge tube and centrifuged for 3 min at 1500 rpm and RT. The medium was aspirated and the cell pellet was resuspended in 1ml of fresh medium. Cells were then split 1:5 to 1:10 depending on their growth rate and 10 ml of the fresh complete growth medium was added to the flask.

2.2.3.3 Cell counting and seeding

Cells were treated as for sub-culturing. After centrifugation medium was aspirated and cells were resuspended in 10 ml of the appropriate fresh medium. The number of cells was determined by cell counting using a Neubauer counting chamber. Depending on the cell type, growth rate and surface area of used cell culture dishes, cell seeding density was as indicated in the Table 2.23.

Cell line	6-well plate	12-well plate containing coverslips	6-well plate containing coverslips
16HBE14o-	2.0×10^5	-	2.0×10^5
Caco-2	3.0×10^5	1.5×10^5	3.0×10^5
Cos-7	2.5×10^5	-	-
HEK293	2.5×10^5	1.0×10^5	2.5×10^5
HeLa	1.5×10^5	-	-
MDCKII	1.0×10^5	-	1.5×10^5

Table 2.23 Seeding density for different cell lines depending on size of cell culture dishes with or without coverslips

2.2.3.4 Cryopreservation of mammalian cells

Cells were treated as for sub-culturing. After centrifugation medium was aspirated and cells were resuspended with appropriate fresh medium containing 10% DMSO (50% FCS + 40% MEM + 10% DMSO for 16HBE14o- cells). Cells from T-75 flask were aliquoted into 1-2 cryogenic vials. First, the vials were placed in

a -20°C freezer for a couple of hours and then in a - 80°C freezer overnight. For long-term storage, cells were frozen in liquid nitrogen.

2.2.3.5 Thawing cells

The vial of frozen cells was taken from liquid nitrogen and thawed in a water bath at 37°C. Cells were resuspended in 5 ml of the appropriate pre-warmed medium and centrifuged for 3 min at 1500 rpm and RT. Without disturbing the cell pellet, DMSO-containing medium was aspirated, cells were resuspended in 10 ml of the fresh medium and transferred into a new sterile T-75 flask. Cells were incubated overnight in an incubator at 37°C with 5% CO_2 and the next day all un-attached dead cells were aspirated and the medium was changed.

2.2.3.6 Cell transfection

One day before transfection cells were seeded in multi-well plates as described above in section 2.2.3.3. Cells were allowed to attach overnight (two days for Caco-2 cells as they attached slower than other cells) and transfected using Lipofectamine2000 the following day at the low confluency of 20-30% according to the manufacturer's instructions. The amount of DNA/siRNA and Lipofectamine2000 (LF2000) for 6-well plate format as well as transfection conditions are indicated below in the Table 2.24.

Cell line	DNA transfection	siRNA transfection
16HBE14o	-	- day 1: 50 nM siRNA + 5 µl LF2000 in medium without P/S - medium changed after 6 h - incubation time: 72 h
Caco-2	-	- day 1: 50 nM siRNA + 5 µl LF2000 - medium changed after 6 h - day3: 50 nM siRNA + 5 µl LF2000 in medium without P/S - medium changed after 6 h - incubation time: 72 h
Cos-7		-

	- day 1: 1,0 µg DNA + 2,5 µl LF2000 in medium without P/S - medium changed after 6 h - incubation time: 48 h	
HEK293	- day 1: 1,0 µg DNA + 2,5 µl LF2000 in medium without P/S - medium changed after 6 h - incubation time: 48 h	- day 1: 50 nM siRNA + 5 µl LF2000 in medium without P/S - medium changed after 6 h - incubation time: 72 h
HeLa	- day 1: 1,0 µg DNA + 2,5 µl LF2000 in medium without P/S - medium changed after 6 h - incubation time: 48 h	- day 1: 50 nM siRNA + 5 µl LF2000 in medium without P/S - medium changed after 6 h - incubation time: 72 h
MDCKII	- day 1: 1,6 µg DNA + 6,0 µl LF2000 in Opti-MEM - medium changed after 6 h - incubation time: 48 h	- day 1: 80 nM siRNA + 5 µl LF2000 in Opti-MEM - medium changed after 6 h - day2: 80 nM siRNA + 5 µl LF2000 in Opti-MEM - medium changed after 6 h - incubation time: 72 h
Cell line	**shRNA transfection**	
HeLa	- day1: 1,0 µg shRNA + 2,5 µl LF2000 in medium without P/S - medium changed after 6 h - incubation time: 72 h	
Cell line	**shRNA + DNA transfection**	**siRNA + DNA transfection**
HEK293	- day1: 1,0 µg shRNA + 2,5 µl LF2000 in medium without P/S - medium changed after 6 h - day2: 0,5 µg shRNA + 0,5 µg DNA 2,5 µl LF2000 in medium without P/S - medium changed after 6 h - incubation time: 72 h	-
MDCKII	-	- day 1: 1,0 µg DNA + 2,5 µl LF2000 in medium without P/S - after 6 h: 80 nM siRNA + 5 µl LF2000 in Opti-MEM - medium changed after 6 h

		- day2, 24h after first siRNa transfection: 80 nM siRNA + 5 µl LF2000 in Opti-MEM - medium changed after 6 h - incubation time: 72 h

Table 2.24 Transfection conditions for different cell lines

2.2.3.7 Generating stable MDCK II cell lines

Stable MDCK II cell lines were generated by transfecting cells with plasmids carrying a neomycin resistance gene pcDNA 3.1 myc-BirA* or pcDNA 3.1 myc-BirA*-FRMPD2. Positive clones were selected in the presence of selection antibiotic G-418 sulfate at the concentration 500 µg/ml.

MDCK II cells were seeded on 35 mm dishes and transfected as indicated in the Table 2.23 and Table 2.24 respectively. After 48 h cells were split 1:3 into 10 cm dishes in normal complete growth medium (Table 2.22). Cells were allowed to attach overnight and the following day the medium was changed to the selection medium containing G-418 sulfate. The selection medium was refreshed every 1-2 days depending on the cell death rate. After 10-14 days, cells started to form colonies from which around 20 were picked and further expanded in two 60 mm dishes (one dish for cell maintenance and one dish for tests). Initially, all colonies were verified by Western Blot and those which were positive were further assessed by immunofluorescence microscopy, verifying proper cellular localisation of transgene products.

2.2.4 Cell mechanics and migration

2.2.4.1 Microfluidic optical stretcher

Microfluidic optical stretcher (OS) is a technic used to characterise changes in cell mechanics which was invented and very well described by Prof Jochen Guck (Guck et al., 2001). All experiments presented in this study were performed in his lab (Biotechnology Center of the TU Dresden, Germany) during a one month secondment to Germany.

OS SETUP

Cells were driven through the microfluidic flow chamber containing two optical fibers aligned perpendicularly to a capillary delivering cell suspension. The chamber was mounted on an inverted phase contrast microscope (Eclipse TE2000U) containing plan Fluor ELWD 40x/0.60 NA objective (Nikon). All deformed cells were acquired with a camera (AVT MARLIN F-146B, 50 frames/s, Firstsight Vision) attached to the microscope. The laser used in OS device was a single-mode, continuous-wave fiber laser at the wavelength 1064 nm (YLM-5-1070-LP, IPG Photonics). The cell flow was adjusted manually through the difference in the heights of inlet and outlet of the reservoirs connected to the capillary.

CELL PREPARATION AND OS MEASUREMENT PROCEDURE

HeLa cells were initially seeded and transfected with siRNA or shRNA in the 6-well plates according to the procedures used for this cell line in the current study described in the Table 2.23 and Table 2.24. 72 hours post transfection the medium was removed and cells were washed twice with 1x PBS without Mg^{2+} and Ca^{2+} and trypsinized. After 80-90% cells detached from the surface the medium was added to the plate wells to stop trypsinization and cells were pipetted repeatedly to break up any clumps. The cell suspension was transferred into 15 ml centrifuge tube and centrifuged for 5 min at 115 g and RT. The medium was aspirated and the cell pellet was re-suspended in 1x PBS without Mg^{2+} and Ca^{2+}. The cell suspension was drawn avoiding air bubbles into a 1-ml syringe which was subsequently connected to the inlet reservoir of microfluidic chamber. When the cell was in the right position in the middle of the capillary, the flow was stopped and cell got trapped for 1 second by the lasers (Figure 2.2, A). Subsequently, lasers were turned on to the higher intensity and cell was stretched for 4 seconds along the laser beam axis (Figure 2.2, B). After stretching, cells underwent relaxation for 2 seconds before measurement procedure was repeated for the next cell. All data were analysed with a custom-built LABVIEW software (National Instruments) using an edge detection algorithm tracking the cell shape during the stretching. In the single experiment around 70 - 100 cells were analysed and all measurements were carried out at RT.

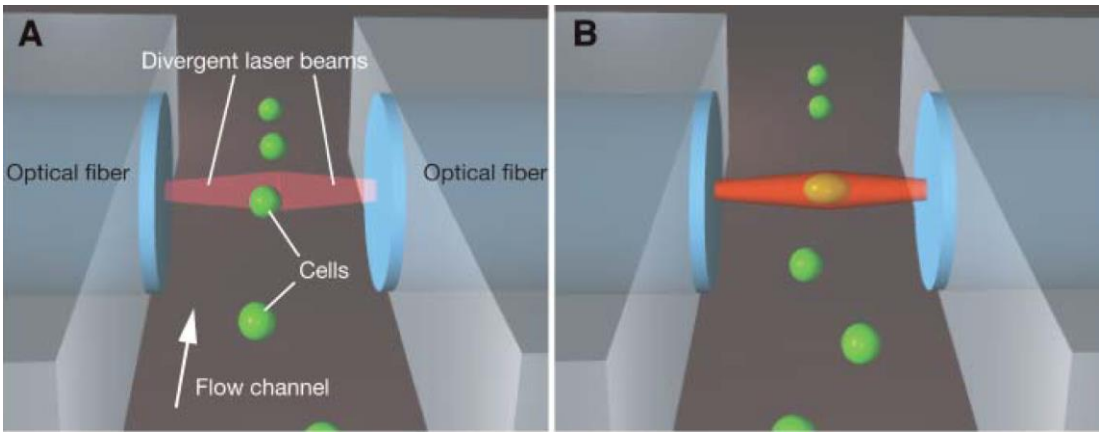

Figure 2.2 The basic principles of microfluidic optical stretcher (OS)

(A) *In an experimental setup cells in suspension flow through the microfluidic channel,* ***(B)*** *are stably trapped and subsequently deformed by the optical forces from two opposing divergent laser beams (Guck et al., 2005)*

Cell mechanical properties were represented by creep compliance measurements. Cell size and relative deformation were recorded by video-microscopy during the measurement procedure. Cell refractive index (RI) required for the calculation of applied stress was determined by immersion refractometry using BSA solutions as described before (Guck et al., 2005). Stress magnitude and distribution were subsequently calculated based on applied power, refractive index, laser beam parameters and the size of the trapped cell as described previously (Guck et al., 2001). Stress distribution was used further to determine the geometric factor, *GGF* (Ananthakrishnan et al., 2006). The relative deformation measured at the last second of stretching time was subsequently normalised by the stress magnitude and the geometric factor, that resulted in the creep compliance or deformability of the cell, *D(t)*.

Results from three independent experiments were analysed using GraphPad Prism software and represented as bar charts with error bars corresponding to the SEM (Standard Error of the Mean). Statistical significance was calculated using one-way ANOVA. All box plots included whiskers at min and max values, horizontal box lines at 25–75% range, median line, and the mean marked by '+'.

2.2.4.2 Real-time deformability cytometry

Real-time deformability cytometry (RT-DC) is a novel technic used to characterise cell mechanical properties at much shorter timescales than an

optical stretcher. RT-DC was developed and very well described by Prof Jochen Guck group (Otto et al., 2015). All experiments presented in this study were performed in his lab (Biotechnology Center of the TU Dresden, Germany) during a one month secondment to Germany.

RT-DC SETUP

The basic principle of RT-DC is to measure the cell deformation triggered by shear stress and pressure gradients during the cell flow through the microfluidic channel constriction of the PDMS chip. The PDMS microfluidic chip was a home-made chip containing two reservoirs connected by 300 µm-long channel with 20 x 20 µm (for HEK293 cells) or 30 x 30 µm square cross-section (for HeLa cells). Channel size was selected based on the cells size and was 1.1 – 2.0 times bigger than cells, what allowed to deform cells only by the shear gradients without contact with the channel. Microfluidic chip was assembled on an Axiovert 200M inverted microscope (Zeiss) and connected to a syringe pump (NemeSys, Cetoni) by which cell suspension was driven through the channel with the flow rate between 0.16 µl/s and 0.32 µl/s. Cells during translocation through the channel constriction were illuminated by a high-power LED (CBT-120, 462 nm, Luminus Devices) and all deformed cells were synchronously acquired with a high-speed CMOS camera (MC1362, Mikroton) connected to the standard PC via camera link interface (NI-1433 Frame Grabber, National Instruments) (Figure 2.3, A).

CELL PREPARATION AND RT-DC MEASUREMENT PROCEDURE

Cells were prepared as described in section 2.2.4.1 for OS experiments. After centrifugation medium was aspirated and the cell pellet was re-suspended in 1x PBS without Mg^{2+} and Ca^{2+} and 0.5% methylcellulose to a final concentration of around 10^6 cells/ml. The addition of methylcellulose helped to reduce sedimentation of the cells during the experiment. The cell suspension was drawn avoiding air bubbles into a 1-ml syringe which was subsequently connected to the inlet of the microfluidic chip. While cells were pumped through the chip, they got deformed from the spherical to a bulletlike shape within the channel constriction (Figure 2.3, B). All data acquisition was carried out at the rear of 300 µm-long channel where the cell shape reached the steady state. Cells deformation and size were analysed in real-time and displayed as a scatter plot (Figure 2.3, C).

All data were analysed with ShapeOut 0.7.0 software made available by Prof Jochen Guck group and the average cell deformation was defined as a peak of the fitted distribution. In a single experiment around 2000 cells were analysed and as a reference, cell deformation in the reservoir was measured as well.

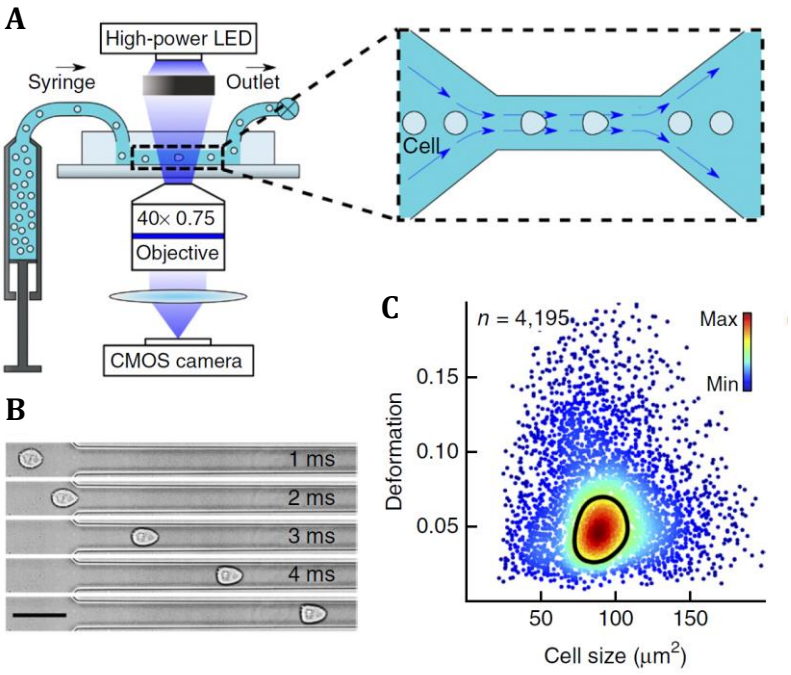

Figure 2.3 The basic principles of real-time deformability cytometry (RT-DC)

(A) *The setup of RT-DC and measurement procedure. The inset shows the channel constriction where cells are getting deformed and analysed.* ***(B)*** *Time series of the cell deformed from the spherical to a bulletlike shape within the channel constriction. Scale bar, 50 µm.* ***(C)*** *Scatter plot of deformation versus cell size representing results from the single experiment. Colour represents linear density scale (Otto et al., 2015)*

2.2.4.3 Migration assay

SOLUTIONS

1x PBS	137mM NaCl, 2.7 mM KCl, 10 mM N Na_2HPO_4, 1.8 mM KH_2PO_4; pH 7.2-7.4
PFA	4% PFA, 1x PBS; pH 7.2-7.4
0.5 % crystal violet	500 mg crystal violet 25 ml methanol 75 ml water

HeLa cells were initially seeded and transfected in the 6-well plates according to the procedures used for this cell line in the current study described in the Table 2.23 and Table 2.24. 40 hours post-transfection the medium was removed and cells were washed twice with 1x PBS. PBS was removed and cells were starved overnight in serum-free medium containing 0.2% BSA. 2 hours before next step, 24-well plate containing ThinCerts™Inserts was incubated with serum-free medium containing 0.2% BSA in the upper compartment of the insert and complete medium with 10% FCS in the lower compartment of the plate well in a cell culture incubator at 37°C and 5% CO_2. Cells were trypsinized, resuspended in serum-free medium with 0.2% BSA and counted to an appropriate final cell concentration 2.5 x 10^5/ml. Media from the plate kept beforehand in the incubator was discarded and 600 µl of the fresh medium with 10% FCS and 200 µl of the cell suspension were added to each well of the cell culture plate and cell culture inserts respectively. Cells were incubated for 18 hours in a cell culture incubator at 37°C and 5% CO_2. Subsequently, the medium was removed, inserts were washed twice with 1x PBS and cells were fixed with PFA for 2 min at RT. After fixation, cells were washed twice with 1x PBS and permeabilized with 100% methanol for 20 min. Next, cells were washed again twice with 1x PBS and stained with 0.5% crystal violet for 20 min. Excess of crystal violet was removed by washing inserts with 1x PBS. Cells that did not migrate through the pores of the membrane and remained on the upper side of the membrane were gently removed with a moist cotton swab. Stained cells were visualised with a brightfield inverted microscope with an objective in 10x magnification and images were captured using Digi-Pad 9556.5600 M attached to the microscope. For each sample, 5 non-overlapping images, representing different regions of the insert membrane, were taken and migrated cells were counted using ImageJ software. Results from three independent experiments were analysed using GraphPad Prism software and represented as bar charts with error bars corresponding to the SEM (Standard Error of the Mean). Statistical significance was calculated using one-way ANOVA or paired t-test.

2.2.5 Immunofluorescence microscopy

2.2.5.1 Coating of coverslips

Immunofluorescence experiments performed with HEK293 cells required poly-L-lysine coated coverslips. 12 mm glass coverslips were placed into the sterile 6- or 12-well plate and covered with 0.1% poly-L-lysine solution diluted 10 times with distilled autoclaved water. The coverslips were coated for 45 min at RT. Subsequently, the solution was aspirated and coverslips were left uncovered to dry for 1.5 h under the hood.

2.2.5.2 Fixation and immunostaining

BUFFERS

1x PBS	137mM NaCl, 2.7 mM KCl, 10 mM Na_2HPO_4, 1.8 mM KH_2PO_4; pH 7.2-7.4
PFA	4% PFA, 1x PBS; pH 7.2-7.4
quenching solution	0.1 M glycine, 1x PBS
permeabilization and blocking solution	0.2% Triton X-100, 5% FCS, 1x PBS

Cells were initially seeded on coverslips and transfected with siRNA and/or DNA in the multi-well plates. Two or three days after transfection the medium was removed, cells were washed twice with 1x PBS and fixed with PFA for 20 min at RT. After fixation, cells were washed once with 1x PBS and remaining PFA was quenched with quenching solution for 5 min at RT. The quenching solution was then removed and cells were washed twice with 1x PBS. Subsequently cells were simultaneously permeabilized and blocked with permeabilization and blocking solution for 10 min at RT. In the meantime the humidity chamber was prepared in the Petri dish covered with tissue paper soaked by water and overlaid with the parafilm. The respective primary antibodies were prepared in the permeabilization buffer at their recommended concentrations as indicated in Table 2.1 and 20-30 µl of the primary antibody solution was aliquoted onto the parafilm. The coverslips were removed from the multi-well plates with forceps

and excess of permeabilization buffer was drained off using tissue paper. The coverslip's side containing cells was placed on the drop of primary antibody solution and incubated for 1 h at RT. After incubation coverslips were removed and excess of primary antibody solution was drained off using tissue paper. Coverslips were placed back into the multi-well plate and washed three times with permeabilization buffer. The cells were incubated then with the respective secondary antibodies at their recommended concentrations as indicated in Table 2.2 in a similar manner to the primary antibody for 1 h at RT. After incubation coverslips were washed three times with permeabilization buffer and then three times with 1x PBS. Finally the cells were mounted onto microscope slides with 10 µl of DAPI-containing mounting medium and left to dry for at least 2 h (ideally overnight) in the dark at RT. The next day cells were observed under the microscope.

2.2.5.3 Microscopy

Stained cells were visualised with the Perkin Elmer Ultraview Vox spinning disc confocal system running on an inverted Olympus IX81 motorised microscope with oil immersion objective lens Uplan Apo 60x. All images were captured using Hamamatsu C9100-50 EM-CCD camera and Volocity software. Images were taken using Z-stack function and were represented as single xy plane or merged multiple xy planes (please refer to the figure legends). Images quality was improved using contrast enhancement tool in Velocity software. Images were exported as TIFF files and further processed and analysed using ImageJ software.

2.2.5.4 Quantification of tight junction formation

Tight junction formation in polarised epithelial MDCKII cells was quantified based on the cell staining with zonula occludens-1 (ZO-1) antibody which served as a tight junction marker. For each sample, 15-20 non-overlapping images, representing different regions of the coverslip, were taken as described above in section 2.2.4.3. In each experimental repeat, approximately 600 cells per sample were counted and each cell was assessed with respect to tight junction integrity. Cells were classified into two groups: having continuous, intact ZO-1 staining and having discontinuous, punctate or no ZO-1 staining. Mitotic cells were not

included in the analysis due to disruption in their tight junction staining. Results from three independent experiments were analysed using GraphPad Prism software and represented as bar charts with error bars corresponding to the SEM (Standard Error of the Mean). Statistical significance was calculated using one-way ANOVA.

2.2.6 ZEBRAFISH METHODS

2.2.6.1 Zebrafish husbandry

2.2.6.1.1 Adult zebrafish maintenance

Adult zebrafish were maintained in accordance with the UK Home Office regulations and UK Animals (Scientific Procedures) Act 1986. All experiments were performed under project licenses 40/3624 and 40/3727 issued to Dr Jarema Malicki and Dr Anton Nikolaev respectively and under personal license I44817F09 issued to me. Adult zebrafish were maintained on a 14:10 hours light/dark cycle at 28.5°C in a recirculating aquarium system. Adults were fed with live *Artemia nauplia* larvae or dry food twice daily and kept at the maximum density of 5 fish per litre of aquarium water.

2.2.6.2 Zebrafish strains

All experiments utilising wild-type zebrafish were performed with AB strain. *frmpd2*^{sa18532}*+/-* mutant line, generated by ENU mutagenesis, was obtained from the Sanger Institute. The original mutation was induced in AB/TL (Tupfel long wild-type strain) background but later the strain was maintained by out-crossing to an AB wild-type strain. Homozygous mutant *frmpd2*^{sa18532}*-/-* was created by incrossing of *frmpd2*^{sa18532}*+/-* line.

2.2.6.3 Pairwise breeding of individual fish for embryo collection

All embryos were obtained by pairwise breeding of individual male and female adult fish. In the late afternoon male and female fish were placed into the clean plastic container containing diagonal plastic divider and breeding trap, that prevents adults from ingesting embryos. On the next day, when the lights came on, dividers were removed and fish were left for at least 30-60 min to breed. Fish

were returned to their tanks and embryos were harvested by pouring them on a collecting net. Embryos were washed several times with fresh water and sorted into groups of 40. Collected embryos were placed in Petri dishes containing fresh E3 medium supplemented with methylene blue acting as a fungicide and antibacterial agent in an incubator at 28.5°C. Unfertilized eggs, empty chorions or dead embryos were removed daily and the E3 medium was refreshed to minimise any detrimental effect on embryo growth and development. All embryos prior to 5.2 dpf, not raised for adult stocks, were destroyed in a bleach solution. Older fish were culled according to the Schedule 1 of regulated procedures.

2.2.6.4 High-throughput genotyping

Mutant line *frmpd2*^{sa18532}*+/-* obtained from the Sanger Institute and its new generations created as a result of out-cross of heterozygote carriers to wild-type AB strain as well as homozygous mutant *frmpd2*^{sa18532}*-/-*, created by in-crossing of the *frmpd2*^{sa1853}*+/-* line, required to identify transmitting founder fish and subsequent mutation-bearing individuals by fin-clipping and PCR. The method for high-throughput PCR-based genotyping was adapted from Dr Robert Wilkinson (Wilkinson et al., 2013) and used for both embryos and adult fish. All mutants were genotyped by sequencing.

2.2.6.4.1 Zebrafish anaesthesia

Genotyping of live zebrafish embryos and adult fish required to perform anaesthesia which was conducted in Tricaine solution (stock concentration 4 mg/ml):

a) adult fish: 4.2 ml of Tricaine in 100 ml of aquarium water in the beaker
b) embryos: 0.42 ml of Tricaine in 10 ml of E3 medium in the Petri dish.

2.2.6.4.2 Fin clip

2.2.6.4.2.a Zebrafish larvae

Zebrafish larvae at 3 dpf were anaesthetised in Tricaine solution and watched under a dissecting microscope until they become motionless for more than 10 sec. A single larvae was transferred using a P20 micropipette and cut-off tip on the Petri dish lid overlaid with 2-3 strips of autoclave tape to form a thicker layer

and the lid was placed under the dissecting microscope. Excess E3 medium was removed and the tip of the caudal fin was cut beyond the circulating blood (Figure 2.4, a) with a clean scalpel, perpendicularly to the surface. The fin biopsy with a minimum amount of liquid was transferred using a P20 micropipette into a 0.5 ml PCR tube containing 50 µl of 50 mM NaOH and the fin-clipped embryo was placed into a 12-well plate with fresh E3 medium to recover.

2.2.6.4.2.b Zebrafish adult

Adult zebrafish was immersed in a beaker containing Tricaine solution and watched until the motility gradually decreased. Sedation reached target level when all voluntary movement was lost and fish stayed motionless more than 10 sec. Fish were subsequently lifted out of the anaesthetic with a small metal spoon and oriented in such way that the caudal fin was exposed. The index finger of one hand was placed gently on the fish and using a clean pair of scissors (scissors were first immersed in water, then in 100% ethanol and subsequently dried) the fin was cut in one-third of the whole tail length (Figure 2.4, b). The clipped tail fragment was collected using a clean pair of tweezers and placed into the 0.5 ml PCR tube containing 200 µl of 50 mM NaOH. The fin-clipped fish was placed into a separate tank with fresh aquarium water and monitored until recovered by itself.

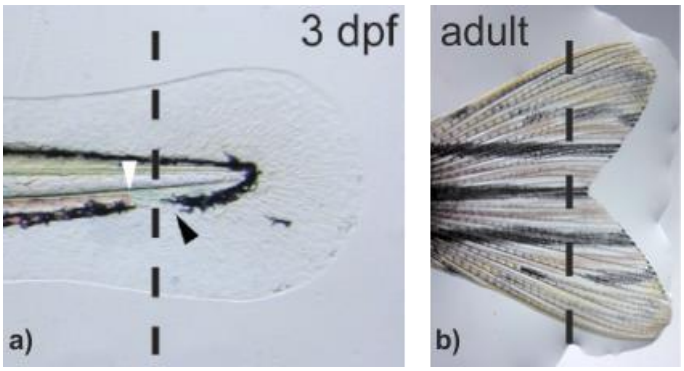

Figure 2.4 Fin transection in zebrafish embryo at 3 dpf and adult fish

(a) Dotted line represents the site of transection at three days post-fertilization (dpf), black arrowhead highlights the pigment gap; white arrowhead, highlights the caudal limit of blood circulation (Wilkinson et al., 2013). (b) Dotted line represents the site of fin transection of adult fish.

2.2.6.4.3 Genomic DNA extraction from tail biopsies

PCR tubes containing fin biopsies from embryos or adult fish were tightly closed and incubated in a PCR machine for 10 – 15 min at 98°C and subsequently cooled down to RT. Once incubation was completed, the DNA mixture was neutralised by adding 1/10 volume of 1M Tris-HCl pH 8.0 to each tube, mixed by pipetting and spun down to clear the DNA solution of any of undissolved particles. At this stage, DNA could be frozen or used directly for further procedures like PCR amplification.

2.2.6.4.4 PCR and sequencing

The genotyping PCR was performed with primers generating DNA fragment around 150 bp and using genomic DNA extracted from tail biopsies as a template. The primers were designed in the way that the mutation site was located in the middle of the amplified DNA fragment. The PCR was performed with *2x ReddyMix PCR Master Mix* and reaction was prepared as indicated in the Table 2.25.

Reaction component	Amount
2x ReddyMix PCR Master Mix	10 µl
template – genomic DNA	2 µl
primer I (forward) (10µM)	1 µl
primer II (reverse) (10µM)	1 µl
H_2O	6 µl

Table 2.25 Genotyping PCR reaction components

Amplification of the DNA fragments was carried out in the thermal cycler with a heated lid using the parameters outlined in the Table 2.26.

Cycle step	Temperature	Time	Cycles
Initial denaturation	95°C	2 min	1
Denaturation	95°C	20 sec	35
Annealing	55°C	20 sec	

Extension	72°C	45 sec	
Final extension	72°C	3 min	1

Table 2.26 Cycling parameters for genotyping PCR reaction

5 µl of PCR reaction was loaded on a 1% agarose gel and amplified DNA fragments were separated by agarose gel electrophoresis (section 2.2.1.2.2). Remaining 15 µl of PCR reactions, along with primer I (forward), were sent for sequencing to the Core Genomic Facility at the University of Sheffield. DNA sequencing was performed using Applied Biosystems' 3730 DNA Analyser.

2.2.6.5 High-resolution *in situ* hybridization to whole-mount zebrafish embryos

Whole-mount in situ hybridization (WISH) allows determining spatial and temporal expression pattern of particular genes in zebrafish embryos and early larvae. The protocol for WISH was adapted from standard method published by Thisse and Thisse (Thisse and Thisse, 2008), modified and improved according to the protocol from Dr Henry H. Roehl lab from MRC Centre for Developmental and Biomedical Genetics at the University of Sheffield.

BUFFERS

Pronase solution stock	10 mg/ml in water
1x PBST	1x PBS, 0.1% Tween 20
PFA	4% PFA, 1x PBS; pH 7.2-7.4
bleaching solution	10% H_2O_2, 5% deionized formamide, 0.5x SSC
Proteinase K stock	10 mg/ml in 1x PBST
HM^+	50% deionized formamide, 5x SSC, 0.1% Tween20, 50 µg/ml heparin, 500 µg/ml RNase-free tRNA pH 6.0 by adding citric acid (460 µl of 1M citric acid solution for 50 ml HM^+)

HM^-	HM^+ without heparin and RNase-free tRNA
20x SSC	3 M NaCl, 0.3 M citric acid trisodium
Blocking solution	2% sheep serum, 2 mg/ml BSA, 1x PBST
Staining solution	100 mM Tris-HCl pH 9.5, 100 mM NaCl, 50 mM $MgCl_2$, 0.1% Tween20
Labeling solution	50 ml staining solution, 225 µl of 50 mg/ml NBT, 175 µl of 50 mg/ml BCIP
Stop solution	1 mM EDTA, 1x PBST

EGG COLLECTION AND CHORIONS REMOVAL

All embryos were obtained by pairwise breeding of individual male and female adult fish as described in section 2.2.6.3. Zebrafish embryos at early developmental stages prior to the hatching period (48 – 72 h) required removal of chorions. Embryos were placed on the Petri dish coated with a layer of solidified 2% agarose in E3 medium to prevent embryos from sticking to the plastic surface. 15 ml of pronase solution at final concentration 2 mg/ml and warmed up to 28.5°C was poured on the embryos and incubated for around 3 min. After incubation, pronase solution was slowly poured out and embryos were rinsed at least five times with water by gentle swirling. Pronase treatment softened chorions which were removed completely during following washes.

EMBRYO FIXATION AND DEHYDRATATION

Dechorionated embryos and embryos after hatching period at the appropriate developmental stage were collected in a 2.0 ml tube (10 – 15 embryos per tube). Excess of E3 medium was removed and embryos were fixed in freshly prepared or beforehand frozen 4% PFA in 1x PBS overnight at 4°C. The next day embryos were rinsed twice with 1x PBST and gradually dehydrated in successive dilutions of methanol in 1x PBST with gentle agitation: 25% (vol/vol) methanol, 50% (vol/vol) methanol, 75% (vol/vol) methanol and 100% (vol/vol) methanol for 10

min at RT. Embryos were stored in 100% methanol at -20°C until the procedure was continued.

IN SITU DAY 1

REHYDRATATION AND BLEACHING

Embryos were rehydrated gradually in successive dilutions of methanol in 1x PBST with gentle agitation: 75% (vol/vol) methanol, 50% (vol/vol) methanol, 25% (vol/vol) methanol and subsequently were washed four times with 1x PBST for 10 min at RT. Rehydrated embryos at the stage 24 hpf and older required depigmentation which was performed in bleaching solution for 30 min with gentle mixing at 10 min intervals at 37°C. After incubation, depigmented embryos were washed five times with 1x PBST for 10 min at RT.

PERMEABILIZATION

Embryos permeabilization was performed by digestion with proteinase K in 1x PBST at a final concentration 10 μg/ml at RT. Permeabilization allows the RNA probe to penetrate and its duration depended on embryo developmental stage as shown in the Table 2.27.

Developmental stage	Duration of proteinase K (10 μg/ml) treatment
1 cell – 1 somite stage	30 sec
1 – 8 somite stage	1 min
9 – 18 somite stage	3 min
18 somite – 24 somite stage	10 min
24 hpf	15 min
36 – 48 hpf	30 min
3 dpf	50 min

Table 2.27 Duration of proteinase K treatment for different zebrafish embryonic stages

Proteinase K digestion was stopped by fixing embryos in freshly prepared or beforehand frozen 4% PFA in 1x PBS for 20 min at RT. After fixation embryos were washed four times with 1x PBST for 10 min at RT.

HYBRIDIZATION

Permeabilized embryos were prehybridized in 500 µl of HM^+ solution for 3 h at 70°C in a water bath or a dry heat block set up at the diagonal position. HM^+ was discarded and replaced with fresh 200 µl HM^+ solution pre-warmed to 70°C and containing 450 ng of sense or antisense DIG-labelled RNA probe. Zebrafish embryos were hybridised overnight at 70°C.

IN SITU DAY 2

WASHING

All washes at 70°C were performed with pre-warmed to 70°C solutions and continued in a water bath or dry heat block set up at the diagonal position.

The hybridization solution was discarded and embryos were washed with HM^- solution for 15 min. Subsequently HM^- was gradually changed to 2x SSC through a series of 15 min washes at 70°C in successive dilutions of HM^- in 2x SSC solution: 75% HM^-, 50% HM^-, 25% HM^- and 100% of 2x SSC. Embryos were washed twice with 0.2x SSC for 45 min at 70°C and subsequently cooled to RT. 0.2x SSC was gradually changed to 1x PBST through a series of 15 min washes at RT in successive dilutions of 0.2x SSC in 1x PBST with gentle agitation: 75% 0.2x SSC, 50% 0.2x SSC, 25% 0.2x SSC and 100% of 1x PBST.

BLOCKING AND INCUBATION WITH ANTIBODY

Extensive washing of embryos was followed by incubation in the blocking solution for 3 h at RT with gentle agitation. Subsequently, embryos were incubated with anti-DIG antibody conjugated to alkaline phosphatase diluted at 1:10 000 in the blocking solution overnight at 4°C with gentle agitation.

IN SITU DAY 3

WASHING

The next day, antibody solution was discarded and embryos were briefly washed with 1x PBST at RT. Washing with 1x PBST was continued for next 1.5 h with 15 min intervals at RT with gentle agitation.

STAINING

Excess of 1x PBST was removed and embryos were washed twice with a staining solution for 10 min at RT. The staining solution was discarded and replaced with freshly prepared labelling solution containing a substrate for alkaline phosphatase. Staining was performed at RT or overnight 4°C in the dark and reaction colour was monitored periodically using a dissecting microscope. Embryos were placed in a spot plate and they were observed every 15 min until desired staining intensity was reached. The reaction was terminated by rinsing embryos three times with stop solution for 15 min at RT.

WASHING AND METHANOL CLEARING

Embryos were fixed in freshly prepared or beforehand frozen 4% PFA in 1x PBS for 20 min at RT and subsequently washed three times in 1x PBST for 10 min at RT with gentle agitation. The staining background was removed by progressive washing with successive dilutions of methanol in 1x PBST as described in paragraph EMBRYOS FIXATION AND DEHYDTRATATION. Embryos were subsequently incubated in 100% methanol for 2 h at RT with gentle agitation during which the colour of stained embryos changed from purple to blue and background became brighter. Washing with reversed methanol dilutions was performed as described in paragraph REHYDRATATION AND BLEACHING and embryos were washed 3 more times with 1x PBST for 10 min at RT.

MOUNTING AND IMAGING

Excess of the solution was discarded, embryos were mounted first in 50% glycerol for 15 min at RT and subsequently in 100% glycerol. Embryos were stored in the dark at RT and imaged using Nikon stereomicroscope with Nikon DS-Fi1 colour camera and Nikon Element software.

CHAPTER 3 - Identifying interacting partners of FRMPD2 protein

3.1 Introduction

All biological processes that drive cellular machinery in the living cell are regulated at various levels including gene expression, protein modification and interactions. The latter create large cellular networks that are very similar in all cells. It has been estimated that over 80% of proteins do not operate alone but in complexes (Berggard et al., 2007), therefore identifying new protein-protein interactions can advance our understanding of unidentified protein functions within the cell and how these proteins form interacting modules and molecular networks. Recent tremendous expansion of the protein-protein interaction maps has been fuelled by powerful biochemical and genetic techniques enabling to perform large-scale studies. Protein-protein interaction networks can be generated using many innovative methods like yeast two-hybrid screen (Y2H) combined with computational approaches (Vinayagam et al., 2011), high-throughput Affinity-Purification Mass Spectrometry (AP-MS) (Huttlin et al., 2015), Tandem Affinity Purification (TAP) combined with mass spectrometry (Gavin et al., 2002, Gavin et al., 2006, Krogan et al., 2006) or recently developed proximity-dependent biotinylation (BioID) (Roux et al., 2012). Although many new protein interactions have been predicted using those approaches, all of them are characterised by some advances and limitations.

The yeast two-hybrid screen is a very useful tool to detect many protein interactions on a genome-wide scale but simultaneously this technique is limited by high positive and false negative rates and cannot be used to identify multiprotein complexes. Some types of protein interactions can be missed in Y2H due to required post-translational modifications and protein self-activation (Bruckner et al., 2009). Also, the AP-MS method may be limited by several factors like protein expression level, abnormal folding or inappropriate intracellular localisation of overexpressed bait protein and stringency of the washes used to reduce nonspecific binding of contaminating proteins. Problems with the identification of transient or weak interactions using conventional techniques

were recently overcome by the newly developed BioID method (Roux et al., 2012). This approach uses the ability of a mutated form of biotin ligase enzyme BirA*, fused to the protein of interest, to promiscuously biotinylate proteins in the closest neighbourhood. The addition of exogenous biotin allows to label vicinal proteins which are purified from the cell extracts by streptavidin and later identified by mass spectrometry (MS). The BioID method uses proximity-dependent biotinylation, therefore, obtained MS results show direct or indirect interactions in the surrounding neighbourhood of the protein of interest (Varnaite and MacNeill, 2016). Nevertheless the BioID method was successfully used in several studies exploring interaction networks of e.g. nuclear pore complex (Kim et al., 2014), centrosome (Comartin et al., 2013), Hippo signalling pathway (Couzens et al., 2013) and cell junctions in mammalian cells (Van Itallie et al., 2013, Van Itallie et al., 2014, Fredriksson et al., 2015) and all promising interactions were further validated using different methods like co-IP or colocalization assays using microscopy.

To study protein-protein interactions of our protein of interest, FRMPD2, we decided to validate promising interactions obtained from a Y2H screen and Affinity Purification Mass Spectrometry, performed by former members of Dr Kai Erdmann laboratory. Selection of protein candidates from the screens was targeted and aimed to characterise components of the FRMPD2-mediated protein complex with respect to signalling and membrane trafficking in epithelial cells relevant to inflammatory bowel disease, epithelial cell polarisation and actin cytoskeleton dynamics. We chose five potential interacting partners: BANK1 (*B-cell Scaffold Protein with Ankyrin Repeats*) was selected due to the fact that it is a known susceptibility gene for psoriasis, a disease very often associated with Crohn's disease (Zhang et al., 2011); SEPTIN10, Filamin B and Plectin-1 are known to be connected with the actin cytoskeleton, therefore their potential interactions with FRMPD2 would give a new insight into FRMPD2 role as a cytoskeleton regulator; and finally, RAPGEF2 protein, which plays versatile roles in epithelial polarisation and its potential interaction with FRMPD2 would help to elucidate new functions of FRMPD2 in epithelial polarity.

Initial Y2H screen was performed with human kidney cDNA library and the KIND domain, the FERM domain and PDZ1-3 domains of FRMPD2 (unpublished data by Christian Fetzer, Erdmann laboratory). Subsequent Y2H screens with an individual domains confirmed that potential new interaction partners indicated affinity to particular domains of FRMPD2 (unpublished data by Nina Stenzel, Erdmann laboratory). BANK1 specifically interacted with the FERM domain of FRMPD2 (Figure 3.1) while SEPTIN10 was found to interact with the FERM domain of FRMPD2 and PTP-BL (Figure 3.2), another protein related to FRMPD2. It has been shown that Filamin B (fragment corresponding to the length of 750 bp) interacts with FERM and PDZ1-3 domains of FRMPD2 although the signal with the PDZ1-3 domain was much weaker than with the FERM domain itself (Figure 3.3). Another potential protein candidate, RAPGEF2 (*Rap guanine nucleotide exchange factor 2*), was found as one of the hits interacting with the PDZ2 domain of FRMPD2 (data not shown). Among the hits obtained from AP-MS (performed by Mass Spectrometry Facility at University of Bochum) using MDCKII stable cell line expressing GFP and GFP-FRMPD2, was Plectin-1, which was characterised by one of the highest scores (data not shown) and was selected for further validation studies.

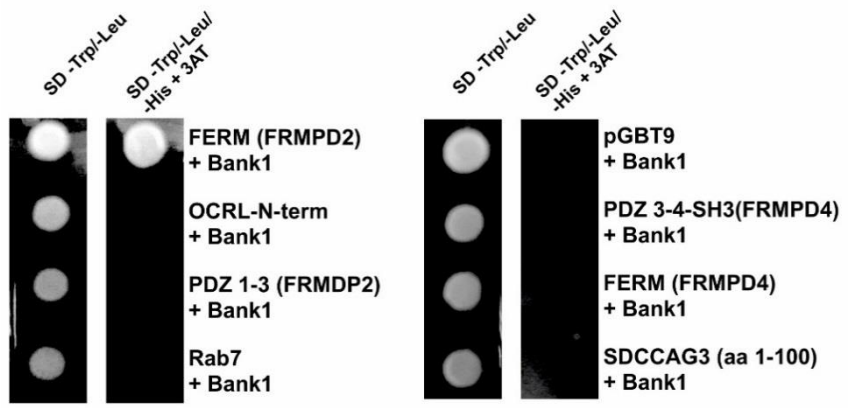

Figure 3.1 Y2H analysis of interaction between BANK1 and the FERM domain of FRMPD2

FERM domain of FRMPD2, N-terminus of OCRL, PDZ1-3 domains of FRMPD2, Rab7, PDZ3-4 plus SH3 domains of FRMPD4, FERM domain of FRMPD4 and SDCCAG3 (aa 1-100) were separately cloned into the vector pGBT9 and BANK1 was cloned into a pGAD vector. The constructs were co-transformed into a YRG2 yeast strain. Each transformed yeast strain was assayed on the plates with the indicated media. Unpublished data by Nina Stenzel, Erdmann lab.

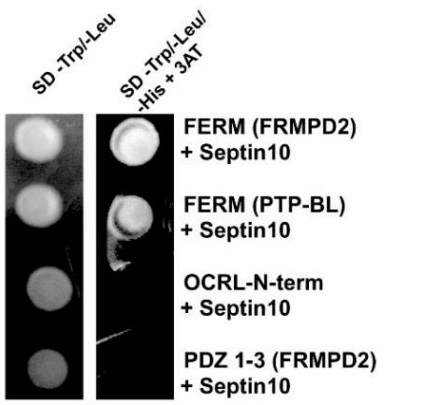

Figure 3.2 Y2H analysis of interaction between SEPTIN10 and the FERM domain of FRMPD2

FERM domain of FRMPD2, FERM domain of PTP-BL, N-terminus of OCRL, PDZ1-3 domains of FRMPD2 were separately cloned into the vector pGBT9 and SEPTIN10 was cloned into a pGAD vector. The constructs were co-transformed into a YRG2 yeast strain. Each transformed yeast strain was assayed on the plates with the indicated media. Unpublished data by Nina Stenzel, Erdmann lab.

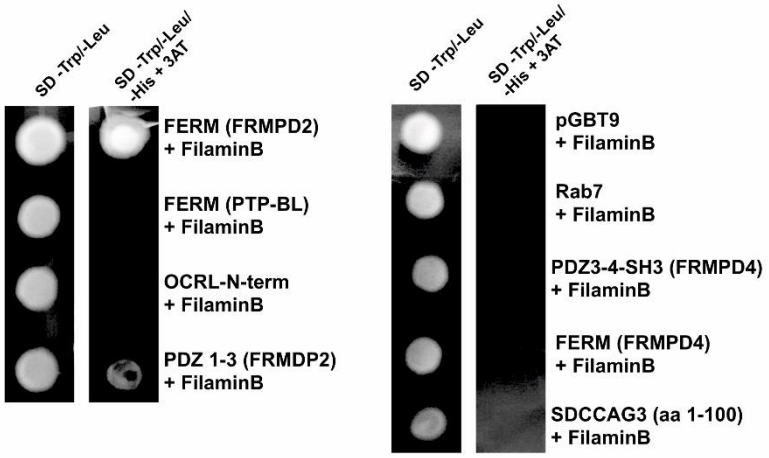

Figure 3.3 Y2H analysis of interaction between Filamin B and the FERM domain of FRMPD2

FERM domain of FRMPD2, FERM domain of PTP-BL, N-terminus of OCRL, PDZ1-3 domains of FRMPD2, Rab7, PDZ3-4 plus SH3 domains of FRMPD4, FERM domain of FRMPD4 and SDCCAG3 (aa 1-100) were separately cloned into the vector pGBT9 and 750 bp fragment of Filamin B was cloned into a pGAD vector. The constructs were co-transformed into a YRG2 yeast strain. Each transformed yeast strain was assayed on the plates with the indicated media. Unpublished data by Nina Stenzel, Erdmann lab.

Although previously performed screens provided a substantial number of potential protein candidates, to have a broader view on the FRMPD2 interactome and explore further its potential functions in epithelial polarisation, we also decided to apply proximity-dependent biotinylation.

3.2 Aim

The aim of experiments performed within this chapter was to validate potential interaction partners discovered by the Y2H screen and AP-MS, mentioned in the introduction part to this chapter. Furthermore, the idea was to characterise in more detail FRMPD2-mediated protein complex using recently developed innovative techniques combined with MS. To verify potential protein-protein interactions and to explore the FRMPD2 interactome the following approaches were used:

1. co-immunoprecipitation with various types of commercially available resins and antibodies
2. proximity-dependent biotin identification, BioID, using MDCK II stable cell line expressing myc-tagged BirA*FRMPD2.

3.3 Results

3.3.1 Validating Yeast Two-Hybrid screen and Mass Spectrometry results

Validation of all potential protein candidates, identified either by Y2H screen or Mass Spectrometry, was conducted using a co-immunoprecipitation approach. Cells were single transfected with GFP- or myc-tagged expression constructs or co-transfected with differentially tagged two expression constructs of potentially interacting partners. Subsequently, tagged proteins were immunoprecipitated by the GFP or c-myc antibodies immobilised to the agarose beads and Western Blot analysis was performed using antibodies against endogenously expressed or overexpressed tagged proteins.

3.3.1.1 FRMPD2 interaction with BANK1 and SEPTIN-10

Originally interaction between FRMPD2 and BANK1 or SEPTIN-10 was detected by Y2H screen using the FERM domain of FRMPD2 as a bait and human adult kidney cDNA as a prey library. To validate these two interactions we performed co-immunoprecipitation assays using the FERM domain of FRMPD2 and myc-tagged full-length protein candidates. Both experiments were conducted simultaneously and Western Blot analysis showed that GFP-FERM was efficiently

precipitated on the *GFP-Trap®_A* beads (Figure 3.4 and 3.5, lower panel). Subsequently, the samples were blotted with c-myc antibody, that revealed immunoprecipitation of myc-BANK, but not myc-SEPTIN-10, with GFP-tagged FERM domain (Figure 3.4 and 3.5, upper panel).

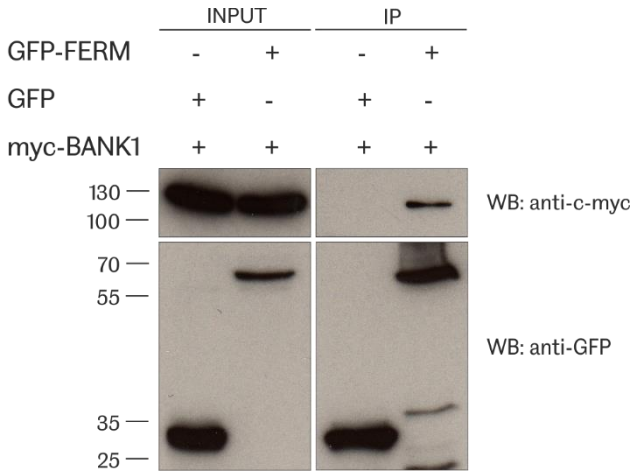

Figure 3.4 myc-BANK1 interacts with GFP-tagged FERM domain of FRMPD2

HEK293 cells were transiently co-transfected with expression constructs of myc-tagged BANK1 and GFP or GFP-tagged FERM domain of FRMPD2. 48 hours post-transfection cell lysates were collected and co-immunoprecipitation was conducted using GFP-Trap®_A. Fusion proteins were detected by Western Blot using anti-c-myc and anti-GFP antibody followed by secondary HRP antibody Input represents around 2% of the total cell lysate. (N=2)

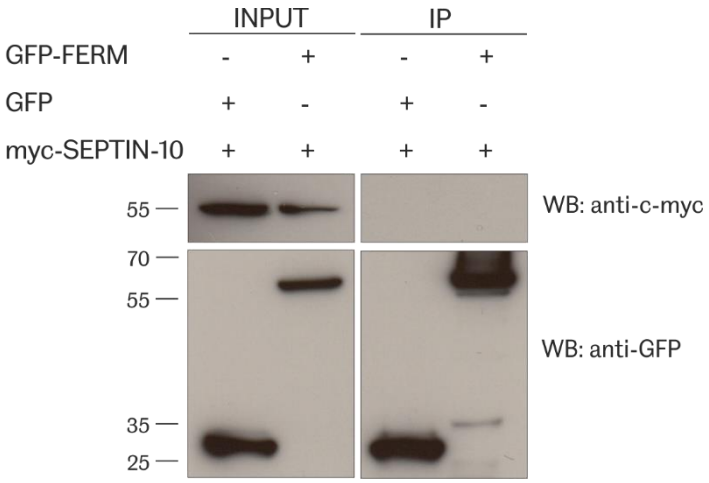

Figure 3.5 myc-SEPTIN-10 does not co-immunoprecipitate with GFP-tagged FERM domain of FRMPD2

HEK293 cells were transiently co-transfected with expression constructs of myc-tagged SEPTIN-10 and GFP or GFP-tagged FERM domain of FRMPD2. 48 hours post-transfection cell lysates were collected and co-immunoprecipitation was conducted using GFP-

Trap®_A. Fusion proteins were detected by Western Blot using anti-c-myc and anti-GFP antibody followed by secondary HRP antibody. Input represents around 2% of the total cell lysate. (N=2)

Further attempts to validate both interactions demonstrated that neither BANK1 nor SEPTIN-10 interacts with full-length FRMPD2 when co-expressed together in HEK293 cells (Figure 3.6), however, low expression level of myc-tagged FRMPD2 in total cell lysate could also affect its detection in pulldown samples. On the other hand, endogenous FRMPD2 was immuno-isolated with GFP-BANK1, but not with GFP-SEPTIN-10 (Figure 3.7), confirming the interaction between FRMPD2 and BANK1.

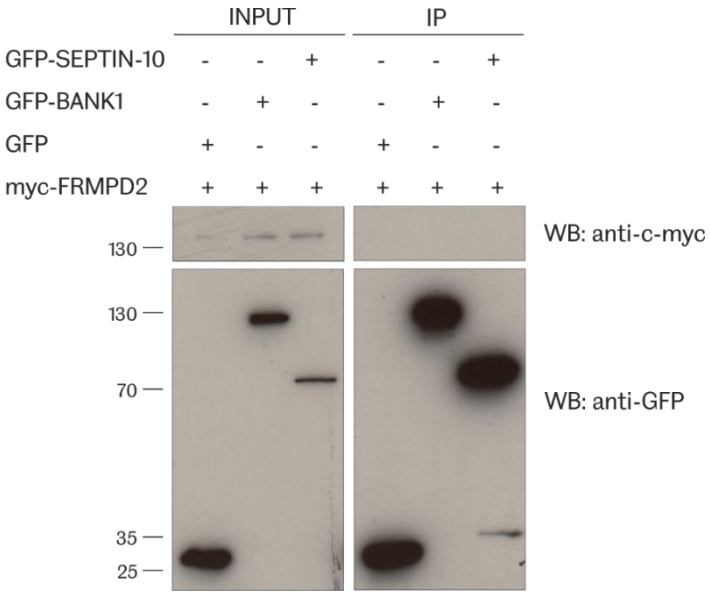

Figure 3.6 GFP-tagged BANK1 and SEPTIN-10 are not detected as interacting partners of myc-tagged FRMPD2

HEK293 cells were transiently co-transfected with expression constructs of myc-tagged FRMPD2 and GFP or GFP-tagged BANK1 or GFP-tagged SEPTIN-10. 48 hours post-transfection cell lysates were collected and co-immunoprecipitation was conducted using GFP-Trap®_A. Fusion proteins were detected by Western Blot using anti-c-myc and anti-GFP antibody followed by secondary HRP antibody. Input represents around 2% of the total cell lysate. (N=2)

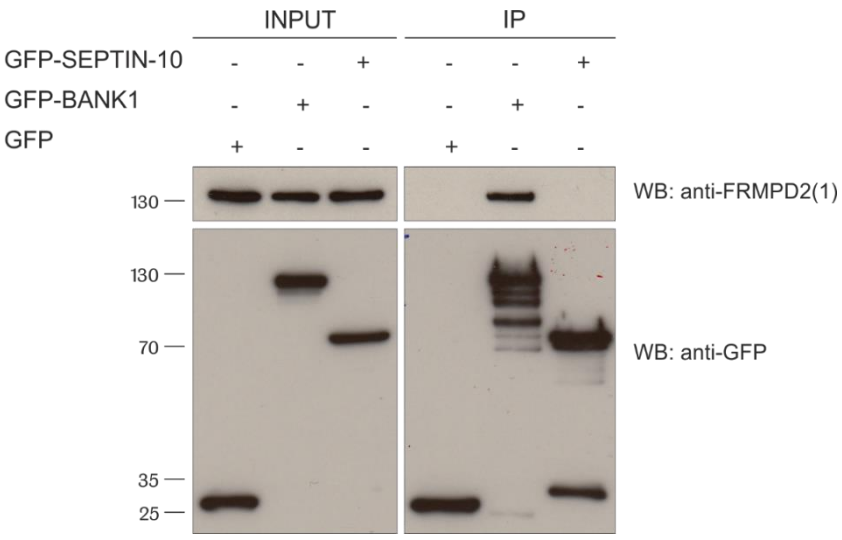

Figure 3.7 GFP-tagged BANK1 co-immunoprecipitates endogenous FRMPD2

HEK293 cells were transiently transfected with expression constructs of GFP or GFP-tagged BANK1 or GFP-tagged SEPTIN-10. 48 hours post-transfection cell lysates were collected and co-immunoprecipitation was conducted using GFP-Trap®_A. Fusion proteins and endogenous proteins were detected by Western Blot using anti-GFP and anti-FRMPD2(1) antibody respectively. Input represents around 2% of the total cell lysate. (N=2)

3.3.1.2 FRMPD2 interaction with FILAMIN B

Similarly to Y2H screen, validation of the interaction between FRMPD2 and FILAMIN B was performed using constructs containing FRMPD2 domains and a fragment of FILAMIN B consisting of 250 aa. All GFP-tagged proteins were efficiently precipitated on the *GFP-Trap®_A* beads, but unfortunately, none of them precipitated myc-tagged FILAMIN $B_{2041\text{-}2290}$ (Figure 3.8). To test whether the predicted FILAMIN B fragment shows an affinity to the full-length FRMPD2, two additional co-IP experiments were conducted. In both cases, Western Blot analysis revealed that neither full length transfected (Figure 3.9) nor endogenous FRMPD2 (Figure 3.10) interacted with FILAMIN $B_{2041\text{-}2290}$. Thus, obtained data suggested that FILAMIN B may not interact with FRMPD2. All experiments validating the interaction between FRMPD2 and FILAMIN $B_{2041\text{-}2290}$ were conducted together with co-IP assays between FRMPD2 and BANK1, which served here as a positive control.

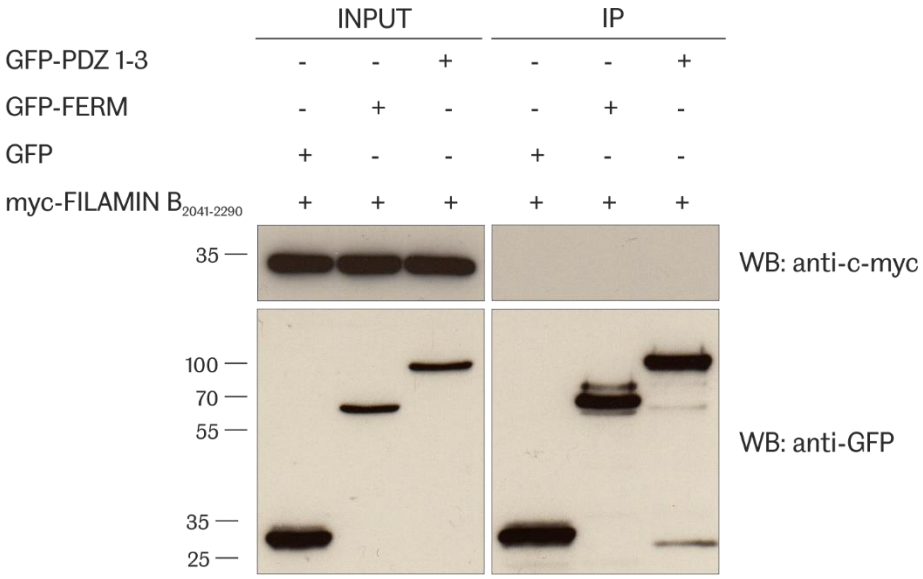

Figure 3.8 myc-FILAMIN B interacts with none of the FRMPD2 domains

HEK293 cells were transiently co-transfected with expression constructs of myc-tagged FILAMIN $B_{2041-2290}$ and GFP or GFP-tagged FERM domain or GFP-tagged PDZ 1-3 domains of FRMPD2. 48 hours post-transfection cell lysates were collected and co-immunoprecipitation was conducted using GFP-Trap®_A. Fusion proteins were detected by Western Blot using anti-c-myc and anti-GFP antibody followed by secondary HRP antibody. Input represents around 2% of the total cell lysate. (N=2)

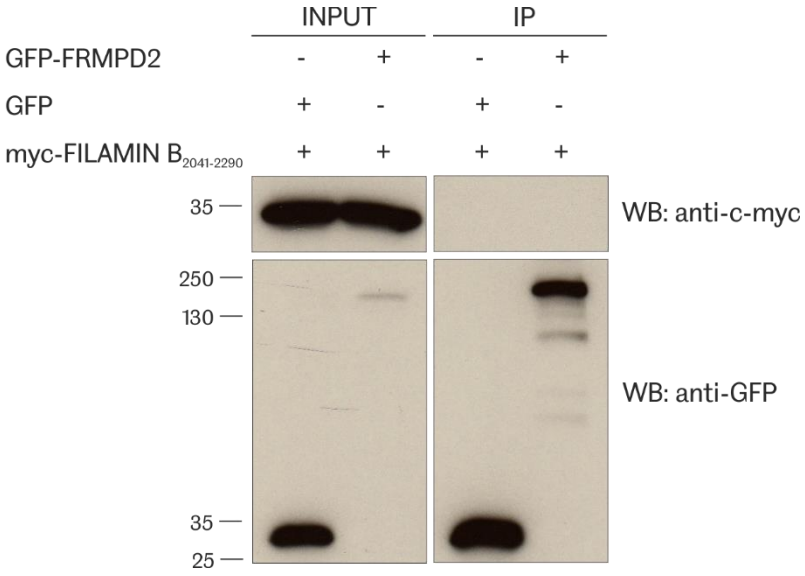

Figure 3.9 myc-FILAMIN B does not co-immunoprecipitate with GFP-tagged FRMPD2

HEK293 cells were transiently co-transfected with expression constructs of myc-tagged FILAMIN $B_{2041-2290}$ and GFP or GFP-tagged FRMPD2. 48 hours post-transfection cell lysates were collected and co-immunoprecipitation was conducted using GFP-Trap®_A. Fusion proteins were detected by Western Blot using anti-c-myc and anti-GFP antibody followed by secondary HRP antibody. Input represents around 2% of the total cell lysate. (N=2)

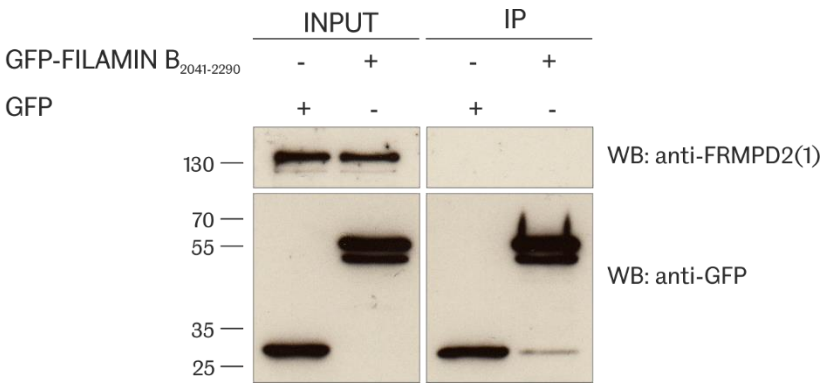

Figure 3.10 Endogenous FRMPD2 does not co-immunoprecipitate with GFP-tagged FILAMIN $B_{2041-2290}$

HEK293 cells were transiently transfected with expression constructs of GFP or GFP-tagged FILAMIN $B_{2041-2290}$. 48 hours post-transfection cell lysates were collected and co-immunoprecipitation was conducted using GFP-Trap®_A. Fusion proteins and endogenous proteins were detected by Western Blot using anti-GFP and anti-FRMPD2(1) antibody respectively followed by secondary HRP antibody. Input represents around 2% of the total cell lysate. (N=2)

3.3.1.3 FRMPD2 interaction with RAPGEF2

RAPGEF2 was found as one of the potential interacting partners of FRMPD2 showing affinity to its PDZ2 domain. To further validate this interaction two co-IP experiments, between overexpressed GFP-RAPGEF2 and myc-FRMPD2, were performed. In the first attempt, GFP-RAPGEF2 was precipitated on the *GFP-Trap®_A* beads and the samples analysed by Western Blot using anti-c-myc antibody revealed that myc-FRMPD2 was efficiently immunoprecipitated with the protein candidate, but not with GFP itself (Figure 3.11). The second co-IP was conducted in a very similar way but Protein A-agarose resin with coupled c-myc antibody was used instead of *GFP-Trap®_A* beads. myc-FRMPD2 was efficiently trapped by the antibody and Western Blot analysis showed that also this time GFP-RAPGEF2 was precipitated with myc-FRMPD2 (Figure 3.12), although the signal of GFP-RAPGEF2 in pulldown sample was much weaker in comparison to the first co-IP experiment. This may be explained by the fact that in the second experiment binding between proteins could hinder access to the antibody binding site. This would result in the reduced detection level of GFP-RAPGEF2 in the pulldown sample, while detection in input samples was comparable between two experiments.

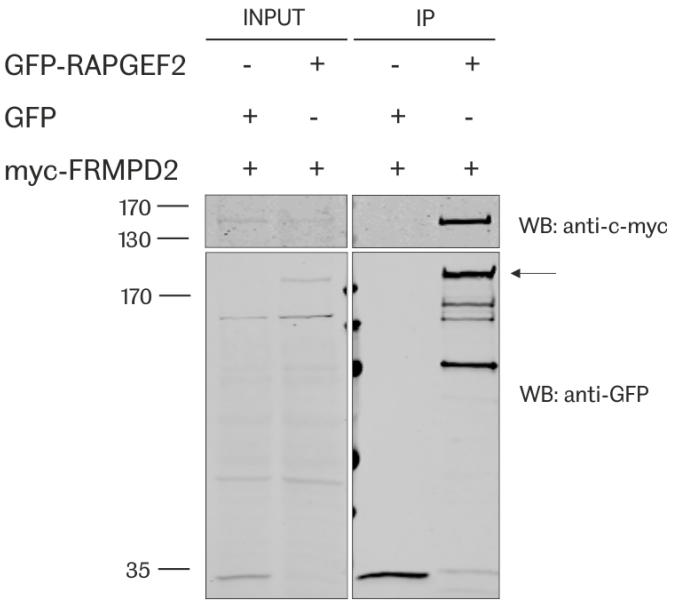

Figure 3.11 myc-FRMPD2 interacts with GFP-tagged RAPGEF2

HEK293 cells were transiently co-transfected with expression constructs of GFP or GFP-tagged RAPGEF2 and myc-tagged FRMPD2. 48 hours post-transfection cell lysates were collected and co-immunoprecipitation was conducted using GFP-Trap®_A. Fusion proteins were detected by Western Blot using anti-c-myc and anti-GFP antibody followed by anti-rabbit Alexa Fluor® 680 and anti-mouse DyLight™ 800 antibody respectively. Input represents around 2% of the total cell lysate. The right size of the GFP-RAPGEF2 was indicated by the arrow. (N=2)

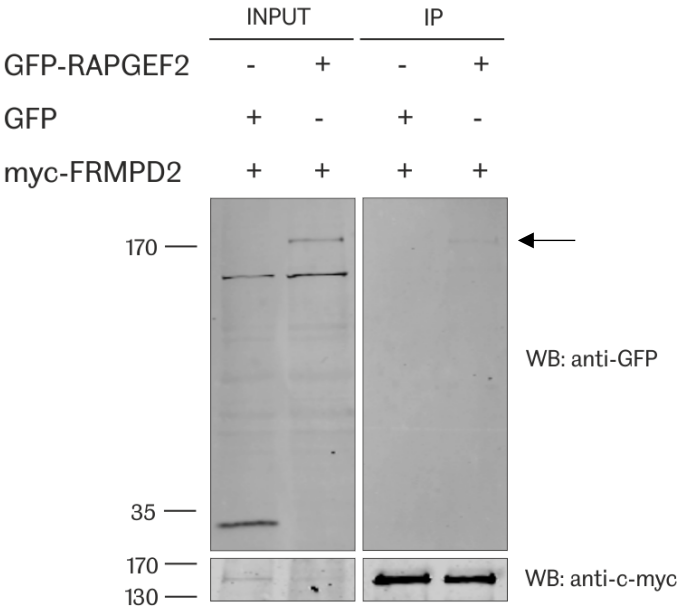

Figure 3.12 GFP-tagged RAPGEF2 co-immunoprecipitates with myc-FRMPD2

HEK293 cells were transiently co-transfected with expression constructs of myc-tagged FRMPD2 and GFP or GFP-tagged RAPGEF2. 48 hours post-transfection cell lysates were collected and co-immunoprecipitation was conducted using Protein A-agarose resin with coupled c-myc antibody. Fusion proteins were detected by Western Blot using anti-c-myc

and anti-GFP antibody followed by anti-rabbit Alexa Fluor® 680 and anti-mouse DyLight™ 800 antibody respectively. Input represents around 2% of the total cell lysate. The right size of the GFP-RAPGEF2 was indicated by the arrow. (N=2)

3.3.1.4 FRMPD2 interaction with PLECTIN-1

Plectin-1 was one of the potential interacting partners of FRMPD2 protein found by Affinity Purification-Mass Spectrometry. A co-IP experiment was performed with GFP and GFP-FRMPD2 overexpressed in HEK293 cells to confirm the interaction. GFP-tagged proteins were precipitated on *GFP-Trap®_A* beads and samples were subsequently blotted with the anti-Plectin-1 antibody. Western Blot analysis revealed that Plectin-1 was precipitated with both GFP and GFP-FRMPD2, although the amount of precipitated Plectin-1 by GFP itself was considerably smaller than with GFP-FRMPD2 (Figure 3.13). Detection of Plectin-1 in the control sample could be also explained by the fact that there was a considerably large amount of precipitated GFP in comparison to GFP-FRMPD2. The same result was obtained twice and although the number of washings in the co-IP protocol was increased, Plectin-1 was still precipitated by GFP protein. Due to its high molecular weight of around 500 kDa, Plectin-1 was quite hard to detect using standard protein transfer conditions. Although a few different protocols for protein transfer were tested (transfer buffer with 20% methanol, transfer buffer with 10% methanol and SDS, transfer buffer without methanol and with SDS), Plectin-1 was detected only when *Trans-Blot® Turbo™ Transfer System* and *Bio-Rad* preprogrammed protocol HIGH MW were applied, however not always we were able to detect Plectin-1 in the total cell lysate. Hence, those two factors – unrepeatable protein transfer and non-specific binding to GFP protein, made it impossible to come to a clear conclusion whether Plectin-1 interacts with FRMPD2.

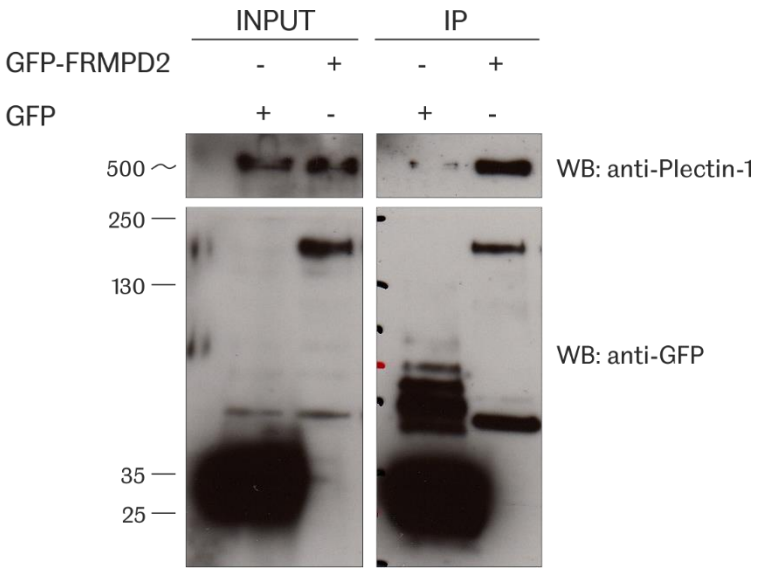

Figure 3.13 Plectin-1 co-immunoprecipitates with GFP and GFP-tagged FRMPD2

HEK293 cells were transiently transfected with expression constructs of GFP or GFP-tagged FRMPD2. 48 hours post-transfection cell lysates were collected and co-immunoprecipitation was conducted using GFP-Trap®_A. Fusion proteins and endogenous proteins were detected by Western Blot using anti-GFP and anti-Plectin-1 antibody respectively followed by secondary HRP antibody. Input represents around 2% of the total cell lysate. (N=2)

3.3.2 Generating and testing BirA*FRMPD2 using BioID approach

To identify new FRMPD2-associated proteins and to define further the FRMPD2 protein interaction network, we took advantage of recently developed BioID approach (Roux et al., 2012), which identifies protein candidates adjacent to and/or interacting with the protein of interest. Full-length human FRMPD2 was amplified by standard PCR, using available in the lab pcDNA3-GFP-FRMPD2 vector, and subsequently cloned within the vector pcDNA3.1-mycBioID at the 3' end of the tag myc-BirA* (Figure 3.14).

Figure 3.14 Schematic representation of myc-BirA*-FRMPD2 construct

The construct contains N-terminal myc tag fused to BirA gene containing the R118G mutation (highly promiscuous form), KIND (kinase non-catalytic C-lobe) domain, FERM (Four-point-one, ezrin, radixin, moesin) domain and three PDZ (PSD95/Dlg/ZO1-homologous peptide-binding) domains.*

Before proceeding to the appropriate experiments on polarised epithelial cells, initial trials were performed in non-polarised HEK293 epithelial cells. To examine the subcellular localisation of myc-BirA* and newly generated myc-BirA*-FRMPD2, the two corresponding constructs were transiently transfected into HEK293 cells and 48 hours post transfection immunofluorescence analysis was performed. Staining with anti-c-myc antibody revealed that myc-BirA* was found predominantly in the cytoplasm and nucleus and was characterised by a punctate staining, while when fused with FRMPD2, myc-BirA* was showing a specific pattern suggesting membrane localisation (Figure 3.15). Such localisation of myc-BirA*FRMPD2 was in line with previously published data demonstrating membrane localisation of both endogenous and overexpressed myc- and GFP-tagged FRMPD2 (Stenzel et al., 2009).

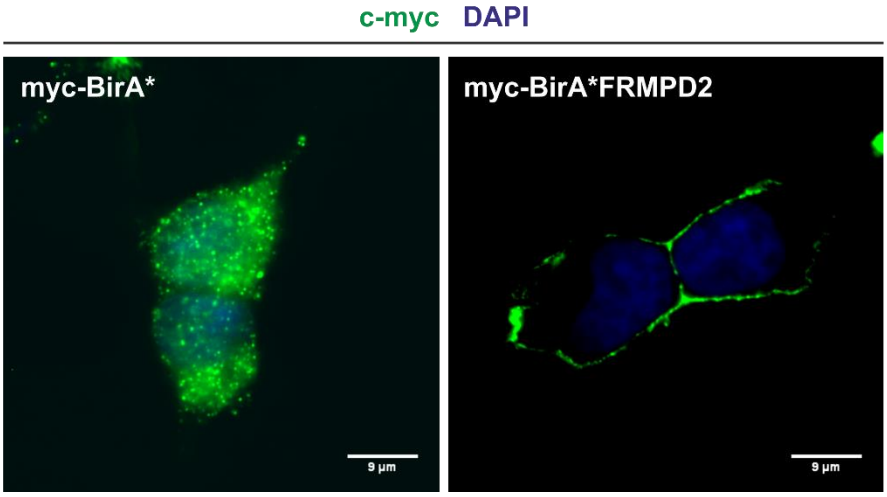

Figure 3.15 myc-BirA*FRMPD2 is localised to the plasma membrane of HEK293 cells

HEK293 cells grown on coverslips were transiently transfected with myc-BirA and myc-BirA*-FRMPD2 constructs. The cells were fixed and stained with primary anti-c-myc mouse antibody followed by secondary anti-mouse Alexa Fluor® 488. Images were taken using a spinning disc confocal microscope. Scale bar represents 9 µm.*

The second step of preliminary analysis aimed to test the ability of BirA* to promiscuous biotinylation of proteins. To this end HEK293 cells, transiently expressing myc-BirA* and myc-BirA*-FRMPD2 were incubated with and without 50 µM biotin for 24 hours. Cell lysates were prepared and all biotinylated endogenous proteins were purified using streptavidin agarose beads as described before (Chapter 2, sections 2.2.2.1.2 and 2.2.2.1.3). Immunoblotting with anti-c-myc antibody revealed bands at around 37 kDa and 180 kDa

corresponding to myc-BirA* and myc-BirA*-FRMPD2 respectively. Both proteins were also successfully purified on streptavidin agarose beads from the samples incubated with 50 μM exogenous biotin (Figure 3.16, upper panel). Labelling efficiency by biotin and streptavidin-mediated pulldown was assessed by immunoblotting with streptavidin HRP. In the absence of exogenous biotin only a few bands were detected in the pulldown samples (higher exposure, data not shown), while the presence of 50 μM biotin effectively stimulated biotinylation of endogenous proteins by BirA* enzyme. In the case of myc-BirA*-FRMPD2 sample incubated with exogenous biotin, proteins were also successfully biotinylated but to a lesser extent than by myc-BirA* itself (Figure 3.16, lower panel). A smaller fraction of proteins biotinylated by myc-BirA*-FRMPD2 in comparison to control sample could suggest that biotinylation was more specific and restricted to myc-BirA*-FRMPD2 subcellular localisation (Figure 3.15). It also can prove the main concept of the BioID method that only proteins accumulated in the closest vicinity are biotinylated and biotinylation is strongly restricted to the localisation of the overexpressed protein. Overall preliminary experiments performed in HEK293 cells suggested, that myc-BirA*-FRMPD2 showed correct subcellular localisation and is capable of biotinylated endogenous proteins in mammalian cells.

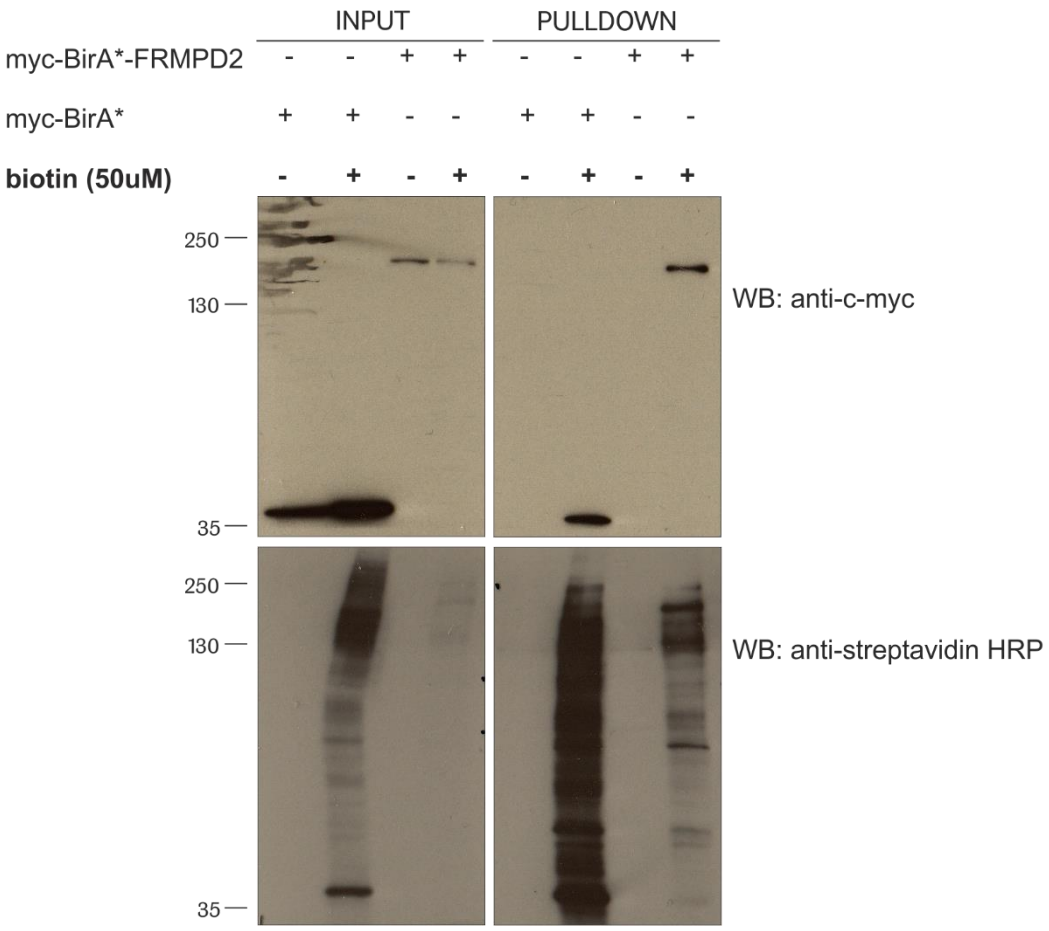

Figure 3.16 myc-BirA* and myc-BirA*-FRMPD2 promiscuously biotinylate proteins in HEK293 cells

HEK293 cells were transiently transfected with myc-BirA or myc-BirA*-FRMPD2 constructs. 24 hours post transfection cells were incubated without (-) or with (+) 50 µM biotin for another 24 hours. Cell lysates were prepared and pulldown experiment was conducted using streptavidin beads. Fusion proteins were detected by Western Blot using anti-c-myc and followed by anti-mouse HRP antibody. Biotinylation efficiency was tested by immunoblotting using streptavidin HRP antibody. Input represents around 2% of the total cell lysate. (N=2)*

3.3.2.1 Generation of BirA* and BirA*FRMPD2 stable cell lines

Characterization of the FRMPD2-mediated protein complex with respect to epithelial cell polarisation required experiments using suitable cell lines. In general, cell lines with retained polarisation properties like Caco-2 or MDCK II cells are difficult to transfect using standard protocols adapted for HEK293 or HeLa cells. However, literature review and consultation with Dr Gordon Cooper (Department of Biomedical Science, University of Sheffield, United Kingdom) resulted in the establishment of a new transfection protocol for MDCK II cells (Chapter 2, Table 2.24). Transient transfection of MDCK II cells didn't guarantee

satisfactory expression level of desired proteins, therefore to provide controllable and high expression level of myc-BirA* and myc-BirA*-FRMPD2 proteins, MDCK II stable cell lines were generated as described in Chapter 2 and section 2.2.3.7. All selected clones were screened by Western Blot using anti-myc and anti-FRMPD2(5) antibody. FRMPD2(5) antibody was used to verify the signal obtained from immunoblotting with an anti-c-myc antibody (Figure 3.17). The presence of overexpressed proteins was confirmed by comparison to non-transfected MDCK II cells, while the correct size of all transfectants was compared to two control samples C1 and C2, corresponding to transiently transfected MDCK II cells overexpressing myc-BirA* and myc-BirA*FRMPD2 respectively.

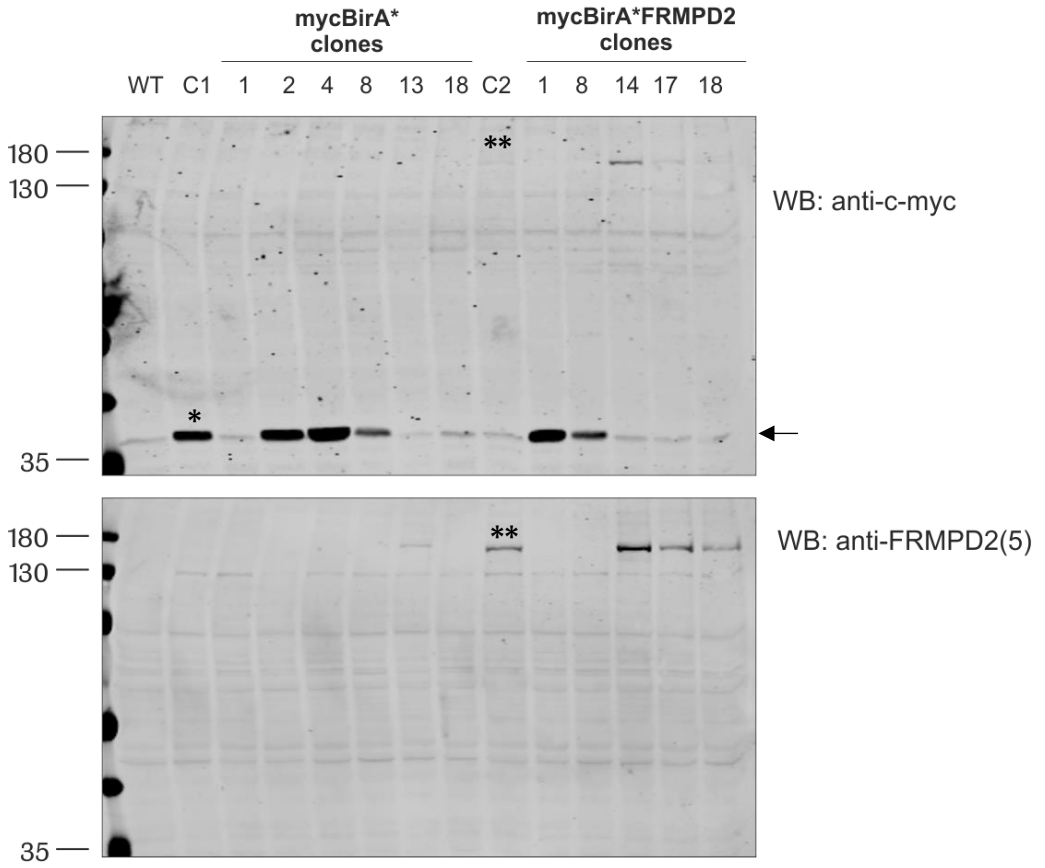

Figure 3.17 Western blot analysis of selected stable MDCK II transfectants overexpressing myc-BirA* and myc-BirA*FRMPD2

MDCK II transfectants were grown on 60 mm dishes and whole cell lysates were prepared after cells reached 90 – 100% confluency. Appropriate control samples were prepared: WT – non-transfected MDCK II cells, C1 – MDCK II cells transiently transfected with myc-BirA-pCDNA3.1 and C2 – MDCK II cells transiently transfected with myc-BirA*-FRMPD2-pCDNA3.1. Membranes were probed for the fusion proteins with anti-c-myc and anti-FRMPD2(5) antibodies followed by anti-mouse DyLight™ 800 and anti-rabbit Alexa Fluor® 680 antibody respectively. (top panel: single asterisk marks the size of myc-BirA* alone and double asterisk indicates the size of myc-BirA*-FRMPD2; bottom panel: double asterisk*

*marks the size of myc-BirA*FRMPD2). The non-specific signal from anti-c-myc antibody is indicated by an arrow. Samples represent around 10% of the total cell lysate. (N=1)*

All positive clones were further verified by immunofluorescence and compared to non-transfected MDCK II cells. Staining with anti-c-myc antibody confirmed previously obtained data from HEK293 cells. myc-BirA* was distributed throughout the cells while myc-BirA*FRMPD2 displayed the specific, observed before, plasma membrane localisation pattern (Figure 3.18). All further experiments were performed using clone 2 of MDCK II myc-BirA* and clone 14 of MDCK II myc-BirA*-FRMPD2 stable cell lines.

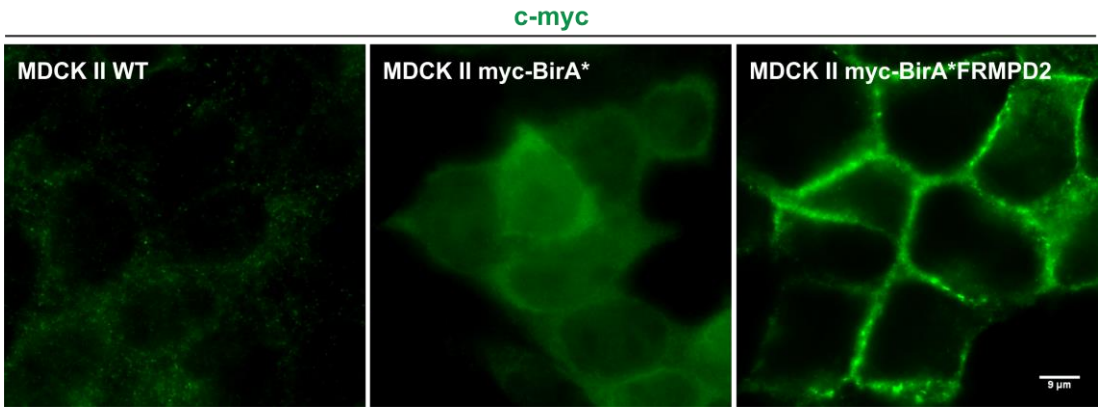

Figure 3.18 myc-BirA* is diffusely distributed in the cytoplasm while myc-BirA*FRMPD2 is localised to the plasma membrane of MDCK II cells

MDCK II WT, clone 2 of MDCK II myc-BirA and clone 14 of MDCK II myc-BirA*FRMPD2 were grown on coverslips until cells reached 90 – 100% confluency. The cells were then fixed and stained with anti-c-myc followed by anti-mouse Alexa Fluor® 488. Images were taken using a spinning disc confocal microscope. Scale bar, 9 µm. (N=2)*

3.3.2.2 Localisation of Biotin Ligase FRMPD2 fusion protein

Initial experiments in HEK293 cells and verification of newly generated stable MDCKII cell lines demonstrated that myc-tagged biotin ligase fused to the N-terminal end of FRMPD2 was characterised by specific, possibly plasma membrane localisation. Previously it has been shown, that in polarised epithelial cells FRMPD2 localises at the basolateral membrane and to a limited extent also at tight junctions (Stenzel et al., 2009). To examine whether myc-BirA*FRMPD2 colocalizes with commonly used adherens and tight junctions markers, stable MDCK II cell line expressing myc-BirA*FRMPD2 was grown on coverslips and subsequently, immunolocalization studies were performed. Staining with anti-c-

myc and β-catenin antibodies revealed that FRMPD2 tagged with myc-BirA* indeed localised to the basolateral membrane of polarised epithelial cells (Figure 3.19, A). Furthermore, colocalization studies with the tight junction protein marker, Zonula occludens-1 (ZO-1), confirmed that biotin ligase fusion protein can be a part of the junctional complex too (Figure 3.19, B).

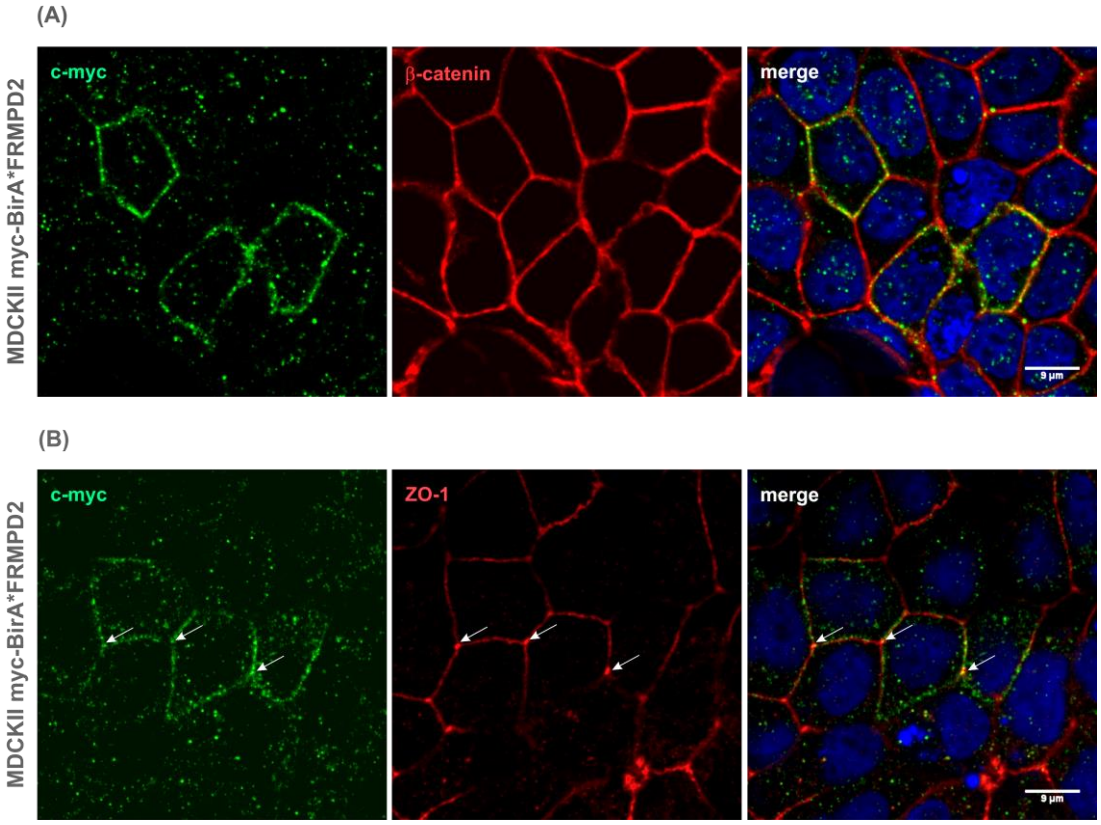

Figure 3.19 myc-BirA*FRMPD2 is localised to the basolateral membrane and partially at tight junctions in polarised MDCK II cells

(A) *Stable MDCK II cell line expressing myc-BirA*-FRMPD2 were grown on coverslips until cells reached 90 – 100% confluency. The cells were then fixed and stained with anti-c-myc and anti-β-catenin followed by anti-rabbit Alexa Fluor® 488 and anti-mouse Alexa Fluor® 594. Images were taken using a spinning disc confocal microscope and Z-stack function. Images represent single xy planes of the basal area of the epithelium. (N=3)* ***(B)*** *Stable MDCK II cell line expressing myc-BirA*FRMPD2 were grown on coverslips until cells reached 90 – 100% confluency. The cells were then fixed and stained with anti-c-myc and anti-ZO-1 followed by anti-mouse Alexa Fluor® 488 and anti-rabbit Alexa Fluor® 594. Colocalization of myc-BirA*FRMPD2 with ZO-1 is pointed out by arrows. Images were taken using a spinning disc confocal microscope and Z-stack function. Images represent single xy planes of the apical area of the epithelium. Scale bar, 9 µm. (N=3)*

Knowing that myc-BirA*FRMPD2 localised to the correct cellular compartments and increased biotinylation of endogenous proteins in mammalian cells depends on the presence of biotin ligase and exogenous biotin, in the next step we verified subcellular localisation of biotinylated proteins. To confirm that BirA* biotinylated proteins specifically only in the closest vicinity to FRMPD2 and such labelling is triggered only by the presence of biotin ligase first we tested the specificity of the streptavidin conjugated antibody. To this end, MDCKII wild-type cells were incubated in the absence and presence of 50 µM exogenous biotin. Immunofluorescence microscopy demonstrated that in WT cells cultured without exogenous biotin, streptavidin antibody detected some endogenously biotinylated proteins in mitochondria (Figure 3.20, left panel, white arrows). On the other hand, staining of MDCKII cells treated with exogenous biotin was more prominent and suggested that streptavidin recognised free, non-bound biotin distributed throughout the cells (Figure 3.20, right panel). For further experiments, this staining pattern can be considered as a background.

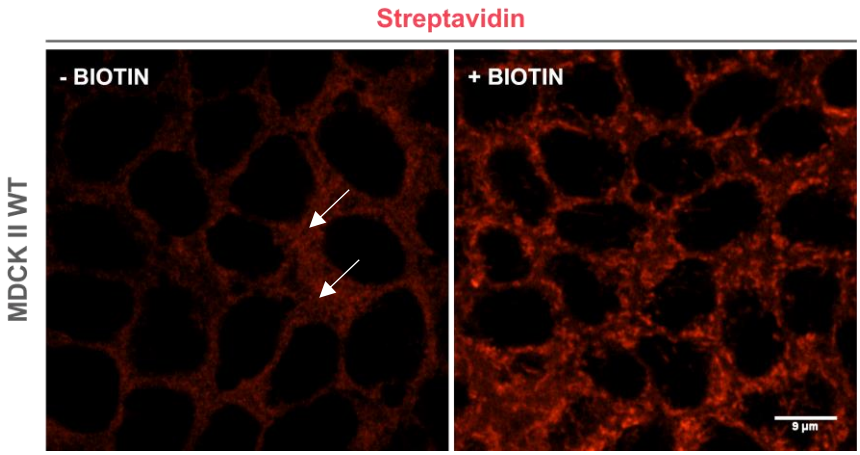

Figure 3.20 Immunofluorescence analysis of streptavidin antibody specificity

MDCK II wild-type cells were grown on coverslips until cells reached 80% confluency and subsequently they were incubated without (left panel) and with 50 µM exogenous biotin (right panel) for 24 hours. The cells were then fixed and stained with streptavidin Alexa Fluor® 594 conjugated antibody. White arrows highlight endogenously biotinylated proteins in mitochondria. Images were taken with the same exposure time using a spinning disc confocal microscope and Z-stack function. Images represent single xy planes of the basal area of the epithelium. Scale bar, 9 µm. (N=2)

Delayed tight junction formation upon the knockdown of FRMPD2 (Stenzel et al., 2009) and shown in this thesis myc-BirA*FRMPD2 localisation at tight junctions shed the light on the possible discovery of a FRMPD2-mediated protein complex

controlling signalling pathways involved in the formation of tight junctions in polarised epithelial cells. To this end, stable MDCK II cell line expressing myc-BirA*FRMPD2 was incubated in the absence and presence of 50 μM exogenous biotin for 18 hours. Subsequently, cells were fixed and stained with anti-c-myc, fluorescence streptavidin antibody and anti-ZO-1 antibody. Microscopic analysis demonstrated that subcellular pattern of biotinylated proteins was similar to signal from myc-BirA*FRMPD2 detected by c-myc antibody and also to some extent overlapping with ZO-1 staining (Figure 3.21). Admittedly, there was also streptavidin staining indicating more diffuse presence of biotinylated proteins in the cytoplasm, but this pattern was very similar to the streptavidin distribution in MDCK II WT cells treated with exogenous biotin (Figure 3.20). Therefore, it is likely that strong cytoplasmic signal comes from free exogenous biotin, but at the same time, we cannot exclude the possibility, that some of the signals may be associated with proteins biotinylated by myc-BirA*FRMPD2. This result can suggest that proximity dependent biotinylation can be used to identify proteins in the closest neighbourhood of FRMPD2 in polarised epithelial cells and potentially forming FRMPD2-mediated protein complex regulating tight junction formation.

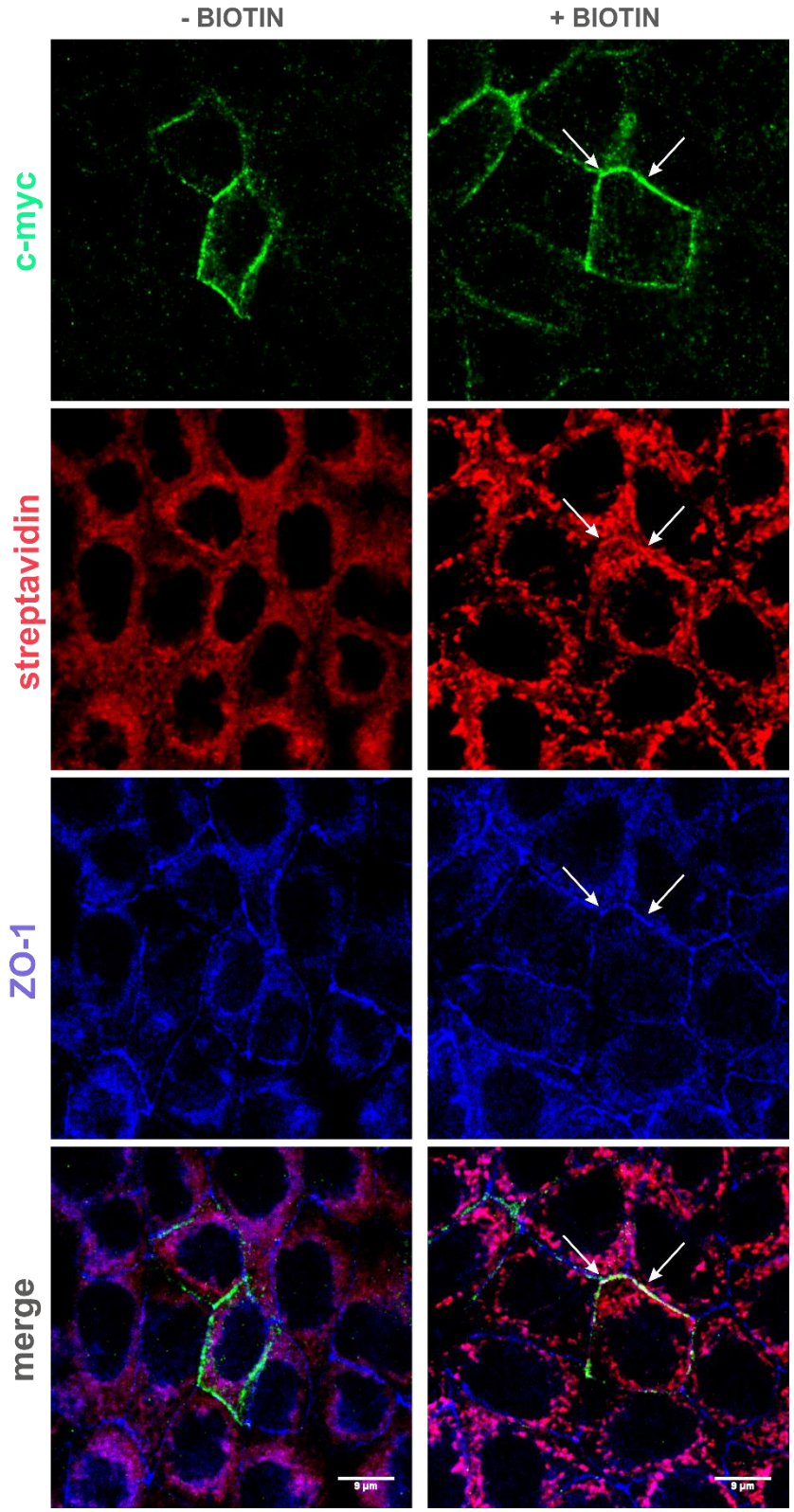

Figure 3.21 myc-BirA*FRMPD2 biotinylates proteins in the closest proximity of tight junctions

*Stable MDCK II cell line expressing myc-BirA*FRMPD2 were grown on coverslips until cells reached 80% confluency and subsequently they were incubated without and with 50 µM exogenous biotin for 18 hours. The cells were then fixed and stained with anti-ZO-1, anti-c-myc followed by anti-rabbit Alexa Fluor® 350, anti-mouse Alexa Fluor® 488 and additionally with streptavidin Alexa Fluor® 594 conjugated antibody. Overlapping signals*

*of ZO-1, myc-BirA*FRMPD2 and biotinylated proteins are pointed out by arrows. Images were taken with the same exposure time using a spinning disc confocal microscope and Z-stack function. Images represent single xy planes of the apical area of the epithelium. Scale bar, 9 µm. (N=3)*

3.3.2.3 Identifying PRK2 as a proximal protein to FRMPD2 in MDCK II cells using BioID approach

All experimental procedures performed to validate the proximity-dependent biotinylation method coincided with the new idea, that FRMPD2, due to its high similarity to PTPN13, can have the same interacting partners and share similar functions in polarised epithelial cells. Moreover, at the time when BioID experiments were carried out, Huttlin and others shared results of their study on human interactome in the BioGRID database (https://thebiogrid.org/), which provided additional evidence of the interaction between FRMPD2 and PRK2 (serine-threonine-protein kinase N2, PKN2) (Huttlin et al., 2015) and therefore supported our hypothesis.

To demonstrate the validity of our hypothesis biotinylation assay was performed and tested for the presence of PRK2 protein, which is known to associate with mouse PTPN13 (Gross et al., 2001). To this end, stable MDCK II cell lines expressing myc-BirA* used here as a control, and myc-BirA*FRMPD2 were cultured in the absence and presence of 50 µM biotin for 18 hours. Cell lysates were prepared and all biotinylated endogenous proteins were purified using streptavidin agarose beads and subsequently detected by anti-streptavidin antibody (Figure 3.22, lower panel). Immunobloting with anti-c-myc antibody revealed the presence of myc-BirA* and myc-BirA*FRMPD2 in the total cell lysate (Figure 3.22 A, INPUT, middle panel). Both proteins were also successfully purified on streptavidin agarose beads from the samples incubated with 50 µM exogenous biotin (Figure 3.22 A, PULLDOWN, middle panel). Western Blot with anti-PRK2 antibody revealed the presence of the PRK2 protein in the total cell lysates from samples non-treated or treated with biotin (Figure 3.22 A, INPUT, upper panel). In the absence of exogenous biotin endogenous PRK2 was detected neither with myc-BirA* nor myc-BirA*-FRMPD2, however in the samples treated with biotin, PRK2 was biotinylated by both, myc-BirA* and myc-BirA*-FRMPD2 (Figure 3.22 A, PULLDOWN, upper panel). The relative PRK2 signal intensity measured for samples treated with biotin demonstrated that PRK2 is almost 5.4-

fold enriched in the sample from cells expressing myc-BirA*FRMPD2 compared with cells expressing biotin ligase only (Figure 3.22 B). The presented experiment, however, was performed only once and would require more repeats to conclude that PRK2 is located in the closest vicinity of FRMPD2 and may form FRMPD2-mediated protein complex in MDCK II polarised epithelial cells.

(A)

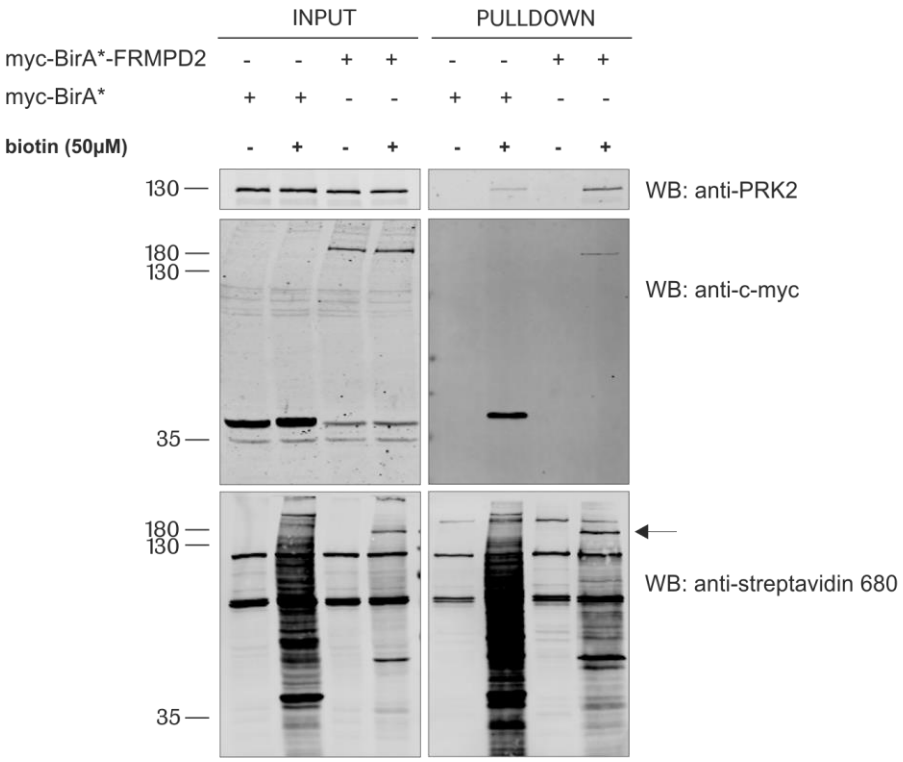

(B)

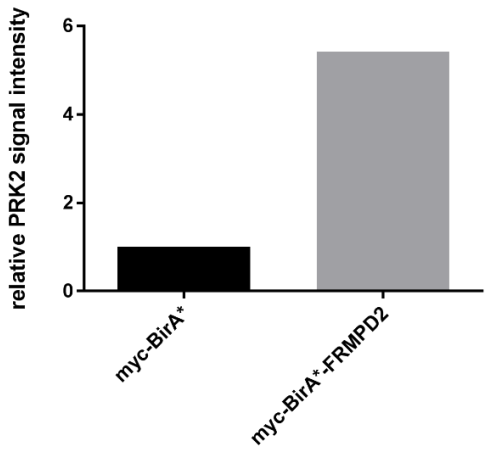

Figure 3.22 PRK2 is promiscuously biotinylated by myc-BirA* and myc-BirA*-FRMPD2 in MDCK II cells

(A) *Stable MDCK II cell line expressing myc-BirA* or myc-BirA*FRMPD2 were grown on 60 mm dishes until cells reached 80% confluency and subsequently, they were incubated without (-) and with (+) 50 µM exogenous biotin for 18 hours. Cell lysates were prepared and pulldown experiment was conducted using streptavidin beads. Fusion proteins and endogenous PRK2 were detected using anti-c-myc and anti-PRK2 respectively followed by anti-rabbit Alexa Fluor® 680 and anti-mouse DyLight™ 800 antibody respectively. Biotinylated proteins were detected using streptavidin Alexa Fluor® 680 antibody. The signal of biotinylated myc-BirA*-FRMPD2 was pointed out by an arrow. Input represents around 2% of the total cell lysate. (N=1)* ***(B)*** *Signal intensity of PRK2 in PULLDOWN samples was normalised to the signal intensity of PRK2 measured in the total cell lysates (INPUT) of samples treated with biotin – myc-BirA* and myc-BirA*-FRMPD2. Obtained values were compared and represented as fold change of PRK2 signal intensity in myc-BirA* sample. Signal intensity was measured using analysis tool of Image Studio™ Lite software. Signal area was the same for all samples. (N=1)*

3.4 Discussion

The FRMPD2-mediated protein complex remains largely unexplored and besides two interactions suggesting its role in epithelial cell polarisation (Stenzel et al., 2009) and host immune defense in epithelial cells (Lipinski et al., 2012), there are no further reports exploring this research area. As a highly modular multi-PDZ domain protein, FRMPD2 is considered as a scaffolding protein and component of potential molecular hubs integrating elements of the actin cytoskeleton, signalling and membrane trafficking machinery relevant to epithelial cell polarisation and Crohn's disease. A current study discovered new potential interacting partners and revealed new possibilities to explore FRMPD2 function in cellular processes mentioned above.

3.4.1 BANK1

BANK1 (B-cell Scaffold Protein with Ankyrin Repeats) was a promising candidate found in the Y2H screen to interact with the FERM domain of FRMPD2. We have now demonstrated that full-length overexpressed BANK1 interacts with either the FERM domain of FRMPD2 or endogenous FRMPD2. The interest in the function of BANK1 protein increased when FRMPD2 was found to be related to inflammatory bowel disease by regulating NOD2 signalling (Lipinski et al., 2012). BANK1 has been identified as a susceptibility gene for psoriasis, a disease affecting skin and very often associated with Crohn's disease (Zhang et al., 2011).

Both disorders cause weakening of the epithelial barriers of the skin and bowel respectively and facilitate penetration of bacteria into deeper tissues. It was hypothesised, that FRMPD2 positively regulates BANK1-mediated signalling and similarly to the NOD2 mechanism, assembles BANK-1 signalling complex at the basolateral membrane of epithelial cells. Although the interaction between FRMPD2 and BANK1 was positive, the precise function of FRMPD2 in the molecular mechanism of action of IBD still remains elusive. We decided to focus on the interaction between FRMPD2 and PRK2, and additional experiments with BANK1 protein were suspended.

3.4.2 SEPTIN-10

Septins belong to the family of proteins with GTPase activity, ubiquitously expressed in mammalian cells and along with actin filaments, microtubules and intermediate filaments are considered as a fourth cytoskeletal component. It has been shown, that septins interact with microtubule-associated proteins (MAPs) and modulate microtubule stability and dynamics (Kremer et al., 2005). Moreover, in polarised epithelial cells, septins spatially guide microtubule organisation along the lateral membrane (Bowen et al., 2011). Such microtubule arrangement is required for establishment and maintenance of epithelial polarity and is crucial for targeted vesicle trafficking, that allows preservation of the different content of the apical and basolateral membranes (Musch, 2004). Among all septins, SEPTIN-10 remains quite unknown, but similarly to another septins, it modulates microtubule stability through the interaction with the microtubule associated protein MAP4 (Xu et al., 2012a). Since FRMPD2 is an important membrane-associated protein we hypothesised that through interaction with SEPTIN-10, FRMPD2 links microtubules to the plasma membrane and therefore regulates their spatial organisation and vesicle trafficking along microtubules in epithelial cells. Although SEPTIN-10 was discovered as an interacting partner in Y2H screen, it is not yet possible to detect its interaction with FRMPD2 by co-immunoprecipitation. We excluded technical problems with the protocol as all co-IPs were performed in parallel with assays with BANK1 protein. However, lack of detectable interaction could be explained by a number of different factors like inadequately optimised co-IP conditions for this type of interaction, weak or

transient nature of the interaction or inappropriate folding of overexpressed proteins that prevents the right exposure of the protein binding sites.

3.4.3 FILAMIN B

Filamins are a group of proteins including three isoforms: filamin A, filamin B and filamin C, that function as actin crosslinkers, but also interact with a large number of proteins, such as ion channels or kinases, suggesting that they act as signalling scaffolds. Filamin B has been shown to localise at the apical region of epithelial tissues in avian embryos and its knockdown promoted epithelium disruption within the neural tube. Moreover, it was proven that filamin B is required for accumulation of E-cadherin and ZO-1 in adherens and tight junction complexes of MDCK cells and its depletion led to the failure of epithelium formation (Wakamatsu et al., 2011). A recent study demonstrated that filamin B promoted invasiveness of cancer cells through the phosphorylation of myosin regulatory chain (MRLC) and focal adhesion kinase (FAK), which are actively involved in cell migration, by generating contractile actomyosin forces and regulating focal adhesion turnover respectively (Iguchi et al., 2015). Filamin B was found as one of the most promising hits in the Y2H screen, but unfortunately, none of the co-immunoprecipitation assays, performed within the current study, confirmed interaction with overexpressed or endogenous FRMPD2. All co-IP attempts were technically challenging and under standard conditions, FRMPD2-Filamin $B_{2041-2290}$ complex could not be immuno-isolated. There is a possibility, that the FRMPD2 binding site in filamin B expressed in mammalian cells is surrounded by many other protein complexes, which preclude detection of the interaction. It is still feasible that FRMPD2 acts as an anchor for filamin B, helping in proper maintenance of the actin filament network and therefore affecting mechanical properties of epithelial cells. On the other hand, we hypothesised that in filamin B-depleted cells localisation of FRMPD2 at cell-cell contacts and tight junctions might be secondary due to the absence of E-cadherin. It will be also interesting to see whether there is any correlation between filamin B and FRMPD2 in migrating cells.

3.4.4 RAPGEF2

RAPGEF2 (Rap guanine nucleotide exchange factor 2, PDZ-GEF1) is a PDZ domain protein exchanging guanine nucleotides and regulating the activity of Rap1 (de Rooij et al., 1999), which has been presented as a key regulator of E-cadherin cell-cell junction formation (Kooistra et al., 2007). It has been shown that RAPGEF2 localises at the plasma membrane with simultaneous co-localization and interaction with β-catenin and ZO-1 proteins, components of adherens and tight junctions (Kawajiri et al., 2000, Kim et al., 2015). Moreover, RAPGEF2 contributes to intestinal epithelial barrier function via regulation of apical cytoskeleton contractility (Monteiro et al., 2013) and induction of brush border formation at the apical membrane of polarised intestinal epithelial cells (Consonni et al., 2014). A recent study demonstrated that RAPGEF2 controls migration of neurons during cerebral cortex development as well as migration and invasion of breast cancer cells, and that activity is regulated by phosphorylation (Magliozzi et al., 2013, Ye et al., 2014). All presented studies about RAPGEF2 showed evidence that its function in epithelial polarity is versatile, therefore we considered this protein as a promising interaction partner for FRMPD2. This study proved that RAPGEF2 binds efficiently to FRMPD2 and it would be interesting to see how these two proteins form a complex and cooperate together in establishing and/or maintaining the polarity of epithelial cells. Also, the key question would be whether their function depends on each other or whether they are forming a scaffolding hub for other signalling molecules along the basolateral membrane. Although the current study revealed interaction between RAPGEF2 and FRMPD2, due to the time constraints further experiments could not be performed.

3.4.5 PLECTIN-1

Plectin is a large, 500 kDa protein, known as a cytoskeletal linker that binds three main components of the cellular cytoskeleton, which consists of intermediate filaments, actin filaments and microtubules. Plectin is characterised by a multi-domain protein structure and binds to a variety of molecules including receptors, peripheral membrane proteins, nuclear envelope proteins or kinases (Castanon et al., 2013). Additionally, it was detected by mass spectrometry as a component of the protein complex associated with the tight junction protein, ZO-1 (Chen et

al., 2006). Hence, the role of Plectin is also versatile, but at the same time mainly auxiliary as it acts as a scaffold for signaling molecules and structurally reinforces the cytoskeleton, particularly in cells and tissues like epithelia or skeletal muscle that are subjected to mechanical stress (Wiche et al., 1983, Wiche et al., 1984). Plectin-1 was found as an interacting protein of FRMPD2 in MDCK cells by Affinity Purification-Mass Spectrometry, however co-IP assays revealed that Plectin-1 immunoprecipitated with both, GFP and GFP-FRMPD2. Although the amount of Plectin-1 co-precipitating with GFP-FRMPD2 was largely increased compared with GFP alone, it is worth noting that Plectin-1, among other cytoskeletal components, was found as a protein that may co-purify with GFP and therefore it can be regarded as a potential contamination (Trinkle-Mulcahy et al., 2008). Thus the interaction between Plectin and FRMPD2 detected by MS and later by co-IP should be interpreted with caution.

3.4.6 Detection of novel putative interactions by BioID-FRMPD2

Until now several studies have been performed using the BioID method to detect novel interactions and explore protein networks controlling cell polarity (Van Itallie et al., 2013, Van Itallie et al., 2014, Fredriksson et al., 2015). Experiments performed within this study allowed to create a new tool, which can be successfully applied to identify new vicinal and/or interacting in vivo proteins within the FRMPD2 network. It is extremely important that protein fused to BirA* is targeted appropriately to specific subcellular compartments as wild-type or endogenous protein (Roux et al., 2012). We have shown that myc-BirA*FRMPD2 stably expressed in MDCK II cells localised to the appropriate subcellular compartments like the basolateral membrane or tight junctions in polarised epithelial cells and that was consistent with the previously published data (Stenzel et al., 2009). We have now presented that biotinylation triggered by myc-BirA*FRMPD2 was spatially specific and the FRMPD2 biotinylated proteins in the close vicinity. Taken together we concluded that proximity-dependent biotinylation may be used for detection of components of the FRMPD2-mediated protein complex at the basolateral membrane of polarised epithelial cells as well as at tight junctions.

As mentioned previously, FRMPD2 belongs to the multi-PDZ domain protein family and has significant similarity to PTPN13 – protein tyrosine phosphatase, non-receptor type 13 (mouse orthologue known as PTP-BL – protein tyrosine phosphatase-basophil like). Interestingly, FRMPD2 and PTP-BL demonstrated complementary localisation in polarised epithelial cells (Stenzel et al., 2009), therefore, we hypothesised, that to some extent these two proteins may have the same interacting partners and share similar functions too. This assumption and previously shown distribution pattern of biotinylated proteins by myc-BirA*FRMPD2 at the plasma membrane and tight junctions led to the hypothesis that FRMPD2 may interact with PRK2 (PKN2, serine/threonine protein kinase N2), which was found in the protein network of PTP-BL (Gross et al., 2001). We have shown that PRK2 was promiscuously biotinylated by both, myc-BirA* and myc-BirA*FRMPD2, however PRK2 was more abundant in the sample of the latter fusion protein. Co-precipitation of PRK2 with myc-BirA* could be explained by the fact that PRK2 localises to other subcellular compartments, independently from FRMPD2 or myc-BirA* alone can diffuse to cell-cell contacts as well.

In summary, this study revealed a number of interesting new potential protein-protein interactions which show new possibilities for exploration of FRMPD2 function in epithelial cell polarisation. Some of the interactions were detected at the beginning of the study, but some like RAPGEF2 very late, therefore due to the time constraints and other priorities we could not continue to study the function of the FRMPD2-RAPGEF2 complex. Furthermore, the BioID method was demonstrated to be a powerful technique that allowed the detection of PRK2 as a part of the FRMPD2 complex and was also supported by the proteomic data published by Huttlin and others (Huttlin et al., 2015). Detection of the potential interaction between FRMPD2 and PRK2 shifted our priorities, therefore mass spectrometry experiments and proteomic analysis will be performed at a later time point.

CHAPTER 4 - PRK2 as a binding partner of FRMPD2

4.1 Introduction

To understand the FRMPD2 function in establishment and/or maintenance of cell polarity and the mechanisms by which FRMPD2 activity is regulated within the cell, it is important to consider the role of its interaction partners. The previously obtained data suggested that through protein-protein interactions FRMPD2 may have not only a versatile role in signalling mechanisms related to epithelial cell polarisation (Stenzel et al., 2009, Lipinski et al., 2012), but its function may also be associated with cytoskeleton organisation, as suggested by its interaction with PRK2. The BioID method revealed that these two proteins could form a complex. However, the identity of the complex was unclear at that stage; whether it is formed via a direct interaction between the two molecules or whether this interaction is bridged by other proteins. At the same time, when the BioID experiments were carried out, Huttlin and others (Huttlin et al., 2015) published data regarding the BioPlex network exploring the human interactome. Among 24000 protein-protein interactions identified in HEK293T cells by high-throughput AP-MS, they found a possible interaction between FRMPD2 and PRK2 and thus demonstrated that PRK2 might form a stable complex with FRMPD2.

PRK2 is a PKC-related serine/threonine-protein kinase containing three conserved domains: three tandem HR1 (homology region 1) domains, a C2-like domain (similar to the lipid-binding C2 domain in PKC kinase) and a serine-threonine kinase domain (homologous to the PKC kinase domain). It has been shown that PRK2 can be activated by binding to the three Rho isoforms (RhoA, RhoB and RhoC) as well as Rac1 (Quilliam et al., 1996, Vincent and Settleman, 1997, Hutchinson et al., 2013) however, of all the Rho molecules, RhoB indicates the strongest affinity to PRK2 (Hutchinson et al., 2013). Several studies have suggested that PRK2 acts as a downstream effector of RhoA (Vincent and Settleman, 1997, Calautti et al., 2002, Wallace et al., 2011). It has been shown that expression of PRK2 kinase-deficient mutant leads to loss of actin stress fibers, with a parallel increase in the level of subcortical actin. Therefore, it has been suggested that through the RhoA-mediated signalling pathway PRK2 plays a role

in the organisation of the actin cytoskeleton in NIH 3T3 cells (Vincent and Settleman, 1997).

Further studies provided evidence that PRK2 kinase activity increases in differentiating keratinocytes and promotes keratinocyte cell-cell adhesion. It has been shown that PRK2 operates as a direct effector of the RhoA signalling pathway and induces localisation of E-cadherin at cell-cell contacts, tyrosine phosphorylation of β- and γ-catenin, as well as Fyn kinase activation, all of which are implicated in establishment of keratinocyte cell-cell adhesion (Calautti et al., 2002).

PRK2 has also been found as a regulator of apical junction formation in human bronchial epithelial cells and its role in this process was demonstrated to be kinase- and RhoA binding-dependent. Specifically, PRK2-depleted cells were not able to form apical junctions, therefore it has been suggested that PRK2 actively participates in the processes involved in the transition from primordial to mature apical junctions (Wallace et al., 2011).

Interestingly, PRK2 has been shown as a regulator of entry into mitosis and exit from cytokinesis, processes also controlled by Rho GTPases (Schmidt et al., 2007). It has been demonstrated that PRK2 activates Cdc25B, which is required for G2 to M transition in cell cycle progression and moreover PRK2 depletion inhibits cytokinesis, which results in multinucleated cells. In another study, PRK2 depletion was shown to affect collective cell migration of 5637 bladder tumour cells through disruption of cell-cell contacts, which resulted in inhibition of 2D and 3D cell migration (Lachmann et al., 2011).

Apart from in vitro studies presenting a role for PRK2 in cell adhesion and migration, there is also some data suggesting that the function of PRK2 in these processes may also be reflected in vivo during embryogenesis (Lu and Settleman, 1999, Quetier et al., 2016, Danno et al., 2017). It has been shown that loss of PRK2 in both *Drosophila melanogaster* and mice resulted in growth retardation and lethality. More specifically, in *Drosophila* constitutive disruption of PRK2 gene function leads to dorsal closure failure, which depends on epidermal cells

migration and adhesion (Lu and Settleman, 1999), while in mice, *PRK2* null mutants display defects in mesenchymal growth and have neural tube defects (Quetier et al., 2016, Danno et al., 2017). Taken together, these in vivo studies may suggest that evolutionarily, PRK2 function may be conserved.

Published data on PRK2 provides evidence that it is an important regulator of cell polarity as well as cell migration and adhesion. The main aim of this study was to investigate FRMPD2 function in all these processes, therefore it was interesting that PRK2 was detected as a potential interacting partner of FRMPD2, suggesting that these two proteins may form a complex and act together. Given the published data and results from the BioID experiments shown in the previous chapter of this thesis, which were obtained from two different mammalian cell lines originating from distinct species, we decided to validate this interaction and study its biological relevance with respect to epithelial cell adhesion/cell polarisation.

4.2 Aim

We hypothesised that FRMPD2 interacts with PRK2 and both proteins act together in a complex to regulate apical junction formation. Therefore we further speculated that PRK2 would be recruited by FRMPD2 and its function will depend on spatial restriction to the basolateral membrane and/or tight junctions. Hence the main aim of this part of the study was:

1. To validate interaction between FRMPD2 and PRK2 by co-IP assays.
2. To characterise FRMPD2-PRK2 interaction in more details.
3. To identify the role of the FRMPD2-PRK2 complex in epithelial cell adhesion/cell polarisation.

4.3 Results

4.3.1 Examination of the interaction between FRMPD2 and PRK2

4.3.1.1 Validation of the FRMPD2-PRK2 interaction

To verify the interaction with PRK2, we performed co-IP experiments in HEK293 cells. First, the co-IP assay was performed using the two full-length proteins, and

a corresponding immunoblot demonstrated that full-length GFP-FRMPD2 was able to co-precipitate myc-tagged PRK2 but GFP alone was not, supporting the interaction between these two proteins (Figure 4.1).

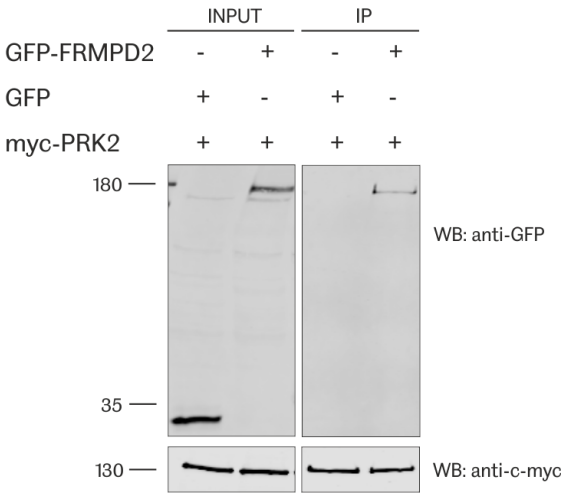

Figure 4.1 PRK2 interacts with FRMPD2

HEK293 cells were transiently co-transfected with expression constructs of myc-tagged PRK2 and GFP or GFP-tagged FRMPD2. 48 hours post-transfection cell lysates were collected, and co-immunoprecipitation was conducted using c-myc antibody coupled to Protein A-agarose resin. Fusion proteins were detected by Western Blot using anti-c-myc and anti-GFP antibody followed by anti-rabbit Alexa Fluor® 680 and anti-mouse DyLight™ 800 antibody respectively. Input represented around 2% of the total cell lysate. (N=3)

4.3.1.2 PRK2 interacts selectively with PDZ3 domain of FRMPD2

Proteins are composed of several domains (building blocks), which mediate protein-protein interactions. As previously mentioned, FRMPD2 is characterised by a modular structure and consists of five separate domains, which establish all of the already known FRMPD2 interactions (Stenzel et al., 2009, Lipinski et al., 2012). To demonstrate, that interaction with PRK2 is also mediated by one of the domains, GFP-tagged KIND, FERM and PDZ1-3 domains were overexpressed together with myc-tagged PRK2 in HEK293 cells and subsequently subjected to co-immunoprecipitation assay. Immunoblot analysis revealed that interaction with myc-PRK2 was domain specific and was exclusively observed with PDZ1-3 domains (Figure 4.2, A). A similar experiment was performed with endogenous PRK2 and also proved its association with PDZ1-3 domains of FRMPD2 (Figure 4.2, B).

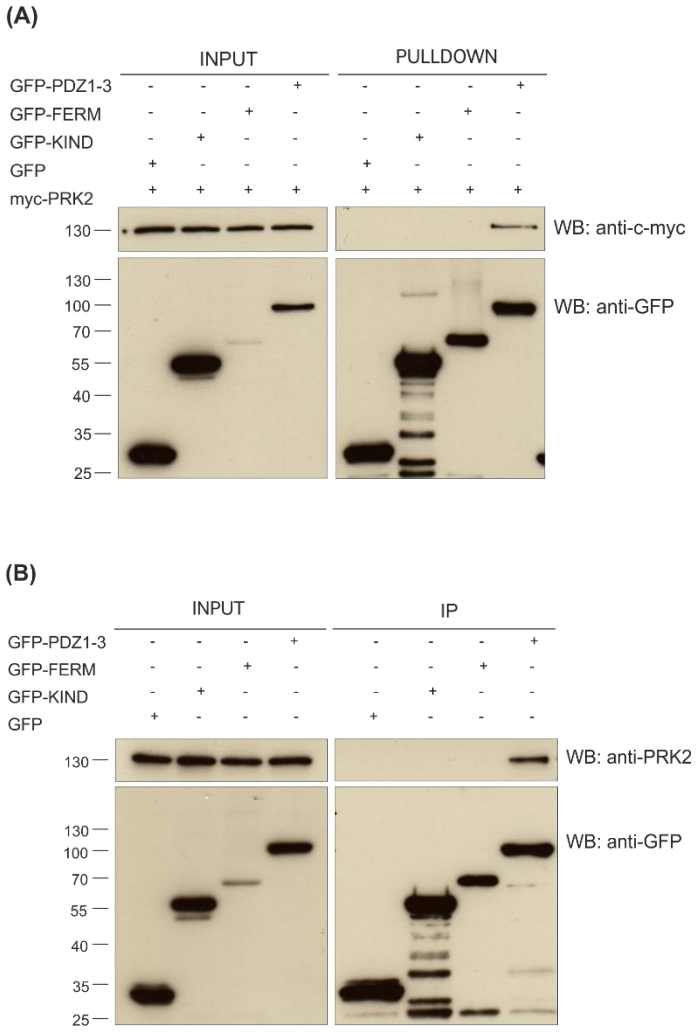

Figure 4.2 Exogenous and endogenous PRK2 co-precipitate exclusively with PDZ1-3 domains of FRMPD2

(A) *HEK293 cells were transiently co-transfected with expression constructs of myc-tagged PRK2 and GFP, GFP-KIND, GFP-FERM or GFP-PDZ1-3. 48 hours post-transfection cell lysates were collected, and co-immunoprecipitation was conducted using GFP-Trap®_A. Fusion proteins were detected by Western Blot using anti-c-myc and anti-GFP antibody followed by secondary HRP antibody. Input represented around 2% of the total cell lysate. (N=3)* ***(B)*** *HEK293 cells were transiently transfected with expression constructs of GFP, GFP-KIND, GFP-FERM or GFP-PDZ1-3. 48 hours post-transfection cell lysates were collected, and co-immunoprecipitation was conducted using GFP-Trap®_A. Fusion proteins and endogenous PRK2 were detected by Western Blot using anti-GFP and anti-PRK2 antibody respectively followed by secondary HRP antibody. Input represented around 2% of the total cell lysate. (N=3)*

All PDZ domains share a similar structure and contain a unique carboxylate-binding loop, which is responsible for binding specific sequence motifs at the carboxyl terminus of target proteins. Thus binding mediated by PDZ domains can be considered as a general mechanism and may unravel unknown PDZ domain interactions (Fanning and Anderson, 1996). We hypothesised that the interaction with PRK2 could be mediated by the PDZ3 domain of FRMPD2, similarly to the previously described interaction between mouse PTPN13 and PRK2 (Gross et al., 2001). Our assumption was supported by the fact that PDZ3 domains of mouse PTPN13 (PTP-BL) and human FRMPD2 share high sequence similarity within the carboxylate binding loop (Figure 4.3).

Figure 4.3 Sequence alignment of mPTPN13 and hFRMPD2 PDZ3 domains

Multiple sequence alignment of PDZ3 domains of mouse PTPN13 and human FRMPD2 proteins. Residues of the carboxylate-binding loop are highlighted in grey. The arrow indicates the conserved basic amino acid. Carboxylate binding site is underlined in blue. Sequences of PDZ3 domains were retrieved from UniProt (http://www.uniprot.org/), and multiple sequence alignment was run using Clustal Omega tool available on the website: http://www.ebi.ac.uk/Tools/msa/clustalo/

To test our hypothesis all the PDZ domains of FRMPD2, separately fused to GFP-tagged FERM domain, were co-expressed with myc-tagged PRK2 and subjected to co-IP assay. The obtained immunoblots demonstrated that only the GFP-FERM-PDZ3 domains successfully co-precipitated myc-PRK2 (Figure 4.4, A). Similar experiments with endogenous PRK2 revealed that PRK2 protein interacted only with the PDZ3 domain of FRMPD2, although the signal was relatively weak (Figure 4.4, B). Overall, experiments demonstrated that both overexpressed and endogenous PRK2 interacted selectively with the PDZ3 domain of FRMPD2 and confirmed the proposed hypothesis.

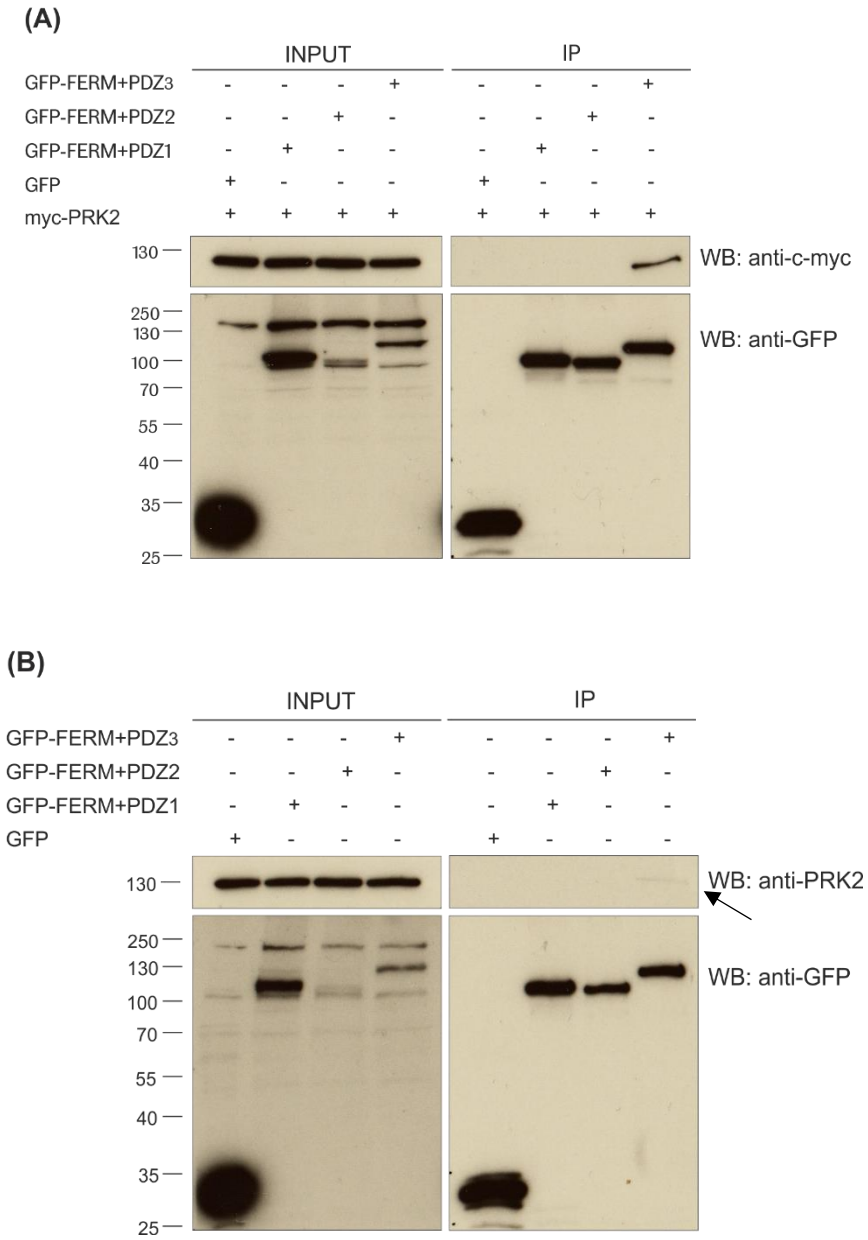

Figure 4.4 Exogenous and endogenous PRK2 interact selectively with PDZ3 domain of FRMPD2

(A) *HEK293 cells were transiently co-transfected with expression constructs of myc-tagged PRK2 and GFP, GFP-FERM-PDZ1, GFP-FERM-PDZ2 or GFP-FERM-PDZ3. 48 hours post-transfection cell lysates were collected, and co-immunoprecipitation was conducted using GFP-Trap®_A. Fusion proteins were detected by Western Blot using anti-c-myc and anti-GFP antibody followed by secondary HRP antibody. Input represented around 2% of the total cell lysate. (N=3)* ***(B)*** *HEK293 cells were transiently transfected with expression constructs of GFP, GFP-FERM-PDZ1, GFP-FERM-PDZ2 or GFP-FERM-PDZ3. 48 hours post-transfection cell lysates were collected, and co-immunoprecipitation was conducted using GFP-Trap®_A. Fusion proteins and endogenous PRK2 were detected by Western Blot using anti-GFP and anti-PRK2 antibody respectively followed by secondary HRP antibody. Input represents around 2% of the total cell lysate. (N=3)*

The basic amino acid within the carboxylate-binding loop (Figure 4.3, lysine - K highlighted by an arrow) is a crucial determinant of the target protein binding, and its substitution can alter PDZ domain affinity for its ligands (Gee et al., 2000). Based on this premise, a point mutation replacing lysine 1084 to glutamate (K1084E) was first introduced into the full-length GFP-tagged FRMPD2 and later into other construct containing GFP-tagged PDZ1-3 domains. First, a co-IP experiment demonstrated that the introduced mutation within PDZ3 domain of FRMPD2 abolished the interaction with myc-PRK2 (Figure 4.5, A). Nevertheless, the GFP signal in pulldown samples was quite weak, therefore to further test the hypothesis we conducted other co-IP assay. To this end, GFP-tagged PDZ1-3 domains together with the corresponding point mutant, carrying the same mutation in the PDZ3 domain as the full-length FRMPD2, were co-expressed with myc-PRK2 in HEK293 cells and subjected to co-immunoprecipitation. Immunobloting revealed that myc-PRK2 was not co-precipitated with the protein containing the mutation (Figure 4.5, B). Therefore, we concluded that a single-amino acid substitution of lysine 1084 in the carboxylate-binding loop of the PDZ3 domain of FRMPD2 can lead to a complete abolishment of interaction with PRK2.

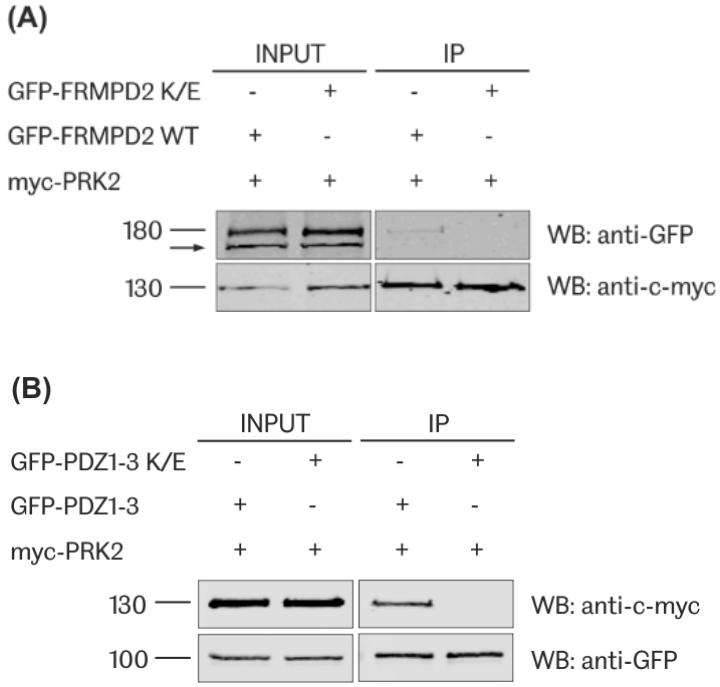

Figure 4.5 Point mutation in carboxylate-binding loop of PDZ3 domain of FRMPD2 abolishes interaction with PRK2

(A) *HEK293 cells were transiently co-transfected with expression constructs of myc- PRK2 and GFP-FRMPD2 WT or GFP-FRMPD2 K/E. 48 hours post-transfection cell lysates were collected, and co-immunoprecipitation was conducted using c-myc antibody coupled to Protein A-agarose resin. (N=3)* ***(B)*** *HEK293 cells were transiently co-transfected with expression constructs of myc-PRK2 and GFP-PDZ1-3 or GFP-PDZ1-3 K/E. 48 hours post-transfection cell lysates were collected, and co-immunoprecipitation was conducted using GFP-Trap®_A. In both experiments, fusion proteins were detected by Western Blot using anti-GFP and anti-c-myc antibody followed by anti-rabbit Alexa Fluor® 680 and anti-mouse DyLight™ 800 antibody respectively. Input represents around 2% of the total cell lysate. An arrow marked the non-specific signal of anti-GFP antibody. (N=3)*

4.3.1.3 The C-terminal cysteine of PRK2 is essential for interaction with FRMPD2

Similar to the published data that identified the interaction between PRK2 and PTP-BL (Gross et al., 2001), the current study also showed PRK2 affinity to the PDZ3 domain of another multi-PDZ domain protein - FRMPD2. Like previously, it was essential to demonstrate that the extreme C-terminal cysteine of PRK2 serves here as part of a PDZ domain binding motif as well. myc-PRK2 K686R, the so-called kinase-dead mutant which harbours a point mutation in the ATP-binding site that reduces autophosphorylation of PRK2 was already available (Gross et al., 2001) but two other myc-tagged PRK2 mutants were generated: myc-PRK2 DEL with the deletion of the last three amino acids (the same mutation abolished PRK2 interaction with PTPN13, a FRMPD2 paralog), and finally myc-PRK2 C/S that contains a point mutation of C-terminal cysteine to serine (cysteine replacement by serine was justified by structural similarity between these two amino acids and also by the fact that the same mutation abolished PRK2 interaction with PTPN13). Lysates of HEK293 cells co-transfected with an expression vector of GFP-tagged PDZ1-3 domains of FRMPD2 and mutated forms of myc-tagged PRK2, along with myc-PRK2 WT used as a control, were subjected to co-immunoprecipitation. Both mutations of the C-terminal part of PRK2 did not co-precipitate, suggesting that in mammalian cells the extreme C-terminal cysteine of PRK2 is engaged in the interaction with FRMPD2 (Figure 4.6). Thus it can be concluded that deletion of the last three amino acids of PRK2 can lead to a complete abolishment of the interaction. However, substitution of only C-

terminal cysteine by serine was sufficient for the disruption of the interaction with FRMPD2.

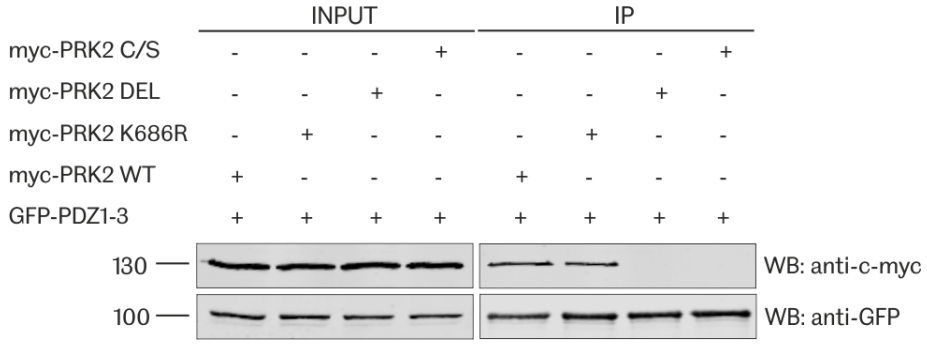

Figure 4.6 The C-terminus of PRK2 is essential for interaction with FRMPD2

HEK293 cells were transiently co-transfected with an expression constructs of GFP-tagged-PDZ1-3 domains of FRMPD2 and different forms of myc-tagged PRK2 (PRK2 WT – wild type, PRK2 K686R – kinase-dead mutant - point mutation in ATP-binding site reducing autophosphorylation of PRK2, PRK2 DEL – deletion of last three amino acids, PRK2 C/S – mutation of the C-terminal cysteine to serine). 48 hours post-transfection cell lysates were collected, and co-immunoprecipitation was conducted using GFP-Trap®_A. Fusion proteins were detected by Western Blot using anti-GFP and anti-c-myc antibody followed by anti-rabbit Alexa Fluor® 680 and anti-mouse DyLight™ 800 antibody respectively. Input represents around 2% of the total cell lysate. (N=3)

4.3.2 PRK2 co-localizes with FRMPD2

4.3.2.1 FRMPD2 recruits PRK2 to the cell membrane in non-polarized epithelial cells

Validation and characterization of the FRMPD2-PRK2 interaction using a biochemical approach were complemented with colocalization assays. Immunostained FRMPD2 localises to the basolateral membrane of polarised epithelial cells and at the plasma membrane of non-polarised epithelial cells (Stenzel et al., 2009). PRK2, however, was found in the apical membrane of polarised epithelial cells and was distributed intracellularly in both polarised and non-polarised cells (Gross et al., 2001, Wallace et al., 2011). The lack of a suitable antibody made it impossible to detect endogenous proteins, therefore subcellular localisation was assessed by fluorescence microscopy of HEK293 cells with transfected tagged versions of FRMPD2 and PRK2. When these two proteins were overexpressed together, intracellular distribution of PRK2 strongly depended on FRMPD2 plasma membrane localisation and overlapped with β-catenin, used

here as a marker of cell-cell contacts (Figure 4.7, upper panel, colocalisation highlighted by the white arrow). This specific distribution was distinctly visible in all double transfected cells, while cells transfected either with GFP-FRMPD2 or myc-PRK2 displayed membrane or cytoplasmic staining respectively. Experiments performed in the current study demonstrated that both PRK2 mutations: deletion of the last three amino acids and substitution of C-terminal cysteine by serine, abolished the interaction with FRMPD2. It was important to check how these mutations affected cellular distribution of PRK2 co-overexpressed with FRMPD2. When overexpressed with GFP-FRMPD2, both myc-PRK2 DEL and myc-PRK2 C/S showed a diffused cytoplasmic staining, however, FRMPD2 staining was still restricted to the cell membrane (Figure 4.7, middle and lower panel). Hence it can be concluded that PRK2 mutations altered not only the interaction with FRMPD2 but also its co-localization with FRMPD2 at the membrane. Moreover, based on these new findings, it can be hypothesised that FRMPD2 recruits PRK2 to the membrane in non-polarized epithelial HEK293 cells.

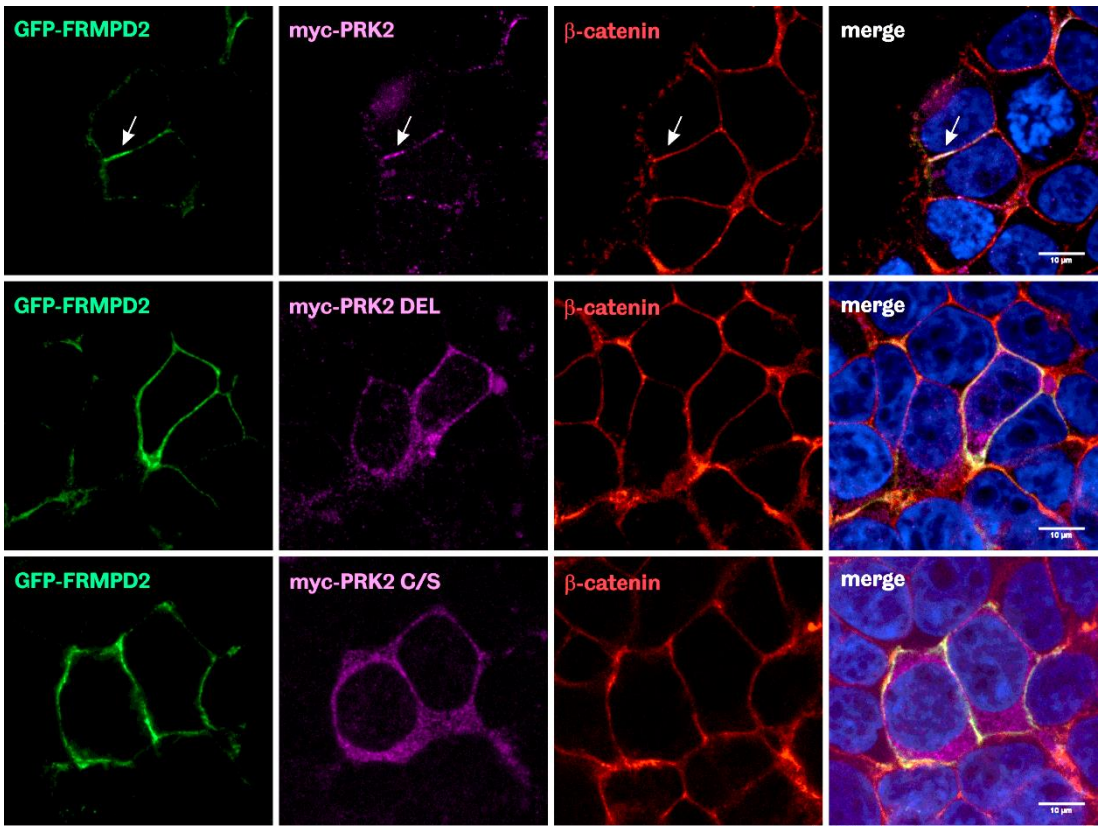

Figure 4.7 The C-terminal cysteine of PRK2 is required for colocalization with FRMPD2

HEK293 cells were grown on coverslips and transiently co-transfected with expression constructs of GFP-tagged FRMPD2 and different forms of myc-tagged PRK2: myc-PRK2, PRK2 DEL – deletion of last three amino acids, PRK2 C/S – mutation of the C-terminal cysteine to serine). 48 hours post transfection cells were fixed and stained with anti-β-catenin and anti-c-myc followed by anti-mouse Alexa Fluor® 568 and anti-rabbit Alexa Fluor® 647 antibody respectively. Overlapping signals of GFP-FRMPD2, myc-PRK2 and β-catenin are pointed out by arrows. Images were taken using a spinning disc confocal microscope and Z-stack function. Images represent single xy planes. Scale bar, 10 µm. (N=3)

Previously described experimental data (section 4.3.1.2) proved that single-amino-acid substitution of lysine 1084 in the carboxylate-binding loop of the PDZ3 domain of FRMPD2 disrupted interaction with PRK2. To investigate the impact of the FRMPD2 mutation on cellular localisation of PRK2, both proteins were overexpressed in HEK293 cells and analysed using fluorescence microscopy. Cells expressing wild-type forms of FRMPD2 and PRK2 clearly indicated protein colocalization at the plasma membrane, and also overlapped with β-catenin (Figure 4.8, upper panel). However, PRK2 expressed together with the K1084E FRMPD2 mutant did not co-localise with FRMPD2 at the plasma membrane, but remained diffuse in the cytoplasm (Figure 4.8, lower panel). This result explicitly showed that alteration of the conserved amino acid in carboxylate binding loop of PDZ3 domain changed the ability of FRMPD2 to recruit PRK2 to the cell-cell contacts.

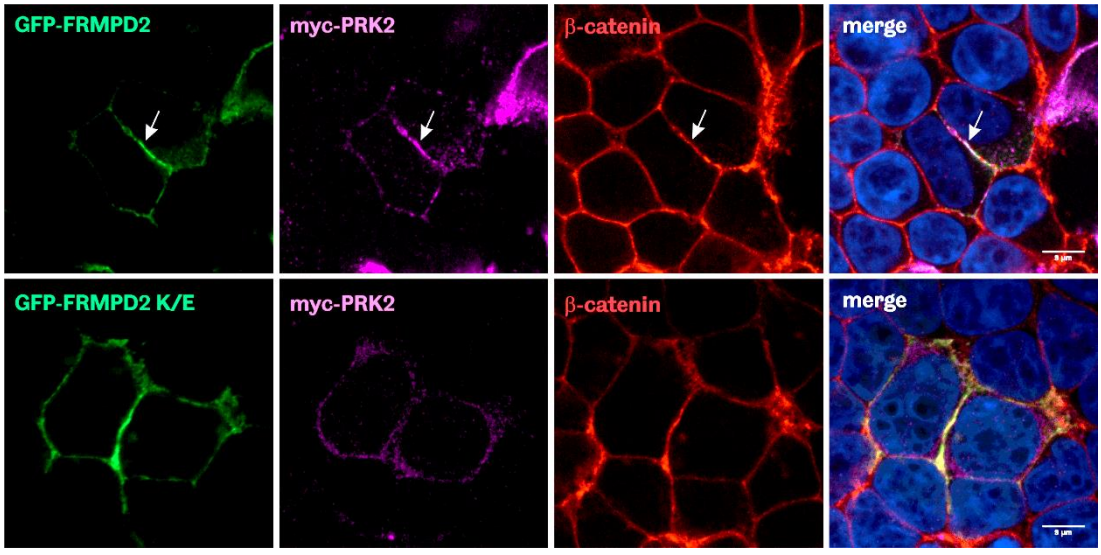

Figure 4.8 Mutated FRMPD2 does not recruit PRK2 to the cell-cell contacts

HEK293 cells were grown on coverslips and transiently co-transfected with expression constructs of myc-PRK2 and GFP-tagged FRMPD2 or GFP-tagged FRMPD2 K/E. 48 hours post transfection cells were fixed and stained with anti-β-catenin and anti-c-myc followed by anti-mouse Alexa Fluor® 568 and anti-rabbit Alexa Fluor® 647 antibody respectively. Overlapping signals of GFP-FRMPD2, myc-PRK2 and β-catenin are pointed out by arrows. Images were taken using a spinning disc confocal microscope and Z-stack function. Images represent single xy planes. Scale bar, 9 µm. (N=3)

4.3.2.2 FRMPD2 regulates PRK2 localisation in polarised epithelial cells

To test whether the new role of FRMPD2 in PRK2 recruitment to the cell membrane has a similar function in different epithelial cells, both proteins were examined for colocalization in polarised epithelial MDCK II cells. Although the transfection efficiency for MDCK II cells was usually low, the optimised protocol tested in the current study allowed to obtain up to 30-40% transfected cells. Similar to the previous co-localization study in the non-polarised HEK293 epithelial cells, GFP-FRMPD2 and myc-PRK2 were overexpressed together in MDCK II cells. Subsequent immunostaining revealed that a fraction of PRK2 colocalized with FRMPD2 at the cell membrane. The overlapping signal of both proteins with β-catenin demonstrated that FRMPD2-PRK2 protein complex localised at the basolateral membrane adjacent to other cells (Figure 4.9, upper panel, colocalisation highlighted by white arrows). It is perhaps worth mentioning that this specific distribution was visible on the Z-stack images of all cell sections, which therefore confirms the co-localization of the two proteins along the basolateral membrane of the epithelial cells. Both of the already tested PRK2 mutations affected PRK2 localisation at the plasma membrane and the mutant proteins remained in the cytoplasm (Figure 4.9, middle panels). Also, a mutation in the carboxylate-binding loop of the PDZ3 domain of FRMPD2 caused PRK2 dislocation from the plasma membrane compartments (Figure 4.9, lower panel). These data are consistent with immunolocalization study performed in non-polarised cells.

Given the fact that FRMPD2 partially localises at tight junctions (Stenzel et al., 2009) and PRK2 regulates apical junction formation (Wallace et al., 2011), it was interesting to investigate whether both proteins co-localize at tight junctions. Immunolocalization analysis using ZO-1 as a tight junction marker revealed occasional colocalization of GFP-FRMPD2 and myc-PRK2 with ZO-1 but to less

extent than with β-catenin (Figure 4.10, upper panel, colocalization pointed out by white arrows). Nevertheless, both mutations of PRK2, as well as a mutation in the PDZ3 domain of FRMPD2, affected the intracellular distribution of PRK2, and its staining was only visible in the cytoplasm as previously shown (Figure 4.10, middle and lower panels).

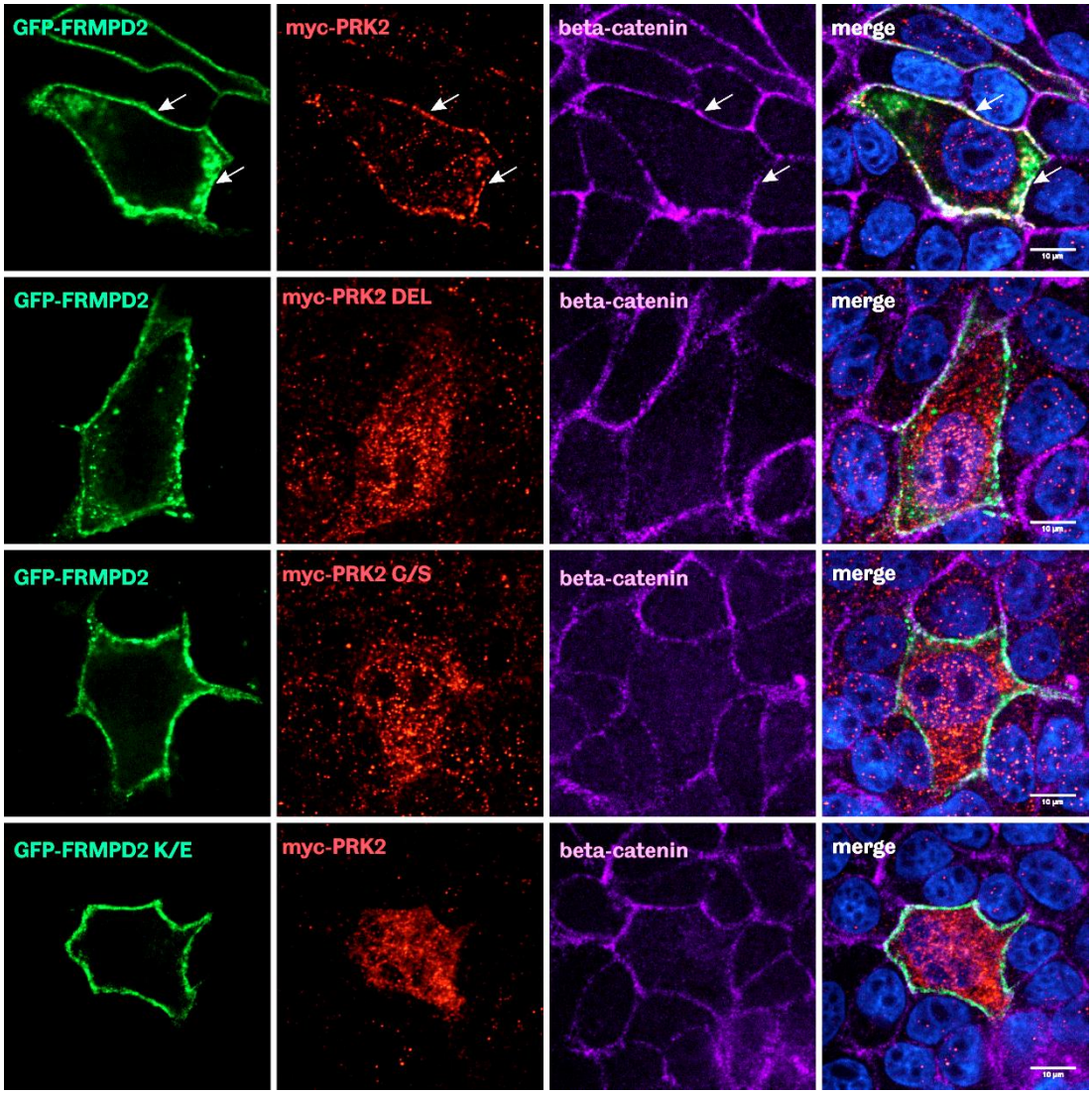

Figure 4.9 FRMPD2 recruits PRK2 to the basolateral membrane of polarised epithelial MDCK II cells

MDCKII cells were grown on coverslips and transiently co-transfected with expression constructs of GFP-tagged FRMPD2 and different forms of myc-tagged PRK2: myc-PRK2, PRK2 DEL – deletion of last three amino acids, PRK2 C/S – mutation of the C-terminal cysteine to serine) or GFP-tagged FRMPD2 K/E and myc-tagged PRK2. 48 hours post transfection cells were fixed and stained with anti-c-myc and anti-β-catenin antibody followed by anti-rabbit Alexa Fluor® 568 and anti-mouse Alexa Fluor® 647 antibody respectively. Overlapping signals of GFP-FRMPD2, myc-PRK2 and β-catenin are pointed out by arrows. Images were taken using a spinning disc confocal microscope and Z-stack function. Images represent single xy planes. Scale bar, 10 µm. (N=3)

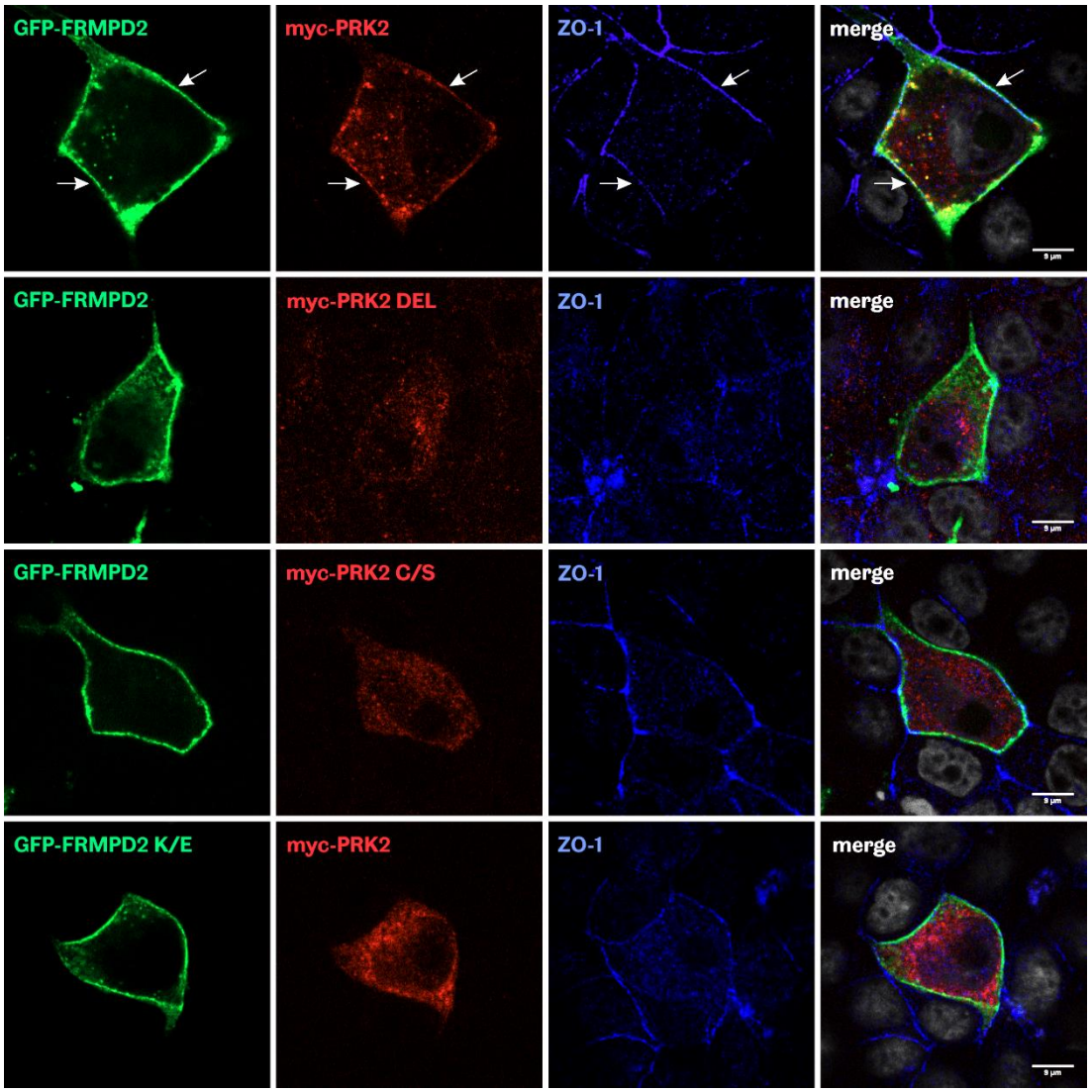

Figure 4.10 FRMPD2 recruits PRK2 to the tight junctions

MDCKII cells were grown on coverslips and transiently co-transfected with expression constructs of GFP-tagged FRMPD2 and different forms of myc-tagged PRK2: myc-PRK2, PRK2 DEL – deletion of last three amino acids, PRK2 C/S – mutation of the C-terminal cysteine to serine) or GFP-tagged FRMPD2 K/E and myc-tagged PRK2. 48 hours post transfection cells were fixed and stained with anti-c-myc and anti-ZO-1 antibody followed by anti-mouse Alexa Fluor® 568 and anti-rabbit Alexa Fluor® 647 antibody respectively. Overlapping signals of GFP-FRMPD2, myc-PRK2 and ZO-1 are pointed out by arrows. Images were taken using a spinning disc confocal microscope and Z-stack function. Images represent single xy planes. Scale bar, 9 µm. (N=3)

4.3.3 Investigating the role of the FRMPD2-PRK2 complex in apical junction formation

The new possible role of FRMPD2, acting as a scaffolding protein and recruiting PRK2 to the membrane of polarised epithelial cells, allowed us to formulate a possible model for PRK2 recruitment to cell/cell junctions. We postulated that

FRMPD2 spatially directs PRK2 to the basolateral membrane of polarised epithelial cells and therefore helps to maintain the proper function of PRK2 in apical junction formation.

4.3.3.1 Epithelial cell model for tight junction formation

To investigate the role of the FRMPD2-PRK2 complex in cell polarisation we decided to perform all experiments in 16HBE14o- human bronchial epithelial cell line, which was previously used in the study reporting the role of PRK2 in apical junction formation (Wallace et al., 2011). 16HBE14o- cells were seeded and transfected according to the protocol listed in Table 2.23 and Table 2.24. Single transfection with siRNA duplex1, targeting human PRK2, at the final concentration of 50 nM resulted in efficient PRK2 downregulation confirmed by Western Blot (Figure 4.11, A) and defective tight junction formation (Figure 4.11, B). Immunofluorescence performed with an anti-ZO-1 antibody, used here as a marker of tight junctions, demonstrated a continuous ring of zonula-occludens-1 at cell-cell contacts of non-targeting siRNA (siCTRL) transfected cells, while PRK2-depleted cells were almost devoid of tight junctions. This result was in line with previously published data and confirmed the obtained phenotype.

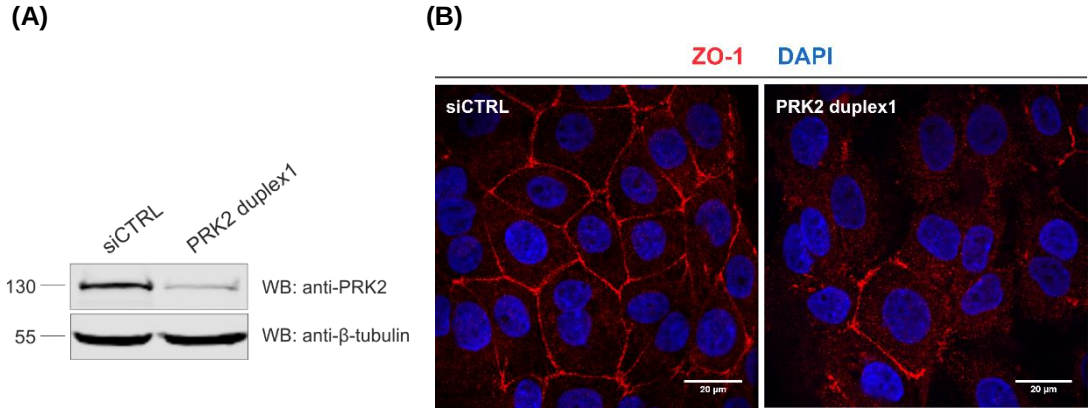

Figure 4.11 PRK2 regulates tight junction formation in 16HBE14o- cells

(A) *16HBE14o- cells were transiently transfected with siCTRL or PRK2 duplex one at the final concentration of 50 nM and incubation time 72 hours. Cell lysates were prepared, and protein concentration was estimated. Endogenous proteins were detected with anti-PRK2 and anti-β-tubulin antibodies followed by anti-mouse DyLight™ 800 antibody. Samples represented around 10% of the total cell lysate. (N=2)* ***(B)*** *16HBE14o- cells were grown on coverslips and transiently with siCTRL or PRK2 duplex 1. 72 hours post transfection cells were fixed and stained with anti-ZO-1 antibody followed by anti-rabbit Alexa Fluor® 594*

antibody respectively. Images were taken using a spinning disc confocal microscope and Z-stack function. Images represent combined multiple xy planes. Scale bar, 20 µm. (N=2)

To test whether PRK2 regulates apical junction formation also in different mammalian cell lines we decided to test Caco-2 cells which were previously used by Stenzel et al. to demonstrate a delay in tight junction formation upon FRMPD2 knockdown (Stenzel et al., 2009). Based on our previous experience with Caco-2 cells, we knew they require entirely different transfection conditions from other cells used in our lab, therefore at first, we determined PRK2 knockdown efficiency. Cells were seeded at a higher density and allowed to adhere and spread for two days before we performed transfection. Cells were transfected twice with siPRK2 duplex1 or siCTRL to a final concentration of 50 nM at day 1 and day 3 with the total incubation time of 96 hours. Western Blot confirmed efficient knockdown of PRK2 (Figure 4.12, A), similar to that obtained with 16HBE14o- cells. Subsequent staining of tight junctions demonstrated an interesting phenotype in the PRK2-depleted Caco-2 cells. Tight junctions in control cells were depicted as a continuous ring of ZO-1, while in the PRK2 devoid cells, ZO-1 staining remained continuous but warped suggesting that tight junctions did not reach the proper stage of maturation (Figure 4.12, B).

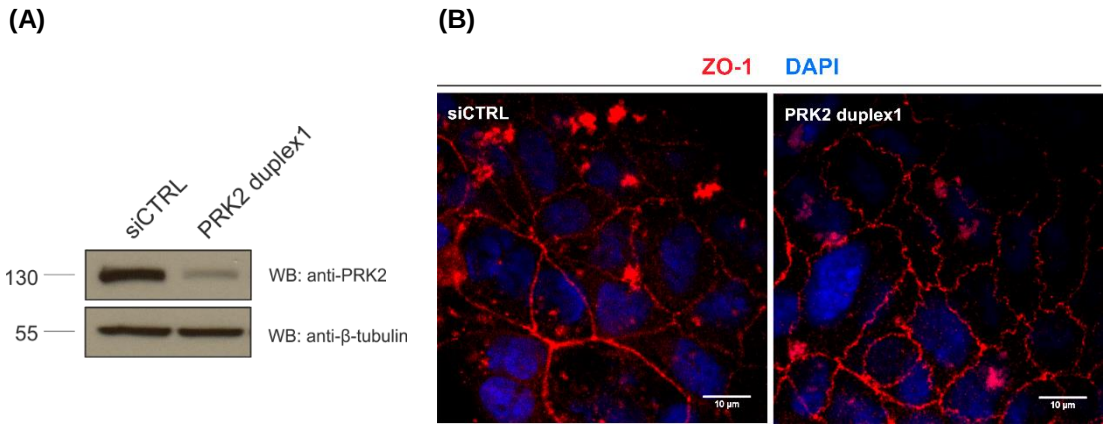

Figure 4.12 PRK2 regulates tight junction maturation in Caco-2 cells

(A) *Caco-2 cells were sequentially transfected with siCTRL or PRK2 duplex one at day 1 and day three at the final concentration 50 nM and incubation time 96 hours. Cell lysates were prepared and protein concentration was estimated. Endogenous proteins were detected with anti-PRK2 and anti-β-tubulin antibodies followed by anti-mouse DyLight™ 800 antibody. Samples represented around 10% of the total cell lysate. (N=2)* ***(B)*** *Caco-2 cells were grown on coverslips and sequentially transfected with siCTRL or PRK2 duplex one at day 1 and day three at the final concentration 50 nM. 96 hours post transfection cells were fixed and stained with anti-ZO-1 antibody followed by anti-rabbit Alexa Fluor® 594*

antibody respectively. Images were taken using a spinning disc confocal microscope and Z-stack function. Images represent combined multiple xy planes. Scale bar, 10 µm. (N=2)

Further studies with Caco-2 cells were not possible due to the problems with obtaining a homogenous monolayer of the wild-type cells, meaning that some regions on the coverslips had cells forming mature junctions and some were still on the premature stage. This prompted us to test another cell line available in the lab, polarised epithelial MDCK II cells, previously used in the current study for generation of the stable cell lines and FRMPD2-PRK2 colocalization assays. Given the fact, that these cells have not been used before in the lab for knockdown experiments, we designed two custom made siRNAs targeting canine PRK2 and tested two different transfection conditions. The first experiment was performed under similar conditions to those used for 16HBE14o- cells: single transfection with siRNA at a final concentration 50 nM and incubation 72 hours. The second test was performed based on the literature (Zuhorn et al., 2007): sequential transfection at day one and day two at a concentration of 80 nM with an incubation of 72 hours. Results from these two knockdown experiments demonstrated reduced PRK2 level, however, Western Blot analysis confirmed that sequentially transfected siRNAs provided better efficiency in PRK2 depletion (Figure 4.13, A). To check, whether altered PRK2 expression affected tight junction formation in canine epithelial cells, we performed immunofluorescence analysis with an anti-ZO-1 antibody, again testing two transfection conditions. Single transfected cells displayed normal and continuous ZO-1 staining regardless of siRNA type. However, staining of sequentially treated cells revealed that PRK2-depleted cells exhibited discontinuous and punctate tight junctions, while in control cells they were preserved in an unchanged form (Figure 4.13, B). Thus further experiments were performed with sequentially transfected cells.

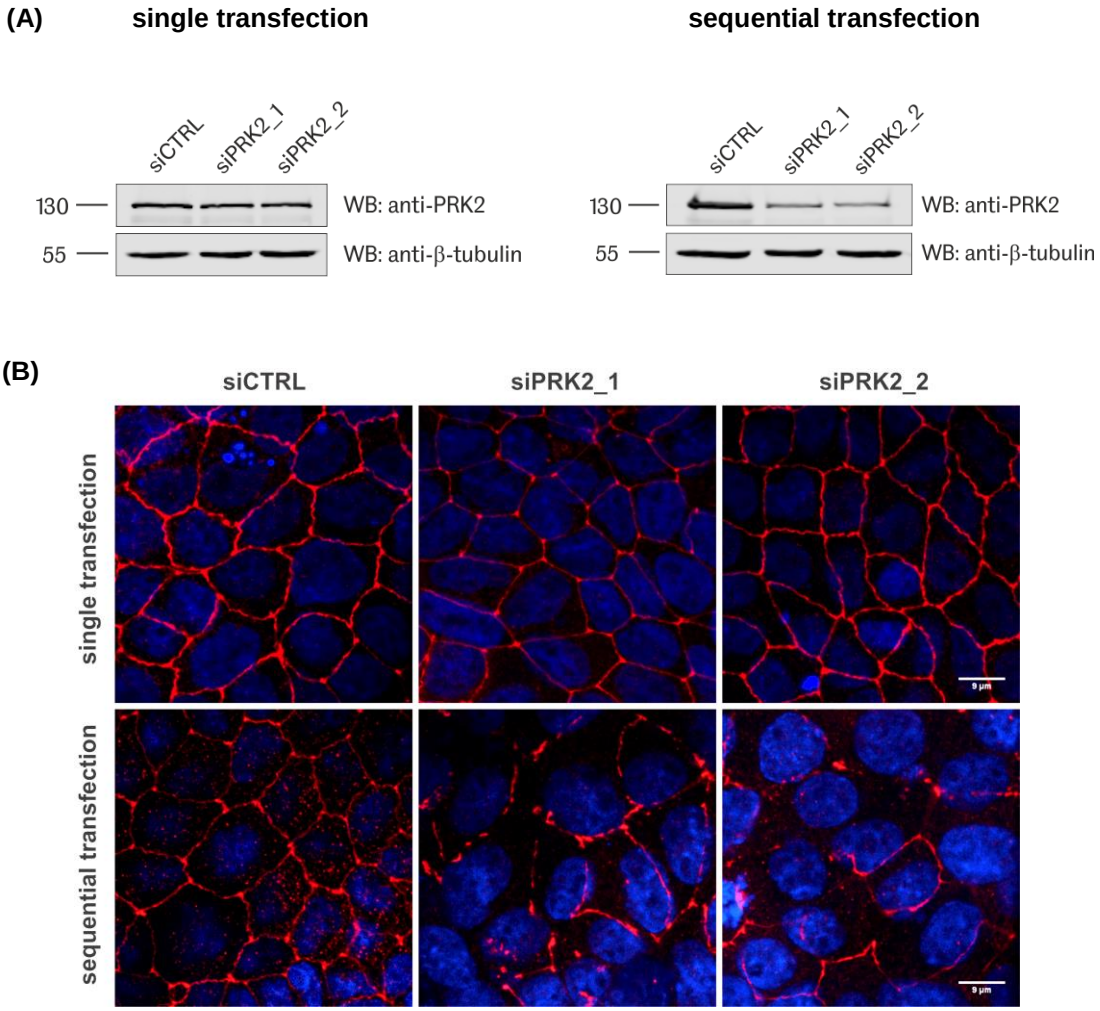

Figure 4.13 PRK2 knockdown efficiency in MDCKII cells

(A) *MDCKII cells were single transfected in serum-free medium with siRNAs: siCTRL, siPRK2_1 and siPRK2_2 at the final concentration of 50 nM and incubation time 72 hours or sequentially at day one and day two at the final concentration 80 nM and incubation time 72 hours. Cell lysates were prepared, and protein concentration was estimated. PRK2 and β-tubulin were detected with anti-PRK2 and anti-β-tubulin antibodies followed by anti-mouse DyLight™ 800 antibody. Samples represented around 10% of the total cell lysate. (N=2)* ***(B)*** *MDCKII were grown on coverslips and transfected as described in (A) and (B). After 72 hours cells were fixed and stained with anti-ZO-1 antibody followed by anti-rabbit Alexa Fluor® 594. Images were taken using a spinning disc confocal microscope and Z-stack function. Images represent combined multiple xy planes. Scale bar, 9 µm. (N=2)*

4.3.3.2 PRK2 regulates apical junction formation in MDCKII cells

Initial experiments allowed us to choose the right epithelial cell model to study apical junction formation and also confirmed that a defect in tight junction formation in MDCK II epithelial cells caused by PRK2 depletion was similar to that observed in human bronchial epithelial cells (Wallace et al., 2011). To

characterise this phenotype in more detail, we performed three independent experiments complemented with immunofluorescence and Western Blot analysis. Depletion of PRK2 caused a significant alteration in apical junction formation in polarised epithelial MDCK II cells and more than 70% of cells displayed weak and punctate staining of ZO-1 (Figure 4.14, A and B). Both siRNA efficiently downregulated PRK2 when compared to the control cells transfected with non-targeting siRNA (siCTRL), but had no effect on other proteins forming tight and adherens junctions (Figure 4.14, C). PRK2 knockdown was confirmed by quantification of signal intensities from Western Blot results from three experiments, which due to some experimental variations was performed using E-cadherin, β-catenin and β-tubulin as normalizers (Figure 4.14, D-F). Although there was a slight difference between the samples treated with siPRK2_1 and siPRK2_2, statistical analysis showed, that in both cases the downregulation of PRK2 was highly significant in comparison to the control cells. It is perhaps worth emphasising, that although in most cells, the tight junctions were not properly formed, ZO-1 expression level was not affected by the PRK2 knockdown. This result was also supported by the fact that transfection with Lipofectamine2000 did not cause any toxic effect on the cells (Figure 4.14 G), therefore it can be concluded that the phenotype seen in PRK2-depleted cells was fully triggered by PRK2 deficiency.

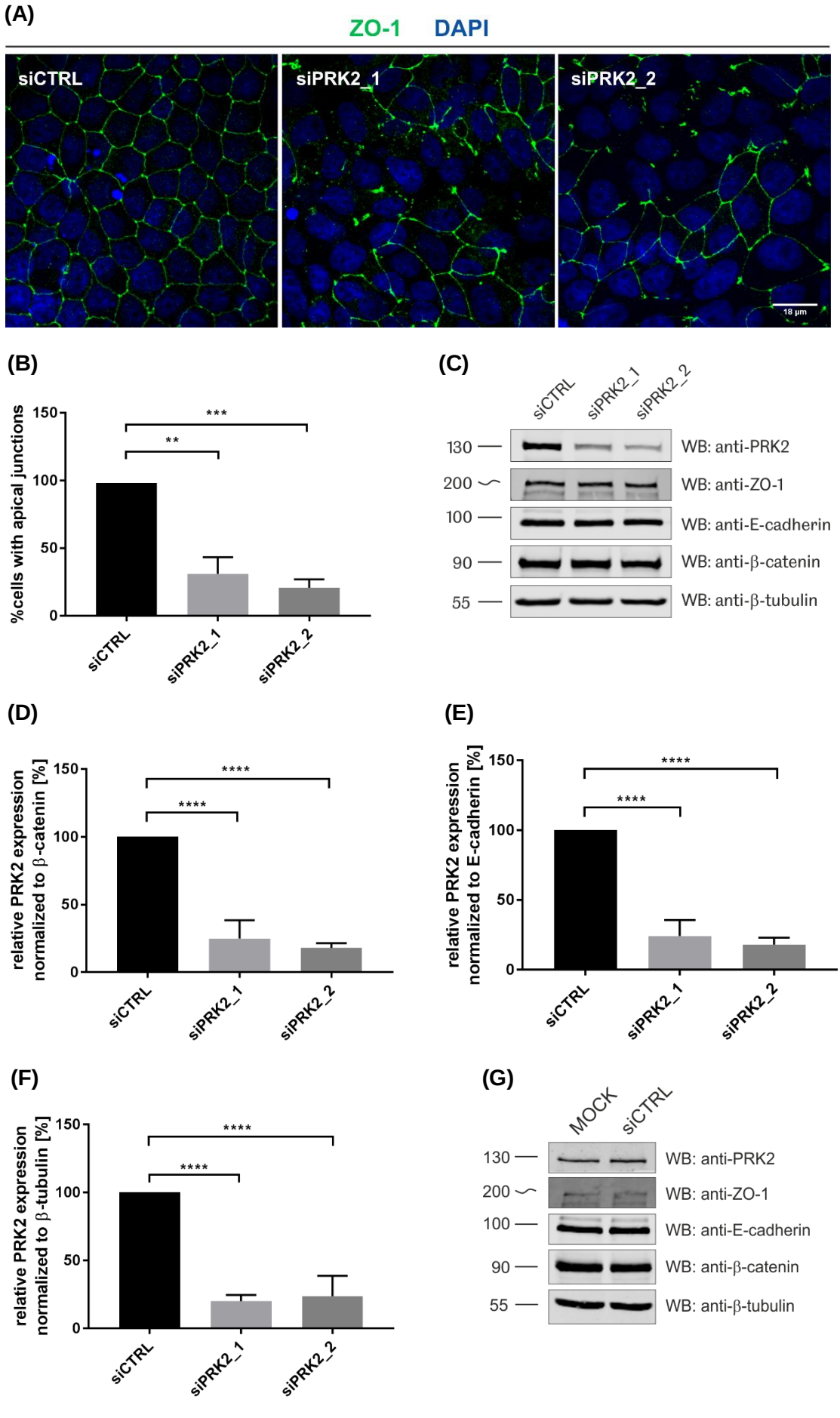
(A)
ZO-1 DAPI
siCTRL
siPRK2_1
siPRK2_2
18 µm
(B)
%cells with apical junctions
150
100
50
0
***
**
siCTRL
siPRK2_1
siPRK2_2
(C)
siCTRL
siPRK2_1
siPRK2_2
130
200
100
90
55
WB: anti-PRK2
WB: anti-ZO-1
WB: anti-E-cadherin
WB: anti-β-catenin
WB: anti-β-tubulin
(D)
relative PRK2 expression normalized to β-catenin [%]
150
100
50
0
****
****
siCTRL
siPRK2_1
siPRK2_2
(E)
relative PRK2 expression normalized to E-cadherin [%]
150
100
50
0
****
****
siCTRL
siPRK2_1
siPRK2_2
(F)
relative PRK2 expression normalized to β-tubulin [%]
150
100
50
0
****
****
siCTRL
siPRK2_1
siPRK2_2
(G)
MOCK
siCTRL
130
200
100
90
55
WB: anti-PRK2
WB: anti-ZO-1
WB: anti-E-cadherin
WB: anti-β-catenin
WB: anti-β-tubulin

Figure 4.14 PRK2 regulates apical junction formation in MDCKII cells

(A) *MDCKII were grown on coverslips and transfected as described in (A). After 72 hours cells were fixed and stained with anti-ZO-1 antibody followed by anti-rabbit Alexa Fluor® 488. Images were taken using a spinning disc confocal microscope and Z-stack function. Images represent combined multiple xy planes. Scale bar, 18 µm. (N=3)* ***(B)*** *Quantification of apical junction formation based on three independent experiments. At least 500 cells were analysed in each experiment (Materials and Methods, section 2.3.4.5). Statistical analysis was performed using one-way ANOVA with posthoc Dunnett's analysis, ** p<0,01, *** p<0,001, error bars represent ±SEM.* ***(C)*** *MDCKII cells were transfected in serum-free medium sequentially at day 1 and day two at the final concentration 80 nM and incubation time 72 hours with siRNAs: siCTRL, siPRK2_1, siPRK2_2. Cell lysates were prepared, and protein concentration was estimated. Endogenous proteins were detected with anti-ZO-1, anti-PRK2, anti-E-cadherin, anti-β-catenin and anti-β-tubulin antibodies followed by anti-rabbit Alexa Fluor®680 and anti-mouse DyLight™ 800 antibody. Samples represented around 5% of the total cell lysate. (N=3) Quantification of PRK2 knockdown efficiency based on three independent experiments. Signal intensity of PRK2 was normalised to the signal intensity of β-tubulin* ***(D)****, E-cadherin* ***(E)*** *or β-catenin* ***(F)*** *measured in the total cell lysates. Obtained values were compared and represented as relative PRK2 expression level. Signal intensity was measured using analysis tool of Image Studio™ Lite software. Signal area was the same for all samples. Statistical analysis was performed using one-way ANOVA with posthoc Dunnett's analysis, **** p<0,0001, error bars represent ±SEM.* ***(G)*** *PRK2 expression level in MDCKII cells is not affected by transfection with Lipofectamine®2000: MDCKII cells were transfected in serum-free medium sequentially at day 1 and day two at the final concentration 80 nM and incubation time 72 hours with control siRNA and additionally MOCK transfection was performed. Cell lysates were prepared, and protein concentration was estimated. Endogenous proteins were detected with anti-ZO-1, anti-PRK2, anti-E-cadherin, anti-β-catenin and anti-β-tubulin antibodies followed by anti-rabbit Alexa Fluor®680 and anti-mouse DyLight™ 800 antibody. Samples represented around 5% of the total cell lysate. (N=3)*

4.3.3.3 Can PRK2 mutants rescue the observed tight junction formation defect?

We already have shown that FRMPD2 recruited PRK2 to the basolateral membrane of polarised epithelial cells and based on this result we suggested that through the binding to FRMPD2, PRK2 maintains its role in apical junction formation. Furthermore, this led us to the assumption that the defect in tight junction formation observed in PRK2-depleted cells might not be rescued by a PRK2 mutant carrying a mutation of the C-terminal cysteine, which does not bind to FRMPD2. To check this possibility we planned to perform a rescue experiment with constructs containing human PRK2. Sequences of siRNAs targeting the PRK2 gene in MDCK II cells were aligned to the sequence of the human gene and such comparison revealed that constructs containing human PRK2 could serve as siRNA-resistant forms suitable for rescue experiments in MDCK II cells treated only with siPRK2_2 (Figure 4.15).

```
hPRK2          GCAAAGAAGGAATGGGATA
siPRK2_1       GCAAAGAAGGAATGGGATA
               ******************

hPRK2          CCTTGGGGCTAGCGAGAAA
siPRK2_2       CCTTGGAGCTGGTGAGAAA
               **********.*.*******
```

Figure 4.15 Sequence alignment of siRNAs targeting canine PRK2 with human PRK2

Multiple sequence alignment of siRNAs targeting canine PRK2: siPRK2_1 and siPRK2_2 with human PRK2. Red asterisks mark Non-matching nucleotides. Sequence of human gene PRK2 was retrieved from https://www.ncbi.nlm.nih.gov/nuccore/NM_006256.3, and multiple sequence alignment was run using Clustal Omega tool available on the website: http://www.ebi.ac.uk/Tools/msa/clustalo/

With the initial experiments, we aimed to test the resistance of human PRK2 to siPRK2_2 targeting the canine version of PRK2. To this end, we co-transfected siCTRL and siPRK2_2 with GFP and CFP-PRK2. CFP-PRK2 unlike myc-PRK2, used in the current study, differed from the endogenous PRK2 by around 25 kDa (due to the tag) and could be easily distinguished on Western Blot. Our experiments demonstrated efficient PRK2 knockdown and good expression level of GFP and CFP-PRK2 but also confirmed that CFP-PRK2 expression was not affected by siPRK2_2. (Figure 4.16).

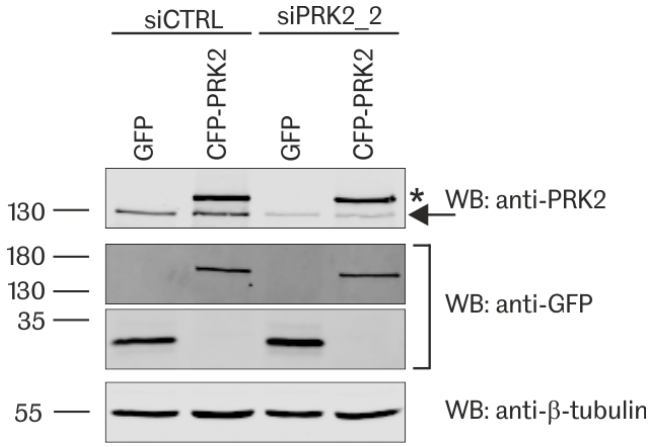

Figure 4.16 Expression of human PRK2 is not affected by siPRK2_2 targeting endogenous PRK2 in MDCK II cells

MDCKII cells were transfected in serum-free medium first with GFP or CFP-PRK2 constructs and after 6 hours with siCTRL or siPRK2_2 sequentially at day one and day two at the final concentration 80 nM and incubation time 72 hours. Cell lysates were prepared, and protein concentration was estimated. Endogenous proteins were detected with anti-PRK2 and anti-β-tubulin antibodies followed by anti-mouse DyLight™ 800 antibody while overexpressed

proteins with anti-GFP antibody followed by anti-rabbit Alexa Fluor® 680. Samples represented around 10% of the total cell lysate. The size of endogenous PRK2 was marked by arrow and size of overexpressed CFP-PRK2 by an asterisk. (N=2)

Although immunoblot results were promising, there was a clear problem with the viability of the transfected cells which were unable to form a tight monolayer (data not shown). Therefore the transfection protocol requires further optimisation.

4.3.3.4 Does FRMPD2 affect apical junction formation in MDCK-II cells?

Previously published data implicated FRMPD2 in tight junction formation in Caco-2 cells, however, the phenotype was represented only by measurements of transepithelial electrical resistance (Stenzel et al., 2009). To check whether FRMPD2 deficiency will have a similar effect on apical junction formation as PRK2 knockdown, we tested two custom made siRNAs targeting canine FRMPD2 in three independent experiments. Cells were transfected sequentially using the same transfection conditions as described before for experiments with PRK2. Immunofluorescence data demonstrated that apical junctions formed a continuous monolayer, represented by a normal and intact ZO-1 staining regardless of the tested siRNA used (Figure 4.17, A). Although some cells displayed a discontinuous or punctate ZO-1 staining upon FRMPD2 knockdown, the statistical analysis showed no significant difference between knockdown and control cells (Figure 4.17 B). Although the result seemed to be quite unambiguous, it needs to be stressed that these experiments have been performed without validation of the FRMPD2 knockdown due to the lack of a suitable antibody. Experiments need to be repeated with validating the knockdown by alternative means like quantitative PCR.

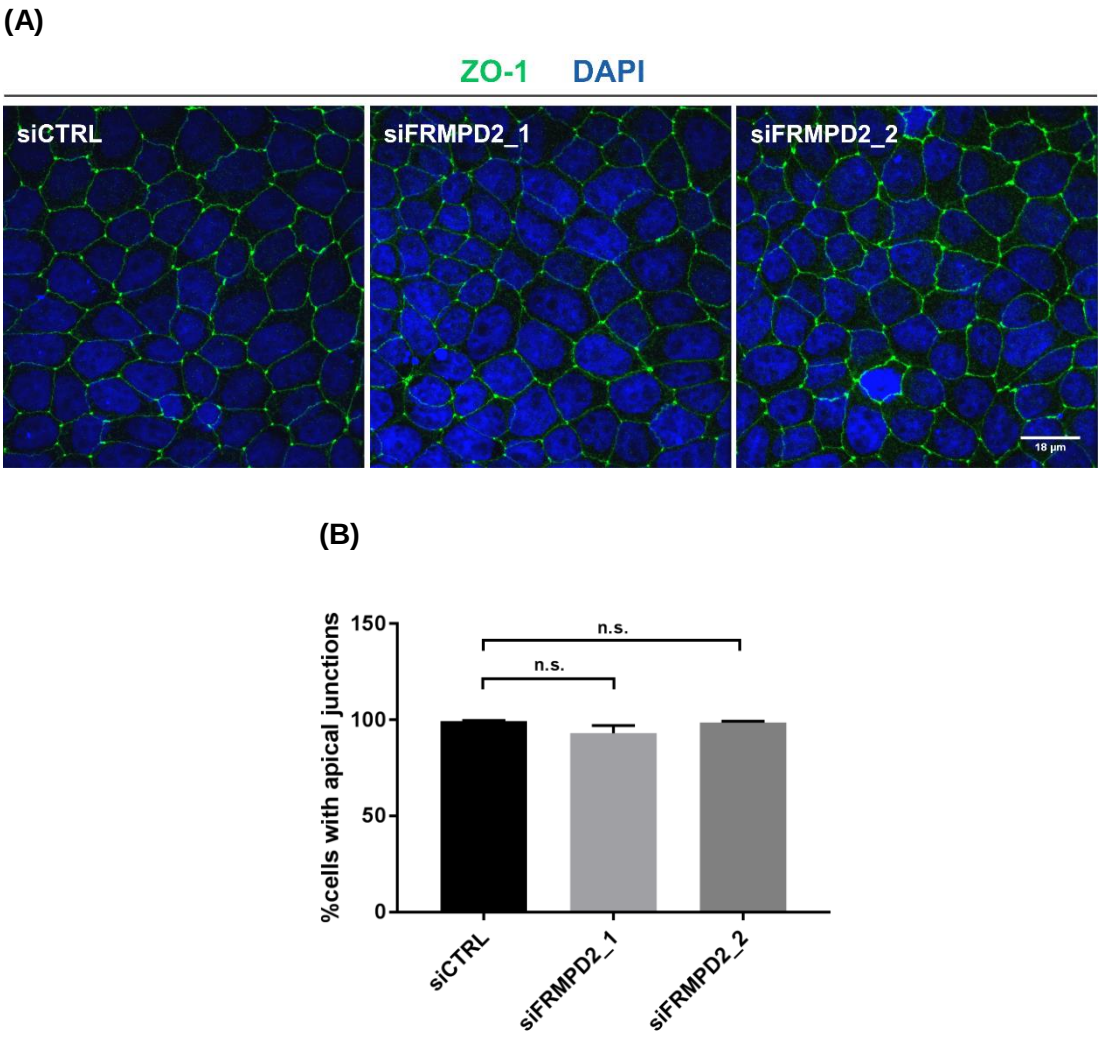

Figure 4.17 FRMPD2 depletion does not affect apical junction formation in MDCK-II cells

(A) *MDCK-II were grown on coverslips and transfected in serum-free medium sequentially at day one and day two at the final concentration 80 nM and incubation time 72 hours with siRNAs: siCTRL, siFRMPD2_1, siFRMPD2_2. After 72 hours cells were fixed and stained with anti-ZO-1 antibody followed by anti-rabbit Alexa Fluor® 488. Images were taken using a spinning disc confocal microscope and Z-stack function. Images represent combined multiple xy planes. Scale bar, 18 µm. (N=3)* ***(B)*** *Quantification of apical junction formation based on three independent experiments. At least 600 cells were analysed in each experiment. Statistical analysis was performed using one-way ANOVA with posthoc Dunnett's analysis, n.s. p<0,05, error bars represent ±SEM.*

4.4 Discussion

The current study provides strong evidence of an interaction between FRMPD2 and the RhoA effector kinase PRK2. PRK2 drew our attention as a potential interaction partner of FRMPD2 as both proteins have been shown to regulate tight junction formation (Stenzel et al., 2009, Wallace et al., 2011). Experiments performed in HEK293 cells proved that both proteins form a complex and interact in a highly specific manner. PRK2 has been shown to interact selectively with the PDZ3 domain of mouse PTPN13 (Gross et al., 2001), which shares a similar domain structure with its human ortholog FRMPD2. In this study we demonstrate that PRK2 binds exclusively only to the PDZ3 domain of FRMPD2, and no interaction could be detected with the other domains of FRMPD2. PDZ domains are essential protein-protein interaction modules containing a specific carboxylate binding loop that bind very short amino acid motifs localised at the extreme C-terminus of the target protein (Saras and Heldin, 1996, Fanning and Anderson, 1996, Lee and Zheng, 2010). Single-amino acid substitution of the conserved lysine or arginine residues in the carboxylate-binding loop is a key determinant for the interactions mediated by PDZ domains (Gee et al., 2000). To examine the importance of the conserved lysine in the binding loop of the PDZ3 domain of FRMPD2, we have used *in vitro* mutagenesis and analysed binding properties of the PDZ3 domain mutant. We found that single-amino-acid replacement of lysine 1084 in the carboxylate-binding loop of the PDZ3 domain of FRMPD2 led to complete abolishment of interaction with PRK2, therefore we concluded that this residue is a critical determinant of PDZ3 domain affinity to PRK2 kinase. Given the fact that interaction with PRK2 is mediated by the PDZ3 domain of mouse PTPN13 (Gross et al., 2001) and human FRMPD2, which share high similarity within the carboxylate binding loop responsible for ligand binding, we hypothesised that these two PDZ domains recognise the same binding motif within the PRK2 sequence. Our coimmunoprecipitation experiments with different PRK2 mutants demonstrated that the interaction with FRMPD2 depends on the C-terminal cysteine in PRK2 sequence, which in fact is strongly conserved in PRK2 homologues from different species (Gross et al., 2001). It can suggest that the C-terminal part of PRK2 has a significant effect on PRK2-mediated signalling, but also that the interaction with FRMPD2 is

conserved between the species. We also speculate that PTPN13 and FRMPD2 proteins assemble the PRK2 complex at two opposing membranes of polarised epithelial cells and provide spatial specificity for PRK2 signalling modules.

All the biochemical assays used for validation and characterisation of FRMPD2-PRK2 interaction were complemented with colocalization studies in non-polarised and polarised epithelial cells. Immunolocalization studies clearly showed that FRMPD2 recruits PRK2 to the plasma membrane in both types of epithelial cell and mutation of the C-terminal cysteine of PRK2 as well as the substitution of lysine 1084 in the PDZ3 domain of FRMPD2 not only impaired the interaction but also PRK2 localisation at cell-cell contacts. In polarised epithelial MDCK II cells, the localisation of the FRMPD2-PRK2 complex can be specifically determined as basolateral, however, we could also show that FRMPD2 directs PRK2 to the tight junctions. Overall our co-localisation studies suggest that PRK2 localises to the same cellular compartments in epithelial cells where FRMPD2 is present. Possible regulation of PRK2 function and signalling by its recruitment to the plasma membrane resembles the mechanism of spatial assembly of NOD2-signaling components mediated by FRMPD2 in polarised epithelial cells (Lipinski et al., 2012). This can further prove the concept that FRMPD2 acts as a scaffold integrating elements of signalosomes relevant to epithelial cell polarisation, but the real function in cell polarisation is mediated by other effector proteins like PRK2 kinase.

As mentioned before, PRK2 has been shown to regulate apical junction formation in human bronchial epithelial cells (Wallace et al., 2011). In this study we demonstrated that PRK2 may regulate the maturation of apical junctions in Caco-2 cells. However, later problems with cell culture conditions prevented us from repeating experiments. Employment of a cell line originating from different species proved that depletion of PRK2 also caused a defect in apical junction formation in the polarised MDCK II cells. It is perhaps worth to mention that siRNA-mediated targeting of PRK2 in MDCK II cells affected the proliferation rate and this was visible in the number of cells counted per image frame. This observation corroborated with the previously reported findings of an inhibited

cytokinesis in PRK2-depleted cells, however we did not observe formation of multinucleated cells (Schmidt et al., 2007).

PRK2 belongs to the AGC kinase family, whose biological function strongly depends on their translocation to the plasma membrane (Peterson and Schreiber, 1999). However, like for most of the AGC kinases, the mechanism of PRK2 membrane localisation remains elusive and requires further investigation. FRMPD2 restriction to the basolateral membrane and PRK2 recruitment to primordial junctions in polarised epithelial cells helped us to formulate the hypothesis that FRMPD2 recruits PRK2 to the basolateral membrane where kinase can effectively regulate apical junction formation. A positive role in the regulation of tight junction formation was already demonstrated for other PDZ domain proteins like PALS1 or Dlg1, which recruited their interaction proteins to the membrane and thereby facilitated tight junction formation (Shin et al., 2005, Stucke et al., 2007). On the other hand, we postulated that loss of the ability to bind FRMPD2 caused by mutation of the C-terminal cysteine of PRK2 would cause a similar defect in maturation of epithelial junctions as PRK2 depletion (Figure 4.18). Difficulties arose, however, when we tried to optimise transfection conditions, which had a clear impact on cell viability. Because these experiments were carried out in the last weeks of current study, there was not enough time to perform further tests.

To test our hypothesis and answer the question whether FRMPD2 plays a significant role in apical junction formation by recruiting PRK2 to the basolateral membrane of polarised epithelial cells, it would be necessary to optimize transfection conditions and perform rescue experiments with a PRK2 mutant carrying mutation of the C-terminal cysteine with further immunoanalysis of junction formation. Another possible experiment would require FRMPD2 knockdown and immunoanalysis of PRK2 localisation in MDCK II cells. However, we would need to confirm FRMPD2 knockdown e.g. by qPCR and find or produce a suitable antibody for PRK2 detection by immunofluorescence.

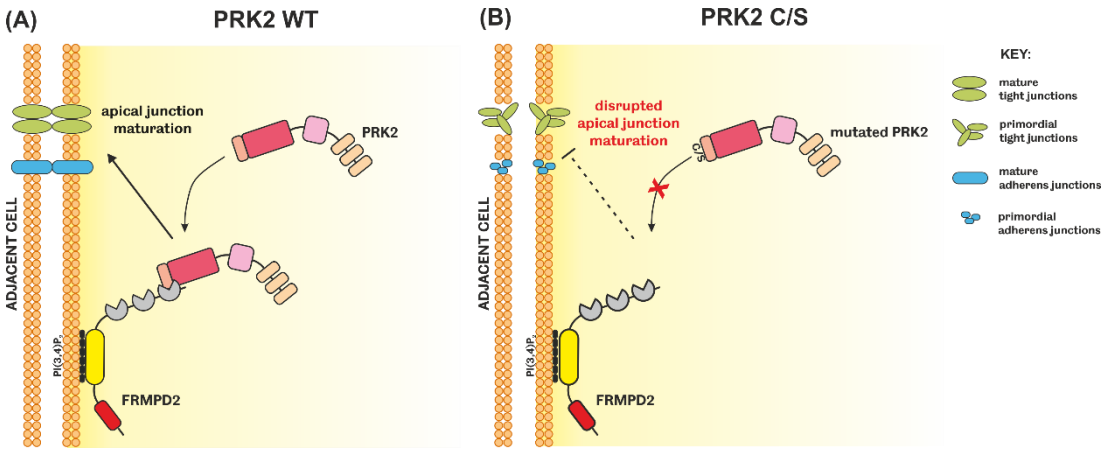

Figure 4.18 Spatial specificity of PRK2-mediated apical junction formation

(A) *PRK2 WT is recruited to the basolateral membrane by FRMPD2 and regulate maturation of primordial junctions in polarised epithelial cells.* ***(B)*** *Mutation of the C-terminal cysteine of PRK2 (PRK C/S) impairs interaction with FRMPD2. PRK2 cannot be translocated to the membrane, and that potentially leads to defect in apical junction formation.*

CHAPTER 5 - The role of FRMPD2 and PRK2 in cell mechanics and migration

5.1 Introduction

Cell polarity relies on two essential features: the unequal distribution of membrane proteins and lipids between opposite poles of the cell, and the orientated arrangement of cytoskeletal components like actin filaments and microtubules. Although the cytoskeleton seems to be a rigid structure, which spatially distributes the content of the cell, it undergoes continual reorganisation and modification to enable cell movement and shape change. Similar to different cellular components, the function of the cytoskeleton depends on the activity of other proteins and organelles. Cytoskeletal structures anchor many building blocks composed of adhesive molecules and scaffolding proteins that integrate with the plasma membrane and apical junctions of polarised epithelial cells. Proteins that are associated with the cytoskeleton and are essential for the establishment and maintenance of cell polarity belongs to the PDZ domain protein family. Some PDZ proteins like ZO-1 and AF-6 that form tight junction complexes, bind actin filaments directly (Mandai et al., 1997, Fanning et al., 1998), but other PDZ family members interact with cytoskeleton-binding proteins, thereby creating a higher-order complexes that stabilise the cytoskeleton structure (Reczek et al., 1997). It has been shown that inflammatory mediators drive apical junction disassembly and alter organisation of actin filaments associated with epithelial junctions (Ivanov et al., 2010a). During inflammation in IBD, disruption of the epithelial junctions leads to the dysfunction of the epithelial barrier and an increased epithelial permeability, which facilitates the entrance of external pathogens into deeper tissue layers (Laukoetter et al., 2008, Michielan and D'Inca, 2015). Epithelial integrity is directly correlated with the integrity of the cell cytoskeleton, therefore changes in the cytoskeleton structure are reflected in different cell mechanical behaviour. FRMPD2 as a scaffold protein is thought to be connected to the cortical actin cytoskeleton, therefore impaired functionality of the FRMPD2-mediated protein complex may result in a direct or indirect change of mechanical properties of the epithelial cells.

5.2 Aim

We hypothesised that FRMPD2 expression and signalling complexes have an effect on the cytoskeleton in epithelial cells and as a potential scaffolding protein representing a linkage between the plasma membrane and the cytoskeleton, an impaired FRMPD2 function would affect the mechanical properties of the epithelial cells. Hence the main aim of this part of the study was:

1. To examine an effect of FRMPD2 and its interaction partner PRK2 on cell mechanical properties
2. To investigate how FRMPD2 and its interaction partner PRK2 affect cell migration
3. To determine FRMPD2 localisation and function in migrating cells

5.3 Results

5.3.1 Depletion of FRMPD2 or PRK2 affects cell mechanical properties

Structure and function of the different cell types, including epithelial cells, are mainly governed by the cytoskeleton, which is formed of an interconnected system of filamentous polymers and other supportive proteins. Cell mechanical properties and also cellular behaviour result from the inner and outer physical stress applied to the cytoskeletal scaffold. Main considerations are currently centred around two questions: 1. how the cytoskeletal network produces, transmits and reacts to mechanical signals? and 2. how to measure this cellular response? Changes in the cytoskeleton structure are reflected directly in the shape and elasticity of the cell, therefore measurement of cell deformability allows to investigate and assess the effect of the applied treatment or gene function on cell mechanics. Cytoskeletal properties differ in adherent and suspended cells mainly due to the absence of actin stress fibers in the latter. It has been shown that cell mechanical properties are subject to change once the cells are transferred from adherent to suspended state (Maloney et al., 2010). There are many available methods that allow assessing mechanical properties of the cell but most of them provide limited information about cell mechanics on an intermediate, subcellular scale and still require physical contact between the cell

and surface (Guck et al., 2010). To determine global cell mechanical effects of FRMPD2 and PRK2 depletion we decided to measure cell deformability in a suspended state with an optical stretcher and real-time deformability cytometry described in more detail the sections 2.2.4.1 and 2.2.4.2. These experiments have been performed at TUD Dresden in collaboration with Prof Jochen Guck during a one-month secondment to Germany.

To investigate changes in mechanical properties of HeLa cells treated with shRNAs or siRNAs targeting FRMPD2 or PRK2 and corresponding non-targeting controls, we measured whole-cell compliance of cells in a suspended state. HeLa cells grown in the adherent state were detached from the plate surface by trypsinization and resuspended in PBS before deformability measurement in an optical stretcher. HeLa cells treated with two shRNAs against FRMPD2 appeared to be more deformable in comparison to control transfected cells, and that was reflected in the higher compliance of FRMPD2-depleted cells (Figure 5.1 A). Increased compliance was also observed when HeLa cells were treated with siRNA targeting PRK2 (Figure 5.1 C). As shown in Figure 5.1 B and D cells depleted of either FRMPD2 or PRK2 exhibited a significantly higher peak compliance than corresponding control cells measured at the end of the stretch period (t = 5s). Knockdown of PRK2 was confirmed by Western Blot (Figure 5.1 E), but FRMPD2 depletion was not verified at the time when OS experiments were carried out (for FRMPD2 knockdown, please refer to Chapter 7 and section 7.3.3). In both cases, OS experiments demonstrated that depletion of either FRMPD2 or PRK2 decreased cell stiffness, therefore we can conclude that these two proteins affect the mechanical properties of HeLa cells. Although the result seemed to be quite unambiguous, it needs to be stressed that these experiments have been performed without validation of the FRMPD2 knockdown due to the lack of a suitable antibody. Experiments need to be repeated with validating the knockdown by alternative means like quantitative PCR.

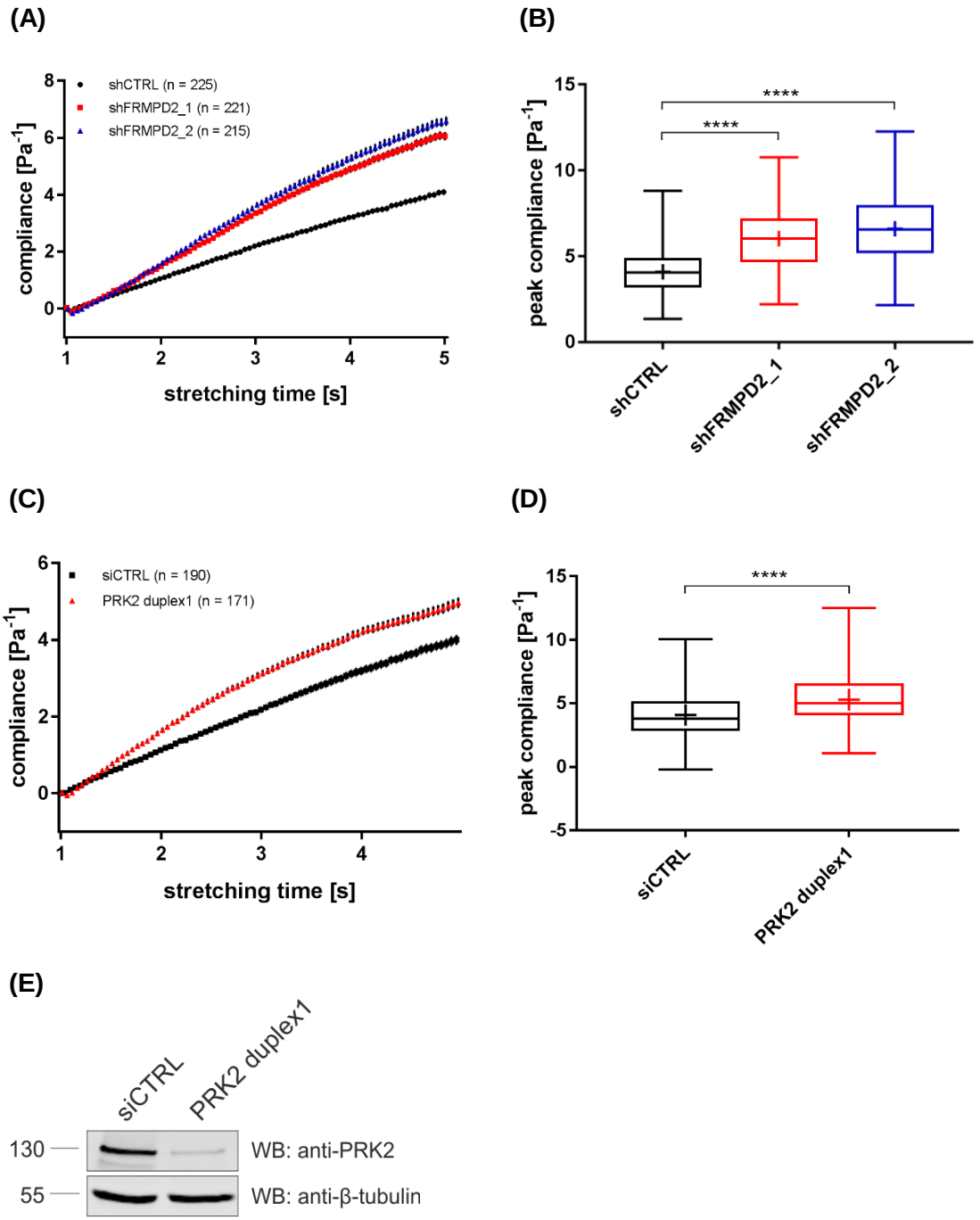

Figure 5.1 Depletion of FRMPD2 or PRK2 soften suspended adherent HeLa cells

(A) *Compliance of HeLa cells treated with shFRMPD2_1 (n = 221) and shFRMPD2_2 (n = 215) compared to control cells treated with non-targeting shCTRL (n = 225); graph presents mean values with error bars representing ±SEM from three independent experiments.* ***(B)*** *Box plots of the peak compliance for HeLa cells treated with shCTRL, shFRMPD2_1 and shFRMPD2_2 measured at the end of the stretch period t = 5s from three independent experiments; whiskers represent min and max values, horizontal box lines 25 – 75% range and median line, the mean is represented by '+'. Statistical analysis was performed using one-way ANOVA with posthoc Dunnett's analysis: shCTRL: 4.098 ± 0.0909, shFRMPD2_1: 6.033 ± 1.303, shFRMPD2_2: 6.605 ± 0.1388; **** p<0,0001.* ***(C)*** *Compliance of HeLa cells treated with PRK2 duplex1 (n = 171) compared to control cells treated with*

non-targeting siCTRL (n = 190); graph presents mean values with error bars representing ±SEM from three independent experiments. ***(D)*** *Box plots of the peak compliance for HeLa cells treated with siCTRL, PRK2 duplex1 measured at the end of the stretch period t = 5s from three independent experiments; whiskers represent min and max values, horizontal box lines 25 – 75% range and median line, the mean is represented by '+'. Statistical analysis was performed using paired t-test: siCTRL: 4.078 ± 0.1124, PRK2 duplex1: 5.292 ± 0.1285; **** p<0,0001.* ***(E)*** *PRK2 knockdown confirmation by Western Blot: HeLa cells were transfected with siCTRL and PRK2 duplex1 at the final concentration 50 nM and incubation time 72 hours. Cell lysates were prepared, and protein concentration was estimated. Endogenous proteins were detected with anti-PRK2 and anti-β-tubulin antibodies followed by anti-mouse DyLight™ 800 antibody. Samples represented around 5% of the total cell lysate. (N=3)*

To demonstrate the effect of FRMPD2 and PRK2 depletion on HeLa cell deformation at a shorter timescale than the one used in the optical stretcher, we employed real-time deformability cytometry technique, which measures cell deformation caused by hydrodynamic stress. HeLa cells were treated in the same way as before and we then performed experiments for FRMPD2 and PRK2-depleted cells along with corresponding controls. All measurements, carried out at three different flow rates for cells treated with shRNA targeting FRMPD2, demonstrated that there was no significant difference in comparison to control cells (Figure 5.2 A-C). The size and deformation of all the examined cells in the reservoir were comparable (data not shown). We observed a variation between experimental repeats, therefore it was difficult to make a final conclusion.

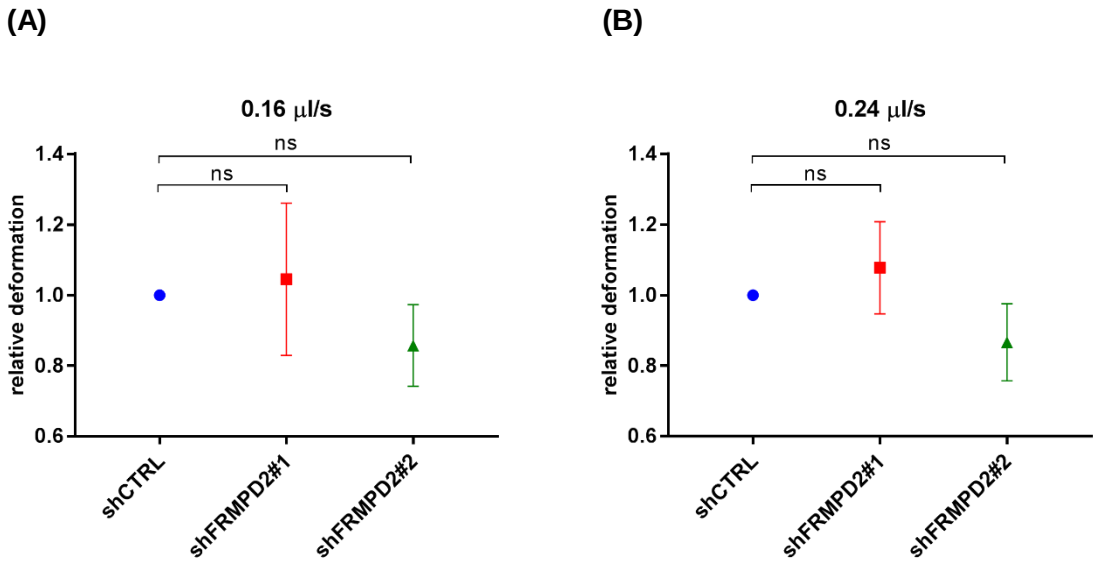

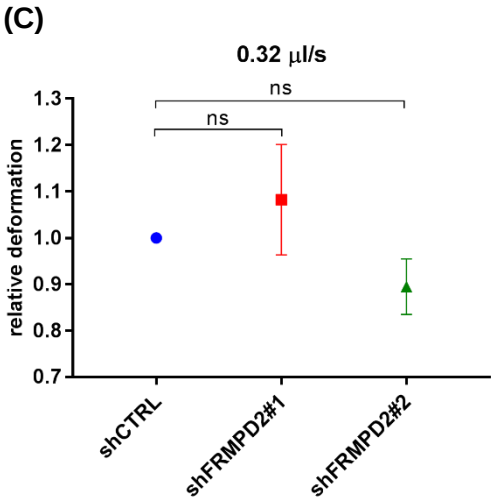

Figure 5.2 Depletion of FRMPD2 does not affect deformability of suspended adherent HeLa cells measured by RT-DC

Deformability of HeLa cells treated with shCTRL, shFRMPD2_1 and shFRMPD2_2 measured at 0.16 µl/s ***(A)****, 0.24 µl/s* ***(B)****, 0.32 µl/s* ***(C)****. Graphs show mean relative deformation values of three replicates. Analysis was performed using ShapeOut 0.7.0 software and enabled extraction of deformation mode values for each population. Statistical analysis data was performed using unpaired t-test.*

The same experiments performed with PRK2-depleted cells revealed that there was a significant difference in the deformability between PRK2-depleted cells and control cells only at the flow rate 0.24 µl/s. The size and deformation of all the examined cells in the reservoir were comparable (data not shown). Although knockdown of PRK2 decreased cell stiffness, and these results were in line with OS data, variation between different flow rates made it difficult to make a final conclusion.

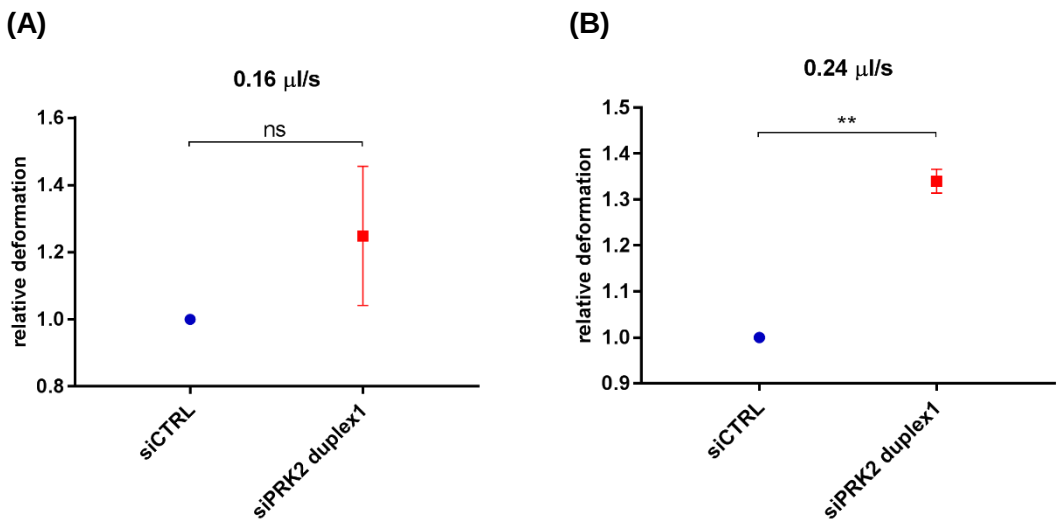

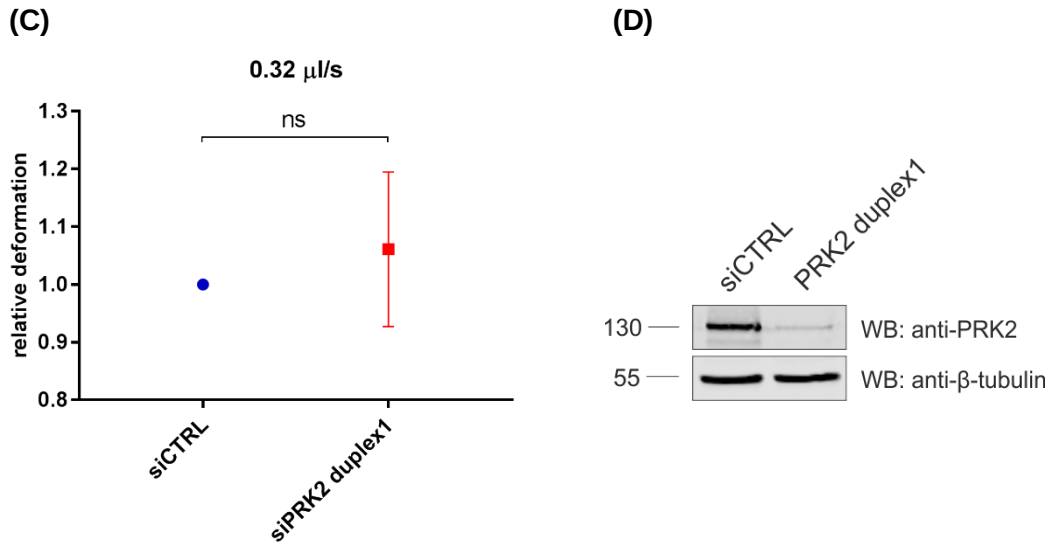

Figure 5.3 Depletion of PRK2 affects deformability of suspended adherent HeLa cells

Deformability of HeLa cells treated with siCTRL and PRK2 duplex1 measured at 0.16 µl/s ***(A)****, 0.24 µl/s* ***(B)****, 0.32 µl/s* ***(C)****. Graphs show mean relative deformation values of two replicates. Analysis was performed using ShapeOut 0.7.0 software and enabled extraction of deformation mode values for each population. Statistical analysis data was performed using unpaired t-test; ** p<0.01.* ***(D)*** *PRK2 knockdown confirmation by Western Blot: HeLa cells were transfected with siCTRL and PRK2 duplex1 at the final concentration 50 nM and incubation time 72 hours. Cell lysates were prepared, and protein concentration was estimated. Endogenous proteins were detected with anti-PRK2 and anti-β-tubulin antibodies followed by anti-mouse DyLight™ 800 antibody. Samples represent around 5% of the total cell lysate.*

5.3.2 FRMPD2 and PRK2 deficiency promotes cell migration

Mechanical properties can be considered as a regulating factor of cell architecture and biological processes within the cell. On the other hand, mechanical behaviour may be triggered by alterations that occur at the level of processes that control signalling and structural modes. Given the fact that mechanical forces are implicated in such processes like cell spreading and migration (du Roure et al., 2005, Lange and Fabry, 2013), and as previously seen, knockdown of either FRMPD2 or PRK2 decreased cell stiffness, further examination was performed towards recognition of a potential function of these proteins in cell migration. To do so, HeLa cells depleted of either FRMPD2 or PRK2 were starved overnight in serum-free medium and subsequently subjected to migration for 18 hours through the 8 µm-pores of the transwell inserts using FCS as chemoattractant. As shown in Figure 5.4 A and B, migration of HeLa cells treated with two different shRNAs targeting FRMPD2 increased significantly as compared to the control

cells. 1.5 times more cells migrated when cells were transfected with shFRMPD2_1, while twice more cells migrated through the filter membrane when FRMPD2 was depleted by shFRMPD2_2.

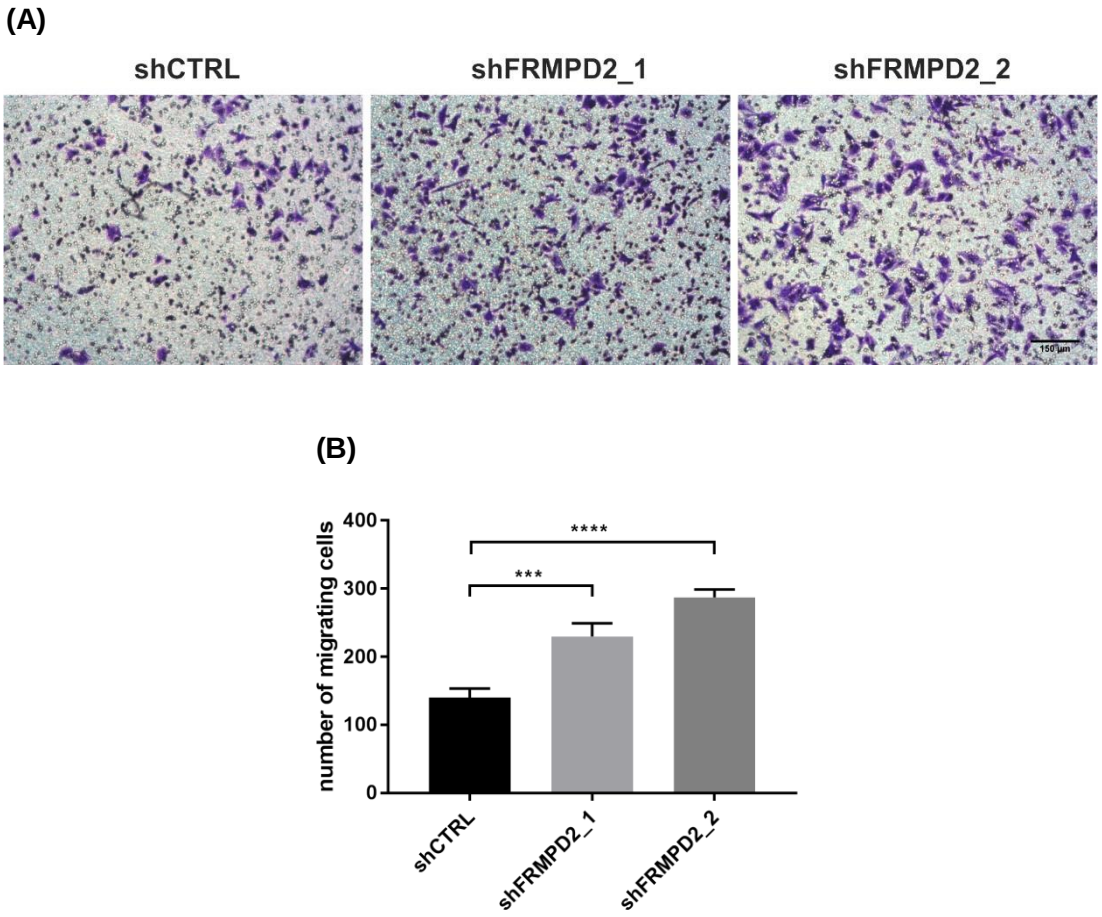

Figure 5.4 Knockdown of FRMPD2 promoted HeLa cells migration

(A) *HeLa cells were grown on 35 mm dish and transfected with shCTRL, shFRMPD2_1 and shFRMPD2_2. 40 h post transfection cells were starved overnight with serum-free medium containing 0.2% BSA. Subsequently, cells were trypsinized, counted and seeded in the upper compartment of the insert while lower compartment was filled with medium containing 10% FCS. Cells were subjected to migration for 18 hours. The filter membrane was fixed, and migrated cells were stained with crystal violet. Images were taken using a brightfield inverted microscope with a Digi-Pad 9556.5600 M. Scale bar, 150 µm. (N=3)* ***(B)*** *Migrated cells were counted using ImageJ software and quantified based on three independent experiments: shCTRL: 140 ± 12.7, shFRMPD2_1: 230 ± 18.3, shFRMPD_2: 287 ± 11.2. Statistical analysis was performed using one-way ANOVA with posthoc Dunnett analysis, *** p<0,001 and **** p<0,0001, error bars represent ±SEM.*

A more prominent effect was also observed when HeLa cells were devoid of PRK2 (Figure 5.5 C) and more than three times more cells migrated after 18 hours as compared to the cells treated with non-targeting siRNA (Figure 5.5 A and B). The significantly increased motility of FRMPD2- and PRK2-depleted HeLa cells suggest that both proteins are required for normal HeLa cell migration and can function as negative regulators in cell migration.

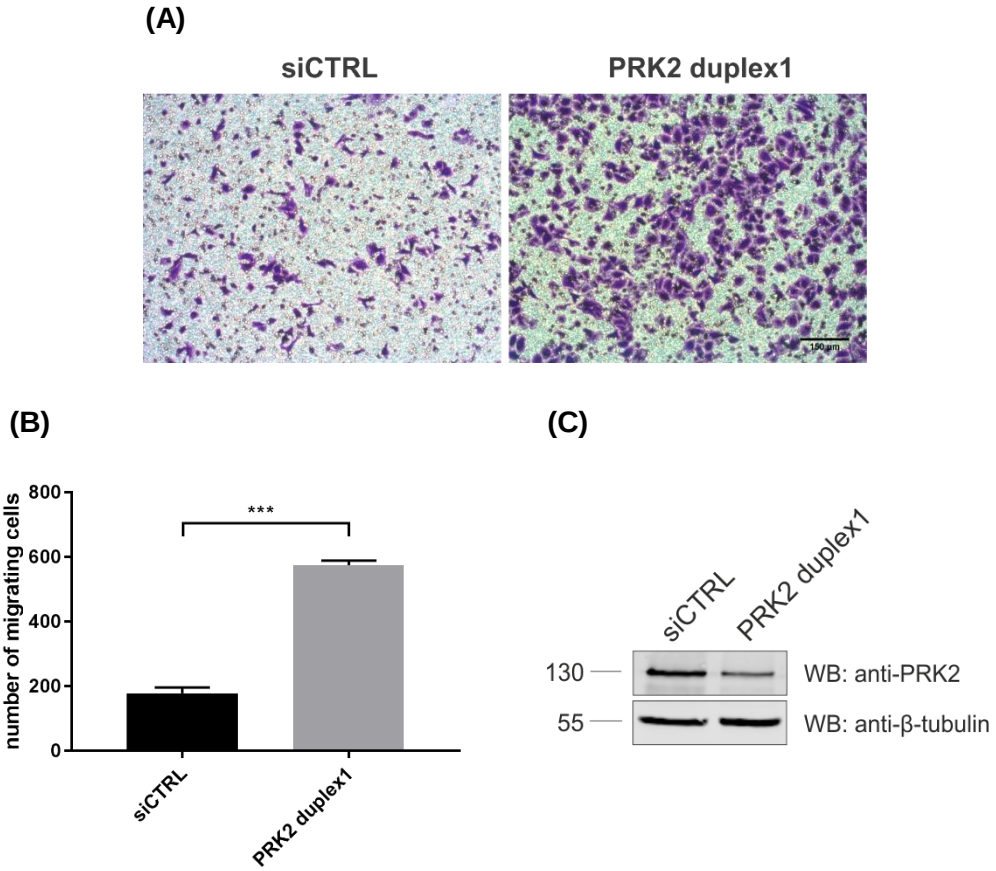

Figure 5.5 Knockdown of PRK2 increases HeLa cells migration

(A) *HeLa cells were grown on 35 mm dish and transfected with siCTRL and PRK2 duplex 1. 40 h post transfection cells were starved overnight with serum-free medium containing 0.2% BSA. Subsequently, cells were trypsinized, counted and seeded in the upper compartment of the insert while lower compartment was filled with medium containing 10% FCS. Cells were subjected to migration for 18 hours. The filter membrane was fixed and migrated cells were stained with crystal violet. Images were taken using a brightfield inverted microscope with a Digi-Pad 9556.5600 M. Scale bar, 150 µm. (N=3)* ***(B)*** *Migrated cells were counted using ImageJ software and quantified based on three independent experiments: siCTRL: 178 ± 11.4, PRK2 duplex1: 576 ± 8.5. Statistical analysis was performed using paired t-test, *** p<0,0001, error bars represent ±SEM.* ***(C)*** *HeLa cells were transiently transfected with siCTRL or PRK2 duplex 1 at the final concentration of 50 nM and incubation time 72 hours. Cells were treated in the same way as described in (A). Cell lysates were prepared, and protein concentration was estimated. Endogenous proteins were detected with anti-PRK2 and anti-β-tubulin antibodies followed by anti-mouse DyLight™ 800 antibody. Samples represented around 10% of the total cell lysate. (N=3)*

5.3.3 FRMPD2 is localised in a polarised fashion in migrating cells

Many studies with cell migration data utilise MDA-MB-231 cells, a highly invasive and metastatic human epithelial breast cancer cells that can migrate spontaneously and in an inducible manner. Therefore, this established cell culture model was further used to examine the more precise function of FRMPD2 in the cell migration process. At first, we aimed to investigate the localisation of FRMPD2 in migrating cells. Due to the lack of a suitable antibody detecting endogenous FRMPD2, FRMPD2 localisation in MDA-MB-231 cells was performed using cells transiently overexpressing FRMPD2. To do so, MDA-MB-231 cells were transfected with GFP-tagged FRMPD2 and subsequently subjected to time-lapse fluorescence microscopy. Serial images of selected GFP-positive cells were taken for at least 6-8 hours at 15-min intervals. FRMPD2 accumulated mainly at the rear or sides of the migrating cells, and such specific localisation was depended on the stage of cell migration (Figure 5.6). At very early time points, when cells exhibited simple and round morphologies without visible protrusions, GFP-FRMPD2 localised uniformly at the plasma membrane (0 min). When cells started to form random protrusions, FRMPD2 accumulated at the sides of the migrating cells (30 min, 60 min and 75 min, white arrows). In response to some external stimuli, like chemical signals or temperature, cells can change their movement direction. At time points between 75 min and 90 min, we observed a change in the movement direction from upper right to the lower right edge and that was accompanied by the change of FRMPD2 localisation from the sides to the rear of the migrating cells (90 min – 120 min, white arrows). Migration terminated when cells lost their guidance or experienced some obstacles on their way like in the presented example (150 min). Cells still elaborated random protrusions but at this stage, they exhibited a morphologically non-polarized round shape, and again FRMPD2 was distributed uniformly at the cell membrane.

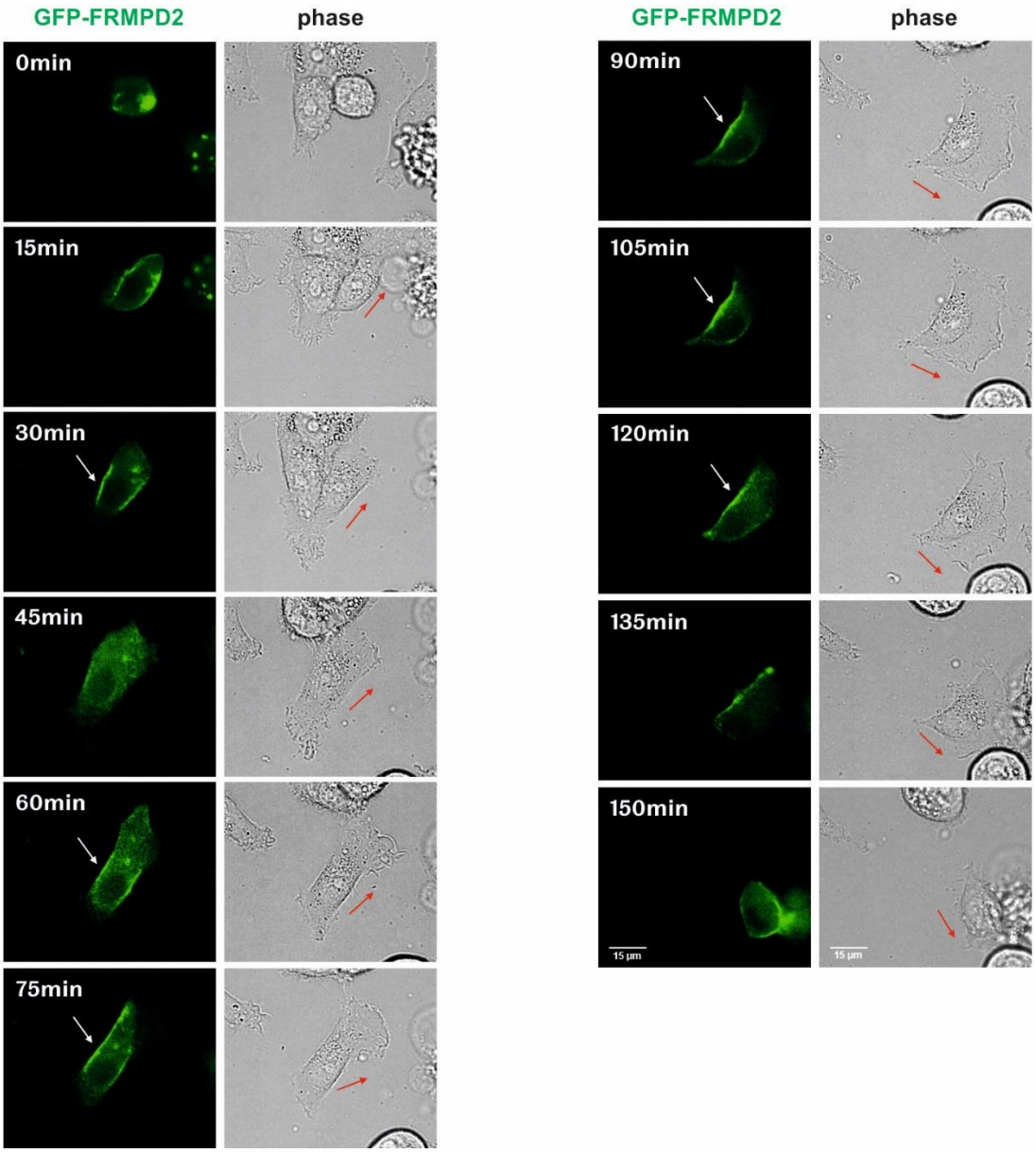

Figure 5.6 FRMPD2 localises at the side and rear of migrating cells

MDA-MB-231 cells were grown 35 mm dish and transfected with the GFP-tagged FRMPD2 construct. 24 h post transfection cells were trypsinized and re-seeded at the low density on glass-bottom dishes. After 16 hours migration of the cells was followed by time-lapse imaging for at least 6 – 8 hours at 15-min intervals. Images were taken using a widefield Nikon dual camera microscope with green channel. White arrows highlight specific localisation of GFP-FRMPD2 at different time points. Red arrows highlight direction of cell migration. Scale bar, 15 µm. (N=3)

In general, GFP-FRMPD2 co-localised with actin as demonstrated by co-transfection with RFP-β-actin followed by live imaging (Figure 5.7) as well as when cells were fixed (Figure 5.8).

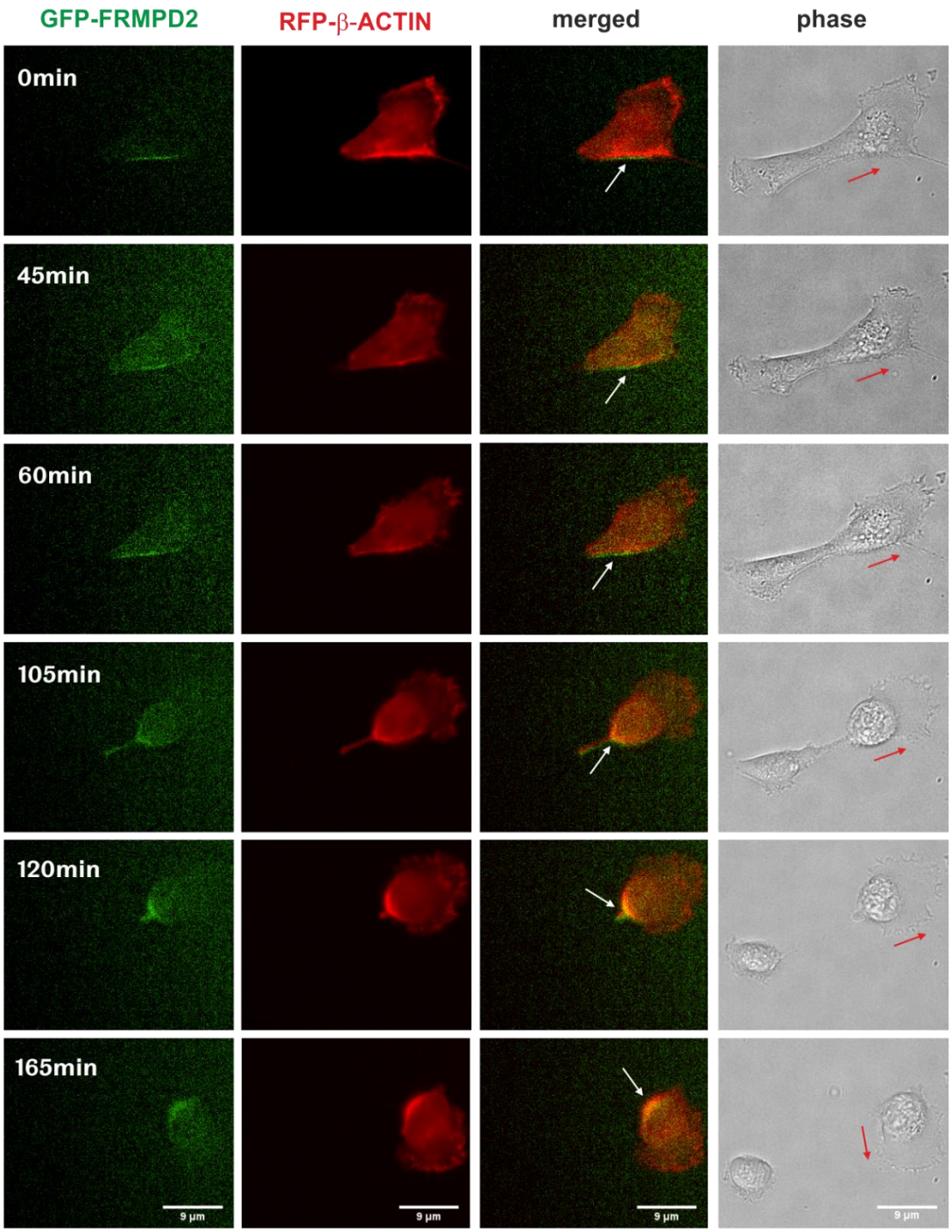

Figure 5.7 FRMPD2 localisation in migrating cells depends on migration stage

MDA-MB-231 cells were grown 35 mm dish and co-transfected with the GFP-tagged FRMPD2 and RFP-tagged Actin constructs. 24 h post transfection cells were trypsinized and re-seeded at the low density on glass-bottom dishes. After 16 hours migration of the cells was followed by time-lapse imaging for at least 6 – 8 hours at 15-min intervals. Images were taken simultaneously using a widefield Nikon dual camera microscope with the green and red channel. Images presented in the figure represent only few time points. White arrows highlight specific localisation of GFP-FRMPD2 and colocalisation with actin at different time points. Red arrows highlight direction of cell migration. Scale bar, 15 µm. (N=3)

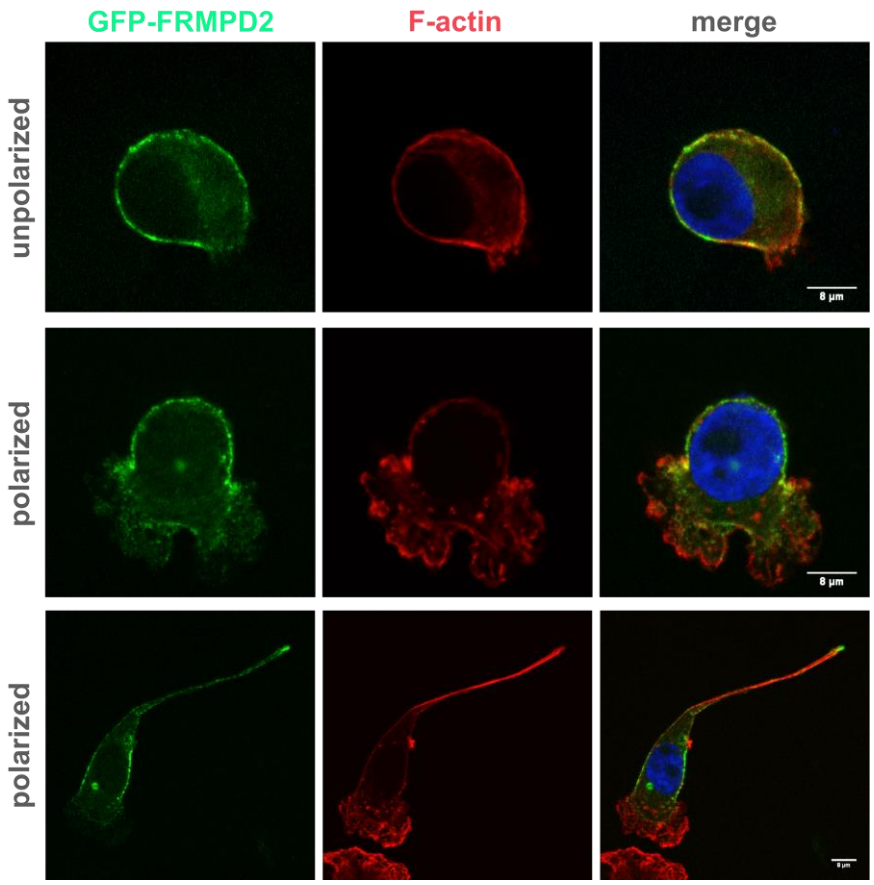

Figure 5.8 FRMPD2 localisation in migrating cells depends on cell polarisation

MDA-MB-231 cells were grown on coverslips and transfected with the GFP-tagged FRMPD2 construct. 48 h post transfection cells were fixed and stained with Phalloidin-Atto 594 binding to F-actin. Images were taken using a spinning disc confocal microscope. Images represent single xy planes. Scale bar, 8 µm. (N=4)

Specific targeting of FRMPD2 to the rear or sides of migrating cells corresponds to previously published data showing its basolateral restriction in polarised epithelial cells, which depends on its FERM and PDZ2 domain (Stenzel et al., 2009). Further investigation of FRMPD2 localisation in migrating cells was carried out to check whether the observed localisation can be attributed to a specific domain of FRMPD2. To this end, MDA-MB-231 cells were transfected with only the FERM domain and subjected to F-actin staining. As shown in Figure 5.9, the FERM domain localised at the plasma membrane, but more prominently at the rear of the migrating cells (localisation highlighted by arrows). Unlike full-length FRMPD2, the FERM domain also accumulated at the leading edge of the cell co-localising with actin in lamellipodia (localisation marked by arrowheads).

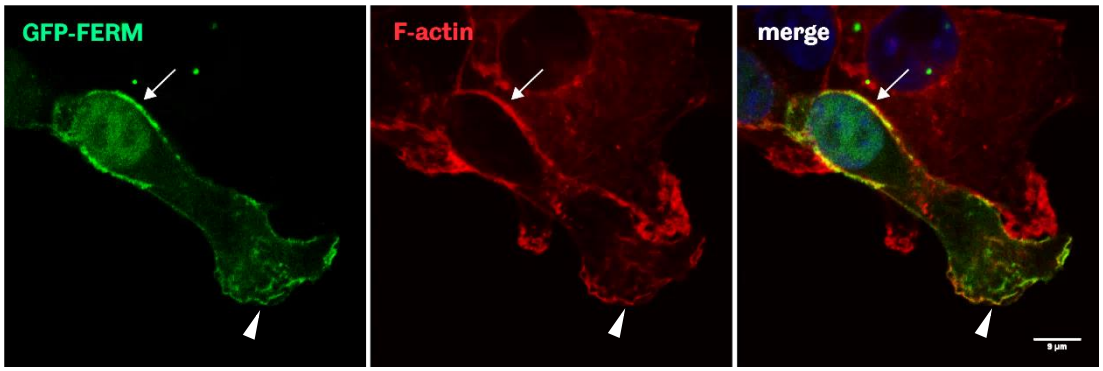

Figure 5.9 FERM domain of FRMPD2 localises mainly at the rear of polarised migrating cells

MDA-MB-231 cells were grown on coverslips and transfected with the GFP-tagged FERM domain construct. 48 h post transfection cells were fixed and stained with Phalloidin-Atto 594 binding to F-actin. Images were taken using a spinning disc confocal microscope. Images represent single xy planes. Arrows highlighted rear and arrowheads lamellipodia localisation. Scale bar, 9 µm. (N=4)

We hypothesised that, as a potential scaffolding protein, FRMPD2 interacts directly or indirectly with actin cytoskeleton components and therefore links the plasma membrane with the actin cytoskeleton. Moreover, FRMPD2 localisation to the rear and sides of polarised migrating cells sheds light on the mechanism driving cell retraction, a process, which involves myosin II activity. Myosin IIa, which actively participates in rear contraction and similarly to FRMPD2 localises at the rear of migrating cells, was found as a potential interacting partner of FRMPD2 using Affinity Purification-Mass Spectrometry (Erdmann, unpublished data). To validate this result, a co-IP experiment was performed using HEK293 cells overexpressing GFP-tagged FRMPD2. Unfortunately, we were unable to detect an interaction between myosin IIa and FRMPD2 (Figure 5.10).

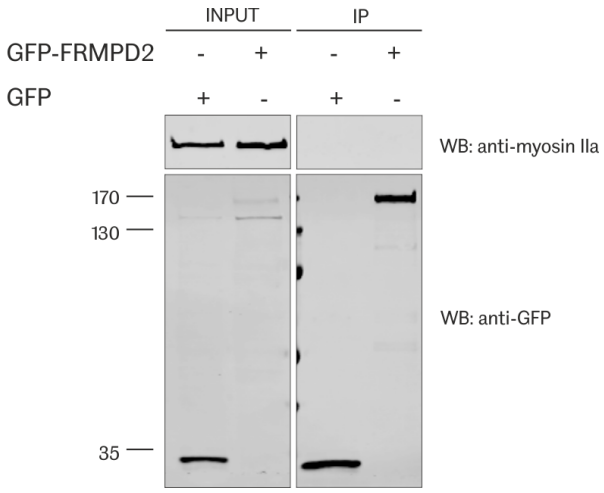

Figure 5.10 Myosin IIa does not interact with GFP-tagged FRMPD2

HEK293 cells were transiently transfected with expression constructs of GFP or GFP-tagged FRMPD2. 48 hours post-transfection cell lysates were collected, and co-immunoprecipitation was conducted using GFP-Trap®_A. Fusion proteins and endogenous proteins were detected by Western Blot using anti-GFP and anti-Myosin IIa antibody respectively followed by anti-rabbit Alexa Fluor® 680 antibody. Input represented around 2% of the total cell lysate. (N=2)

Although direct interaction with myosin IIa was excluded at that stage, possible indirect interaction and proximity between FRMPD2 and myosin IIa were further examined using stable cell line expressing myc-BirA*-FRMPD2 that was generated in the current study. Following an established protocol, all biotinylated proteins were purified using streptavidin agarose beads. Subsequent Western Blot analysis with anti-myosin IIa antibody revealed that myosin IIa was not detected in the pulldown samples (Figure 5.11, PULLDOWN, upper panel). Western Blot with anti-myosin IIa antibodies was performed at the same time as PRK2 (Figure 3.22), which can serve here as a positive control. Confirmation of the interaction between FRMPD2 and myosin IIa was technically challenging and at the moment based on these two results we can conclude that FRMPD2 does not interact with myosin IIa and both proteins are not in the closest neighbourhood.

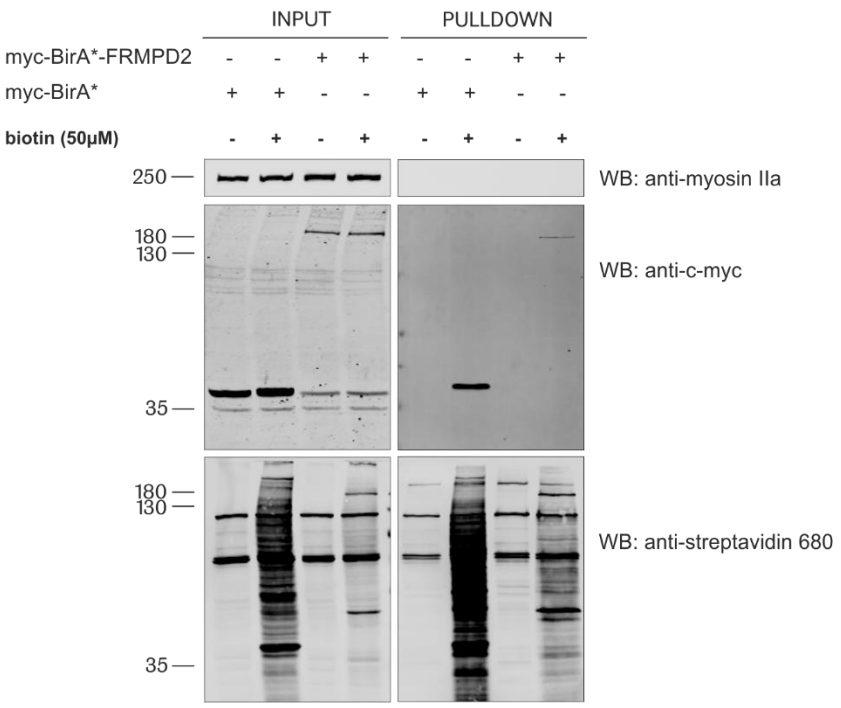

Figure 5.11 Myosin IIa is not biotinylated by myc-BirA*FRMPD2 in MDCK II cells

Stable MDCK II cell line expressing myc-BirA or myc-BirA*-FRMPD2 were grown on 60 mm dishes until cells reached 80% confluency and subsequently, they were incubated without (-) and with (+) 50 µM exogenous biotin for 18 hours. Cell lysates were prepared, and pulldown experiment was conducted using streptavidin beads. Fusion proteins and endogenous PRK2 were detected using anti-c-myc and anti-myosin IIa respectively followed by anti-rabbit Alexa Fluor® 680 and anti-mouse DyLight™ 800 antibody respectively. Biotinylated proteins were detected using streptavidin Alexa Fluor® 680 antibody. The signal of biotinylated myc-BirA*-FRMPD2 was pointed out by an arrow. Input represents around 2% of the total cell lysate. (N=1)*

5.4 Discussion

This study established a new function of the FRMPD2-mediated protein complex in the regulation of cell mechanical properties and migration. We speculated that as a scaffold protein, FRMPD2 may be associated with the actin cytoskeleton and therefore affect epithelial integrity and cell mechanical properties. To do so we measured the effect of knockdown, targeting FRMPD2 as well as its interacting partner PRK2, on cell deformability of suspended HeLa cells using the optical stretcher technology and real-time deformability cytometry. Here we showed that depletion of FRMPD2 as well as PRK2 in HeLa cells, grown in the adherent state and brought into suspension, significantly increased cell compliance measured in the seconds-timescale by the optical stretcher. A possible explanation of the observed change in mechanical properties of HeLa cells after

FRMPD2 depletion is that the cells lost their normal rigidity due to cytoskeleton relaxation. Similarly to ERM protein family acting as crosslinkers between the plasma membrane and the cortical actin network (Fehon et al., 2010), FRMPD2 is characterised by the presence of a plasma membrane-associated FERM domain. It has been shown that inactivation of ERM protein leads to a disconnection between the plasma membrane and the cortical cytoskeleton which results in a substantial increase in cell deformability (Faure et al., 2004). At the moment we cannot explain our results from RT-DC, but to draw a final statement we need to perform more experiments.

Previously published data demonstrated that expression of a kinase-deficient mutant of PRK2 contributed to the loss of actin stress fibers (Vincent and Settleman, 1997), however, all our measurements were carried out for cells in a suspended state, therefore, no stress fibers and focal adhesions were present. As a RhoA effector protein, PRK2 may participate in a wider range of molecular events associated with regulation of the actin cytoskeleton, however, the current knowledge on this subject is limited. Another component of the actin cytoskeleton is myosin II. It has been shown that the myosin II contributes to cell stiffness in an opposite way for cells adherent to a substrate and cells in suspension. It has been shown that changes in mechanical properties of the cells upon inhibition of myosin by blebbistatin measured by two different techniques resulted in contrary results. Cells in suspension were characterised by decreased deformability, while adherent cells softened actin cytoskeleton what resulted in increased deformability (Martens and Radmacher, 2008, Chan et al., 2015). Based on these studies, we can assume that cell deformability strongly depends on the cell state as well as used methodology, however precise mechanism of how PRK2 contribute to cell compliance will require further investigation.

Cell compliance is highly linked to the cytoskeleton and is reflected in cytoskeleton modifications (Elson, 1988). It is also known that cell migration requires changes in cell shape, which are mainly driven by rearrangement of cytoskeleton components. Since our results from the optical stretcher and real-time deformability cytometry showed FRMPD2- and PRK2-dependent cell compliance, we decided to examine the migration behaviour of HeLa cells devoid of these two proteins. We demonstrated that downregulation of both FRMPD2

and PRK2 significantly enhanced migration of HeLa cells and these results corroborated the fact that more compliant cells indicate greater migratory activity. On the other hand, it has been shown that depletion of PRK2 in 5637 bladder tumour cell line inhibited 2D and 3D migration and these results appear contrary to our presented findings (Lachmann et al., 2011). This discrepancy can be clarified by the fact that cell migration of HeLa and 5637 cell lines is characterised by a different type of movement. Migration of the first one occurs through individual cell movement, while the latter cells migrate in sheets – groups of cells kept together by cell adhesion molecules like E-cadherin in the form of collective migration. PRK2 has been shown to regulate cell-cell adhesion (Calautti et al., 2002), therefore it is possible that downregulation of PRK2 can cause disruption of cell adhesion and as a consequence deceleration of migration. These two distinct types of movement, single and collective migration are associated with different requirements, therefore results may vary between the different cell lines.

Increased cellular deformability has been linked to the metastatic potential of human breast epithelial cells as well as ovarian cancer cell lines and correlated with significant changes in actin remodelling pathways (Guck et al., 2005, Xu et al., 2012b). Metastatic progression is associated with the transition from epithelial to mesenchymal phenotype, which is mainly caused by disruption of the epithelial junctions in conjunction with further loss of cell polarity. The obtained results can support our hypothesis that defects in epithelial junction formation caused by FRMPD2 or PRK2 depletion may correlate with decreased cytoskeletal rigidity leading to increased cell compliance and migration. However, confirmation of the close association between these two proteins and cytoskeleton components is crucial for further investigations.

We have shown that FRMPD2 and PRK2 function as suppressors of cell migration, but first we wanted to examine only FRMPD2 function in cell migration. Further experiments were performed with MDA-MB-231 cells, which are commonly used as a model for cell migration. Our time-lapse fluorescence analysis demonstrated that the localisation of FRMPD2 in migrating cells strongly depends on the migration stage in conjunction with cell polarisation. We identified FRMPD2 to

be enriched at the rear and sides of migrating cells, while it was evenly distributed at the membrane of unpolarised resting cells. It seemed that during random cell migration FRMPD2 was localised alongside actin, but colocalization took place only when the rear of migrating cells was retracted (Figure 5.11).

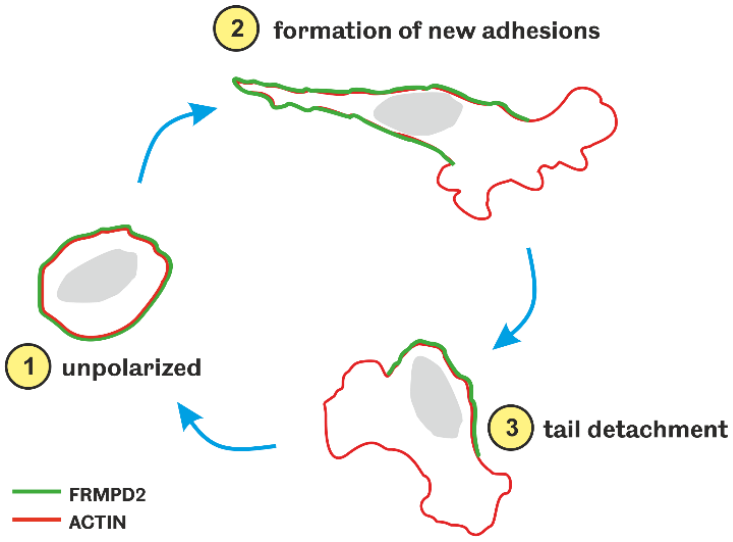

Figure 5.11 Schematic representation of FRMPD2 localisation during different cell migration phases

(1) *In an unpolarised fashionFRMPD2 localises evenly at the membrane of resting cells.* ***(2)*** *In response to some stimulation cells start to form protrusions at the leading edge, and then FRMPD2 accumulates at the rear and sides of polarised migrating cells.* ***(3)*** *During late stage of migration in conjunction with tail, retraction FRMPD2 localises at the rear of migrating cells.*

We also demonstrated that restricted localisation of FRMPD2 at the rear or sides of migrating cells does not depend on its FERM domain only, but most likely engages other domains and corresponding interacting partners. This observation was convergent with FERM domain localisation at the plasma membrane of epithelial cells exhibiting apico-basal polarity (Stenzel et al., 2009). Seeking the new function of FRMPD2 in cell migration, we have tried to connect its role to the processes occurring at the rear of migrating cells. One mechanism, in line with FRMPD2 restricted localisation in migrating cells, seemed to be a role in rear retraction; a process involving myosin IIa activity. We hypothesised that through interaction with myosin II, FRMPD2 might cooperate in actomyosin contractility driving cell detachment. Unfortunately, we were not able to detect association of

these two proteins and currently it is problematic to define a specific function of FRMPD2 in migrating cells.

We speculate that due to the specific localisation at the rear and/or sides of migrating cells, FRMPD2 may be involved in processes responsible for cell adhesion and tail detachment. Currently, we do not know whether FRMPD2 and PRK2 act in a complex inhibiting cell migration. However, FRMPD2 transition from basolateral restriction to the rear of polarised migrating cells may suggest that its protein-protein interactions could be preserved and their function modified to adapt to processes that generate front-rear polarity.

Similarly to CynA and ForA proteins from *Dictyostelium discoideum* showing strong connection with the actin cytoskeleton, FRMPD2 may define processes occurring at the rear of the migrating cells (Swaney et al., 2015, Ramalingam et al., 2015). As a scaffold protein, which is tightly localised at the rear of migrating cells, FRMPD2 may stabilise signalling complexes involved in rear detachment or formation of migration tracks, and prevent them from relocation in response to signals that initiate cell migration. Subsequent stages of cell migration are controlled by many signalling networks, however there is a considerable contribution of Rho GTPase signalling pathways that regulate different processes during cell migration (Hanna and El-Sibai, 2013). For example, it has been shown that tail detachment is regulated by RhoA acting via ROCK (Rho-associated kinase) and inducing actomyosin contractility (Amano et al., 2010). PRK2 is a known RhoA effector, acting in a variety of processes including actin cytoskeleton organisation and E-cadherin-dependent adhesion (Calautti et al., 2002, Vincent and Settleman, 1997). Up until now there has been no evidence of direct association between FRMPD2 and actin, however there is a possibility that through the interaction with PRK2, FRMPD2 may regulate actin cytoskeleton rearrangements promoting cell retraction. On the other hand we were not able to show whether FRMPD2 acts as a positive or negative regulator of PRK2 activity while translocating it to the plasma membrane. Hence, given the second scenario, it could be possible that PRK2 acts in a RhoA-independent manner and therefore can inhibit cell migration.

Many proteins containing FERM domain have been shown to play important role in cellular movements and migration (Bosanquet et al., 2014). Some of them, including Talin, Kindlins and FAK (focal adhesion kinase) interact and regulate integrin functions, the main component of focal adhesions (Tanentzapf and Brown, 2006, Liu et al., 2011, Tancioni et al., 2014). Targeting to the plasma membrane via phosphoinositide binding is a very important mechanism for localisation and functional regulation of many peripheral membrane proteins. It has been shown that phosphatidylinositol-(3,4,5)-trisphosphate (PIP3)-mediated membrane association of kindlin-2 promotes integrin activation by talin, another important component of focal adhesions (Liu et al., 2011). Interestingly both kindlin-2 and talin contain FERM domains and membrane association significantly affects their function. As a FERM domain-containing protein that localises to the rear of migrating cells, FRMPD2, could potentially be involved in the activation of integrins as well. There is a possibility that FRMPD2 could bind to the cytoplasmic tail of integrins, creating focal adhesions at the trailing edge, and form a scaffold for another proteins and signalling pathways. However, on the other hand FRMPD2 may associate with the plasma membrane via phosphatidylinositol-(3,4)-bisphosphate and similarly to kindlin-2 and talin to form a complex with other focal adhesion components involved in the activation of integrins.

During cell migration, integrins are subjected to continuous endocytosis and recycling to the plasma membrane (Caswell and Norman, 2006, Pellinen and Ivaska, 2006, Caswell and Norman, 2008). Although not yet demonstrated, it is possible that PRK2 may control endosomal traffic. Similarly to PRK1, another isoform of protein kinase C-related kinase (PRK), PRK2 could be targeted to endosomes by the small GTPase RhoB (Mellor et al., 1998), which was one of three Rho isoforms showing the strongest affinity to PRK2 (Hutchinson et al., 2013). Endocytosis is a key process regulating focal adhesion turnover and it has been demonstrated that 3-phosphoinositide-dependent protein kinase 1 (PDK1), upstream kinase of PRK2, controls integrin endocytosis during focal adhesion disassembly (di Blasio et al., 2015). The kinase-active form of PDK1 directly associates and phosphorylates β3 integrin thereby controlling its internalisation. It has been shown that PDK1 phosphorylates and activates PRK2 (Dettori et al.,

2009), therefore it would be possible that PRK2 acts downstream of PDK1 and regulates integrin endocytosis too.

Adhesion of cells to the extracellular matrix (ECM) facilitates their directional migration, which is dynamically regulated by continuous formation and turnover of focal adhesions (FAs) at the leading edge as well as disassembly at the rear (Broussard et al., 2008, Webb et al., 2002). Very often focal adhesions are connected to actin stress fibers, which are needed for cell movement (Parri and Chiarugi, 2010) and have been shown to act as transmitters converting mechanical forces into biochemical signals (Vogel, 2006). As demonstrated previously, PRK2 is as a regulator of actin stress fibers formation (Vincent and Settleman, 1997), therefore we hypothesised that FRMPD2 could recruit PRK2 at the sides of migrating cells and therefore support PRK2-mediated stress fibers formation.

In light of most of the above-mentioned theories, FRMPD2 and PRK2 should promote cell migration and adhesion, however our transwell assays suggest the opposite. The discrepancy between hypotheses and obtained results underscores the importance of using different cell model as well as multiple experiments to measure cell migration. Also, there is still not much known about FRMPD2 and PRK2 interaction and other mechanisms involving these proteins requires further investigation. In general, the localisation of FRMPD2 in migrating cells is consistent with front-rear polarity acquired by cells during random migration. Moreover, it seems that processes regulating the symmetry breaking generating apical-basal or front-rear polarities depends on the conserved function of FRMPD2, or help FRMPD2 to maintain a specialised role in the polarised cells. We presented a novel function of FRMPD2 in cell migration, however precise definition requires more experiments.

CHAPTER 6 - FRMPD2 function in zebrafish

6.1 Introduction

The rationale for applying the zebrafish model in the current study was explained before in the 'Chapter 1 – Introduction' of this thesis. The multi-PDZ domain protein FRMPD2 has been identified as a crucial component of the immune host defence in human intestinal epithelial cells (Lipinski et al., 2012), which is perturbed in inflammatory bowel disease (IBD). Interaction with NOD2 places FRMPD2 as the central organization component of a larger protein complex with potential relevance to inflammatory bowel disease as well as epithelial integrity (Lipinski et al., 2012). The fully sequenced zebrafish genome and the significant homology to the human genome implies that many genes involved in human pathologies, including FRMPD2, could have the same function in zebrafish.

A frmpd gene family was identified in the zebrafish genome as well and similarly to the human genome it contains four genes: *frmpd1*, *frmpd2*, *frmpd3 and frmpd4,* which encode proteins with the conserved domain structures of their human orthologues (Figure 1.8, CHAPTER 1). Nevertheless, apart from identification at the genomic level, there is no other information about *frmpd* genes functions in zebrafish development or their physiological relevance available. In more detail, the zebrafish *frmpd2* gene includes two transcript variants encoding proteins of 1116 and 1018 aa long, which share 38% and 37% identity with their human orthologues respectively. Both proteins have a conserved domain structure of the human FRMPD2 protein and contain a N-terminal KIND (kinase non-catalytic C-lobe) domain, followed by a FERM (Four-point-one, ezrin, radixin, moesin) domain and three PDZ domains (Figure 6.7 in this chapter). Although FRMPD2 protein function in zebrafish is not known yet, it is hypothesised that due to the similarity to the human protein, FRMPD2 function is also conserved between the species and that potentially can lead to establishment of a zebrafish disease model for inflammatory bowel disease based on FRMPD2.

6.2 Aim

Based on the hypothesis mentioned above, it was crucial to investigate the basic features and functions of FRMPD2 protein in zebrafish. Hence the aim of this chapter was:

1. to check whether FRMPD2 is expressed during zebrafish development,
2. to determine spatial and temporal FRMPD2 expression pattern in zebrafish embryos/larvae
3. to perform in vivo analysis of FRMPD2 function in zebrafish (determination of the phenotype of FRMPD2 zebrafish mutant obtained from the Sanger Institute).

6.3 Results

6.3.1 Where is FRMPD2 expressed in zebrafish?

6.3.1.1 *in situ* hybridisation for *frmpd2*

To detect expression sites of *frmpd2* gene in zebrafish embryos and early larvae, *in situ* hybridisation was conducted with sense and antisense RNA probes corresponding to the sequence 'probe 1' depicted in the Figure 6.1.

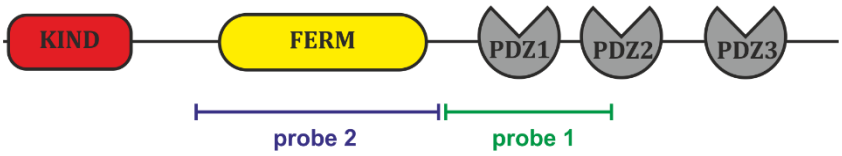

Figure 6.1 Localisation of probe1 and probe2 within FRMPD2 sequence used for in situ hybridisation in zebrafish

Antisense and sense RNA probes for in situ hybridisation were synthesised with T7 or T3 RNA polymerase on the DNA sequences marked as probe 1 and probe 2 and cloned into the vector within a dual promoter cassette with the T7 and T3 promoter. Probe 1 corresponds to the length of 742 bp between 1861 and 2602 bp within frmpd2 gene and probe 2 to the length of 1001 bp between 797 and 1797 bp within frmpd2 gene.

Probes were synthesised with T3 or T7 RNA polymerases and simultaneously labelled with digoxigenin-linked nucleotides as described in section 2.2.1.3.1. Gene expression sites were visualised immunohistochemically with anti-digoxigenin antibody conjugated to alkaline phosphatase and chromogenic

substrate. All *in situ* hybridisation experiments were performed together with antisense and sense probes *tecta*, specific to *α-Tectorin* gene, which served as a positive experimental control (Figure 6.2). Antisense *tecta* probe allowed the detection of the specific mRNA expression sites at otoliths, while sense probe did not demonstrate any specificity and this result was consistent with published data (Stooke-Vaughan et al., 2015).

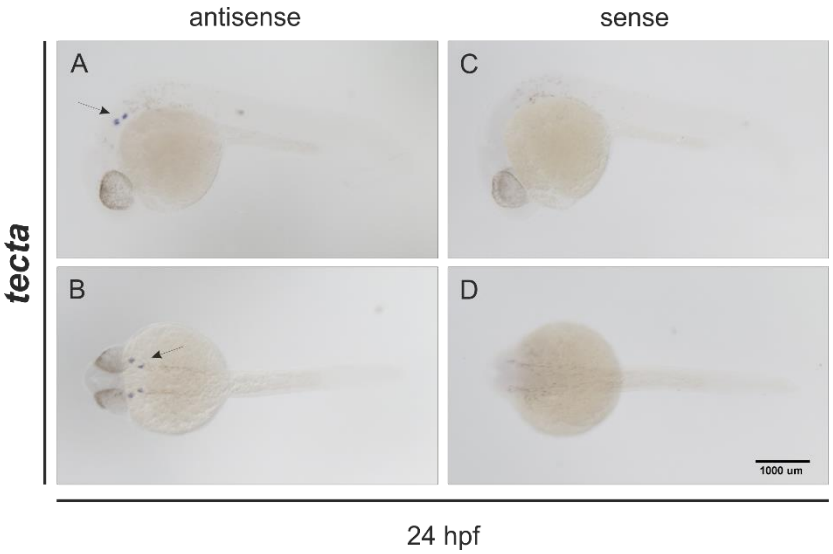

Figure 6.2 Expression pattern of α-Tectorin gene in zebrafish

In situ hybridisation with antisense (panel A, B) and sense (panel C, D) riboprobes against α-Tectorin gene in wild type embryos at 24 hpf (period : pharyngula, stage: prim-5). Otoliths are highlighted by arrows. Panel A and C show lateral view with dorsal to the top, anterior is th the bottom in specimens. Panel B and D show dorsal view, anterior is to the left in specimens. Scale bar, 1000 µm. (N>4) Riboprobes were obtained from Dr Tanya Whitfield, MRC Centre for Developmental and Biomedical Genetics, University of Sheffield

The first *in situ* trial for *frmpd2* was conducted with zebrafish embryos at 14 hpf and 48 hpf using a published protocol (Thisse and Thisse, 2008). Unexpectedly, both samples with sense and antisense probe, showed the same staining pattern and none of the organs could be distinguished (Figure 6.3). Very dark yolk staining is characteristic if embryos are kept longer time in the staining solution. At this stage methanol clearing was not applied. More experiments were performed with more stringent conditions during probe hybridisation (higher temperature within 70 – 72°C) but the staining pattern between sense and antisense probe still remained unchanged. It is perhaps worth to mention here

that in all control samples, *in situ* hybridisation experiments always showed positive staining and there were no deviations from their expression pattern.

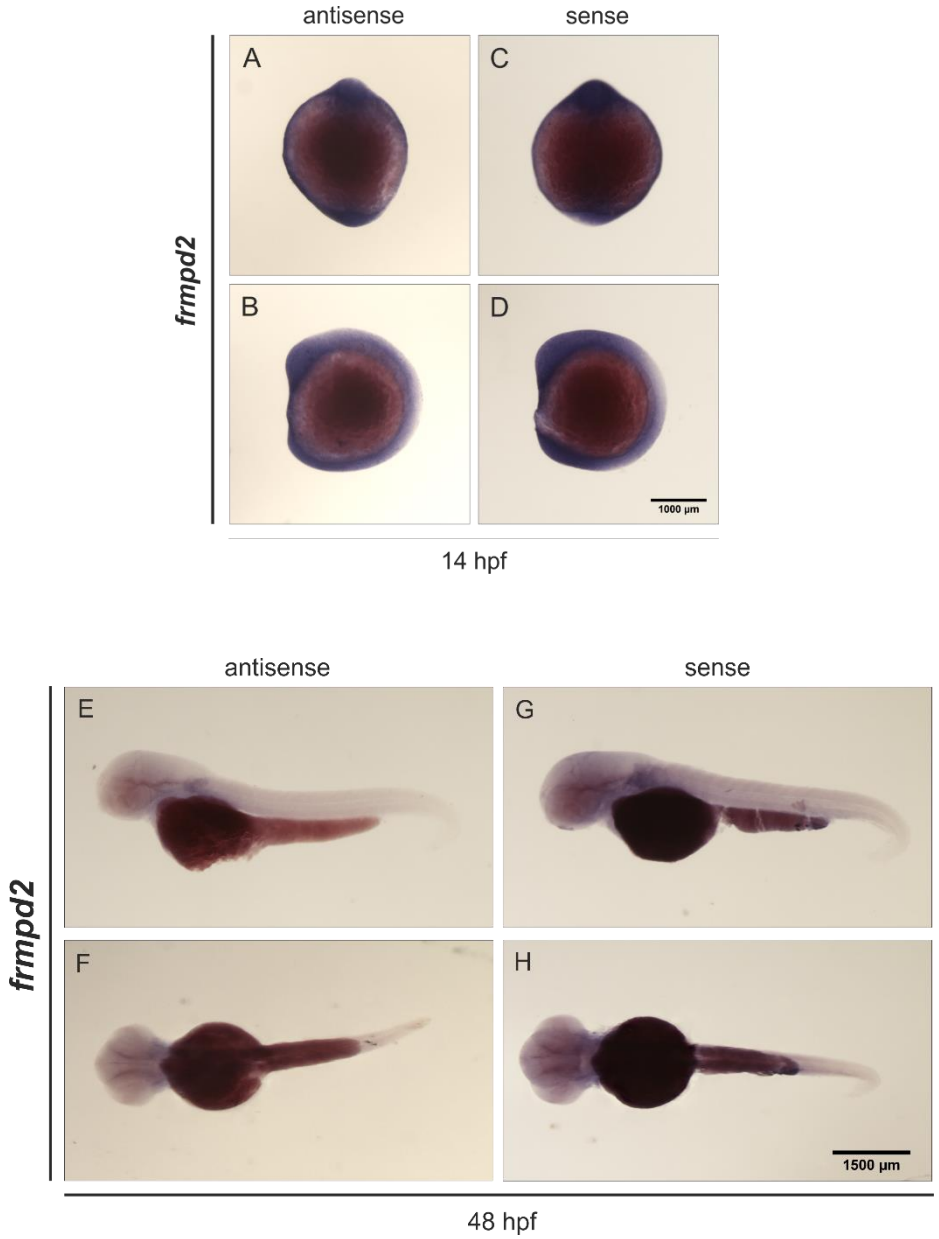

Figure 6.3 Expression analysis of frmpd2 gene in zebrafish using probe 1

In situ hybridisation with antisense (panel A, B, E, F) and sense (panel C, D, G, H) riboprobes 1 against frmpd2 gene in wild type embryos at 14 hpf (period: segmentation, stage: 10-13 somites) and 48 hpf (period: hatching, stage: long-pec). Panel A, C, F and H show dorsal view, anterior is to the top (panel A and C) or to the left (panel F and H) in specimens. Panel B, D, E and G show lateral view with dorsal to the top, anterior is to the left in all specimens. Scale bar for 14 hpf, 1000 µm and scale bar for 48 hpf, 1500 µm (N=3)

To test whether there was a problem with the probe, a new probe against *frmpd2*, corresponding to the sequence 'probe 2' depicted in Figure 6.1, was created and

in situ hybridisation was performed according to the protocol described in section 2.2.6.5. Experiments were conducted with zebrafish embryos at 14 hpf and 48 hpf and an additional embryonic developmental stage of 24 hpf was included. The staining pattern can suggest that *frmpd2* is expressed ubiquitously at 14 hpf and in the anterior part and brain of zebrafish embryo at 24 hpf. Although signal from antisense probe was stronger than that obtained with the sense probe, the staining pattern remained similar. Staining at 48 hpf showed no difference between antisense and sense riboprobe (Figure 6.4). Taken together, at the moment determination of *frmpd2* expression pattern in zebrafish embryos remains elusive.

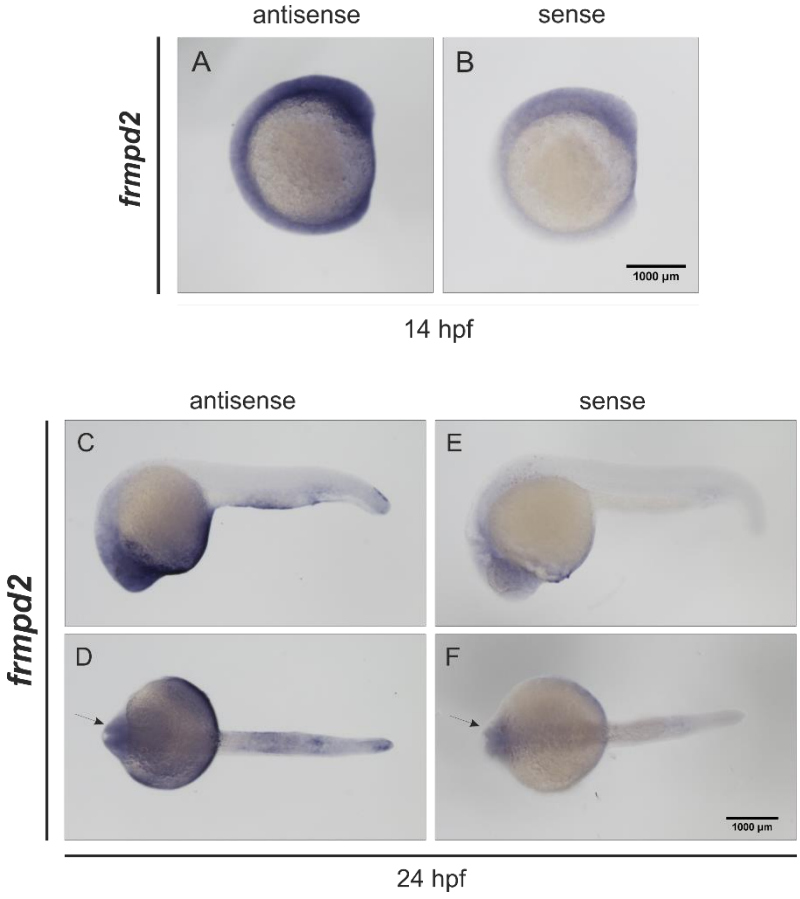

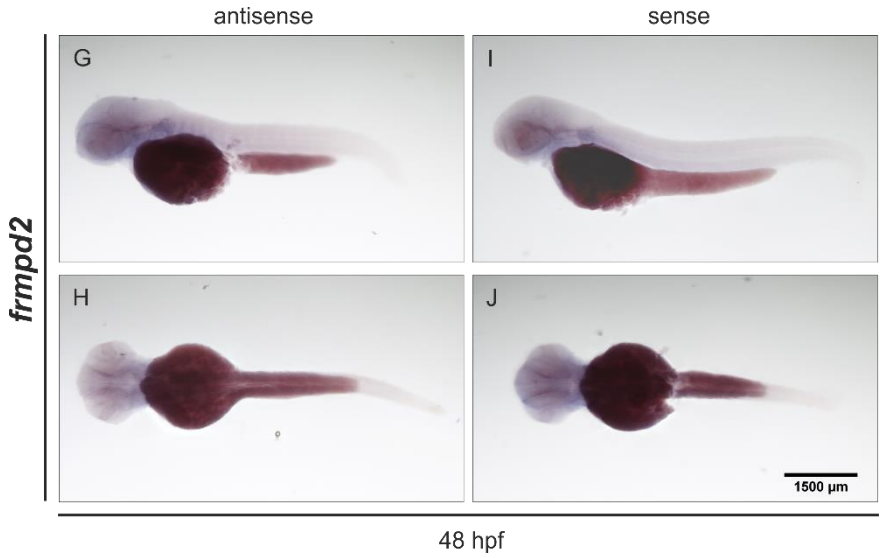

Figure 6.4 Expression analysis of frmpd2 gene in zebrafish using probe 2

In situ hybridisation with antisense (panel A, C, D, G, H) and sense (panel B, E, F, I, J) riboprobes 2 against frmpd2 gene in wild type embryos at 14 hpf (period: segmentation, stage: 10-13 somites), 24 hpf (period: pharyngula, stage: prim-5) and 48 hpf (period: hatching, stage: long-pec). Panel A and B show lateral view with dorsal to the top, anterior to the right in specimens. Panel C, E, G and I show lateral view with dorsal to the top, anterior is to the left in all specimens. Panel D, F, H and J show dorsal view, anterior is to the left in all specimens. Brain staining at 24 hpf is highlighted by arrows. Scale bar for 14 hpf/24 hpf, 1000 µm and scale bar for 48 hpf, 1500 µm (N=3)

At that stage technical problems with the protocol were excluded as *in situ* hybridisation with control probes showed the appropriate expression pattern. To eliminate possible problems with the newly synthesised *frmpd2* probe, the probe against *ptpn13*, another gene of interest studied in the Erdmann lab, was created. *in situ* hybridisation performed with zebrafish embryos at 24 hpf revealed that *ptpn13* was expressed mainly in parts of the central nervous system called rhombomeres (at later stages they form hindbrain) as shown on the Figure 6.5. It can be assumed that the obtained staining pattern was specific as none of the distinctive structure detected with antisense probe was visible in the sample tested with sense probe. Therefore this can lead to the assumption that probe synthesis was carried out in accordance to functioning protocol.

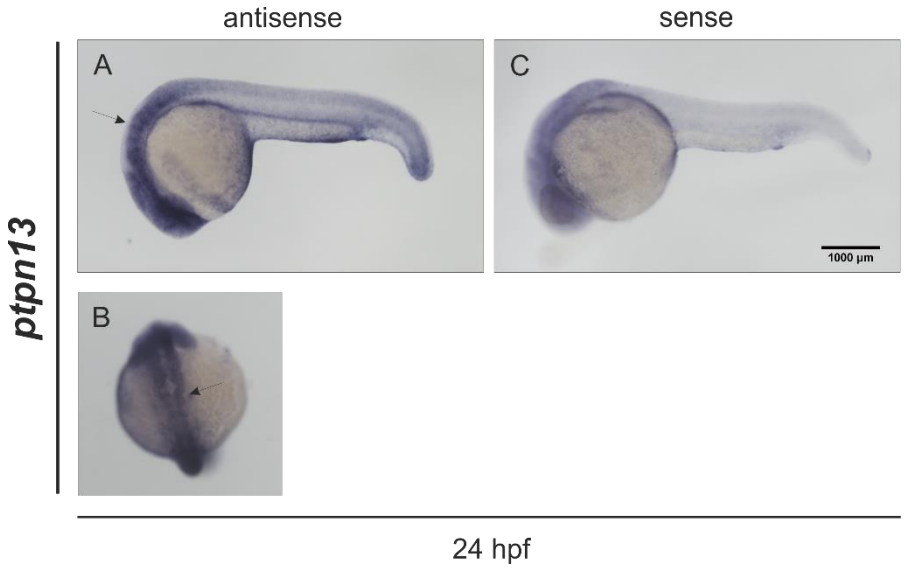

Figure 6.5 Expression analysis of ptpn13 gene in zebrafish

In situ hybridisation with antisense (panel A, B) and sense (panel C) riboprobes against ptpn13 gene in wild type embryos at 24 hpf (period: pharyngula, stage: prim-5). Panel A and C show lateral view with dorsal to the top, anterior to the left in specimens. Panel B shows top view with anterior is to the top in a specimen. Rhombomeres are highlighted by arrows. Scale bar, 1000 µm (N=3)

6.3.2 FRMPD2 is expressed in zebrafish during early development

In situ hybridisation results did not give us specific information about spatial-temporal *frmpd2* expression pattern, therefore to demonstrate that *frmpd2* is expressed during zebrafish development we performed RT-qPCR. Embryos and larvae at different developmental stages as well as adult zebrafish were harvested for RNA extraction that was carried out according to the protocol described in section 2.2.1.1.1. 1 µg of RNA was treated with DNase (see section 2.2.1.1.2) and subsequently converted to cDNA (see section 2.2.1.3.2). Real-time PCR, with corresponding -RT (negative control for reverse transcription) and NTC (no template control) samples, was performed using previously optimised conditions. *frmpd2* mRNA expression level was calculated using the comparative $\Delta\Delta C_t$ method (described in section 2.2.1.3.3 c). The results obtained from the quantitative real-time PCR revealed that at the early developmental stages, *frmpd2* is characterised by a very low expression level ($C_t > 34$), which increases significantly after 72 hpf. Independently from the amount of amplified product and C_t values, sequencing results confirmed *frmpd2* presence in all samples.

Based on the $\Delta\Delta C_t$ method it was estimated that in comparison to the 12 hpf stage, which was used as a calibrator, the highest expression level of *frmpd2* was observed at stages between 96 hpf and 15 dpf, reaching around 190-fold increase (Figure 6.5). There is no clear explanation why the level of *frmpd2* expression dropped at 120 hpf and increased again at further stages. However, it might be the variation in the sample preparation, as the C_t value for *β-actin* differed from the values obtained for other stages at the same time as well.

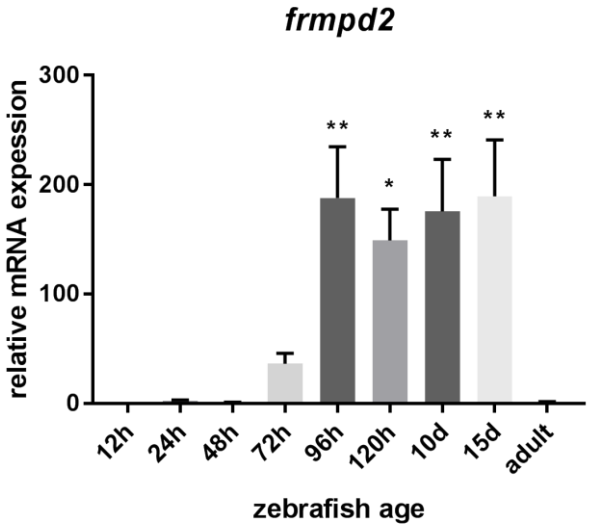

Figure 6.6 frmpd2 is expressed during zebrafish development

*Quantitative real-time PCR examined the mRNA expression level of zebrafish frmpd2. Zebrafish embryos and larvae were harvested at 12 hpf, 24 hpf, 48 hpf, 72 hpf, 96 hpf, 120 hpf, 10 dpf, 15 dpf. RNA was extracted from adult zebrafish as well. frmpd2 expression was normalised to β-actin and all values are relative to 12h stage. Statistical analysis of three independent experiments was performed using ordinary one-way ANOVA with post-hoc Dunnett's analysis, ** p<0,01 and * p<0,05, error bars represent ±SEM.*

6.3.3 Does *frmpd2* mutant zebrafish display a specific phenotype?

To evaluate the developmental and physiological role of *frmpd2*, a zebrafish mutant was obtained from the Zebrafish Mutation Project, an open resource of the Wellcome Trust Sanger Institute. Zebrafish mutants are widely created by ENU (*N*-ethyl-*N*-nitrosourea) induced mutagenesis, introducing random point mutations in the zebrafish genome (de Bruijn et al., 2009). The *frmpd2*^{sa18532} mutant allele contained a nonsense mutation that consequently resulted in a change from tyrosine to premature stop codon (TAT > TAA) at position 531 aa in the FERM C-terminal PH-like domain. This mutation eliminates a significant part

of the FRMPD2 protein including three PDZ domains and part of the FERM domain of FRMPD2 protein (Figure 6.7).

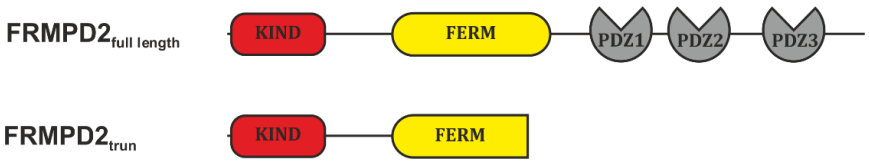

Figure 6.7 Schematic representation of full length and truncated FRMPD2 protein before and after ENU induced mutagenesis

$FRMPD2_{full\ length}$ protein contains KIND (kinase non-catalytic C-lobe) domain, FERM (Four-point-one, ezrin, radixin, moesin) domain and three PDZ (PSD95/Dlg/ZO1-homologous peptide-binding) domains. $FRMPD2_{trun}$ protein was created by ENU triggered mutagenesis and contains only KIND domain followed by truncated FERM domain.

Screening for zebrafish mutants required optimising conditions for genotyping method based on PCR from small zebrafish fin biopsies. All steps of optimisation can be found in Appendix 1. Optimised PCR conditions were subsequently used for high-throughput genotyping, which allowed the selection of zebrafish with the desired genotype only (Figure 6.8).

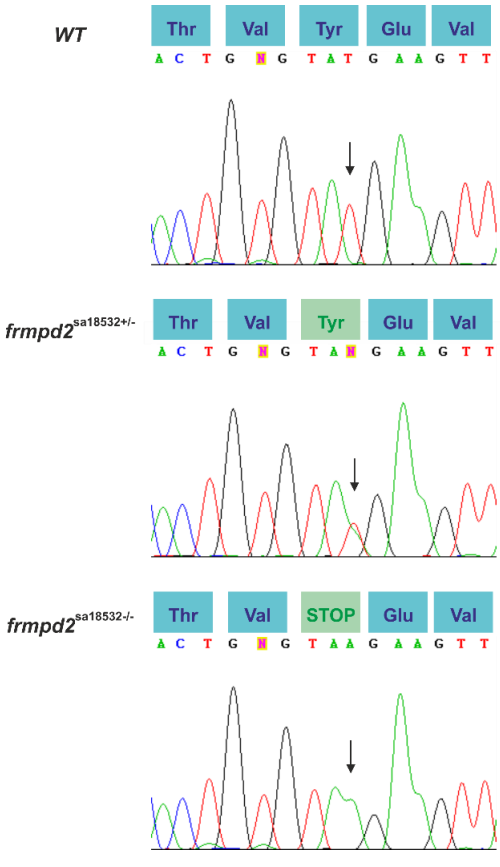

Figure 6.8 Genotype of frmpd2 mutant

Sequence analysis of zebrafish wild-type (WT), heterozygote ($frmpd2^{sa18532+/-}$) and homozygote ($frmpd2^{sa18532-/-}$). Mutation place is indicated by an arrow.

As mentioned earlier, the *frmpd2*^{sa18532} zebrafish mutant allele was obtained from the Sanger Institute. F2 generation of heterozygous carriers was born as a result of in vitro fertilisation of wild-type AB eggs with the frozen sperm of adult males treated with ENU. Due to the very small number of fertilised eggs, F2 heterozygotes were raised to adulthood and subsequently outcrossed to wild-type AB strain giving rise to a F3 generation of zebrafish embryos. 42 embryos obtained from Sanger were raised to adulthood in the aquarium facility at The University of Sheffield. All adult zebrafish of F3 generation were genotyped using PCR-based genotyping and finally 18 heterozygous carriers were identified.

To investigate the possible effect of *frmpd2* mutation on zebrafish development and to determine mutant phenotype, six pairs of F3 heterozygotes were incrossed by pairwise breeding of individual male and female adult fish. Embryos from all pairs were collected and observed during their early development. Interestingly, progeny of only three pairs (pair C, D and E) at 3 dpf started to display a moderate to severe phenotype leading to death. The most commonly observed phenotype was the curved body axis with associated twitching and circling, lack of swim bladder, lack of otoliths or change in head shape (Figure 6.9). All defective embryos were kept under observation until day 6 and finally culled. Progeny of the other three pairs (pair A, B and F) displayed normal wild-type-like phenotype with some larvae without swim bladder similar to the ones in Figure 6.9 E, F. DNA from embryos with a potential phenotype was extracted and genotyped by sequencing. The results revealed that there was no correlation between *frmpd2* genotype and the observed phenotype was equally presented within all genotypes (wild-type, heterozygotes and homozygotes).

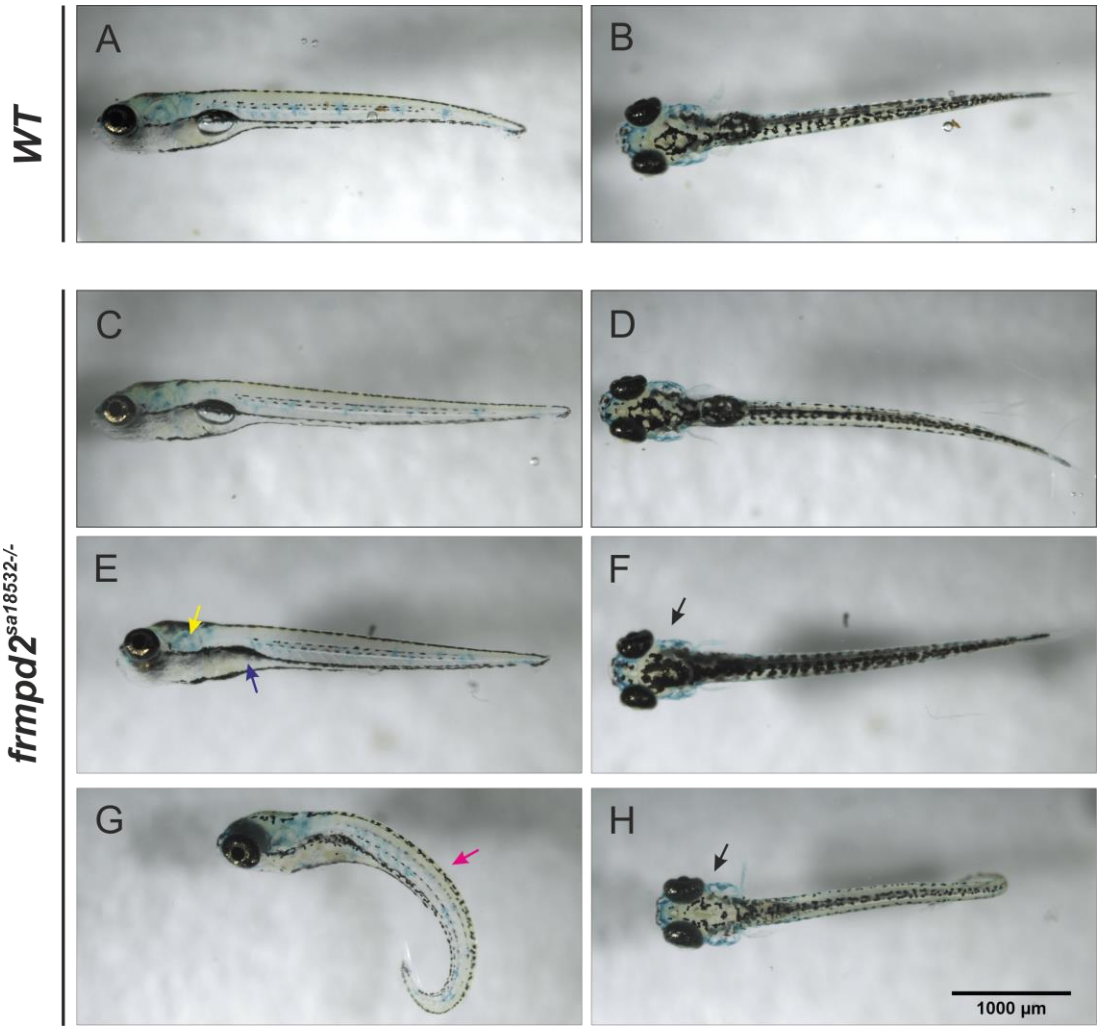

Figure 6.9 Phenotype of F4 generation of frmpd2$^{sa18532-/-}$ mutant

Phenotype of wild-type (panel A, B) and homozygote (panel C, D, E, F, G, H) zebrafish of F4 generation at 6 dpf. The most common phenotypes observed in homozygotes are highlighted by arrows: yellow – lack of otoliths, blue – lack of swim bladder, pink – curved body axis, black – change in head shape. Panel A, C, E and G show lateral view with dorsal to the top, anterior to the left in all specimens. Panel B, D, F and H show dorsal view, anterior to the left in all specimens. Scale bar, 1000µm

To clear background mutations, fish from pair A were out-crossed to wild type AB by pairwise breeding of individual male and female adult fish. The obtained embryos were fin-clipped at 3 dpf and genotyped for heterozygote selection. A total of 23 heterozygous carriers were raised to adulthood, but due to some problems with the adaptation (fish transfer at 7 dpf from petri dishes to the tank) only 5 fish of F4 generation survived. Finally, they differentiated into four females and one male adult fish. In fact, only one fish pair was in-crossed giving around 100 embryos of F5 generation zebrafish. All embryos were fin-clipped at 3 dpf and genotyped based on the established PCR method. Approximately 25% of the

offspring did not have a swim bladder therefore they could not control their buoyancy and were losing their stability at a certain water depth (Figure 6.10). Unfortunately, similar to the earlier generation, the observed phenotype did not correlate with *frmpd2* mutation.

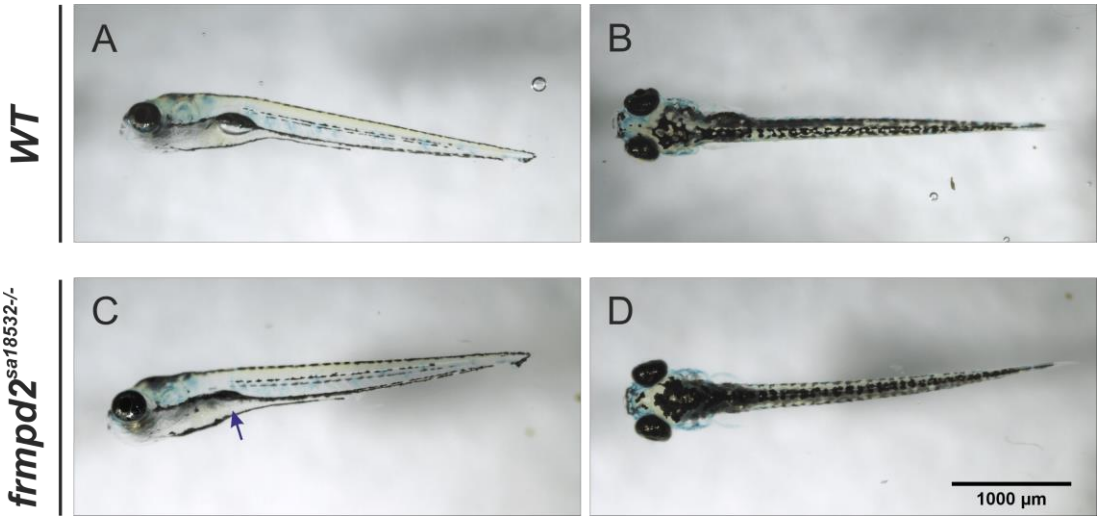

Figure 6.10 Phenotype of F5 generation of frmpd2$^{sa18532-/-}$ mutant

Phenotype of wild-type (panel A, B) and homozygote (panel C, D) zebrafish of F5 generation at 5 dpf. The most common phenotype characterised by lack of swim bladder observed in homozygotes is highlighted by blue arrow. Panel A and C show lateral view with dorsal to the top, anterior to the left in all specimens. Panel B and D show dorsal view, anterior to the left in all specimens. Scale bar, 1000µm

6.3.3.1 Possible effects of FRMPD2 mutation in vitro

Very often in vitro studies aiming to analyse and compare wild-type and mutant proteins allow the verification of the functional effects associated with mutations introduced within the gene of interest. Until now our in vivo study of the zebrafish *frmpd2* mutant did not determine any genotype-phenotype correlation, therefore we decided to pursue an in vitro study with mammalian cell lines.

To demonstrate possible effects of the introduced nonsense mutation in the FERM domain of FRMPD2 protein, we performed an in silico analysis using two computational online tools: MutationTaster2 (Schwarz et al., 2014) and PROVEAN Protein (*Protein Variation Effect Analyser*) (Choi et al., 2012, Choi and Chan, 2015). Both analyses demonstrated that mutation of the conserved tyrosine, in both zebrafish and human protein (Figure 6.11), leading to the formation of a premature termination codon (PTC), most probably would result

in a deleterious effect. Nevertheless, at that stage of analysis we could not predict whether mutation within *frmpd2* gene would cause RNA or protein degradation or whether the created mutant protein would act by a dominant-negative or gain-of-function effects.

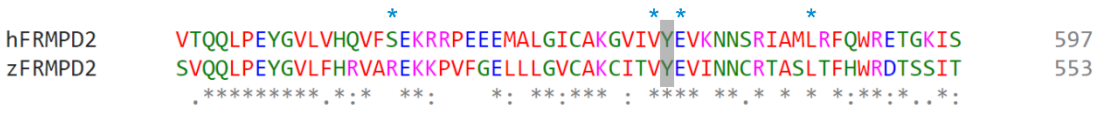

Figure 6.11 Sequence alignment of human and zebrafish FRMPD2 proteins

Sequence alignment of human (hFRMPD2) and zebrafish (zFRMPD2) FRMPD2 proteins. Represented fragment shows alignment of part of FERM domain of FRMPD2 in human and zebrafish. The conserved tyrosine (Y) is highlighted in grey. Putative residues contributing to phosphoinositide binding in human and zebrafish proteins are indicated by blue asterisks. Protein sequences were retrieved from NCBI (http://www.ncbi.nlm.nih.gov/) and multiple sequence alignment was run using Clustal Omega tool available on the website: http://www.ebi.ac.uk/Tools/msa/clustalo/.

It has been shown that the FERM domain of FRMPD2 is sufficient for membrane localisation and binds phosphatidylinositol PtdIns(3,4)P_2 (Stenzel et al., 2009). Mutation at the position Y531 of zebrafish protein or Y575 of human protein may cause the loss of two putative residues contributing to phosphoinositide binding (Figure 6.11), therefore, it was hypothesised that the truncated version of FRMPD2 would interfere with its proper localisation and function. To test this theory, a truncated GFP-tagged human FRMPD2 construct was created and overexpressed in HEK293 cells and MDCKII cells along with the full length GFP-tagged FRMPD2 as a control. Western Blot analysis demonstrated a weak band of the size of around 170 kDa corresponding to full length FRMPD2, and band of the size of around 90 kDa which could correspond to truncated FRMPD2 protein (Figure 6.12, B; white arrow and dotted arrow respectively). Immunofluorescence assay showed that MDCK II cells overexpressing the full length protein displayed characteristic FRMPD2 membrane localization, while the truncated FRMPD2 mutant displayed only cytoplasmic staining (Figure 6.12, A). Given the fact that we were not able to detect expression of truncated FRMPD2 via Western Blot and also based on the IF data, we could not conclude whether signal comes from the truncated FRMPD2 protein or a degradation product. Nevertheless, the results suggest that truncation within the FERM domain caused either partial or complete deletion of PtdIns(3,4)P_2 binding sites, that are

responsible for FRMPD2 attachment to the membrane, or complete degradation of FRMPD2 protein.

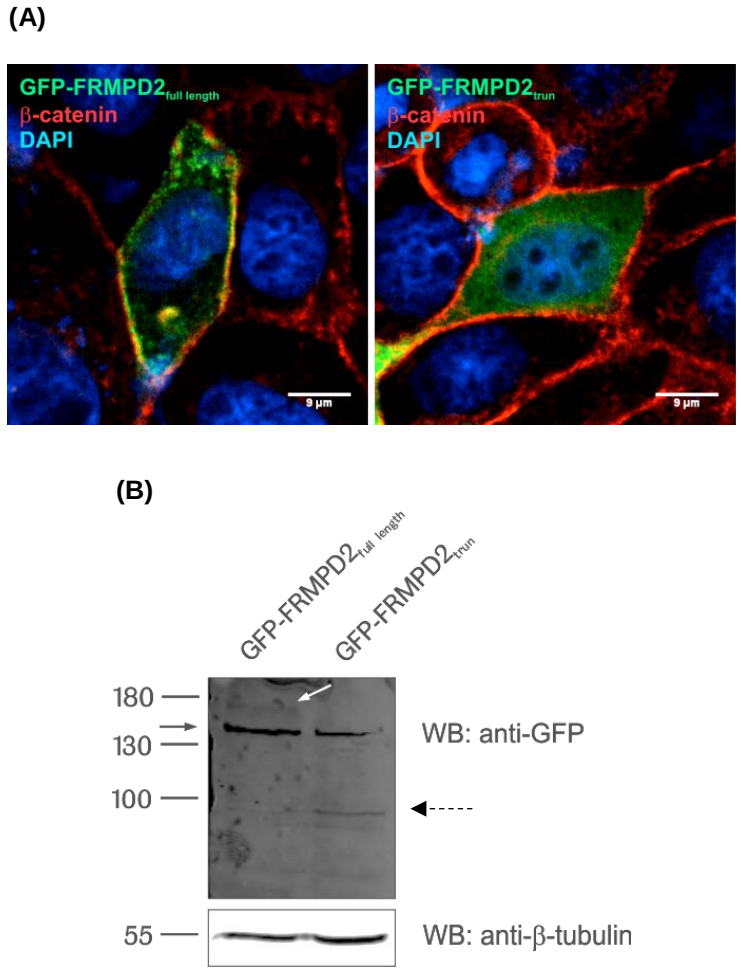

Figure 6.12 Truncated FRMPD2 displays altered localisation pattern in polarized MDCKII epithelial cells

(A) *MDCKII cells were grown on coverslips and transiently transfected with expression constructs of full length and truncated GFP-tagged FRMPD2. 48 hours post transfection cells were fixed and stained with anti-β-catenin followed by anti-mouse Alexa Fluor® 594 antibody. Images were taken using spinning disc confocal microscope and Z-stack function. Images represent single xy planes. Scale bar, 9 µm.* ***(B)*** *HEK293 cells were transiently transfected with expression constructs of full length or truncated GFP-tagged FRMPD2 and whole cell lysates were prepared 48h post-transfection. Membranes were probed with anti-GFP and anti-β-tubulin antibodies followed by anti-rabbit Alexa Fluor® 680 and anti-mouse DyLight™ 800 antibody respectively. Samples represented around 10% of the total cell lysate. Signal from full length and truncated FRMPD2 was indicated by white and dotted arrow respectively. Non-specific signal of anti-GFP antibody was marked by black arrow.*

6.4 Discussion

The data shown provide evidence of *frmpd2* gene expression in zebrafish, and contrast with the previously published data that suggest *frmpd2* and *ptpn20* are the same genes (van Eekelen et al., 2012). Although FRMPD2 and PTPN20 share 53% identity at the protein level, genomic databases imply that these two genes are in fact distinct and possess five and two distinguished transcript variants, respectively. However there is still a possibility that these two genes could evolved due to alternative splicing.

We hypothesised that FRMPD2 protein in zebrafish has the same function as its human equivalent and due to the high similarity between these two species, it may be expressed in epithelial tissues. Spatial and temporal *frmpd2* expression pattern, investigated by performing *in situ* hybridisation, did not appear to be specific. Results obtained with two different riboprobes demonstrated the same staining with anti-sense and sense probe independently from the zebrafish stage. Although the signal with the antisense riboprobe 2 was more prominent, which could suggest *frmpd2* ubiquitous expression during the stage of segmentation period (14 hpf) followed by a more specific expression in the brain structures of an embryo at 24 hpf, the staining pattern obtained with corresponding sense probe was less intense but identical. Therefore, without additional experiments including *frmpd2* knockdown, final data interpretation remains disputable. In situ hybridisation results did not give us specific information about the spatial-temporal *frmpd2* expression pattern, therefore the expression level of *frmpd2* during zebrafish embryogenesis was assessed by real-time PCR. The results indicated that at the early developmental stage of 12 hpf as well as in adult fish *frmpd2* mRNA expression level was very low (with $C_t \sim 38/39$) and even *β-actin* was not detected as early as other stages. Experiments performed within the current study, but not presented in this thesis, also confirmed the presence of *frmpd2* at stages of 1 and 4 hpf, however similar to the presented data, C_t values were very high. It could suggest the problem with amplification efficiency, which would require further optimisation for the stages at the onset of development but on the other hand this could also suggest that *β-actin* may not be a very good normalizer although RT-qPCR optimisation showed amplification efficiency of

around 100% for both *frmpd2* and *β-actin*. At the subsequent developmental stages, the presence of *frmpd2* was evident and its expression level increased significantly after 72 h post-fertilisation and remained at almost the same level until the stage of 15 dpf. We concluded that *frmpd2* may be less important at the onset of development but can play important roles at the later stages of zebrafish growth. This would also explain the problems with the *in situ* hybridisation experiments which were performed prior to the real-time PCR runs. Low detection level and similar staining pattern from antisense and sense probes at the early zebrafish developmental stages can suggest that *frmpd2* expression was not sufficient for detection hence the observed signals indicated some non-specific binding.

In vivo analysis of FRMPD2 function in zebrafish requires methods altering gene activity. Although the most widely used technique was a gene knockdown by morpholino, this method is restricted temporally and could not be used effectively at later stages of embryogenesis or in adult fish. Therefore, after the recommendation from researchers at MRC Centre at University of Sheffield, we decided to breed *frmpd2*^{sa18532} mutant from the Sanger Institute. An initial genetic screen identified heterozygous carriers which did not demonstrate any abnormalities, however the first generation of their offspring displayed a mixture of severe phenotypes. Although all of them suggested some neurological or epithelial defects, potentially compatible with the hypothesis of conserved *frmpd2* function among the species, genotyping results did not correlate with the observed phenotype. Given the sequencing results as well as the mixed phenotype within the same generation, the zebrafish mutants obtained from Sanger continued to contain the background mutations or transgenic insertions that were not listed in the genotype and appeared during ENU mutagenesis. A next generation of heterozygotes, obtained as a result of outcrossing of zebrafish from Sanger to wild-type strain, anatomically and behaviourally were similar to the previous generation. Their progeny did not display such severe phenotypes as before, but approximately 25% of them did not have a swim bladder. Unfortunately, the phenotype did not match with the *frmpd2* homozygote genotype. Moreover, it suggested that the existing background mutation(s)

causing loss of swim bladder can be conserved throughout the generations, and was therefore hard to eliminate.

Creation of a premature termination codon (PTC) usually contribute to the formation of defective products at the mRNA or protein level. In most cases incorporation of the PTC activates the nonsense-mediated mRNA decay (NMD) pathway, that recognizes abnormal transcripts and eliminates them, thus preventing synthesis of aberrant proteins (Culbertson and Leeds, 2003). However, if elimination of such mRNA products is unsuccessful, it may result in the synthesis of abnormal proteins potentially acting through dominant-negative or gain-of-function effects. On the other hand, aberrant proteins are usually misfolded and therefore are not able to gain a proper three-dimensional structure. Like other nascent proteins in cells, misfolded products undergo a protein quality control, which recognizes them as detrimental and directs them, through ubiquitin proteasome system, to degradation (Popp and Maquat, 2013). Although until now *frmpd2* in vivo function in zebrafish remains unclear, in silico analysis suggested that creation of a premature termination codon (PTC) within the FERM domain of FRMPD2 could have a deleterious effect on protein stability and function. We have shown that a corresponding human mutant with premature stop codon within the FERM domain would lose its ability to localise at the plasma membrane, however the expression of the truncated FRMPD2 protein remains questionable. We have not been able to prove yet whether introduction of the PTC led to creation of the truncated FRMPD2 protein or complete degradation due to its misfolding and instability. Nevertheless, truncation of FRMPD2 protein as well as its complete degradation would have a negative impact on FRMPD2-related signaling mechanisms and PDZ domain-related interactions with e.g. NOD2 (Lipinski et al., 2012) or even PRK2 as presented in this thesis.

In summary, qPCR data demonstrated that *frmpd2* expression significantly increases after 72 h post-fertilisation, but the spatial and temporal expression pattern requires further investigation. *frmpd2* mutant phenotype still remains elusive, however we did not perform detailed analysis of the zebrafish phenotype and only looked at potential abnormalities visible by eye. On the other hand, we

analysed only embryos and early larvae of zebrafish, but certainly we should observe phenotypes of adult homozygotes. Based on the data obtained from an in vitro study in mammalian cells, nonsense mutation within the FERM domain would most likely affect not only the protein itself but also all related biological mechanisms.

CHAPTER 7 - FRMPD2 detection

7.1 Introduction

Almost all experimental procedures in the studies unravelling protein function require protein detection using either a qualitative or quantitative assay. The most popular techniques; Western Blot and immunofluorescence microscopy, utilise antibodies characterised by high specificity and affinity to the target protein. In the current study, pulldown, co-immunoprecipitation or immunofluorescence assays of overexpressed target proteins were detected by widely used commercial antibodies raised against specific epitope tags like GFP or myc. However, endogenous proteins require antibodies which recognise short sequences of the target protein and are designed in a specific way to reduce cross-reactivity. Immunogen sequences usually correspond to the most antigenic regions of the protein of interest, however in many cases, including the current study, even precise design or even a known and previously tested immunogen do not necessarily provide the production of a useful antiserum.

In many studies, analysis of protein function in mammalian cells is determined by knockdown experiments which utilise small interfering RNA (siRNA) or short hairpin RNA (shRNA) to silence gene expression. To validate protein knockdown in this study, Western Blot was the method of choice, which showed a reduction in the expression level of GFP-tagged FRMPD2. However, in many cases, if specific antibodies are unavailable, gene knockdown can be confirmed by detecting mRNA instead of protein, which can be achieved by quantitative real-time PCR (RT-qPCR).

All procedures in the current study required protein detection at the exogenous or endogenous level. We have tested several antibodies against FRMPD2, which are currently available on the market, however none of them were useful for immunoblot or immunofluorescence of the endogenous protein. They were only able to recognise overexpressed protein (data not shown). Hence we decided to make an attempt to produce a custom made antibody against FRMPD2 and to validate FRMPD2 knockdown in mammalian cells using Western Blot technique. At the later time, due to problems with obtaining good quality antibodies, we also tried to validate *frmpd2* gene expression level using qPCR method

7.2 Aim

The main aim of this part of the PhD project was to establish tools for detection of endogenous FRMPD2. With a view to achieve this goal, the following approaches were considered:

1. antibody production against FRMPD2
2. validation of FRMPD2 knockdown by Western Blot
3. validation of FRMPD2 knockdown by qPCR

7.3 Results

7.3.1 Antigen production and generation of antibody against FRMPD2

Previously published data about FRMPD2 (Stenzel et al., 2009) demonstrated that endogenous protein can be easily detected by two independent antibodies and two different techniques including Western Blot and immunofluorescence microscopy. A commercially available antibody from SIGMA (named here as anti-FRMPD2(1)) was successfully used at the beginning of the current study when endogenous FRMPD2 was detected by Western Blot in total cell lysates and also in co-precipitates with BANK1 (Chapter 3, Figure 3.7). Unfortunately, this antibody has been discontinued by the company and although it was replaced by a new one, produced based on a different immunogen, endogenous FRMPD2 was not detectable neither by Western Blot nor by immunofluorescence (data not shown). A custom made FRMPD2 antibody (named here as anti-FRMPD2(3)) was produced several years ago and successfully used in the Erdmann lab before. When we tested this antibody in the current study using several different cell lines of mainly epithelial origin, we identified many non-specific signals and although a prominent band of the expected FRMPD2 size was recognised in Caco-2 and HEK293 lysates as well (Figure 7.2), subsequent knockdown experiments proved, that this signal was non-specific (data not shown). The antibody failed in the immunofluorescence assay as well, but interestingly, it was successful in recognising overexpressed FRMPD2 by Western blot and immunofluorescence microscopy (data not shown). More tests, including cell lysis with different buffers, using a higher total amount of the protein loaded on the gel, transfection

with shRNAs targeting FRMPD2 or co-IP, were performed to figure out whether there is any technical problem preventing FRMPD2 detection. Even though considerable efforts and the extensive troubleshooting were carried out, it was not possible to unravel why the previously active serum could not recognise the endogenous FRMPD2 anymore.

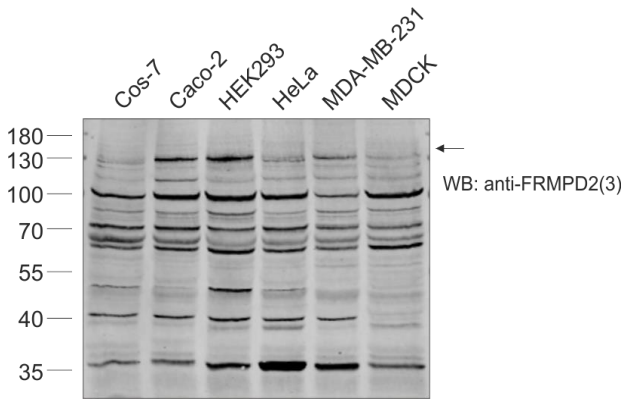

Figure 7.1 FRMPD2 detection by anti-FRMPD2(3) antibody

Different cell lines including Cos-7, Caco-2, HEK293, HeLa, MDA-MB-231 and MDCK cells were grown on 60 mm dishes and whole cell lysates were prepared after cells reached 90 – 100% confluency. Membranes were probed for the endogenous FRMPD2 with anti-FRMPD2(3) antibody followed by anti-rabbit Alexa Fluor® 680 antibody. Samples represented around 10% of the total cell lysate. Estimated size of endogenous FRMPD2 (~144 kDa) was marked by an arrow.

Lack of suitable commercially available antibodies prompted us to the decision of antibody production. We decided to use two different antigens depicted in the Figure 7.2: antigen 1, used before for the production of anti-FRMPD2(3) antibody and antigen2, which corresponded to the immunogen used for the production of anti-FRMPD2(1) antibody by SIGMA.

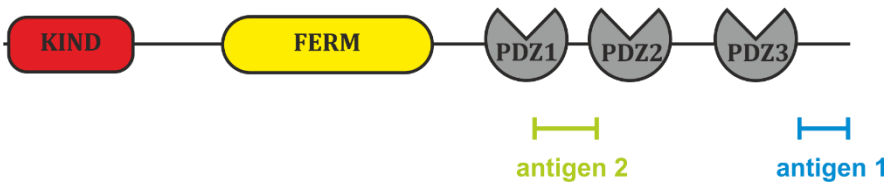

Figure 7.2 Localisation of antigen1 and antigen2 within FRMPD2 sequence used for antibody production

Antibodies against FRMPD2 were produced using two different antigens: antigen1 represents C-terminal part of the protein of the total length 142aa localised within 1168 and 1309aa; antigen2 recognised the sequence of 121aa situated between 832 and 952aa

and covering region between PDZ1 and PDZ2 domains, 30% of PDZ1 and only 2 aa from the PDZ2 domain. Sequences of both antigens were fused to GST protein.

Two antigens were produced and purified from bacteria as GST fusion proteins (Figure 7.3). The purified proteins were subsequently used for antibody production by Eurogentec company.

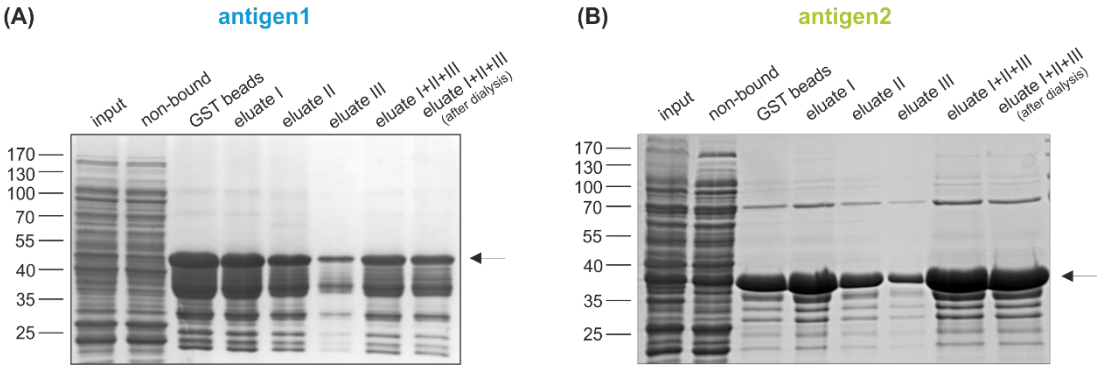

Figure 7.3 Purification of GST-fusion proteins used as antigens for FRMPD2 antibody production

Coomassie stained gels representing samples of different steps from GST purification protocol (refer to Chapter 2 and section 2.2.2.1.1). GST fusion proteins containing sequences of antigen1 ***(A)*** *and antigen2* ***(B)*** *were expressed in bacteria BL21(DE3) and purified from bacteria lysate by GST pulldown. Purified proteins were subsequently eluted from the beads and dialysed into PBS. Protein concentration was estimated and aliquots containing 200µg of protein were prepared (eluate I+II+III, after dialysis). The right size of purified antigens was marked by an arrow. The bands below represented antigen degradation products.*

Prior to immunisation, we had tested pre-immune sera of a few selected animals for the presence of antibodies against FRMPD2 or other cross-reactivities of similar size by Western Blot with samples prepared from a total cell lysate of non-transfected and myc-FRMPD2 and GFP-FRMPD2 transfected HEK293 cells. Animals, whose pre-immune sera gave the lowest background and did not recognise overexpressed FRMPD2, were chosen for immunisation. Immunisation was carried out by the company Eurogentec and animals were immunised four times within a 87-day cycle until the final sera were obtained. All antibodies were tested under the same conditions using whole cell lysates from different cell lines and HEK293 cells overexpressing myc-tagged FRMPD2 which was used as a control to indicate the right size of FRMPD2 (myc-FRMPD2 has a very similar size to endogenous FRMPD2) as well as the presence of antibodies in the tested sera. As shown in Figure 7.4 all antibodies recognised overexpressed myc-FRMPD2

which confirmed successful immunisation by antigen1 and antigen2 of the four selected animals in total. However, the signal from endogenous FRMPD2 could not be detected by any of the newly made antibodies. As mentioned before, additional tests were performed including immunostaining, Western Blot with the much higher total amount of protein loaded into the gel and Western Blot with samples from cells treated with shRNAs targeting FRMPD2 and utilisation of two different detection methods. The results led to a similar conclusion, therefore, it was finally confirmed that all the antibodies failed in recognising endogenous FRMPD2 independently from the detection method.

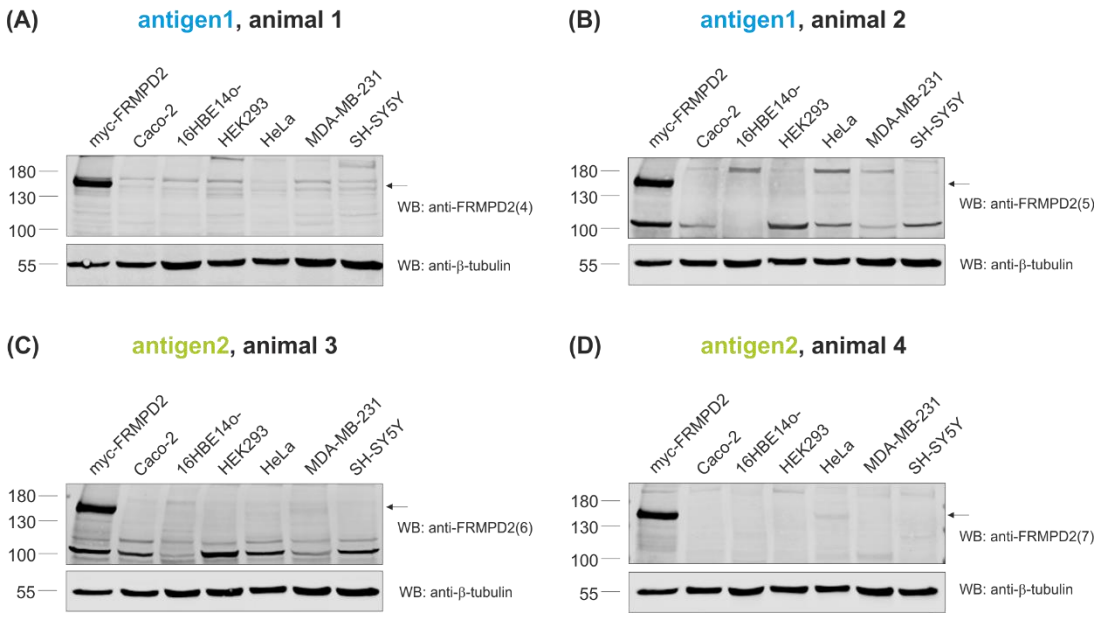

Figure 7.4 FRMPD2 detection by custom made anti-FRMPD2 antibodies (Eurogentec)

Different cell lines including HEK293 cells transfected with myc-FRMPD2, Caco-2, 16HBE14o-, HEK293, HeLa, MDA-MB-231 and SH-SY5Y cells were grown on 35 mm dishes and whole cell lysates were prepared 48h post-transfection or when cells reached 90 – 100% confluency. Membranes were probed for the endogenous FRMPD2 with anti-FRMPD2(4)/(5)/(6)/(7) antibodies followed by anti-rabbit Alexa Fluor® 680 antibody. Samples represent around 10% of the total cell lysate. Estimated size of endogenous FRMPD2 (~144 kDa) was marked by an arrow.

In our second attempt, antibody production was carried out by a different company – Biogenes. This time two animals were immunised with antigen1 and final sera were obtained after three months. Both antibodies were tested using samples from HEK293 cells either overexpressing or depleted of FRMPD2 and similar to previous antibodies, only overexpressed FRMPD2 was detected (Figure 7.5). Additionally, two other tests were performed using antibodies affinity-

purified from the crude sera and subsequently concentrated. Unfortunately, the results were again not positive and endogenous FRMPD2 band was not detectable. Affinity-purification and concentration helped to reduce the signal to background ratio by significantly removing the non-specific signals that were detected when using the crude sera.

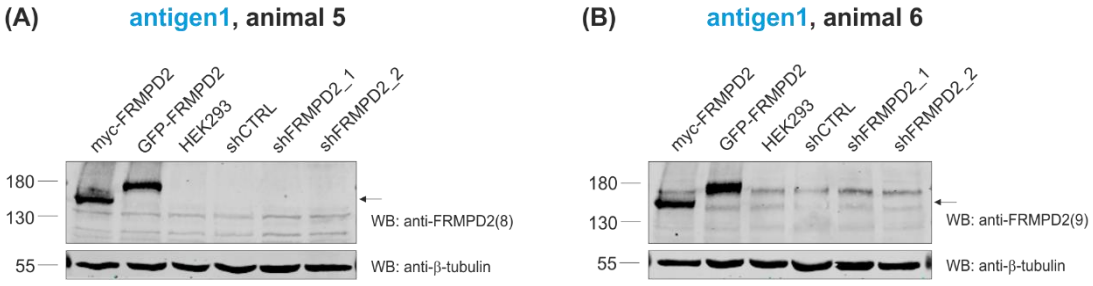

Figure 7.5 FRMPD2 detection by custom made anti-FRMPD2 antibodies (Biogenes)

Wild-type HEK293 cells were grown on 35 mm dishes and transfected with myc-FRMPD2, GFP-FRMPD2, shCTRL, shFRMPD2_1, shFRMPD2_2. Whole cell lysates were prepared 48h post-transfection or when cells reached 90 – 100% confluency. Membranes were probed for the endogenous FRMPD2 with anti-FRMPD2(8)/(9) antibodies followed by anti-rabbit Alexa Fluor® 680 antibody. Samples represent around 10% of the total cell lysate. Estimated size of endogenous FRMPD2 (~144 kDa) was marked by an arrow.

7.3.2 Attempt to validate *frmpd2* knockdown by RT-qPCR

RT-qPCR experiments were run simultaneously with other knockdown validation procedures. Several pairs of primers listed in Table 2.6 were designed as described in section 2.2.1.3.3 c, plus one commercially available pair of primers (*Bio-Rad Laboratories*), for *frmpd2* amplification were tested. In all samples containing cDNA (+RT), negative control for reverse transcription (-RT) samples as well as no template control (NTC) samples, one major product was amplified and that was confirmed by comparison of C_t values and appropriate dissociation curves. Sequencing results of PCR products revealed that they all corresponded to the desired *frmpd2* fragments. At the same time the *GAPDH* gene, used here as a normalizer, was amplified only in samples containing cDNA (+RT) and fluorescence signal in the negative control for reverse transcription (-RT) or no template control (NTC) samples was detected only at the baseline suggesting that there were no traces of contamination. Therefore, it can be concluded that the problem with contamination referred only to the human *frmpd2* gene. To overcome this problem and find the source of contamination, we performed

many standard PCR and qPCR runs with changed conditions or procedure in the template preparation. Unfortunately, the contamination problem has not been solved yet, and due to the time constraints, further experimental procedures have been suspended.

7.3.3 Validation of FRMPD2 expression level by Western Blot

Despite two attempts at antibody generation with two companies and testing two antigens targeting different regions of the FRMPD2 protein, it was not possible to validate the knockdown efficiency of endogenous *frmpd2* using either shRNAs or siFRMPD2 (SMARTpool: siGenome FRMPD2 siRNA) available in the lab via western blotting. Although both tools were tested and validated previously (Stenzel et al., 2009, Lipinski et al., 2012), the optical stretcher, real-time deformability cytometry as well as cell migration experiments conducted in the current study required knockdown confirmation at the time of performing them. Unsuccessful antibody production encouraged us to find an alternative way to confirm knockdown of *frmpd2*. To this end, siFRMPD2 was tested for reduction in the protein level of overexpressed FRMPD2. To check whether siRNA targeting FRMPD2 reduces the level of overexpressed GFP-FRMPD2, samples were probed with anti-GFP antibody and additionally with anti-β-tubulin, used here as a loading control. Immunoblot revealed a substantial decrease of GFP-FRMPD2 expression in cells treated with siFRMPD2 when compared to the cells treated with non-targeting control siRNA (siCTRL) (Figure 7.6, A). The expression level of tubulin in both samples was comparable, therefore the observed decrease in the GFP signal was due to the effect caused only by siRNA targeting *frmpd2*. A very similar experiment was performed with two shRNAs against *frmpd2*, in the current study used for the optical stretcher, RT-DC and cell migration experiments (Chapter 5). Western Blot analysis demonstrated that both shRNAs: shFRMPD2_1 and shFRMPD2_2 effectively reduced protein level of overexpressed GFP-tagged FRMPD2 in comparison to the control sample (Figure 7.6, B). It is probably worth to mention that shFRMPD2_2 was slightly more efficient than shFRMPD2_1 and GFP signal was almost undetectable. Tubulin level in all samples was similar suggesting that both shRNAs efficiently targeted

exogenous FRMPD2. Overall these results proved that either siFRMPD2 or the two shRNAs efficiently reduced the exogenous level of FRMPD2.

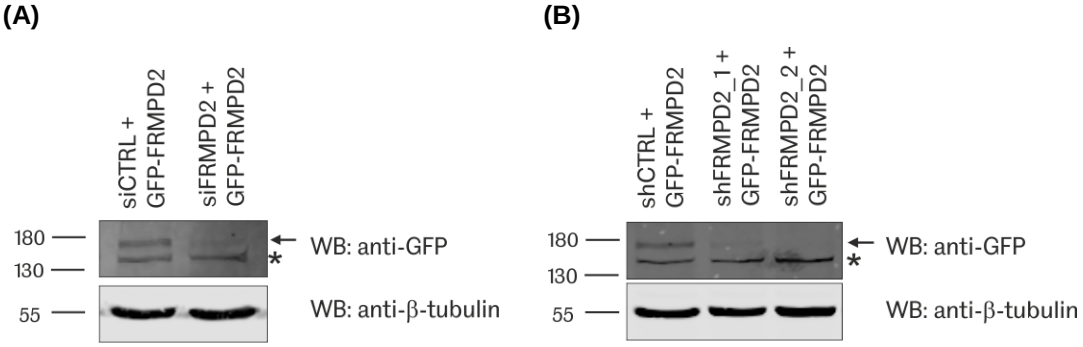

Figure 7.6 siRNA and shRNA targeting FRMPD2 decreases level of overexpressed FRMPD2

HEK293 cells were transfected with GFP-FRMPD2 construct and siCTRL or siFRMPD2 at day 1 at the final concentration 50 nM and incubation time 72 hours (A) or HEK293 cells were transfected with GFP-FRMPD2 construct and shCTRL, shFRMPD2_1 or shFRMPD2_2 at day 1 and incubated for 72 hours (B). Cell lysates were prepared and protein concentration was estimated. Endogenous proteins were detected with anti-β-tubulin antibody followed by anti-mouse DyLight™ 800 antibody, while overexpressed proteins with anti-GFP antibody followed by anti-rabbit Alexa Fluor® 680. Samples represented around 10% of the total cell lysate. The size of overexpressed GFP-FRMPD2 was marked by an arrow. The asterisk indicated some non-specific signal from the anti-GFP antibody.

7.4 Discussion

A significant part of the experimental procedures carried out within this thesis required detection of the endogenous FRMPD2 protein. Moreover, many other experiments, which were planned, could not be performed due to the lack of suitable tools. FRMPD2 expression has already been confirmed using custom made and commercially available antibodies (Stenzel et al., 2009, Lipinski et al., 2012), however currently none of the antibodies available on the market are useful for immunoblot or immunofluorescence of the endogenous protein. Our attempts to produce custom made antibodies against FRMPD2 were unsuccessful as they also recognised only overexpressed protein. One reason for this could be that the protein amount used for immunisation did not contain enough of the good quality antigen due to its degradation. Although we have tested several mammalian cell lines of epithelial origin, known to express FRMPD2, all the antibodies failed to detect endogenous FRMPD2 protein level.

The unavailability of a good quality antibody encouraged us to test quantitative real-time PCR to confirm *frmpd2* knockdown in mammalian cells. Previous results for zebrafish *frmpd2* confirmed that quantitative real-time RT-PCR procedure was highly optimised and characterised by high amplification efficiency. Although qPCR was successfully applied to assess *frmpd2* gene expression in zebrafish, we encountered significant problems with detection of its human ortholog. *frmpd2* was amplified in the samples containing cDNA templates as well as in negative control for reverse transcription (-RT) and no template control (NTC) samples. Despite modification of PCR conditions including *frmpd2* primers annealing temperature, amount or source of the template, C_t values of all amplified products were similar. Additionally, analysis of the dissociation curves, indicating one major peak at the temperature of around 86.0°C, suggested an amplification of specific products and at the same time excluded possibility of primer-dimer formation. All amplified fragments matched the size of the desired gene fragments on gel electrophoresis and the final sequencing results confirmed that the products in the negative control for reverse transcription (-RT) or the no template control (NTC) samples corresponded to the expected *frmpd2* gene fragments. While there was a continuous problem with *frmpd2* detection, *GAPDH* used in all PCR runs as a control was amplified clearly only from the cDNA template and none of the contamination was present in the negative control for reverse transcription (-RT) samples as well as and no template control (NTC) samples. Possible contamination with genomic DNA was also excluded in the very beginning by testing the DNase efficiency and amplification of G*APDH* (data not shown). Moreover, all primers were designed to span exon-exon junctions to avoid amplification of gDNA products, even if some gDNA traces would be present in the RNA samples. Unfortunately, the source of contamination remained undetectable despite extensive troubleshooting and employment of good laboratory practices. Based on all standard PCR and qPCR results, it can be concluded that contamination was introduced at the time of pipetting reaction components into the PCR plates. Most likely it came from some external sources, which were contaminated with plasmids DNA containing ORF of *frmpd2* gene, used very often in other experimental procedures described in this thesis. Extensive troubleshooting was performed within current thesis and included:

1) change in the RNA extraction protocol and cDNA synthesis (the protocol used for zebrafish was implemented for mammalian cells);
2) RNA extraction and cDNA synthesis with newly opened kits;
3) testing samples prepared by different researchers in a different place;
4) testing qPCR reagents from different suppliers;
5) checking gDNA contamination
6) testing different mammalian cell lines;
7) testing different primers;
8) testing different input mass of RNA;
9) using fresh RNase-free water for primers resuspension and for RT-PCR reaction;
10) using disposable filter tips;
11) extensive cleaning of pipettes (ethanol, bleach, UV) and place to prepare templates and qPCR plates (sterile hood).

The one remaining solution which was not tried yet is to outsource performance of qPCR to the core facility at the University of Sheffield, or external company. The lack of suitable antibody and the unsolved contamination problems in real-time PCR hindered the conduction of further experiments that required validation of *frmpd2* knockdown in order to interpret its results undoubtedly. Although shRNAs and siRNA targeting *frmpd2*, used in this thesis, were validated previously (Stenzel et al., 2009, Lipinski et al., 2012), some of the outcomes obtained from the optical stretcher and RT-DC measurements still could not be accompanied with a validation of the knockdown. However, these silencing molecules reduced the level of an overexpressed FRMPD2 and potentially this can suggest that they maintained the same ability to deplete endogenous FRMPD2. This experiment showed a significant reduction of the overexpressed protein level (70 – 80%), therefore, at the moment, it could be used as an alternative way to confirm *frmpd2* knockdown in mammalian cells.

Overview and future perspectives

In this thesis, we provide evidence for several novel interaction partners for the multi-PDZ domain protein FRMPD2. These novel interactions support the previous notion that FRMPD2 may be a key player in establishment and maintenance of epithelial polarity as well as having a broader role in regulating the immune host defense system of the intestine, which is compromised in inflammatory bowel disease. We have presented a novel role of FRMPD2 in regulating cell mechanical properties and cell migration of epithelial cells. Moreover, FRMPD2 also appeared asymmetrically distributed in migrating cells, with clear accumulation at the rear of the migrating cell. This resembles its asymmetric localisation in epithelial monolayers, where FRMPD2 accumulates selectively at the basolateral membrane. Finally, we also demonstrated that FRMPD2 is expressed in zebrafish during early developmental stages, however its spatial expression pattern as well as in vivo function still remains elusive.

8.1 FRMPD2 interactome

Previously published data about FRMPD2 showed its vital role in cell polarity as well as presented a unique linkage between FRMPD2 and signalling mediating host immune defence in colon epithelial cells (Stenzel et al., 2009, Lipinski et al., 2012). The current study aimed to explore the protein interaction network of FRMPD2 to be able to get insight into the possible mechanism of FRMPD2 action in epithelial cell polarity. We took two approaches to identify new interaction partners, including validation of candidates from Y2H and AP-MS screen performed previously in the Erdmann lab, and using a novel technique called proximity-dependent biotinylation – BioID. Numerous co-immunoprecipitation assays performed within the current study revealed three new interactions of FRMPD2, with BANK1, PLECTIN-1 and RAPGEF2. Although all of them, as discussed before, were promising candidates due to our limited knowledge, some technical issues, and time constraints, we have not been able to perform a deeper analysis of their functional effect with respect to epithelial cell polarity and mechanisms of autoimmune disorders. Given the fact that one of those proteins, RAPGEF2 has a very broad functions in processes involved in the maintenance of

epithelial polarity, cytoskeleton contractility and also cell migration, we see a potential to continue the study and to explore the role of the FRMPD2-RAPGEF2 complex further.

The advent of new proteomic approaches, like the BioID method applied in the current study, enables identification of both interacting and neighbouring proteins in the cellular environment of FRMPD2. We have successfully demonstrated that the BioID method worked in polarised epithelial cells and it helped us to discover the novel interaction between FRMPD2 and PRK2. Prioritisation of experimental work in the current study and resource constraints prevented us from performing further mass spectrometry and proteomic analysis of biotinylated complexes, however, we already know that BioID-FRMPD2 would be a very useful tool, which in the future may be used to explore the FRMPD2 signalosome further.

Given the fact that interaction between FRMPD2 and PRK2 was validated by us and also confirmed by another proteomic study (Huttlin et al., 2015), it was hypothesised that these two proteins might act together and regulate apical junction formation in polarised epithelial cells. We have demonstrated that PRK2 interacts selectively with the PDZ3 domain of FRMPD2 and also that a C-terminal cysteine of PRK2 is essential for this binding. Crucial for this study was the fact that these two proteins colocalized in non-polarised and polarised epithelial cells, and this colocalization was abolished by the mutations in their binding sites. This may suggest a broader role of FRMPD2 in membrane-associated PRK2 signalling in non-polarised cells. Additionally, we also proved that FRMPD2 recruits PRK2 to cell-cell contacts of non-polarized and polarized epithelial cells, but we found them colocalizing with tight junction marker in polarized epithelial cells as well. We confirmed that PRK2 is responsible for apical junction formation in not only in bronchial epithelial cells but also in epithelial cells of colon and kidney. Currently, we are not able to test our hypothesis that endogenous FRMPD2 acts as a molecular scaffold recruiting PRK2 to the basolateral membrane and enabling PRK2 to regulate epithelial junction formation. The main limitations in the framework of this study like lack of suitable antibodies and tools to validate the FRMPD2 knockdown prevented us from performing a number of

experiments. Thus it is key for further studies to establish such tools like suitable antibodies or quantitative PCR.

8.2 The role of FRMPD2 in cell mechanical properties

This work lays the foundation for future research into deeper understanding of the role of FRMPD2 in cell mechanics. For the first time, we have reported that FRMPD2 affects cell mechanical properties of detached epithelial cells. Based on two different methods, we showed that depletion of FRMPD2 or PRK2 increased cell deformation, however because of experimental variabilities, more tests are needed to be performed. The presented data suggest that FRMPD2 may be associated with cytoskeletal components, but to get a full picture of FRMPD2 effects on the cytoskeleton, it would be necessary to perform further experiments with the cells being in the adherent state, using different methods like AFM. The same applies to PRK2, however, its connection to the cytoskeleton is known, and future experimental design needs to be considered to understand better the function of the FRMPD2-PRK2 complex in cell mechanics. Following changes in mechanical properties of the cells, we have studied FRMPD2 and PRK2 function in cell migration, and demonstrated for the first time that both proteins act as a suppressors of migration. Moreover, we discovered that localisation of FRMPD2 in polarised migrating cells is asymmetrical, depends on migration stage, and is consistent with front-rear polarity. This finding may be especially of interest with respect to understanding the mechanism of epithelial-mesenchymal transition, an important process contributing to cancer metastasis. Acting as an inhibitor of cell migration, FRMPD2 may be a crucial component of scaffolding complexes maintaining epithelial integrity. This novel function of FRMPD2 requires special attention, and in the future, it may help to resolve molecular mechanism contributing to human diseases like inflammatory bowel disease and cancer.

8.3 The role of FRMPD2 in zebrafish development

The current study confirmed the presence of the *frmpd2* gene in zebrafish, which is distinguished from other genes in contrast to previously published data (van Eekelen et al., 2012). We demonstrated that *frmpd2* is expressed developmentally and in adult zebrafish. However, to elucidate this further we need to determine

frmpd2 expression level in different organs, as an expression in a whole adult zebrafish does not provide precise information. The priority will be to determine the spatial and temporal *frmpd2* expression patterns in zebrafish larvae, as until now it was not successful. Finally, to investigate *frmpd2* function in vivo in zebrafish, the *frmpd2*^{sa18532}*-/-* mutant without background mutations should be created and further tested to investigate phenotypes caused by mutagenesis. Although our current knowledge about FRMPD2 function in vivo in zebrafish is limited, our in vitro results demonstrated that mutation in the FERM domain of FRMPD2 alters FRMPD2 localisation within epithelial cells. The truncated protein was cytosolic compared to the plasma membrane associated localisation of WT FRMPD2. Furthermore, the expression levels of the transfected truncated FRMPD2 were low, suggesting that the truncated protein might be unstable. Hence homozygous offspring of zebrafish mutant are likely to be a good model to study *frmpd2* function in zebrafish development and adulthood.

8.4 Concluding remarks

The work performed in the framework of this thesis has established several potential interacting proteins for FRMPD2. One of these interactions (FRMPD2/PRK2) was studied in detail and has led to a model how Rho-dependent kinase activity can be selectively directed to the basolateral membrane to establish apical junctions. Furthermore, stable epithelial cell lines expressing a biotinylation competent fusion protein of FRMPD2 were established, which will serve as a valuable tool to characterise the FRMPD2 mediated signalosome using proximity-dependent biotinylation assays. The current study also sheds light on a novel function of FRMPD2 in regulating cell mechanical properties and cell migration. This is of particular importance as both inflammatory bowel disease as well as cancer, are characterised by loss of epithelial integrity, which is also reflected in major changes in the cytoskeleton, and this can have a profound effect on the cell´s overall mechanical properties. Although a preliminary analysis of homozygous mutant frmpd2 zebrafish did not reveal an obvious phenotype a much more detailed analysis is at the cell and tissue level is required including a detailed expression study at advanced developmental stages.

To conclude, FRMPD2 is emerging as an important component of complexes regulating epithelial cell polarisation on different levels. FRMPD2 may represents a protein regulating signalling pathways as well as cytoskeleton structure, both essential for maintenance of epithelial integrity.

Appendix 1

Optimization of genotyping conditions

Screening for zebrafish mutants required the optimisation of conditions for high-throughput genotyping method based on PCR from small zebrafish fin biopsies. DNA was extracted either from zebrafish larvae or adult fins, as described in section 2.2.6.4, and subsequently used as a template for PCR. Two pairs of primers: zFR_4_fwd with zFR_9_rev and zFR_5_fwd with zFR_9_rev, amplifying a *frmpd2* gene fragment corresponding to the length of 140 bp and 165 bp respectively, were designed within the exon sequence affected by ENU mutagenesis (Figure A5.1).

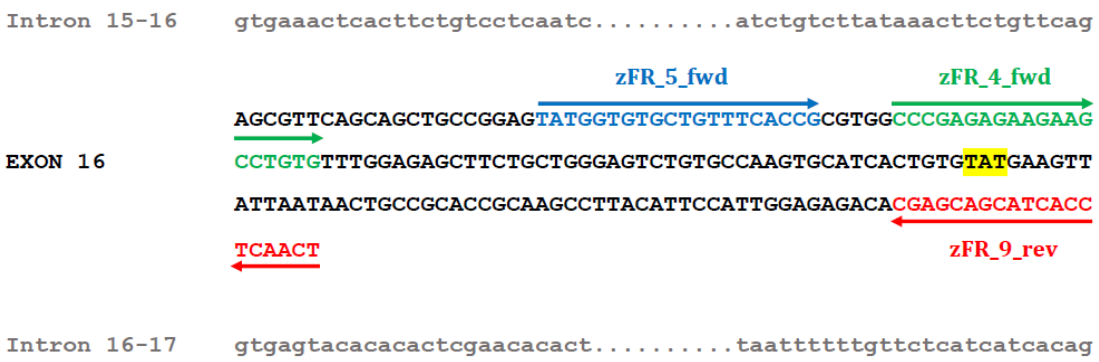

Figure A5.1 Localisation of primers within zebrafish frmpd2 gene sequence used for high-throughput PCR-based genotyping

Sequence of exon 16 of zebrafish frmpd2 gene affected by ENU mutagenesis. Affected tyrosine codon is highlighted in yellow. Represented sequence fragment helped to design primers used for high-throughput PCR-based genotyping. frmpd2 gene sequence was retrieved from Ensembl (http://www.ensembl.org/Danio_rerio/Gene/Summary?db=core;g=ENSDARG00000074119;r=12:2487909-2533727;t=ENSDART00000152567).

The first PCR run aimed to test whether genomic DNA was successfully extracted from zebrafish larvae fin (DNA_2) as well as to show that the *frmpd2* gene can be amplified from this template. To test that, PCR was performed with DNA_1 template from whole zebrafish embryos and Tubby_fwd and Tubby_rev primers amplifying *tubby bipartite transcription factor* gene, both obtained from Dr. Jarema Malicki lab and used here as a control. Amplification of the *tubby* gene as well as *frmpd2* gene using both pairs of primers was successful with both DNA_1 and DNA_2 template. Although more efficient amplification occurred when

DNA_1 was used as a template, this can be explained by the fact that DNA_1 was extracted from zebrafish embryos while DNA_2 only from fin biopsy. Moreover, it appeared that *frmpd2* gene was amplified more efficiently with zFR_4_fwd and zFR_9_rev primers (Figure A5.2).

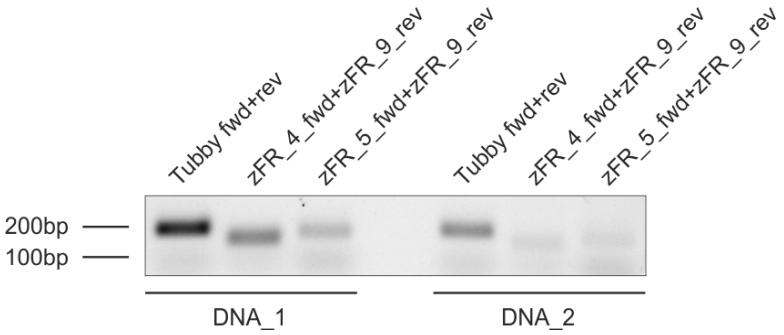

Figure A5.2 PCR test for genomic DNA extracted from zebrafish larvae fin and frmpd2 primers

PCR was run with annealing temperature 60°C. DNA_1 template and Tubby_fwd+Tubby_rev primers were used as a control. Amplified tubby gene fragment corresponds to the length of 200 bp. Amplified frmpd2 gene fragments corresponds to the predicted size of 140 bp and 165 bp when using zFR_4_fwd+zFR_9_rev and zFR_5_fwd+zFR_9_rev respectively.

Further optimisation aimed to find the best annealing temperature for the chosen *frmpd2* primers which provides the most efficient amplification. To this end, PCR with gradient annealing temperature within the range of 55 - 65°C was run using genomic DNA extracted from fin biopsy of zebrafish larvae at 96 hpf. Amplification efficiency gradually increased with the temperature decrease, reaching its peak at the lowest temperature 55°C within the tested temperature range (Figure A5.3).

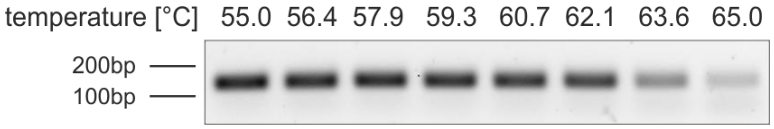

Figure A5.3 Gradient PCR for frmpd2 primers

PCR was run with gradient annealing temperature within the range 55 - 65°C. Genomic DNA extracted from zebrafish larvae at 96 hpf fin biopsy was used as a template. frmpd2 gene fragment was amplified with zFR_4_fwd+zFR_9_rev primers and corresponds to the predicted size of 140 bp.

REFERENCES

ABERLE, H., BUTZ, S., STAPPERT, J., WEISSIG, H., KEMLER, R. & HOSCHUETZKY, H. 1994. Assembly of the cadherin-catenin complex in vitro with recombinant proteins. *J Cell Sci,* 107 (Pt 12)**,** 3655-63.

ADACHI, M., HAMAZAKI, Y., KOBAYASHI, Y., ITOH, M., TSUKITA, S., FURUSE, M. & TSUKITA, S. 2009. Similar and distinct properties of MUPP1 and Patj, two homologous PDZ domain-containing tight-junction proteins. *Mol Cell Biol,* 29**,** 2372-89.

AMANO, M., NAKAYAMA, M. & KAIBUCHI, K. 2010. Rho-kinase/ROCK: A key regulator of the cytoskeleton and cell polarity. *Cytoskeleton (Hoboken),* 67**,** 545-54.

AN, N., BLUMER, J. B., BERNARD, M. L. & LANIER, S. M. 2008. The PDZ and band 4.1 containing protein Frmpd1 regulates the subcellular location of activator of G-protein signaling 3 and its interaction with G-proteins. *J Biol Chem,* 283**,** 24718-28.

ANANTHAKRISHNAN, R., GUCK, J., WOTTAWAH, F., SCHINKINGER, S., LINCOLN, B., ROMEYKE, M., MOON, T. & KAS, J. 2006. Quantifying the contribution of actin networks to the elastic strength of fibroblasts. *J Theor Biol,* 242**,** 502-16.

BALDA, M. S., WHITNEY, J. A., FLORES, C., GONZALEZ, S., CEREIJIDO, M. & MATTER, K. 1996. Functional dissociation of paracellular permeability and transepithelial electrical resistance and disruption of the apical-basolateral intramembrane diffusion barrier by expression of a mutant tight junction membrane protein. *J Cell Biol,* 134**,** 1031-49.

BALKOVETZ, D. F. 2009. Tight junction claudins and the kidney in sickness and in health. *Biochim Biophys Acta,* 1788**,** 858-63.

BARNICH, N., AGUIRRE, J. E., REINECKER, H. C., XAVIER, R. & PODOLSKY, D. K. 2005. Membrane recruitment of NOD2 in intestinal epithelial cells is essential for nuclear factor-{kappa}B activation in muramyl dipeptide recognition. *J Cell Biol,* 170**,** 21-6.

BERGGARD, T., LINSE, S. & JAMES, P. 2007. Methods for the detection and analysis of protein-protein interactions. *Proteomics,* 7**,** 2833-42.

BERREBI, D., MAUDINAS, R., HUGOT, J. P., CHAMAILLARD, M., CHAREYRE, F., DE LAGAUSIE, P., YANG, C., DESREUMAUX, P., GIOVANNINI, M., CEZARD, J. P., ZOUALI, H., EMILIE, D. & PEUCHMAUR, M. 2003. Card15 gene overexpression in mononuclear and epithelial cells of the inflamed Crohn's disease colon. *Gut,* 52**,** 840-6.

BILDER, D. 2003. PDZ domain polarity complexes. *Curr Biol,* 13**,** R661-2.

BOHL, J., BRIMER, N., LYONS, C. & VANDE POL, S. B. 2007. The stardust family protein MPP7 forms a tripartite complex with LIN7 and DLG1 that regulates the stability and localization of DLG1 to cell junctions. *J Biol Chem,* 282**,** 9392-400.

BONEN, D. K., OGURA, Y., NICOLAE, D. L., INOHARA, N., SAAB, L., TANABE, T., CHEN, F. F., FOSTER, S. J., DUERR, R. H., BRANT, S. R., CHO, J. H. & NUNEZ, G. 2003. Crohn's disease-associated NOD2 variants share a signaling defect in response to lipopolysaccharide and peptidoglycan. *Gastroenterology,* 124**,** 140-6.

BOSANQUET, D. C., YE, L., HARDING, K. G. & JIANG, W. G. 2014. FERM family proteins and their importance in cellular movements and wound healing (review). *Int J Mol Med,* 34**,** 3-12.

BOWEN, J. R., HWANG, D., BAI, X., ROY, D. & SPILIOTIS, E. T. 2011. Septin GTPases spatially guide microtubule organization and plus end dynamics in polarizing epithelia. *J Cell Biol,* 194**,** 187-97.

BRENMAN, J. E., CHAO, D. S., GEE, S. H., MCGEE, A. W., CRAVEN, S. E., SANTILLANO, D. R., WU, Z., HUANG, F., XIA, H., PETERS, M. F., FROEHNER, S. C. & BREDT, D. S. 1996. Interaction of nitric oxide synthase with the postsynaptic density protein PSD-95 and alpha1-syntrophin mediated by PDZ domains. *Cell,* 84**,** 757-67.

BROUSSARD, J. A., WEBB, D. J. & KAVERINA, I. 2008. Asymmetric focal adhesion disassembly in motile cells. *Curr Opin Cell Biol,* 20**,** 85-90.

BRUCKNER, A., POLGE, C., LENTZE, N., AUERBACH, D. & SCHLATTNER, U. 2009. Yeast two-hybrid, a powerful tool for systems biology. *Int J Mol Sci,* 10**,** 2763-88.

BRYANT, D. M. & MOSTOV, K. E. 2008. From cells to organs: building polarized tissue. *Nat Rev Mol Cell Biol,* 9**,** 887-901.

BUCKLEY, C. D., TAN, J., ANDERSON, K. L., HANEIN, D., VOLKMANN, N., WEIS, W. I., NELSON, W. J. & DUNN, A. R. 2014. Cell adhesion. The minimal cadherin-catenin complex binds to actin filaments under force. *Science,* 346**,** 1254211.

BURRIDGE, K. & CHRZANOWSKA-WODNICKA, M. 1996. Focal adhesions, contractility, and signaling. *Annu Rev Cell Dev Biol,* 12**,** 463-518.

CALAUTTI, E., GROSSI, M., MAMMUCARI, C., AOYAMA, Y., PIRRO, M., ONO, Y., LI, J. & DOTTO, G. P. 2002. Fyn tyrosine kinase is a downstream mediator of Rho/PRK2 function in keratinocyte cell-cell adhesion. *J Cell Biol,* 156**,** 137-48.

CANTIELLO, H. F. 1996. Role of the actin cytoskeleton in the regulation of the cystic fibrosis transmembrane conductance regulator. *Exp Physiol,* 81**,** 505-14.

CASANOVA, J. E. 2002. Epithelial cell cytoskeleton and intracellular trafficking V. Confluence of membrane trafficking and motility in epithelial cell models. *Am J Physiol Gastrointest Liver Physiol,* 283**,** G1015-9.

CASTANON, M. J., WALKO, G., WINTER, L. & WICHE, G. 2013. Plectin-intermediate filament partnership in skin, skeletal muscle, and peripheral nerve. *Histochem Cell Biol,* 140**,** 33-53.

CASWELL, P. & NORMAN, J. 2008. Endocytic transport of integrins during cell migration and invasion. *Trends Cell Biol,* 18**,** 257-63.

CASWELL, P. T. & NORMAN, J. C. 2006. Integrin trafficking and the control of cell migration. *Traffic,* 7**,** 14-21.

CHAN, C. J., EKPENYONG, A. E., GOLFIER, S., LI, W., CHALUT, K. J., OTTO, O., ELGETI, J., GUCK, J. & LAUTENSCHLAGER, F. 2015. Myosin II Activity Softens Cells in Suspension. *Biophys J,* 108**,** 1856-69.

CHEN, V. C., LI, X., PERREAULT, H. & NAGY, J. I. 2006. Interaction of zonula occludens-1 (ZO-1) with alpha-actinin-4: application of functional proteomics for identification of PDZ domain-associated proteins. *J Proteome Res,* 5**,** 2123-34.

CHEN, X. & MACARA, I. G. 2005. Par-3 controls tight junction assembly through the Rac exchange factor Tiam1. *Nat Cell Biol,* 7**,** 262-9.

CHEN, X., WINTERS, C., AZZAM, R., LI, X., GALBRAITH, J. A., LEAPMAN, R. D. & REESE, T. S. 2008. Organization of the core structure of the postsynaptic density. *Proc Natl Acad Sci U S A,* 105**,** 4453-8.

CHISHTI, A. H., KIM, A. C., MARFATIA, S. M., LUTCHMAN, M., HANSPAL, M., JINDAL, H., LIU, S. C., LOW, P. S., ROULEAU, G. A., MOHANDAS, N., CHASIS, J. A., CONBOY, J. G., GASCARD, P., TAKAKUWA, Y., HUANG, S. C., BENZ, E. J., JR., BRETSCHER, A., FEHON, R. G., GUSELLA, J. F., RAMESH, V., SOLOMON, F., MARCHESI, V. T., TSUKITA, S., TSUKITA, S., HOOVER, K. B. & ET AL. 1998. The FERM domain: a unique module involved in the linkage of cytoplasmic proteins to the membrane. *Trends Biochem Sci,* 23**,** 281-2.

CHOI, Y. & CHAN, A. P. 2015. PROVEAN web server: a tool to predict the functional effect of amino acid substitutions and indels. *Bioinformatics,* 31**,** 2745-7.

CHOI, Y., SIMS, G. E., MURPHY, S., MILLER, J. R. & CHAN, A. P. 2012. Predicting the functional effect of amino acid substitutions and indels. *PLoS One,* 7**,** e46688.

CHOU, J., BURKE, N. A., IWABU, A., WATKINS, S. C. & WELLS, A. 2003. Directional motility induced by epidermal growth factor requires Cdc42. *Exp Cell Res,* 287**,** 47-56.

COMARTIN, D., GUPTA, G. D., FUSSNER, E., COYAUD, E., HASEGAN, M., ARCHINTI, M., CHEUNG, S. W., PINCHEV, D., LAWO, S., RAUGHT, B., BAZETT-JONES, D. P., LUDERS, J. & PELLETIER, L. 2013. CEP120 and SPICE1 cooperate with CPAP in centriole elongation. *Curr Biol,* 23**,** 1360-6.

CONSONNI, S. V., BROUWER, P. M., VAN SLOBBE, E. S. & BOS, J. L. 2014. The PDZ domain of the guanine nucleotide exchange factor PDZGEF directs binding to phosphatidic acid during brush border formation. *PLoS One,* 9**,** e98253.

COUZENS, A. L., KNIGHT, J. D., KEAN, M. J., TEO, G., WEISS, A., DUNHAM, W. H., LIN, Z. Y., BAGSHAW, R. D., SICHERI, F., PAWSON, T., WRANA, J. L., CHOI, H. & GINGRAS, A. C. 2013. Protein interaction network of the mammalian Hippo pathway reveals mechanisms of kinase-phosphatase interactions. *Sci Signal,* 6**,** rs15.

CULBERTSON, M. R. & LEEDS, P. F. 2003. Looking at mRNA decay pathways through the window of molecular evolution. *Curr Opin Genet Dev,* 13**,** 207-14.

DANNO, S., KUBOUCHI, K., MEHRUBA, M., ABE, M., NATSUME, R., SAKIMURA, K., EGUCHI, S., OKA, M., HIRASHIMA, M., YASUDA, H. & MUKAI, H. 2017. PKN2 is essential for mouse embryonic development and proliferation of mouse fibroblasts. *Genes Cells,* 22**,** 220-236.

DE BRUIJN, E., CUPPEN, E. & FEITSMA, H. 2009. Highly Efficient ENU Mutagenesis in Zebrafish. *Methods Mol Biol,* 546**,** 3-12.

DE ROOIJ, J., BOENINK, N. M., VAN TRIEST, M., COOL, R. H., WITTINGHOFER, A. & BOS, J. L. 1999. PDZ-GEF1, a guanine nucleotide exchange factor specific for Rap1 and Rap2. *J Biol Chem,* 274**,** 38125-30.

DEN HOLLANDER, A. I., TEN BRINK, J. B., DE KOK, Y. J., VAN SOEST, S., VAN DEN BORN, L. I., VAN DRIEL, M. A., VAN DE POL, D. J., PAYNE, A. M., BHATTACHARYA, S. S., KELLNER, U., HOYNG, C. B., WESTERVELD, A., BRUNNER, H. G., BLEEKER-WAGEMAKERS, E. M., DEUTMAN, A. F., HECKENLIVELY, J. R., CREMERS, F. P. & BERGEN, A. A. 1999. Mutations in a human homologue of Drosophila crumbs cause retinitis pigmentosa (RP12). *Nat Genet,* 23**,** 217-21.

DETTORI, R., SONZOGNI, S., MEYER, L., LOPEZ-GARCIA, L. A., MORRICE, N. A., ZEUZEM, S., ENGEL, M., PIIPER, A., NEIMANIS, S., FRODIN, M. & BIONDI, R. M. 2009. Regulation of the interaction between protein kinase C-related protein kinase 2 (PRK2) and its upstream kinase, 3-phosphoinositide-dependent protein kinase 1 (PDK1). *J Biol Chem,* 284**,** 30318-27.

DI BLASIO, L., GAGLIARDI, P. A., PULIAFITO, A., SESSA, R., SEANO, G., BUSSOLINO, F. & PRIMO, L. 2015. PDK1 regulates focal adhesion disassembly by modulating endocytosis of alphavbeta3 integrin. *J Cell Sci,* 128**,** 863-77.

DOW, L. E., BRUMBY, A. M., MURATORE, R., COOMBE, M. L., SEDELIES, K. A., TRAPANI, J. A., RUSSELL, S. M., RICHARDSON, H. E. & HUMBERT, P. O. 2003. hScrib is a functional homologue of the Drosophila tumour suppressor Scribble. *Oncogene,* 22**,** 9225-30.

DOW, L. E., KAUFFMAN, J. S., CADDY, J., ZARBALIS, K., PETERSON, A. S., JANE, S. M., RUSSELL, S. M. & HUMBERT, P. O. 2007. The tumour-suppressor Scribble dictates cell polarity during directed epithelial migration: regulation of Rho GTPase recruitment to the leading edge. *Oncogene,* 26**,** 2272-82.

DOYLE, D. A., LEE, A., LEWIS, J., KIM, E., SHENG, M. & MACKINNON, R. 1996. Crystal structures of a complexed and peptide-free membrane protein-binding domain: molecular basis of peptide recognition by PDZ. *Cell,* 85**,** 1067-76.

DU ROURE, O., SAEZ, A., BUGUIN, A., AUSTIN, R. H., CHAVRIER, P., SILBERZAN, P. & LADOUX, B. 2005. Force mapping in epithelial cell migration. *Proc Natl Acad Sci U S A,* 102**,** 2390-5.

EBNET, K., AURRAND-LIONS, M., KUHN, A., KIEFER, F., BUTZ, S., ZANDER, K., MEYER ZU BRICKWEDDE, M. K., SUZUKI, A., IMHOF, B. A. & VESTWEBER, D. 2003. The junctional adhesion molecule (JAM) family members JAM-2 and JAM-3 associate with the cell polarity protein PAR-3: a possible role for JAMs in endothelial cell polarity. *J Cell Sci,* 116**,** 3879-91.

EBNET, K., SCHULZ, C. U., MEYER ZU BRICKWEDDE, M. K., PENDL, G. G. & VESTWEBER, D. 2000. Junctional adhesion molecule interacts with the PDZ domain-containing proteins AF-6 and ZO-1. *J Biol Chem,* 275**,** 27979-88.

EBNET, K., SUZUKI, A., HORIKOSHI, Y., HIROSE, T., MEYER ZU BRICKWEDDE, M. K., OHNO, S. & VESTWEBER, D. 2001. The cell polarity protein ASIP/PAR-3 directly associates with junctional adhesion molecule (JAM). *EMBO J,* 20**,** 3738-48.

ELIAS, G. M. & NICOLL, R. A. 2007. Synaptic trafficking of glutamate receptors by MAGUK scaffolding proteins. *Trends Cell Biol,* 17**,** 343-52.

ELSON, E. L. 1988. Cellular mechanics as an indicator of cytoskeletal structure and function. *Annu Rev Biophys Biophys Chem,* 17**,** 397-430.

ETIENNE-MANNEVILLE, S. & HALL, A. 2001. Integrin-mediated activation of Cdc42 controls cell polarity in migrating astrocytes through PKCzeta. *Cell,* 106**,** 489-98.

ETIENNE-MANNEVILLE, S. & HALL, A. 2003. Cdc42 regulates GSK-3beta and adenomatous polyposis coli to control cell polarity. *Nature,* 421**,** 753-6.

ETIENNE-MANNEVILLE, S., MANNEVILLE, J. B., NICHOLLS, S., FERENCZI, M. A. & HALL, A. 2005. Cdc42 and Par6-PKCzeta regulate the spatially localized association of Dlg1 and APC to control cell polarization. *J Cell Biol,* 170**,** 895-901.

FAGERBERG, L., HALLSTROM, B. M., OKSVOLD, P., KAMPF, C., DJUREINOVIC, D., ODEBERG, J., HABUKA, M., TAHMASEBPOOR, S., DANIELSSON, A., EDLUND, K., ASPLUND, A., SJOSTEDT, E., LUNDBERG, E., SZIGYARTO, C. A., SKOGS, M., TAKANEN, J. O., BERLING, H., TEGEL, H., MULDER, J., NILSSON, P., SCHWENK, J. M., LINDSKOG, C., DANIELSSON, F., MARDINOGLU, A., SIVERTSSON, A., VON FEILITZEN, K., FORSBERG, M., ZWAHLEN, M., OLSSON, I., NAVANI, S., HUSS, M., NIELSEN, J., PONTEN, F. & UHLEN, M. 2014. Analysis of the human tissue-specific expression by genome-wide integration of transcriptomics and antibody-based proteomics. *Mol Cell Proteomics,* 13**,** 397-406.

FAN, S., FOGG, V., WANG, Q., CHEN, X. W., LIU, C. J. & MARGOLIS, B. 2007. A novel Crumbs3 isoform regulates cell division and ciliogenesis via importin beta interactions. *J Cell Biol,* 178**,** 387-98.

FANNING, A. S. & ANDERSON, J. M. 1996. Protein-protein interactions: PDZ domain networks. *Curr Biol,* 6**,** 1385-8.

FANNING, A. S., JAMESON, B. J., JESAITIS, L. A. & ANDERSON, J. M. 1998. The tight junction protein ZO-1 establishes a link between the transmembrane protein occludin and the actin cytoskeleton. *J Biol Chem,* 273**,** 29745-53.

FAURE, S., SALAZAR-FONTANA, L. I., SEMICHON, M., TYBULEWICZ, V. L., BISMUTH, G., TRAUTMANN, A., GERMAIN, R. N. & DELON, J. 2004. ERM proteins regulate cytoskeleton relaxation promoting T cell-APC conjugation. *Nat Immunol,* 5**,** 272-9.

FEHON, R. G., MCCLATCHEY, A. I. & BRETSCHER, A. 2010. Organizing the cell cortex: the role of ERM proteins. *Nat Rev Mol Cell Biol,* 11**,** 276-87.

FENG, W., WU, H., CHAN, L. N. & ZHANG, M. 2008. Par-3-mediated junctional localization of the lipid phosphatase PTEN is required for cell polarity establishment. *J Biol Chem,* 283**,** 23440-9.

FENG, W. & ZHANG, M. 2009. Organization and dynamics of PDZ-domain-related supramodules in the postsynaptic density. *Nat Rev Neurosci,* 10**,** 87-99.

FOGG, V. C., LIU, C. J. & MARGOLIS, B. 2005. Multiple regions of Crumbs3 are required for tight junction formation in MCF10A cells. *J Cell Sci,* 118**,** 2859-69.

FRAME, M. C., PATEL, H., SERRELS, B., LIETHA, D. & ECK, M. J. 2010. The FERM domain: organizing the structure and function of FAK. *Nat Rev Mol Cell Biol,* 11**,** 802-14.

FREDRIKSSON, K., VAN ITALLIE, C. M., APONTE, A., GUCEK, M., TIETGENS, A. J. & ANDERSON, J. M. 2015. Proteomic analysis of proteins surrounding occludin and claudin-4 reveals their proximity to signaling and trafficking networks. *PLoS One,* 10**,** e0117074.

FUJITA, Y., SHIRATAKI, H., SAKISAKA, T., ASAKURA, T., OHYA, T., KOTANI, H., YOKOYAMA, S., NISHIOKA, H., MATSUURA, Y., MIZOGUCHI, A., SCHELLER, R. H. & TAKAI, Y. 1998. Tomosyn: a syntaxin-1-binding protein that forms a novel complex in the neurotransmitter release process. *Neuron,* 20**,** 905-15.

GAVIN, A. C., ALOY, P., GRANDI, P., KRAUSE, R., BOESCHE, M., MARZIOCH, M., RAU, C., JENSEN, L. J., BASTUCK, S., DUMPELFELD, B., EDELMANN, A., HEURTIER, M. A., HOFFMAN, V., HOEFERT, C., KLEIN, K., HUDAK, M., MICHON, A. M., SCHELDER, M., SCHIRLE, M., REMOR, M., RUDI, T., HOOPER, S., BAUER, A., BOUWMEESTER, T., CASARI, G., DREWES, G., NEUBAUER, G., RICK, J. M., KUSTER, B., BORK, P., RUSSELL, R. B. & SUPERTI-FURGA, G. 2006. Proteome survey reveals modularity of the yeast cell machinery. *Nature,* 440**,** 631-6.

GAVIN, A. C., BOSCHE, M., KRAUSE, R., GRANDI, P., MARZIOCH, M., BAUER, A., SCHULTZ, J., RICK, J. M., MICHON, A. M., CRUCIAT, C. M., REMOR, M., HOFERT, C., SCHELDER, M., BRAJENOVIC, M., RUFFNER, H., MERINO, A., KLEIN, K., HUDAK, M., DICKSON, D., RUDI, T., GNAU, V., BAUCH, A., BASTUCK, S., HUHSE, B., LEUTWEIN, C., HEURTIER, M. A., COPLEY, R. R., EDELMANN, A., QUERFURTH, E., RYBIN, V., DREWES, G., RAIDA, M., BOUWMEESTER, T., BORK, P., SERAPHIN, B., KUSTER, B., NEUBAUER, G. & SUPERTI-FURGA, G. 2002. Functional organization of the yeast proteome by systematic analysis of protein complexes. *Nature,* 415**,** 141-7.

GEE, S. H., QUENNEVILLE, S., LOMBARDO, C. R. & CHABOT, J. 2000. Single-amino acid substitutions alter the specificity and affinity of PDZ domains for their ligands. *Biochemistry,* 39**,** 14638-46.

GOMES, E. R., JANI, S. & GUNDERSEN, G. G. 2005. Nuclear movement regulated by Cdc42, MRCK, myosin, and actin flow establishes MTOC polarization in migrating cells. *Cell,* 121**,** 451-63.

GRANDE-GARCIA, A., ECHARRI, A., DE ROOIJ, J., ALDERSON, N. B., WATERMAN-STORER, C. M., VALDIVIELSO, J. M. & DEL POZO, M. A. 2007. Caveolin-1 regulates cell polarization and directional migration through Src kinase and Rho GTPases. *J Cell Biol,* 177**,** 683-94.

GROSS, C., HEUMANN, R. & ERDMANN, K. S. 2001. The protein kinase C-related kinase PRK2 interacts with the protein tyrosine phosphatase PTP-BL via a novel PDZ domain binding motif. *FEBS Lett,* 496**,** 101-4.

GUCK, J., ANANTHAKRISHNAN, R., MAHMOOD, H., MOON, T. J., CUNNINGHAM, C. C. & KAS, J. 2001. The optical stretcher: a novel laser tool to micromanipulate cells. *Biophys J,* 81**,** 767-84.

GUCK, J., LAUTENSCHLAGER, F., PASCHKE, S. & BEIL, M. 2010. Critical review: cellular mechanobiology and amoeboid migration. *Integr Biol (Camb),* 2**,** 575-83.

GUCK, J., SCHINKINGER, S., LINCOLN, B., WOTTAWAH, F., EBERT, S., ROMEYKE, M., LENZ, D., ERICKSON, H. M., ANANTHAKRISHNAN, R., MITCHELL, D., KAS, J., ULVICK, S. & BILBY, C. 2005. Optical deformability as an inherent

cell marker for testing malignant transformation and metastatic competence. *Biophys J,* 88**,** 3689-98.

GUPTON, S. L. & WATERMAN-STORER, C. M. 2006. Spatiotemporal feedback between actomyosin and focal-adhesion systems optimizes rapid cell migration. *Cell,* 125**,** 1361-74.

GUTIERREZ, O., PIPAON, C., INOHARA, N., FONTALBA, A., OGURA, Y., PROSPER, F., NUNEZ, G. & FERNANDEZ-LUNA, J. L. 2002. Induction of Nod2 in myelomonocytic and intestinal epithelial cells via nuclear factor-kappa B activation. *J Biol Chem,* 277**,** 41701-5.

HALL, R. A., PREMONT, R. T., CHOW, C. W., BLITZER, J. T., PITCHER, J. A., CLAING, A., STOFFEL, R. H., BARAK, L. S., SHENOLIKAR, S., WEINMAN, E. J., GRINSTEIN, S. & LEFKOWITZ, R. J. 1998. The beta2-adrenergic receptor interacts with the Na+/H+-exchanger regulatory factor to control Na+/H+ exchange. *Nature,* 392**,** 626-30.

HANNA, S. & EL-SIBAI, M. 2013. Signaling networks of Rho GTPases in cell motility. *Cell Signal,* 25**,** 1955-61.

HARRIS, B. Z. & LIM, W. A. 2001. Mechanism and role of PDZ domains in signaling complex assembly. *J Cell Sci,* 114**,** 3219-31.

HILDEBRANDT, F., ATTANASIO, M. & OTTO, E. 2009. Nephronophthisis: disease mechanisms of a ciliopathy. *J Am Soc Nephrol,* 20**,** 23-35.

HISAMATSU, T., SUZUKI, M., REINECKER, H. C., NADEAU, W. J., MCCORMICK, B. A. & PODOLSKY, D. K. 2003. CARD15/NOD2 functions as an antibacterial factor in human intestinal epithelial cells. *Gastroenterology,* 124**,** 993-1000.

HONG, Y., STRONACH, B., PERRIMON, N., JAN, L. Y. & JAN, Y. N. 2001. Drosophila Stardust interacts with Crumbs to control polarity of epithelia but not neuroblasts. *Nature,* 414**,** 634-8.

HORIKOSHI, Y., SUZUKI, A., YAMANAKA, T., SASAKI, K., MIZUNO, K., SAWADA, H., YONEMURA, S. & OHNO, S. 2009. Interaction between PAR-3 and the aPKC-PAR-6 complex is indispensable for apical domain development of epithelial cells. *J Cell Sci,* 122**,** 1595-606.

HOWE, K., CLARK, M. D., TORROJA, C. F., TORRANCE, J., BERTHELOT, C., MUFFATO, M., COLLINS, J. E., HUMPHRAY, S., MCLAREN, K., MATTHEWS, L., MCLAREN, S., SEALY, I., CACCAMO, M., CHURCHER, C., SCOTT, C., BARRETT, J. C., KOCH, R., RAUCH, G. J., WHITE, S., CHOW, W., KILIAN, B., QUINTAIS, L. T., GUERRA-ASSUNCAO, J. A., ZHOU, Y., GU, Y., YEN, J., VOGEL, J. H., EYRE, T., REDMOND, S., BANERJEE, R., CHI, J., FU, B., LANGLEY, E., MAGUIRE, S. F., LAIRD, G. K., LLOYD, D., KENYON, E., DONALDSON, S., SEHRA, H., ALMEIDA-KING, J., LOVELAND, J., TREVANION, S., JONES, M., QUAIL, M., WILLEY, D., HUNT, A., BURTON, J., SIMS, S., MCLAY, K., PLUMB, B., DAVIS, J., CLEE, C., OLIVER, K., CLARK, R., RIDDLE, C., ELLIOT, D., THREADGOLD, G., HARDEN, G., WARE, D., BEGUM, S., MORTIMORE, B., KERRY, G., HEATH, P., PHILLIMORE, B., TRACEY, A., CORBY, N., DUNN, M., JOHNSON, C., WOOD, J., CLARK, S., PELAN, S., GRIFFITHS, G., SMITH, M., GLITHERO, R., HOWDEN, P., BARKER, N., LLOYD, C., STEVENS, C., HARLEY, J., HOLT, K., PANAGIOTIDIS, G., LOVELL, J., BEASLEY, H., HENDERSON, C., GORDON, D., AUGER, K., WRIGHT, D., COLLINS, J., RAISEN, C., DYER, L., LEUNG, K., ROBERTSON, L., AMBRIDGE, K., LEONGAMORNLERT, D., MCGUIRE, S., GILDERTHORP,

R., GRIFFITHS, C., MANTHRAVADI, D., NICHOL, S., BARKER, G., et al. 2013. The zebrafish reference genome sequence and its relationship to the human genome. *Nature,* 496**,** 498-503.

HU, J. H., YANG, L., KAMMERMEIER, P. J., MOORE, C. G., BRAKEMAN, P. R., TU, J., YU, S., PETRALIA, R. S., LI, Z., ZHANG, P. W., PARK, J. M., DONG, X., XIAO, B. & WORLEY, P. F. 2012. Preso1 dynamically regulates group I metabotropic glutamate receptors. *Nat Neurosci,* 15**,** 836-44.

HUGOT, J. P., CHAMAILLARD, M., ZOUALI, H., LESAGE, S., CEZARD, J. P., BELAICHE, J., ALMER, S., TYSK, C., O'MORAIN, C. A., GASSULL, M., BINDER, V., FINKEL, Y., CORTOT, A., MODIGLIANI, R., LAURENT-PUIG, P., GOWER-ROUSSEAU, C., MACRY, J., COLOMBEL, J. F., SAHBATOU, M. & THOMAS, G. 2001. Association of NOD2 leucine-rich repeat variants with susceptibility to Crohn's disease. *Nature,* 411**,** 599-603.

HUNG, A. Y. & SHENG, M. 2002. PDZ domains: structural modules for protein complex assembly. *J Biol Chem,* 277**,** 5699-702.

HURD, T. W., FAN, S., LIU, C. J., KWEON, H. K., HAKANSSON, K. & MARGOLIS, B. 2003a. Phosphorylation-dependent binding of 14-3-3 to the polarity protein Par3 regulates cell polarity in mammalian epithelia. *Curr Biol,* 13**,** 2082-90.

HURD, T. W., GAO, L., ROH, M. H., MACARA, I. G. & MARGOLIS, B. 2003b. Direct interaction of two polarity complexes implicated in epithelial tight junction assembly. *Nat Cell Biol,* 5**,** 137-42.

HUTCHINSON, C. L., LOWE, P. N., MCLAUGHLIN, S. H., MOTT, H. R. & OWEN, D. 2013. Differential binding of RhoA, RhoB, and RhoC to protein kinase C-related kinase (PRK) isoforms PRK1, PRK2, and PRK3: PRKs have the highest affinity for RhoB. *Biochemistry,* 52**,** 7999-8011.

HUTTLIN, E. L., TING, L., BRUCKNER, R. J., GEBREAB, F., GYGI, M. P., SZPYT, J., TAM, S., ZARRAGA, G., COLBY, G., BALTIER, K., DONG, R., GUARANI, V., VAITES, L. P., ORDUREAU, A., RAD, R., ERICKSON, B. K., WUHR, M., CHICK, J., ZHAI, B., KOLIPPAKKAM, D., MINTSERIS, J., OBAR, R. A., HARRIS, T., ARTAVANIS-TSAKONAS, S., SOWA, M. E., DE CAMILLI, P., PAULO, J. A., HARPER, J. W. & GYGI, S. P. 2015. The BioPlex Network: A Systematic Exploration of the Human Interactome. *Cell,* 162**,** 425-40.

IGUCHI, Y., ISHIHARA, S., UCHIDA, Y., TAJIMA, K., MIZUTANI, T., KAWABATA, K. & HAGA, H. 2015. Filamin B Enhances the Invasiveness of Cancer Cells into 3D Collagen Matrices. *Cell Struct Funct,* 40**,** 61-7.

IKENOUCHI, J., UMEDA, K., TSUKITA, S., FURUSE, M. & TSUKITA, S. 2007. Requirement of ZO-1 for the formation of belt-like adherens junctions during epithelial cell polarization. *J Cell Biol,* 176**,** 779-86.

ISMAILOV, II, BERDIEV, B. K., SHLYONSKY, V. G., FULLER, C. M., PRAT, A. G., JOVOV, B., CANTIELLO, H. F., AUSIELLO, D. A. & BENOS, D. J. 1997. Role of actin in regulation of epithelial sodium channels by CFTR. *Am J Physiol,* 272**,** C1077-86.

ITOH, M., FURUSE, M., MORITA, K., KUBOTA, K., SAITOU, M. & TSUKITA, S. 1999. Direct binding of three tight junction-associated MAGUKs, ZO-1, ZO-2, and ZO-3, with the COOH termini of claudins. *J Cell Biol,* 147**,** 1351-63.

ITOH, M., SASAKI, H., FURUSE, M., OZAKI, H., KITA, T. & TSUKITA, S. 2001. Junctional adhesion molecule (JAM) binds to PAR-3: a possible

mechanism for the recruitment of PAR-3 to tight junctions. *J Cell Biol,* 154**,** 491-7.

IVANOV, A. I., PARKOS, C. A. & NUSRAT, A. 2010a. Cytoskeletal regulation of epithelial barrier function during inflammation. *Am J Pathol,* 177**,** 512-24.

IVANOV, A. I., YOUNG, C., DEN BESTE, K., CAPALDO, C. T., HUMBERT, P. O., BRENNWALD, P., PARKOS, C. A. & NUSRAT, A. 2010b. Tumor suppressor scribble regulates assembly of tight junctions in the intestinal epithelium. *Am J Pathol,* 176**,** 134-45.

IZUMI, Y., HIROSE, T., TAMAI, Y., HIRAI, S., NAGASHIMA, Y., FUJIMOTO, T., TABUSE, Y., KEMPHUES, K. J. & OHNO, S. 1998. An atypical PKC directly associates and colocalizes at the epithelial tight junction with ASIP, a mammalian homologue of Caenorhabditis elegans polarity protein PAR-3. *J Cell Biol,* 143**,** 95-106.

JOBERTY, G., PETERSEN, C., GAO, L. & MACARA, I. G. 2000. The cell-polarity protein Par6 links Par3 and atypical protein kinase C to Cdc42. *Nat Cell Biol,* 2**,** 531-9.

KACHEL, N., ERDMANN, K. S., KREMER, W., WOLFF, P., GRONWALD, W., HEUMANN, R. & KALBITZER, H. R. 2003. Structure determination and ligand interactions of the PDZ2b domain of PTP-Bas (hPTP1E): splicing-induced modulation of ligand specificity. *J Mol Biol,* 334**,** 143-55.

KAECH, S. M., WHITFIELD, C. W. & KIM, S. K. 1998. The LIN-2/LIN-7/LIN-10 complex mediates basolateral membrane localization of the C. elegans EGF receptor LET-23 in vulval epithelial cells. *Cell,* 94**,** 761-71.

KALLURI, R. & NEILSON, E. G. 2003. Epithelial-mesenchymal transition and its implications for fibrosis. *J Clin Invest,* 112**,** 1776-84.

KATOH, K., KANO, Y., AMANO, M., ONISHI, H., KAIBUCHI, K. & FUJIWARA, K. 2001. Rho-kinase--mediated contraction of isolated stress fibers. *J Cell Biol,* 153**,** 569-84.

KAWAJIRI, A., ITOH, N., FUKATA, M., NAKAGAWA, M., YAMAGA, M., IWAMATSU, A. & KAIBUCHI, K. 2000. Identification of a novel beta-catenin-interacting protein. *Biochem Biophys Res Commun,* 273**,** 712-7.

KEMPHUES, K. 2000. PARsing embryonic polarity. *Cell,* 101**,** 345-8.

KENNEDY, M. B. 1995. Origin of PDZ (DHR, GLGF) domains. *Trends Biochem Sci,* 20**,** 350.

KENNEDY, M. B. 2000. Signal-processing machines at the postsynaptic density. *Science,* 290**,** 750-4.

KIM, D. I., BIRENDRA, K. C., ZHU, W., MOTAMEDCHABOKI, K., DOYE, V. & ROUX, K. J. 2014. Probing nuclear pore complex architecture with proximity-dependent biotinylation. *Proc Natl Acad Sci U S A,* 111**,** E2453-61.

KIM, E. & SHENG, M. 2004. PDZ domain proteins of synapses. *Nat Rev Neurosci,* 5**,** 771-81.

KIM, T. Y., SIESSER, P. F., ROSSMAN, K. L., GOLDFARB, D., MACKINNON, K., YAN, F., YI, X., MACCOSS, M. J., MOON, R. T., DER, C. J. & MAJOR, M. B. 2015. Substrate trapping proteomics reveals targets of the betaTrCP2/FBXW11 ubiquitin ligase. *Mol Cell Biol,* 35**,** 167-81.

KIMMEL, C. B., BALLARD, W. W., KIMMEL, S. R., ULLMANN, B. & SCHILLING, T. F. 1995. Stages of embryonic development of the zebrafish. *Dev Dyn,* 203**,** 253-310.

KOHJIMA, M., NODA, Y., TAKEYA, R., SAITO, N., TAKEUCHI, K. & SUMIMOTO, H. 2002. PAR3beta, a novel homologue of the cell polarity protein PAR3, localizes to tight junctions. *Biochem Biophys Res Commun,* 299**,** 641-6.

KOOISTRA, M. R., DUBE, N. & BOS, J. L. 2007. Rap1: a key regulator in cell-cell junction formation. *J Cell Sci,* 120**,** 17-22.

KORNAU, H. C., SCHENKER, L. T., KENNEDY, M. B. & SEEBURG, P. H. 1995. Domain interaction between NMDA receptor subunits and the postsynaptic density protein PSD-95. *Science,* 269**,** 1737-40.

KRAUSE, M., DENT, E. W., BEAR, J. E., LOUREIRO, J. J. & GERTLER, F. B. 2003. Ena/VASP proteins: regulators of the actin cytoskeleton and cell migration. *Annu Rev Cell Dev Biol,* 19**,** 541-64.

KREMER, B. E., HAYSTEAD, T. & MACARA, I. G. 2005. Mammalian septins regulate microtubule stability through interaction with the microtubule-binding protein MAP4. *Mol Biol Cell,* 16**,** 4648-59.

KROGAN, N. J., CAGNEY, G., YU, H., ZHONG, G., GUO, X., IGNATCHENKO, A., LI, J., PU, S., DATTA, N., TIKUISIS, A. P., PUNNA, T., PEREGRIN-ALVAREZ, J. M., SHALES, M., ZHANG, X., DAVEY, M., ROBINSON, M. D., PACCANARO, A., BRAY, J. E., SHEUNG, A., BEATTIE, B., RICHARDS, D. P., CANADIEN, V., LALEV, A., MENA, F., WONG, P., STAROSTINE, A., CANETE, M. M., VLASBLOM, J., WU, S., ORSI, C., COLLINS, S. R., CHANDRAN, S., HAW, R., RILSTONE, J. J., GANDI, K., THOMPSON, N. J., MUSSO, G., ST ONGE, P., GHANNY, S., LAM, M. H., BUTLAND, G., ALTAF-UL, A. M., KANAYA, S., SHILATIFARD, A., O'SHEA, E., WEISSMAN, J. S., INGLES, C. J., HUGHES, T. R., PARKINSON, J., GERSTEIN, M., WODAK, S. J., EMILI, A. & GREENBLATT, J. F. 2006. Global landscape of protein complexes in the yeast Saccharomyces cerevisiae. *Nature,* 440**,** 637-43.

LACHMANN, S., JEVONS, A., DE RYCKER, M., CASAMASSIMA, A., RADTKE, S., COLLAZOS, A. & PARKER, P. J. 2011. Regulatory domain selectivity in the cell-type specific PKN-dependence of cell migration. *PLoS One,* 6**,** e21732.

LAING, K. J., PURCELL, M. K., WINTON, J. R. & HANSEN, J. D. 2008. A genomic view of the NOD-like receptor family in teleost fish: identification of a novel NLR subfamily in zebrafish. *BMC Evol Biol,* 8**,** 42.

LANGE, J. R. & FABRY, B. 2013. Cell and tissue mechanics in cell migration. *Exp Cell Res,* 319**,** 2418-23.

LAPRISE, P., VIEL, A. & RIVARD, N. 2004. Human homolog of disc-large is required for adherens junction assembly and differentiation of human intestinal epithelial cells. *J Biol Chem,* 279**,** 10157-66.

LAUFFENBURGER, D. A. & HORWITZ, A. F. 1996. Cell migration: a physically integrated molecular process. *Cell,* 84**,** 359-69.

LAUKOETTER, M. G., NAVA, P. & NUSRAT, A. 2008. Role of the intestinal barrier in inflammatory bowel disease. *World J Gastroenterol,* 14**,** 401-7.

LEE, H. J. & ZHENG, J. J. 2010. PDZ domains and their binding partners: structure, specificity, and modification. *Cell Commun Signal,* 8**,** 8.

LEE, H. W., CHOI, J., SHIN, H., KIM, K., YANG, J., NA, M., CHOI, S. Y., KANG, G. B., EOM, S. H., KIM, H. & KIM, E. 2008. Preso, a novel PSD-95-interacting FERM and PDZ domain protein that regulates dendritic spine morphogenesis. *J Neurosci,* 28**,** 14546-56.

LEE, O. K., FRESE, K. K., JAMES, J. S., CHADDA, D., CHEN, Z. H., JAVIER, R. T. & CHO, K. O. 2003. Discs-Large and Strabismus are functionally linked to plasma membrane formation. *Nat Cell Biol,* 5**,** 987-93.

LEGOUIS, R., JAULIN-BASTARD, F., SCHOTT, S., NAVARRO, C., BORG, J. P. & LABOUESSE, M. 2003. Basolateral targeting by leucine-rich repeat domains in epithelial cells. *EMBO Rep,* 4**,** 1096-102.

LEMMERS, C., MEDINA, E., DELGROSSI, M. H., MICHEL, D., ARSANTO, J. P. & LE BIVIC, A. 2002. hINADI/PATJ, a homolog of discs lost, interacts with crumbs and localizes to tight junctions in human epithelial cells. *J Biol Chem,* 277**,** 25408-15.

LEMMERS, C., MICHEL, D., LANE-GUERMONPREZ, L., DELGROSSI, M. H., MEDINA, E., ARSANTO, J. P. & LE BIVIC, A. 2004. CRB3 binds directly to Par6 and regulates the morphogenesis of the tight junctions in mammalian epithelial cells. *Mol Biol Cell,* 15**,** 1324-33.

LI, H., COGHLAN, A., RUAN, J., COIN, L. J., HERICHE, J. K., OSMOTHERLY, L., LI, R., LIU, T., ZHANG, Z., BOLUND, L., WONG, G. K., ZHENG, W., DEHAL, P., WANG, J. & DURBIN, R. 2006. TreeFam: a curated database of phylogenetic trees of animal gene families. *Nucleic Acids Res,* 34**,** D572-80.

LI, Y., KARNAK, D., DEMELER, B., MARGOLIS, B. & LAVIE, A. 2004. Structural basis for L27 domain-mediated assembly of signaling and cell polarity complexes. *EMBO J,* 23**,** 2723-33.

LIN, D., EDWARDS, A. S., FAWCETT, J. P., MBAMALU, G., SCOTT, J. D. & PAWSON, T. 2000. A mammalian PAR-3-PAR-6 complex implicated in Cdc42/Rac1 and aPKC signalling and cell polarity. *Nat Cell Biol,* 2**,** 540-7.

LIPINSKI, S., GRABE, N., JACOBS, G., BILLMANN-BORN, S., TILL, A., HASLER, R., ADEN, K., PAULSEN, M., ARLT, A., KRAEMER, L., HAGEMANN, N., ERDMANN, K. S., SCHREIBER, S. & ROSENSTIEL, P. 2012. RNAi screening identifies mediators of NOD2 signaling: implications for spatial specificity of MDP recognition. *Proc Natl Acad Sci U S A,* 109**,** 21426-31.

LIU, J., FUKUDA, K., XU, Z., MA, Y. Q., HIRBAWI, J., MAO, X., WU, C., PLOW, E. F. & QIN, J. 2011. Structural basis of phosphoinositide binding to kindlin-2 protein pleckstrin homology domain in regulating integrin activation. *J Biol Chem,* 286**,** 43334-42.

LOFTUS, E. V., JR. 2004. Clinical epidemiology of inflammatory bowel disease: Incidence, prevalence, and environmental influences. *Gastroenterology,* 126**,** 1504-17.

LU, Y. & SETTLEMAN, J. 1999. The Drosophila Pkn protein kinase is a Rho/Rac effector target required for dorsal closure during embryogenesis. *Genes Dev,* 13**,** 1168-80.

MAGLIOZZI, R., LOW, T. Y., WEIJTS, B. G., CHENG, T., SPANJAARD, E., MOHAMMED, S., VAN VEEN, A., OVAA, H., DE ROOIJ, J., ZWARTKRUIS, F. J., BOS, J. L., DE BRUIN, A., HECK, A. J. & GUARDAVACCARO, D. 2013. Control of epithelial cell migration and invasion by the IKKbeta- and CK1alpha-mediated degradation of RAPGEF2. *Dev Cell,* 27**,** 574-85.

MAKAROVA, O., ROH, M. H., LIU, C. J., LAURINEC, S. & MARGOLIS, B. 2003. Mammalian Crumbs3 is a small transmembrane protein linked to protein associated with Lin-7 (Pals1). *Gene,* 302**,** 21-9.

MALONEY, J. M., NIKOVA, D., LAUTENSCHLAGER, F., CLARKE, E., LANGER, R., GUCK, J. & VAN VLIET, K. J. 2010. Mesenchymal stem cell mechanics from the attached to the suspended state. *Biophys J,* 99**,** 2479-87.

MANDAI, K., NAKANISHI, H., SATOH, A., OBAISHI, H., WADA, M., NISHIOKA, H., ITOH, M., MIZOGUCHI, A., AOKI, T., FUJIMOTO, T., MATSUDA, Y., TSUKITA, S. & TAKAI, Y. 1997. Afadin: A novel actin filament-binding protein with one PDZ domain localized at cadherin-based cell-to-cell adherens junction. *J Cell Biol,* 139**,** 517-28.

MANTOVANI, F. & BANKS, L. 2003. Regulation of the discs large tumor suppressor by a phosphorylation-dependent interaction with the beta-TrCP ubiquitin ligase receptor. *J Biol Chem,* 278**,** 42477-86.

MANTOVANI, F., MASSIMI, P. & BANKS, L. 2001. Proteasome-mediated regulation of the hDlg tumour suppressor protein. *J Cell Sci,* 114**,** 4285-92.

MARTENS, J. C. & RADMACHER, M. 2008. Softening of the actin cytoskeleton by inhibition of myosin II. *Pflugers Arch,* 456**,** 95-100.

MATTER, K. & BALDA, M. S. 2003. Signalling to and from tight junctions. *Nat Rev Mol Cell Biol,* 4**,** 225-36.

MAUDSLEY, S., ZAMAH, A. M., RAHMAN, N., BLITZER, J. T., LUTTRELL, L. M., LEFKOWITZ, R. J. & HALL, R. A. 2000. Platelet-derived growth factor receptor association with Na(+)/H(+) exchanger regulatory factor potentiates receptor activity. *Mol Cell Biol,* 20**,** 8352-63.

MCCARTHY, K. M., SKARE, I. B., STANKEWICH, M. C., FURUSE, M., TSUKITA, S., ROGERS, R. A., LYNCH, R. D. & SCHNEEBERGER, E. E. 1996. Occludin is a functional component of the tight junction. *J Cell Sci,* 109 (Pt 9)**,** 2287-98.

MEDINA, E., LEMMERS, C., LANE-GUERMONPREZ, L. & LE BIVIC, A. 2002a. Role of the Crumbs complex in the regulation of junction formation in Drosophila and mammalian epithelial cells. *Biol Cell,* 94**,** 305-13.

MEDINA, E., WILLIAMS, J., KLIPFELL, E., ZARNESCU, D., THOMAS, G. & LE BIVIC, A. 2002b. Crumbs interacts with moesin and beta(Heavy)-spectrin in the apical membrane skeleton of Drosophila. *J Cell Biol,* 158**,** 941-51.

MELLOR, H., FLYNN, P., NOBES, C. D., HALL, A. & PARKER, P. J. 1998. PRK1 is targeted to endosomes by the small GTPase, RhoB. *J Biol Chem,* 273**,** 4811-4.

MERTENS, A. E., PEGTEL, D. M. & COLLARD, J. G. 2006. Tiam1 takes PARt in cell polarity. *Trends Cell Biol,* 16**,** 308-16.

METAIS, J. Y., NAVARRO, C., SANTONI, M. J., AUDEBERT, S. & BORG, J. P. 2005. hScrib interacts with ZO-2 at the cell-cell junctions of epithelial cells. *FEBS Lett,* 579**,** 3725-30.

MICHEL, D., ARSANTO, J. P., MASSEY-HARROCHE, D., BECLIN, C., WIJNHOLDS, J. & LE BIVIC, A. 2005. PATJ connects and stabilizes apical and lateral components of tight junctions in human intestinal cells. *J Cell Sci,* 118**,** 4049-57.

MICHIELAN, A. & D'INCA, R. 2015. Intestinal Permeability in Inflammatory Bowel Disease: Pathogenesis, Clinical Evaluation, and Therapy of Leaky Gut. *Mediators Inflamm,* 2015**,** 628157.

MIZUNO, K., SUZUKI, A., HIROSE, T., KITAMURA, K., KUTSUZAWA, K., FUTAKI, M., AMANO, Y. & OHNO, S. 2003. Self-association of PAR-3-mediated by

the conserved N-terminal domain contributes to the development of epithelial tight junctions. *J Biol Chem,* 278**,** 31240-50.

MOLEIRINHO, S., TILSTON-LUNEL, A., ANGUS, L., GUNN-MOORE, F. & REYNOLDS, P. A. 2013. The expanding family of FERM proteins. *Biochem J,* 452**,** 183-93.

MONTEIRO, A. C., SUMAGIN, R., RANKIN, C. R., LEONI, G., MINA, M. J., REITER, D. M., STEHLE, T., DERMODY, T. S., SCHAEFER, S. A., HALL, R. A., NUSRAT, A. & PARKOS, C. A. 2013. JAM-A associates with ZO-2, afadin, and PDZ-GEF1 to activate Rap2c and regulate epithelial barrier function. *Mol Biol Cell,* 24**,** 2849-60.

MORAIS-DE-SA, E., MIROUSE, V. & ST JOHNSTON, D. 2010. aPKC phosphorylation of Bazooka defines the apical/lateral border in Drosophila epithelial cells. *Cell,* 141**,** 509-23.

MUSCH, A. 2004. Microtubule organization and function in epithelial cells. *Traffic,* 5**,** 1-9.

MUSCH, A., COHEN, D., YEAMAN, C., NELSON, W. J., RODRIGUEZ-BOULAN, E. & BRENNWALD, P. J. 2002. Mammalian homolog of Drosophila tumor suppressor lethal (2) giant larvae interacts with basolateral exocytic machinery in Madin-Darby canine kidney cells. *Mol Biol Cell,* 13**,** 158-68.

MUTHUSWAMY, S. K. & XUE, B. 2012. Cell polarity as a regulator of cancer cell behavior plasticity. *Annu Rev Cell Dev Biol,* 28**,** 599-625.

NAGAI-TAMAI, Y., MIZUNO, K., HIROSE, T., SUZUKI, A. & OHNO, S. 2002. Regulated protein-protein interaction between aPKC and PAR-3 plays an essential role in the polarization of epithelial cells. *Genes Cells,* 7**,** 1161-71.

NAISBITT, S., KIM, E., TU, J. C., XIAO, B., SALA, C., VALTSCHANOFF, J., WEINBERG, R. J., WORLEY, P. F. & SHENG, M. 1999. Shank, a novel family of postsynaptic density proteins that binds to the NMDA receptor/PSD-95/GKAP complex and cortactin. *Neuron,* 23**,** 569-82.

NAVARRO, C., NOLA, S., AUDEBERT, S., SANTONI, M. J., ARSANTO, J. P., GINESTIER, C., MARCHETTO, S., JACQUEMIER, J., ISNARDON, D., LE BIVIC, A., BIRNBAUM, D. & BORG, J. P. 2005. Junctional recruitment of mammalian Scribble relies on E-cadherin engagement. *Oncogene,* 24**,** 4330-9.

NELSON, W. J. 2003. Adaptation of core mechanisms to generate cell polarity. *Nature,* 422**,** 766-74.

NELSON, W. J. & NUSSE, R. 2004. Convergence of Wnt, beta-catenin, and cadherin pathways. *Science,* 303**,** 1483-7.

NGUYEN, M. M., RIVERA, C. & GRIEP, A. E. 2005. Localization of PDZ domain containing proteins Discs Large-1 and Scribble in the mouse eye. *Mol Vis,* 11**,** 1183-99.

NIETHAMMER, M., KIM, E. & SHENG, M. 1996. Interaction between the C terminus of NMDA receptor subunits and multiple members of the PSD-95 family of membrane-associated guanylate kinases. *J Neurosci,* 16**,** 2157-63.

NIETHAMMER, M., VALTSCHANOFF, J. G., KAPOOR, T. M., ALLISON, D. W., WEINBERG, R. J., CRAIG, A. M. & SHENG, M. 1998. CRIPT, a novel postsynaptic protein that binds to the third PDZ domain of PSD-95/SAP90. *Neuron,* 20**,** 693-707.

NOREN, N. K., LIU, B. P., BURRIDGE, K. & KREFT, B. 2000. p120 catenin regulates the actin cytoskeleton via Rho family GTPases. *J Cell Biol,* 150**,** 567-80.

OEHLERS, S. H., FLORES, M. V., HALL, C. J., SWIFT, S., CROSIER, K. E. & CROSIER, P. S. 2011. The inflammatory bowel disease (IBD) susceptibility genes NOD1 and NOD2 have conserved anti-bacterial roles in zebrafish. *Dis Model Mech,* 4**,** 832-41.

OGURA, Y., BONEN, D. K., INOHARA, N., NICOLAE, D. L., CHEN, F. F., RAMOS, R., BRITTON, H., MORAN, T., KARALIUSKAS, R., DUERR, R. H., ACHKAR, J. P., BRANT, S. R., BAYLESS, T. M., KIRSCHNER, B. S., HANAUER, S. B., NUNEZ, G. & CHO, J. H. 2001a. A frameshift mutation in NOD2 associated with susceptibility to Crohn's disease. *Nature,* 411**,** 603-6.

OGURA, Y., INOHARA, N., BENITO, A., CHEN, F. F., YAMAOKA, S. & NUNEZ, G. 2001b. Nod2, a Nod1/Apaf-1 family member that is restricted to monocytes and activates NF-kappaB. *J Biol Chem,* 276**,** 4812-8.

OGURA, Y., LALA, S., XIN, W., SMITH, E., DOWDS, T. A., CHEN, F. F., ZIMMERMANN, E., TRETIAKOVA, M., CHO, J. H., HART, J., GREENSON, J. K., KESHAV, S. & NUNEZ, G. 2003. Expression of NOD2 in Paneth cells: a possible link to Crohn's ileitis. *Gut,* 52**,** 1591-7.

OLSEN, O., LIU, H., WADE, J. B., MEROT, J. & WELLING, P. A. 2002. Basolateral membrane expression of the Kir 2.3 channel is coordinated by PDZ interaction with Lin-7/CASK complex. *Am J Physiol Cell Physiol,* 282**,** C183-95.

OSMANI, N., VITALE, N., BORG, J. P. & ETIENNE-MANNEVILLE, S. 2006. Scrib controls Cdc42 localization and activity to promote cell polarization during astrocyte migration. *Curr Biol,* 16**,** 2395-405.

OTTO, O., ROSENDAHL, P., MIETKE, A., GOLFIER, S., HEROLD, C., KLAUE, D., GIRARDO, S., PAGLIARA, S., EKPENYONG, A., JACOBI, A., WOBUS, M., TOPFNER, N., KEYSER, U. F., MANSFELD, J., FISCHER-FRIEDRICH, E. & GUCK, J. 2015. Real-time deformability cytometry: on-the-fly cell mechanical phenotyping. *Nat Methods,* 12**,** 199-202, 4 p following 202.

PARRI, M. & CHIARUGI, P. 2010. Rac and Rho GTPases in cancer cell motility control. *Cell Commun Signal,* 8**,** 23.

PEGTEL, D. M., ELLENBROEK, S. I., MERTENS, A. E., VAN DER KAMMEN, R. A., DE ROOIJ, J. & COLLARD, J. G. 2007. The Par-Tiam1 complex controls persistent migration by stabilizing microtubule-dependent front-rear polarity. *Curr Biol,* 17**,** 1623-34.

PELLINEN, T. & IVASKA, J. 2006. Integrin traffic. *J Cell Sci,* 119**,** 3723-31.

PENKERT, R. R., DIVITTORIO, H. M. & PREHODA, K. E. 2004. Internal recognition through PDZ domain plasticity in the Par-6-Pals1 complex. *Nat Struct Mol Biol,* 11**,** 1122-7.

PETERSON, R. T. & SCHREIBER, S. L. 1999. Kinase phosphorylation: Keeping it all in the family. *Curr Biol,* 9**,** R521-4.

PETERSON, S. M. & FREEMAN, J. L. 2009. RNA isolation from embryonic zebrafish and cDNA synthesis for gene expression analysis. *J Vis Exp*.

PLANT, P. J., FAWCETT, J. P., LIN, D. C., HOLDORF, A. D., BINNS, K., KULKARNI, S. & PAWSON, T. 2003. A polarity complex of mPar-6 and atypical PKC binds, phosphorylates and regulates mammalian Lgl. *Nat Cell Biol,* 5**,** 301-8.

POPP, M. W. & MAQUAT, L. E. 2013. Organizing principles of mammalian nonsense-mediated mRNA decay. *Annu Rev Genet,* 47**,** 139-65.

PRAT, A. G., XIAO, Y. F., AUSIELLO, D. A. & CANTIELLO, H. F. 1995. cAMP-independent regulation of CFTR by the actin cytoskeleton. *Am J Physiol,* 268**,** C1552-61.

QIN, Y., CAPALDO, C., GUMBINER, B. M. & MACARA, I. G. 2005. The mammalian Scribble polarity protein regulates epithelial cell adhesion and migration through E-cadherin. *J Cell Biol,* 171**,** 1061-71.

QUETIER, I., MARSHALL, J. J., SPENCER-DENE, B., LACHMANN, S., CASAMASSIMA, A., FRANCO, C., ESCUIN, S., WORRALL, J. T., BASKARAN, P., RAJEEVE, V., HOWELL, M., COPP, A. J., STAMP, G., ROSEWELL, I., CUTILLAS, P., GERHARDT, H., PARKER, P. J. & CAMERON, A. J. 2016. Knockout of the PKN Family of Rho Effector Kinases Reveals a Non-redundant Role for PKN2 in Developmental Mesoderm Expansion. *Cell Rep,* 14**,** 440-8.

QUILLIAM, L. A., LAMBERT, Q. T., MICKELSON-YOUNG, L. A., WESTWICK, J. K., SPARKS, A. B., KAY, B. K., JENKINS, N. A., GILBERT, D. J., COPELAND, N. G. & DER, C. J. 1996. Isolation of a NCK-associated kinase, PRK2, an SH3-binding protein and potential effector of Rho protein signaling. *J Biol Chem,* 271**,** 28772-6.

RAGHURAM, V., MAK, D. O. & FOSKETT, J. K. 2001. Regulation of cystic fibrosis transmembrane conductance regulator single-channel gating by bivalent PDZ-domain-mediated interaction. *Proc Natl Acad Sci U S A,* 98**,** 1300-5.

RAJASEKARAN, A. K., HOJO, M., HUIMA, T. & RODRIGUEZ-BOULAN, E. 1996. Catenins and zonula occludens-1 form a complex during early stages in the assembly of tight junctions. *J Cell Biol,* 132**,** 451-63.

RAMALINGAM, N., FRANKE, C., JASCHINSKI, E., WINTERHOFF, M., LU, Y., BRUHMANN, S., JUNEMANN, A., MEIER, H., NOEGEL, A. A., WEBER, I., ZHAO, H., MERKEL, R., SCHLEICHER, M. & FAIX, J. 2015. A resilient formin-derived cortical actin meshwork in the rear drives actomyosin-based motility in 2D confinement. *Nat Commun,* 6**,** 8496.

RECZEK, D., BERRYMAN, M. & BRETSCHER, A. 1997. Identification of EBP50: A PDZ-containing phosphoprotein that associates with members of the ezrin-radixin-moesin family. *J Cell Biol,* 139**,** 169-79.

REIG, G., PULGAR, E. & CONCHA, M. L. 2014. Cell migration: from tissue culture to embryos. *Development,* 141**,** 1999-2013.

RIDLEY, A. J., SCHWARTZ, M. A., BURRIDGE, K., FIRTEL, R. A., GINSBERG, M. H., BORISY, G., PARSONS, J. T. & HORWITZ, A. R. 2003. Cell migration: integrating signals from front to back. *Science,* 302**,** 1704-9.

ROH, M. H., FAN, S., LIU, C. J. & MARGOLIS, B. 2003. The Crumbs3-Pals1 complex participates in the establishment of polarity in mammalian epithelial cells. *J Cell Sci,* 116**,** 2895-906.

ROH, M. H., LIU, C. J., LAURINEC, S. & MARGOLIS, B. 2002a. The carboxyl terminus of zona occludens-3 binds and recruits a mammalian homologue of discs lost to tight junctions. *J Biol Chem,* 277**,** 27501-9.

ROH, M. H., MAKAROVA, O., LIU, C. J., SHIN, K., LEE, S., LAURINEC, S., GOYAL, M., WIGGINS, R. & MARGOLIS, B. 2002b. The Maguk protein, Pals1, functions

as an adapter, linking mammalian homologues of Crumbs and Discs Lost. *J Cell Biol,* 157**,** 161-72.

ROMERO, G., VON ZASTROW, M. & FRIEDMAN, P. A. 2011. Role of PDZ proteins in regulating trafficking, signaling, and function of GPCRs: means, motif, and opportunity. *Adv Pharmacol,* 62**,** 279-314.

ROUX, K. J., KIM, D. I., RAIDA, M. & BURKE, B. 2012. A promiscuous biotin ligase fusion protein identifies proximal and interacting proteins in mammalian cells. *J Cell Biol,* 196**,** 801-10.

RUAN, J., LI, H., CHEN, Z., COGHLAN, A., COIN, L. J., GUO, Y., HERICHE, J. K., HU, Y., KRISTIANSEN, K., LI, R., LIU, T., MOSES, A., QIN, J., VANG, S., VILELLA, A. J., URETA-VIDAL, A., BOLUND, L., WANG, J. & DURBIN, R. 2008. TreeFam: 2008 Update. *Nucleic Acids Res,* 36**,** D735-40.

SARAS, J. & HELDIN, C. H. 1996. PDZ domains bind carboxy-terminal sequences of target proteins. *Trends Biochem Sci,* 21**,** 455-8.

SATO, T., FUJITA, N., YAMADA, A., OOSHIO, T., OKAMOTO, R., IRIE, K. & TAKAI, Y. 2006. Regulation of the assembly and adhesion activity of E-cadherin by nectin and afadin for the formation of adherens junctions in Madin-Darby canine kidney cells. *J Biol Chem,* 281**,** 5288-99.

SCANNEVIN, R. H. & HUGANIR, R. L. 2000. Postsynaptic organization and regulation of excitatory synapses. *Nat Rev Neurosci,* 1**,** 133-41.

SCHLUTER, M. A., PFARR, C. S., PIECZYNSKI, J., WHITEMAN, E. L., HURD, T. W., FAN, S., LIU, C. J. & MARGOLIS, B. 2009. Trafficking of Crumbs3 during cytokinesis is crucial for lumen formation. *Mol Biol Cell,* 20**,** 4652-63.

SCHMIDT, A., DURGAN, J., MAGALHAES, A. & HALL, A. 2007. Rho GTPases regulate PRK2/PKN2 to control entry into mitosis and exit from cytokinesis. *EMBO J,* 26**,** 1624-36.

SCHREIBER, F., PATRICIO, M., MUFFATO, M., PIGNATELLI, M. & BATEMAN, A. 2014. TreeFam v9: a new website, more species and orthology-on-the-fly. *Nucleic Acids Res,* 42**,** D922-5.

SCHULZKE, J. D., GITTER, A. H., MANKERTZ, J., SPIEGEL, S., SEIDLER, U., AMASHEH, S., SAITOU, M., TSUKITA, S. & FROMM, M. 2005. Epithelial transport and barrier function in occludin-deficient mice. *Biochim Biophys Acta,* 1669**,** 34-42.

SCHWARZ, J. M., COOPER, D. N., SCHUELKE, M. & SEELOW, D. 2014. MutationTaster2: mutation prediction for the deep-sequencing age. *Nat Methods,* 11**,** 361-2.

SFAKIANOS, J., TOGAWA, A., MADAY, S., HULL, M., PYPAERT, M., CANTLEY, L., TOOMRE, D. & MELLMAN, I. 2007. Par3 functions in the biogenesis of the primary cilium in polarized epithelial cells. *J Cell Biol,* 179**,** 1133-40.

SHENG, M. & HOOGENRAAD, C. C. 2007. The postsynaptic architecture of excitatory synapses: a more quantitative view. *Annu Rev Biochem,* 76**,** 823-47.

SHIN, K., FOGG, V. C. & MARGOLIS, B. 2006. Tight junctions and cell polarity. *Annu Rev Cell Dev Biol,* 22**,** 207-35.

SHIN, K., STRAIGHT, S. & MARGOLIS, B. 2005. PATJ regulates tight junction formation and polarity in mammalian epithelial cells. *J Cell Biol,* 168**,** 705-11.

SHIN, K., WANG, Q. & MARGOLIS, B. 2007. PATJ regulates directional migration of mammalian epithelial cells. *EMBO Rep,* 8**,** 158-64.

SHORT, D. B., TROTTER, K. W., RECZEK, D., KREDA, S. M., BRETSCHER, A., BOUCHER, R. C., STUTTS, M. J. & MILGRAM, S. L. 1998. An apical PDZ protein anchors the cystic fibrosis transmembrane conductance regulator to the cytoskeleton. *J Biol Chem,* 273**,** 19797-801.

ST JOHNSTON, D. & SANSON, B. 2011. Epithelial polarity and morphogenesis. *Curr Opin Cell Biol,* 23**,** 540-6.

STENZEL, N., FETZER, C. P., HEUMANN, R. & ERDMANN, K. S. 2009. PDZ-domain-directed basolateral targeting of the peripheral membrane protein FRMPD2 in epithelial cells. *J Cell Sci,* 122**,** 3374-84.

STERN, C. D. 2006. Evolution of the mechanisms that establish the embryonic axes. *Curr Opin Genet Dev,* 16**,** 413-8.

STOOKE-VAUGHAN, G. A., OBHOLZER, N. D., BAXENDALE, S., MEGASON, S. G. & WHITFIELD, T. T. 2015. Otolith tethering in the zebrafish otic vesicle requires Otogelin and alpha-Tectorin. *Development,* 142**,** 1137-45.

STRAIGHT, S. W., PIECZYNSKI, J. N., WHITEMAN, E. L., LIU, C. J. & MARGOLIS, B. 2006. Mammalian lin-7 stabilizes polarity protein complexes. *J Biol Chem,* 281**,** 37738-47.

STRAIGHT, S. W., SHIN, K., FOGG, V. C., FAN, S., LIU, C. J., ROH, M. & MARGOLIS, B. 2004. Loss of PALS1 expression leads to tight junction and polarity defects. *Mol Biol Cell,* 15**,** 1981-90.

STUCKE, V. M., TIMMERMAN, E., VANDEKERCKHOVE, J., GEVAERT, K. & HALL, A. 2007. The MAGUK protein MPP7 binds to the polarity protein hDlg1 and facilitates epithelial tight junction formation. *Mol Biol Cell,* 18**,** 1744-55.

SWANEY, K. F., BORLEIS, J., IGLESIAS, P. A. & DEVREOTES, P. N. 2015. Novel protein Callipygian defines the back of migrating cells. *Proc Natl Acad Sci U S A,* 112**,** E3845-54.

TAKAHASHI, K., NAKANISHI, H., MIYAHARA, M., MANDAI, K., SATOH, K., SATOH, A., NISHIOKA, H., AOKI, J., NOMOTO, A., MIZOGUCHI, A. & TAKAI, Y. 1999. Nectin/PRR: an immunoglobulin-like cell adhesion molecule recruited to cadherin-based adherens junctions through interaction with Afadin, a PDZ domain-containing protein. *J Cell Biol,* 145**,** 539-49.

TAKAI, Y., IKEDA, W., OGITA, H. & RIKITAKE, Y. 2008. The immunoglobulin-like cell adhesion molecule nectin and its associated protein afadin. *Annu Rev Cell Dev Biol,* 24**,** 309-42.

TAKAI, Y. & NAKANISHI, H. 2003. Nectin and afadin: novel organizers of intercellular junctions. *J Cell Sci,* 116**,** 17-27.

TAKEUCHI, K., KAWASHIMA, A., NAGAFUCHI, A. & TSUKITA, S. 1994. Structural diversity of band 4.1 superfamily members. *J Cell Sci,* 107 (Pt 7)**,** 1921-8.

TANCIONI, I., URYU, S., SULZMAIER, F. J., SHAH, N. R., LAWSON, C., MILLER, N. L., JEAN, C., CHEN, X. L., WARD, K. K. & SCHLAEPFER, D. D. 2014. FAK Inhibition disrupts a beta5 integrin signaling axis controlling anchorage-independent ovarian carcinoma growth. *Mol Cancer Ther,* 13**,** 2050-61.

TANENTZAPF, G. & BROWN, N. H. 2006. An interaction between integrin and the talin FERM domain mediates integrin activation but not linkage to the cytoskeleton. *Nat Cell Biol,* 8**,** 601-6.

THISSE, C. & THISSE, B. 2008. High-resolution in situ hybridization to whole-mount zebrafish embryos. *Nat Protoc,* 3**,** 59-69.

TOMAIC, V., GARDIOL, D., MASSIMI, P., OZBUN, M., MYERS, M. & BANKS, L. 2009. Human and primate tumour viruses use PDZ binding as an

evolutionarily conserved mechanism of targeting cell polarity regulators. *Oncogene,* 28**,** 1-8.

TRINKLE-MULCAHY, L., BOULON, S., LAM, Y. W., URCIA, R., BOISVERT, F. M., VANDERMOERE, F., MORRICE, N. A., SWIFT, S., ROTHBAUER, U., LEONHARDT, H. & LAMOND, A. 2008. Identifying specific protein interaction partners using quantitative mass spectrometry and bead proteomes. *J Cell Biol,* 183**,** 223-39.

TSUKITA, S., YAMAZAKI, Y., KATSUNO, T., TAMURA, A. & TSUKITA, S. 2008. Tight junction-based epithelial microenvironment and cell proliferation. *Oncogene,* 27**,** 6930-8.

ULLMER, C., SCHMUCK, K., FIGGE, A. & LUBBERT, H. 1998. Cloning and characterization of MUPP1, a novel PDZ domain protein. *FEBS Lett,* 424**,** 63-8.

VAN DE PAVERT, S. A., KANTARDZHIEVA, A., MALYSHEVA, A., MEULEMAN, J., VERSTEEG, I., LEVELT, C., KLOOSTER, J., GEIGER, S., SEELIGER, M. W., RASHBASS, P., LE BIVIC, A. & WIJNHOLDS, J. 2004. Crumbs homologue 1 is required for maintenance of photoreceptor cell polarization and adhesion during light exposure. *J Cell Sci,* 117**,** 4169-77.

VAN EEKELEN, M., RUNTUWENE, V., MASSELINK, W. & DEN HERTOG, J. 2012. Pair-wise regulation of convergence and extension cell movements by four phosphatases via RhoA. *PLoS One,* 7**,** e35913.

VAN ITALLIE, C. M., APONTE, A., TIETGENS, A. J., GUCEK, M., FREDRIKSSON, K. & ANDERSON, J. M. 2013. The N and C termini of ZO-1 are surrounded by distinct proteins and functional protein networks. *J Biol Chem,* 288**,** 13775-88.

VAN ITALLIE, C. M., TIETGENS, A. J., APONTE, A., FREDRIKSSON, K., FANNING, A. S., GUCEK, M. & ANDERSON, J. M. 2014. Biotin ligase tagging identifies proteins proximal to E-cadherin, including lipoma preferred partner, a regulator of epithelial cell-cell and cell-substrate adhesion. *J Cell Sci,* 127**,** 885-95.

VARNAITE, R. & MACNEILL, S. A. 2016. Meet the neighbors: Mapping local protein interactomes by proximity-dependent labeling with BioID. *Proteomics,* 16**,** 2503-2518.

VINAYAGAM, A., STELZL, U., FOULLE, R., PLASSMANN, S., ZENKNER, M., TIMM, J., ASSMUS, H. E., ANDRADE-NAVARRO, M. A. & WANKER, E. E. 2011. A directed protein interaction network for investigating intracellular signal transduction. *Sci Signal,* 4**,** rs8.

VINCENT, S. & SETTLEMAN, J. 1997. The PRK2 kinase is a potential effector target of both Rho and Rac GTPases and regulates actin cytoskeletal organization. *Mol Cell Biol,* 17**,** 2247-56.

VOGEL, V. 2006. Mechanotransduction involving multimodular proteins: converting force into biochemical signals. *Annu Rev Biophys Biomol Struct,* 35**,** 459-88.

WAKAMATSU, Y., SAKAI, D., SUZUKI, T. & OSUMI, N. 2011. FilaminB is required for the directed localization of cell-cell adhesion molecules in embryonic epithelial development. *Dev Dyn,* 240**,** 149-61.

WALLACE, S. W., MAGALHAES, A. & HALL, A. 2011. The Rho target PRK2 regulates apical junction formation in human bronchial epithelial cells. *Mol Cell Biol,* 31**,** 81-91.

WANG, H. R., ZHANG, Y., OZDAMAR, B., OGUNJIMI, A. A., ALEXANDROVA, E., THOMSEN, G. H. & WRANA, J. L. 2003. Regulation of cell polarity and protrusion formation by targeting RhoA for degradation. *Science,* 302**,** 1775-9.

WANG, Q., CHEN, X. W. & MARGOLIS, B. 2007. PALS1 regulates E-cadherin trafficking in mammalian epithelial cells. *Mol Biol Cell,* 18**,** 874-85.

WANG, Q., HURD, T. W. & MARGOLIS, B. 2004. Tight junction protein Par6 interacts with an evolutionarily conserved region in the amino terminus of PALS1/stardust. *J Biol Chem,* 279**,** 30715-21.

WANG, S., YUE, H., DERIN, R. B., GUGGINO, W. B. & LI, M. 2000. Accessory protein facilitated CFTR-CFTR interaction, a molecular mechanism to potentiate the chloride channel activity. *Cell,* 103**,** 169-79.

WATTS, J. L., ETEMAD-MOGHADAM, B., GUO, S., BOYD, L., DRAPER, B. W., MELLO, C. C., PRIESS, J. R. & KEMPHUES, K. J. 1996. par-6, a gene involved in the establishment of asymmetry in early C. elegans embryos, mediates the asymmetric localization of PAR-3. *Development,* 122**,** 3133-40.

WEBB, D. J., PARSONS, J. T. & HORWITZ, A. F. 2002. Adhesion assembly, disassembly and turnover in migrating cells -- over and over and over again. *Nat Cell Biol,* 4**,** E97-100.

WICHE, G., KREPLER, R., ARTLIEB, U., PYTELA, R. & ABERER, W. 1984. Identification of plectin in different human cell types and immunolocalization at epithelial basal cell surface membranes. *Exp Cell Res,* 155**,** 43-9.

WICHE, G., KREPLER, R., ARTLIEB, U., PYTELA, R. & DENK, H. 1983. Occurrence and immunolocalization of plectin in tissues. *J Cell Biol,* 97**,** 887-901.

WILKINSON, R. N., ELWORTHY, S., INGHAM, P. W. & VAN EEDEN, F. J. 2013. A method for high-throughput PCR-based genotyping of larval zebrafish tail biopsies. *Biotechniques,* 55**,** 314-6.

WILLOTT, E., BALDA, M. S., FANNING, A. S., JAMESON, B., VAN ITALLIE, C. & ANDERSON, J. M. 1993. The tight junction protein ZO-1 is homologous to the Drosophila discs-large tumor suppressor protein of septate junctions. *Proc Natl Acad Sci U S A,* 90**,** 7834-8.

WU, H., FENG, W., CHEN, J., CHAN, L. N., HUANG, S. & ZHANG, M. 2007. PDZ domains of Par-3 as potential phosphoinositide signaling integrators. *Mol Cell,* 28**,** 886-98.

XU, M., TAKANASHI, M., OIKAWA, K., NISHI, H., ISAKA, K., YOSHIMOTO, T., OHYASHIKI, J. & KURODA, M. 2012a. Identification of a novel role of Septin 10 in paclitaxel-resistance in cancers through a functional genomics screen. *Cancer Sci,* 103**,** 821-7.

XU, W., MEZENCEV, R., KIM, B., WANG, L., MCDONALD, J. & SULCHEK, T. 2012b. Cell stiffness is a biomarker of the metastatic potential of ovarian cancer cells. *PLoS One,* 7**,** e46609.

YAMAMOTO, T., HARADA, N., KANO, K., TAYA, S., CANAANI, E., MATSUURA, Y., MIZOGUCHI, A., IDE, C. & KAIBUCHI, K. 1997. The Ras target AF-6 interacts with ZO-1 and serves as a peripheral component of tight junctions in epithelial cells. *J Cell Biol,* 139**,** 785-95.

YAMANAKA, T., HORIKOSHI, Y., IZUMI, N., SUZUKI, A., MIZUNO, K. & OHNO, S. 2006. Lgl mediates apical domain disassembly by suppressing the PAR-

3-aPKC-PAR-6 complex to orient apical membrane polarity. *J Cell Sci,* 119**,** 2107-18.

YAMANAKA, T., HORIKOSHI, Y., SUGIYAMA, Y., ISHIYAMA, C., SUZUKI, A., HIROSE, T., IWAMATSU, A., SHINOHARA, A. & OHNO, S. 2003. Mammalian Lgl forms a protein complex with PAR-6 and aPKC independently of PAR-3 to regulate epithelial cell polarity. *Curr Biol,* 13**,** 734-43.

YAP, A. S., NIESSEN, C. M. & GUMBINER, B. M. 1998. The juxtamembrane region of the cadherin cytoplasmic tail supports lateral clustering, adhesive strengthening, and interaction with p120ctn. *J Cell Biol,* 141**,** 779-89.

YE, T., IP, J. P., FU, A. K. & IP, N. Y. 2014. Cdk5-mediated phosphorylation of RapGEF2 controls neuronal migration in the developing cerebral cortex. *Nat Commun,* 5**,** 4826.

ZHANG, X., FEI, Z., WAN, J., XU, J., YU, B. & GUAN, M. 2011. Association analysis of BANK1 gene with psoriasis in Southern Han Chinese. *Int J Immunogenet,* 38**,** 507-12.

ZUHORN, I. S., KALICHARAN, D., ROBILLARD, G. T. & HOEKSTRA, D. 2007. Adhesion receptors mediate efficient non-viral gene delivery. *Mol Ther,* 15**,** 946-53.